CHEMICAL REVIEWS

pubs.acs.org/CR

Review

Orbital-Free Density Functional Theory: An Attractive Electronic Structure Method for Large-Scale First-Principles Simulations

Wenhui Mi,*,† Kai Luo,*,† S. B. Trickey,*,† and Michele Pavanello*,†

Cite This: *Chem. Rev.* 2023, 123, 12039−12104

Read Online

ACCESS | Metrics & More | Article Recommendations

ABSTRACT: Kohn−Sham Density Functional Theory (KSDFT) is the most widely used electronic structure method in chemistry, physics, and materials science, with thousands of calculations cited annually. This ubiquity is rooted in the favorable accuracy vs cost balance of KSDFT. Nonetheless, the ambitions and expectations of researchers for use of KSDFT in predictive simulations of large, complicated molecular systems are confronted with an intrinsic computational cost-scaling challenge. Particularly evident in the context of first-principles molecular dynamics, the challenge is the high cost-scaling associated with the computation of the Kohn−Sham orbitals. Orbital-free DFT (OFDFT), as the name suggests, circumvents entirely the explicit use of those orbitals. Without them, the structural and algorithmic complexity of KSDFT simplifies dramatically and near-linear scaling with system size irrespective of system state is achievable. Thus, much larger system sizes and longer simulation time scales (compared to conventional KSDFT) become accessible; hence, new chemical phenomena and new materials can be explored. In this review, we introduce the historical contexts of OFDFT, its theoretical basis, and the challenge of realizing its promise via approximate kinetic energy density functionals (KEDFs). We review recent progress on that challenge for an array of KEDFs, such as one-point, two-point, and machine-learnt, as well as some less explored forms. We emphasize use of exact constraints and the inevitability of design choices. Then, we survey the associated numerical techniques and implemented algorithms specific to OFDFT. We conclude with an illustrative sample of applications to showcase the power of OFDFT in materials science, chemistry, and physics.

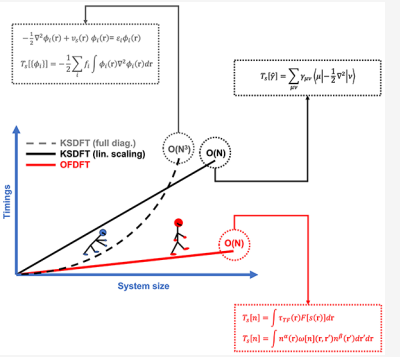

CONTENTS

Received: October 31, 2022
Published: October 23, 2023

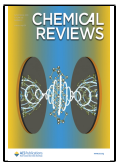

1. INTRODUCTION

1.1. Motivation

The extraordinarily widespread use of density functional theory (DFT) in its conventional computational form via Kohn–Sham (KS) orbitals and their eigenvalues[1] masks a remarkable fact: those orbitals are not essential to Kohn–Sham DFT (KSDFT). This review focuses on exploitation of that fact in the electronic structure method known as orbital-free density functional theory (OFDFT). In a very real sense it is the more fundamental form of KSDFT. OFDFT literally puts the density back into centrality in DFT, both formally and in practice.

The immediate motivation is plain. Given the need to consider only the electron density as the main ingredient of the method, OFDFT can have a computational cost scaling linearly with system size *irrespective of system state*. Therefore, OFDFT is on the verge of becoming the alternative to conventional KSDFT in at least two limiting categories: (1) systems for which the size is too large or the number of simulations is too large to be tackled by conventional KSDFT and (2) systems with temperature and/or density too large to be tractable with conventional KSDFT. These two categories, especially the first, are becoming increasingly relevant as chemistry and materials physics push into systems of high molecular and structural complexity.

We say OFDFT "is on the verge" because it involves a problem analogous with one familiar in conventional KSDFT, namely construction of accurate approximate density functionals. The difference is that OFDFT needs kinetic energy density functionals (KEDFs) as well as the exchange-correlation (XC) functionals familiar in conventional KSDFT.[2]

The reader may have noticed the terminology "conventional KSDFT". Perhaps this seems an unmotivated complication. But the reasons for making the distinction are deep and will become clear soon. The essential point is simple. OFDFT is a way of doing KSDFT. But it does not use the KS orbitals explicitly. Instead it uses KEDFs. KEDFs connect the theory to the earliest days of quantum mechanics. It is perhaps underappreciated that the earliest forms of OFDFT preceded the Hohenberg–Kohn theorems[3] of modern DFT. That earlier work provided the intellectual foundations and ample precedent for treating many-electron problems via a suitably constructed effective non-interacting system. We do not pretend to be historians of science. Nonetheless, the centrality of that non-interacting system concept motivates our historically oriented account of those pre-Hohenberg–Kohn roots. In it we try to do justice to the great effort of many researchers. That effort built the context that distinguishes conventional KSDFT in its ubiquitous practical form and KSDFT in its most basic form, namely OFDFT. We then lay out the relevant parts of formal DFT and use that to clarify the distinctive differences between conventional KSDFT and OFDFT. There follows a survey of modern KEDFs, with pointers to earlier ones via prior reviews. We devote a section to the software implementations of OFDFT in its various flavors and another to some of the most notable contemporary applications.

In all, we attempt to give a clear, candid account of the state of the art in OFDFT functional development and its algorithmic realizations in advanced electronic structure software, describing both the limitations and the opportunities for applications in chemistry and materials science.

1.2. Curse of Computational Scaling

In recent years, some chemists, materials scientists, and physicists have speculated upon "lab 2.0".[4] It is conceived as a scientific inquiry mode in which computer simulations replace experiments for tasks such as materials design and combinatorial search of chemical space. Even though computationally aided materials design and chemical discovery via tools such as high-throughput workflows now are daily occurrences,[5,6] the computational cost scaling of adequately accurate quantum-mechanical methods hinders progress severely. "lab 2.0" thus still largely belongs to the future.

Disparity between desired computational approaches and available computational resources is not a new problem. At each stage of computational resource development, from pen and paper to abacus, slide rule, rotary calculator,[7,8] desk calculator, analog machine, ENIAC,[9] ..., it has been easy to define calculations intractable on currently available resources.

More profoundly, nature imposes some computational scaling lower bounds.[10,11] The focus issue is electronic structure. It underlies the periodic table, which is normative for the chemistry of materials and their molecular constituents. In the simplest case, the nuclei are fixed and the electrons are treated by some model that makes them independent in a mean-field of the others, e.g. Hartree–Fock (HF)[12] or KSDFT.[1] In both, the straightforward implementation, in terms of a determinant (HF or conventional KSDFT) and standard XC approximants, causes the number of operations to grow as the cube of the number of electrons (i.e., $O(N_e^3)$ or simply $O(N^3)$ hereafter) because of the orthogonalization of the one-electron orbitals. In addition, the straightforward approach of expanding in a basis of local orbitals can lead to large additional costs caused by quadratic scaling for building the needed matrices. Scaling of this sort can be mitigated by employing techniques such as distance-based screening coupled with sparse linear algebra[13−15] and/or fast Fourier transforms[16] to recover almost linear scaling algorithms for matrix build and Hamiltonian-wave function operations, albeit with a large prefactor[11,17] and restriction to systems wherein

https://doi.org/10.1021/acs.chemrev.2c00758
Chem. Rev. 2023, 123, 12039−12104

Table 1. Chronology of Orbital-Free Density Functional Theory[a]

Year	Milestone	Method
1927	Thomas and Fermi present their approximate method that satisfies the Pauli principle while avoiding the Schrödinger equation	TF[22,23]
1930	TF is applied to atoms such as Fe yielding qualitative agreement with experimental sequential ionization energies[24]	
1930	Dirac extends TF to include exchange effects	TFD[25]
1935	Slater extends TF to the condensed phase and applies it to metals, but no binding is found[26]	
1935	von Weizsäcker proposes the first gradient correction	TFvW, TFvWD[27]
1945	The ENIAC computer is built; patent filed in 1948[9]	
1949	Reitz implements TFD on ENIAC for computation of electronic properties of atoms[28]	
1949	Feynman, Metropolis, and Teller extend the finite-temperature Thomas−Fermi theory[29]	
1957−1982	Extensions of TFvWD and the gradient expansion approximation	GEA[30−34] and TFλvW[35−38]
1962	Teller proves that TF cannot lead to molecular bonding[39]	
1964	Formal footing of DFT	Hohenberg−Kohn theorems[3]
1965	Mapping to a non-interacting electron system and employment of the exact non-interacting KEDF	KSDFT[1]
1964−1965	Introduction of polarizability in the construction of the KEDF	Nonlocal KEDF[3,40]
1981−1983	Computational proof that a gradient correction to TF (e.g., TFvWD) leads to molecular binding[41,42]	
1985−ongoing	Nonlocal (two-point) KEDFs for condensed phases	CAT,[43] WT,[44] WGC,[45] SM,[46] Perrot,[47] Chai−Weeks,[48] XWM[49] KEDFs, real space,[50−53] and reciprocal space[54,55]
1986	Generalized gradient approximation for the exchange and correlation energy functional	GGA XC[56,57]
1991	Conjointness conjecture[58]	GGA KEDFs[58−63,63−76]
2010−ongoing	Nonlocal (two-point) KEDF for semiconductors	HC,[77] WGCD,[78] EvW-WGC,[79] KGAP,[80] MGP[81]
2012−ongoing	Machine-learnt KEDFs[82−84]	
2013−ongoing	General-purpose semilocal (one-point) KEDFs	VT84F,[85] LKT,[86] PGSL[87]
2019−ongoing	Nonlocal (two-point) KEDF for finite systems and subsystem DFT	LMGP,[88,89] LDAK[90] and revHC[91]

[a]KEDF stands for kinetic energy density functional.

sparsity is physically realistic. More complicated explicit wave function methods simply worsen the scaling.[18−21]

The curse of computational scaling in quantum mechanics has been known since its inception. Dirac's oft-quoted 1929 remark raises the problem at the end:

> *"The underlying physical laws necessary for the mathematical theory of a large part of physics and the whole of chemistry are thus completely known, and the difficulty is only that the exact application of these laws leads to equations much too complicated to be soluble. It therefore becomes desirable that approximate practical methods of applying quantum mechanics should be developed, which can lead to an explanation of the main features of complex atomic systems without too much computation."*[92]

Back then researchers addressed computational scaling barriers by making clever but drastic simplifications to the quantum mechanical approach. Only much later, in the mid-1940s, did the first Turing complete computer (i.e., a digital computer in the modern sense) surface, the ENIAC project.[28] In anticipation of the main focus of this review, we note that Dirac's ambition, to give "···an explanation of the main features···", was modest compared to today's ambition to achieve predictive calculations.

In any event, the late 1920s and the 1930s were replete with pen-and-paper calculations of atoms[93] and materials[26] which avoided the use of any computationally challenging manipulations such as diagonalization of large matrices. Heroic numerical solutions on manual calculators[7,94−96] also were achieved.

It was in this environment that Thomas[23] and Fermi[22] independently proposed a method that required no diagonalizations. Instead, their approach focuses on a single, central quantum-mechanical quantity, the electron number density, and results in a single differential equation. This is the justly famous Thomas−Fermi theory (TF hereafter). It is the primordial version of OFDFT. Table 1 provides an overview of OFDFT development milestones from then until today.

Because its clear analytical structure incorporates the basic features of many-Fermion systems generally, TF theory has been the subject of intense mathematical scrutiny; hence, much is known about its content and properties. See reviews by March,[30] Lieb and Simon,[97] Spruch,[98] March,[99] and Solovej[100] as well as the book by Englert,[101] among many resources. Basic development of TF theory is treated in many books, e.g. by Parr and Yang,[102] Slater,[103,104] Giuliani and Vignale,[105] and Engel and Dreizler,[106] so we sketch only the idea and display relevant bits here.

The foundational insight in TF theory is that a set of electrons in a neutral system can be idealized as behaving much like a non-interacting, uniform gas. That is, one assumes that the real system of interest is nearly indistinguishable from a homogeneous electron gas (HEG). The HEG in turn is assumed to occupy a volume V uniformly with number density $n = \frac{N_e}{V}$. (Remark: We adopt the notation prevalent in the physics literature, n. In the chemistry literature, often ρ is used.) The hard-walled volume forces quantization into discrete energy levels. The electrons must satisfy the Pauli exclusion principle; thus, at most two of them can occupy a given level. This leads to a maximum occupied energy level

https://doi.org/10.1021/acs.chemrev.2c00758
Chem. Rev. 2023, 123, 12039−12104

related to the charge density. In turn, there is a total kinetic energy (there is no interaction energy) given by

$$T = \frac{3}{10}(3\pi^2)^{2/3} n^{5/3} \equiv c_{TF} n^{5/3} \tag{1}$$

Note that here and henceforth, unless stated otherwise, we are using Hartree atomic units, $\hbar = m_e = q_e = 1$ with m_e and q_e the electron mass and charge magnitude, respectively.

The key conceptual leap then is to make the local density approximation, namely that locally a physical system behaves like an HEG of the density locally. The resulting generalization to inhomogeneous systems is

$$T_{TF}[n] = c_{TF} \int_{\mathbb{R}^3} d\mathbf{r} n^{5/3}(\mathbf{r}) \equiv \int_{\mathbb{R}^3} d\mathbf{r} \tau_{TF}(\mathbf{r}) \tag{2}$$

Along with this, one can associate an electrostatic potential that is as deep as the maximum energy (a simple shift of energy zero) and gives, via Poisson's equation, the proper charge density. This is the prescription for the TF atom, for example. For details not needed here, we refer the reader to Appendix 17 of ref 103.

It often has been remarked that TF theory is the ancestor of DFT (see Table 1). Early interest in TF theory arose, in fact, from its computational feasibility for treating many-electron atoms. When spherical symmetry is present, the TF equations are pseudo-one-dimensional and their solution can be approached with pen and paper. Among the early applications of TF theory is the work of Baker[24] aimed at predicting multiple atomic ionizations. This was an important topic that also was pursued by Hartree[12,107] as an application of the HF method. It, unfortunately, is intractable for pen-and-paper calculation. Using TF theory, Baker[24] predicted semiquantitative agreement with experimental ionization potentials (IPs) for atoms such as O and Fe. See Figure 1.

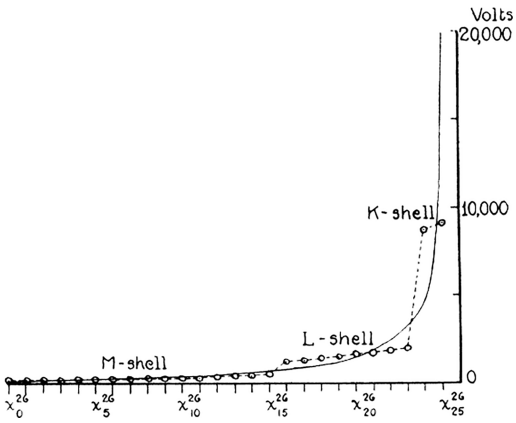

Figure 1. First computation of ionization potentials using Thomas–Fermi theory (full curve). Calculated values for Fe compared to experiment (dashed curve and data points). Reprinted with permission from ref 24. Copyright (1930) American Physical Society.

Dirac became interested in finding commonality between the HF ansatz and TF theory. In 1930 he showed[25] that application of the HF approach to an HEG produces a stabilizing exchange term proportional to the maximum momentum attainable by the HEG. It follows that the exchange energy density is proportional to $n^{4/3}$ and thus the associated exchange potential is proportional to $n^{1/3}$.

Dirac's analysis yielded two achievements. First, it justified TF theory (for which there was only a heuristic grounding until then) by constructing the quasi-classical counterpart of the HF problem for a nearly uniform density system. [Remark: Dirac[25] achieved the quasi-classical counterpart of the HF approach in a way that nowadays is standard practice.[108,109] He took what we now call the Wigner transform (introduced in 1927 by Weyl[110] and formally only two years later by Wigner[111]) of a dynamical variable to transform the exchange and Coulomb operators into classical phase space functions (i.e., p and q). That led to an expression for the Hamiltonian also as a function of only p and q. Then he evaluated the Poisson bracket with the electron density matrix, which was also assumed to be Wigner-transformed to a function of p and q, and approximated by $\rho(p, q) = 2$ if $p < P$ and zero otherwise (P here is a maximum momentum attainable in the infinitesimal volume of phase space, $(2\pi\hbar)^3$, at point p, q). As the energy is conserved, the Poisson brackets need to be zero, $\{H, \rho\} = 0$. This procedure led him to find the Thomas–Fermi equation (i.e., the functional derivative of eq 2 with respect to the electron density) for atoms, augmented by an additional term stemming from the exchange operator and proportional to the maximum momentum P.] Second, Dirac showed that an exchange term should be added to the TF energy and potential.

However, already in the 1930s there were indications that the TF approximation did not support chemical bonds. Slater extended TF to treat metals by constructing the bulk as a sum of locally spherical atomic fragments.[26] Disappointingly, the result was repulsive energy curves. Thus it appeared that, at least for metals, TF theory could not predict binding. Years later Teller (who was a good friend of Fermi[112]) confirmed the difficulty rigorously[39] with the demonstration that molecular binding cannot happen in the TF model.

But in 1935 that problem was tackled by von Weizsäcker.[27] He contrived a correction to the TF model which involved the use of an ad-hoc orbital proportional to the square-root of the electron density. The kinetic energy from such an orbital certainly contains a density gradient term and, thus, introduces explicit treatment of inhomogeneity. The derivation itself is incorrect,[113] but the idea is consequential.

Let us revisit the von Weizsäcker idea via an alternative development. Note that there are several other derivations, for example refs 114 and 115, that follow a density matrix-centric route. We anticipate OFDFT and suppose that one orbital is enough in some sense to capture the essential information in the wave function of the system. Such a "collective orbital" can take the form

$$\psi(\mathbf{r}) = (a + b(\mathbf{r}))e^{i\mathbf{p}\cdot\mathbf{r}} \tag{3}$$

with a a real constant such that $a \exp(i\mathbf{p}\cdot\mathbf{r})$ represents the part of the system most similar to the HEG, $b(\mathbf{r})$ is a real function that represents the deviation from uniformity, and $\mathbf{p}$ is an average momentum associated with the collective orbital. The kinetic energy of the system can be evaluated as

https://doi.org/10.1021/acs.chemrev.2c00758
Chem. Rev. 2023, 123, 12039–12104

$$
\begin{aligned}
T[\psi] &= \frac{1}{2}\langle \nabla\psi | \nabla\psi \rangle \\
&= \frac{1}{2}\int d\mathbf{r}(-i\mathbf{p}a + \nabla b(\mathbf{r}) - ib(\mathbf{r})\mathbf{p}) \\
&\quad (i\mathbf{p}a + \nabla b(\mathbf{r}) + ib(\mathbf{r})\mathbf{p}) \\
&= \frac{1}{2}\int d\mathbf{r}(p^2[a + b(\mathbf{r})]^2 + |\nabla b(\mathbf{r})|^2) \\
&= \frac{1}{2}\int d\mathbf{r}(p^2 n(\mathbf{r}) + |\nabla\sqrt{n(\mathbf{r})}|^2)
\end{aligned}
\tag{4}
$$

We recognize the first term, $\int p^2 n(\mathbf{r})d\mathbf{r}$, as the TF functional by comparison with eq 1 and the realization that for the uniform system we can identify

$$
p^2 = \frac{3}{5}(3\pi)^{2/3} n^{2/3} \tag{5}
$$

Insertion of eq 5 in eq 4 leads to the Thomas–Fermi–von Weiszäcker (TFvW) functional,

$$
\begin{aligned}
T_{TFvW}[n] &= c_{TF}\int d\mathbf{r} n^{5/3}(\mathbf{r}) + \frac{1}{2}\int d\mathbf{r}\nabla\sqrt{n(\mathbf{r})}\,\nabla\sqrt{n(\mathbf{r})} \\
&= T_{TF}[n] + T_{vW}[n]
\end{aligned}
\tag{6}
$$

We remark that TF and TFvW can be combined with Dirac's exchange,[25] to lead to TFD and TFvWD, respectively. For later reference, we note

$$
\begin{aligned}
T_{vW}[n] &:= \frac{1}{2}\int d\mathbf{r}|\nabla n^{1/2}(\mathbf{r})|^2 \equiv \frac{1}{8}\int d\mathbf{r}\frac{|\nabla n(\mathbf{r})|^2}{n(\mathbf{r})} \\
&\equiv \int d\mathbf{r}\tau_{vW}[n](\mathbf{r})
\end{aligned}
\tag{7}
$$

At least so far as sophistication of formulation is concerned, TFvW clearly is superior to TF. But the differential equations involved are not amenable to analytical solution.[30] Widespread use began only decades after von Weizsäcker's original conception. Building from the work of Kirzhnitz,[31] whose derivations led him to compute the first gradient expansion approximation (GEA) to the TF model, the first thorough probe of TFvW on realistic physical systems seems to be application to atoms by Yonei and Tomishima.[38,116] They found that the TFλvW functional

$$
T_{TF\lambda vW}[n] = T_{TF}[n] + \lambda T_{vw}[n] \tag{8}
$$

with $\lambda = 0.2$ (rather than the GEA value of $\lambda = \frac{1}{9}$) yielded closest agreement with their quantum mechanical data, which were from the HF method with hydrogenic atomic orbitals (by the same authors).

Benguria et al.[41] and later Berk[42] did a mathematical analysis of the TFvW method and found that the von Weizsäcker correction must lead to binding between atoms. Thus, it is not surprising that investigations using TFvW theory appeared[117,118] and have continued for decades.[119−122]

Although more inclusive of quantum mechanical effects than TF, TFλvW has major drawbacks. As Figure 2 shows, no TFλvW variant reproduces atomic shell structure. As will become clearer below, this is a consequence of a more general limitation of TFλvW, namely that it contains no information about the polarizability of the electronic system.[40] Similarly, Friedel oscillations[123] (density oscillations around an impurity in a metal) are among the so-called quantum oscillations that

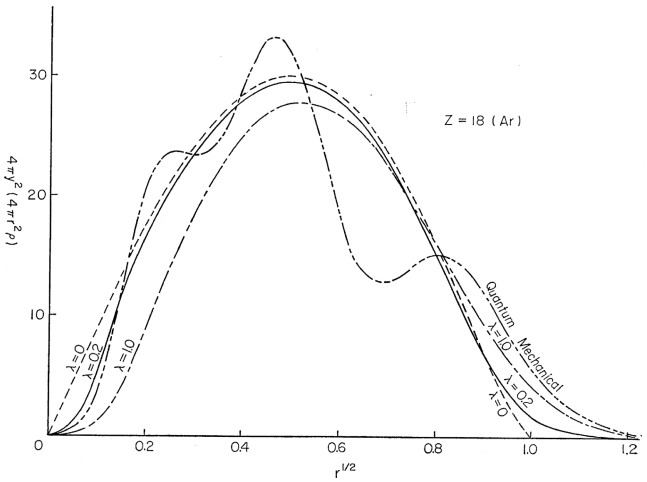

Figure 2. First probe of the TFλvW functional on realistic systems. Shown is the radial electron density for the Ar atom. "Quantum Mechanical" results are Hartree–Fock. Reprinted with permission from ref 38. Copyright (1965) The Physical Society of Japan.

TF and TFvW miss completely. The ability of some TFvW-type functionals to reproduce, at least semiquantitatively, the kinetic energy of atoms has been ascribed to major error cancellation.[124,125] As we will explain in Section 2, TFλvW with $\lambda < 1$ are non-N-representable functionals and, therefore, are not expected to be generally accurate. Nevertheless, there have been interesting applications of TFλvW to metal clusters.[119,126−128] In them, TFλvW was found to produce converged Carr–Parrinello or Born–Oppenheimer molecular dynamics and provide useful predictions related to melting and alloying; see Section 4.

1.3. Connecting the Early TF and TFvWD Functionals with Modern OFDFT

TF and TFvW, as already remarked, are density functionals. Given an electron density, each one gives back an energy. But the demonstration that the exact many-electron system ground state is expressible variationally as a density functional came only in 1964 with the famous Hohenberg–Kohn theorems,[3] though there had been suggestive antecedents in the 1950s.[129,130]

Only the barest essentials of DFT are needed at this point to connect TF and TFvW to modern advances. More details are in Section 2. The Hohenberg–Kohn existence theorems state that for a system of N_e electrons in an external potential $v_{ext}(\mathbf{r})$, there exists a functional of the density $\mathcal{E}[n]$ that gives the total ground-state energy E_0 variationally by

$$
\begin{aligned}
E_0[n_0] &= \min_n\{\mathcal{E}[n] + E_{ext}[n]\} \\
\mathcal{E}[n] &:= T[n] + U_{ee}[n]
\end{aligned}
\tag{9}
$$

Here $T[n]$ is the *total* many-electron kinetic energy, U_{ee} is the *total* many-electron Coulomb interaction energy (Hartree, exchange, and correlation), and n_0 is the ground-state electron density. To make connection with the non-interacting electron concept of the TF and TFvW schemes, we insert the non-interacting kinetic energy (denoted, for reasons lost in history, as $T_s[n]$) and make a trivial addition and subtraction rearrangement

$$
\mathcal{E}[n] = T_s[n] + \{U_{ee}[n] + T[n] - T_s[n]\} \tag{10}
$$

https://doi.org/10.1021/acs.chemrev.2c00758
Chem. Rev. 2023, 123, 12039−12104

Structurally, this is the same as TFD or TFvWD: a noninteracting kinetic energy and some Coulombic (and other) corrections, all density functionals. Obviously the formal grounding and content are very different. The HK theorems prove that the TFvW, TFvWD concept is correct, even though the functionals themselves are not.

Because one-electron states ("Kohn–Sham orbitals") commonly are introduced to make the DFT variational problem tractable by giving an explicit, calculable form for T_s, we emphasize that the form just given is "orbital-free", OFDFT. (Remark: Shortly it will be apparent that "one orbital" would be more precise, in the same spirit as our summary of TFvW, eq 3 above. But by now "orbital-free" is standard.) The crucial distinction is that KSDFT[1] in the conventional orbital form has become the pre-eminent many-electron formulation for calculations on materials and their molecular constituents. Annual citation counts in the thousands in both quantum chemistry and materials physics[131] attest to this point, as does the 1998 Nobel Prize in Chemistry. It was shared by Walter Kohn, for DFT itself,[132] and John Pople for quantum chemical methods.[133] Conventional KSDFT with semilocal approximate XC functionals can produce remarkably accurate and useful results, despite known drawbacks.[2]

The dominant position of conventional KSDFT means that overcoming computational scaling barriers while simultaneously building more accurate XC density functional approximations (DFAs) are two critically important tasks. The KS orbitals put these two in tension. Interestingly, Pople was a late convert to DFT who focused on the explicit use of the KS orbitals in XC DFAs.[134] Conversion of the majority chemistry community soon occurred,[135] followed by a proliferation of orbital-dependent exchange-correlation DFAs. From the perspective of computational cost scaling, that proliferation is a retrograde step. Though introduction of the KS orbitals[1] was crucial because it meant that early band structure and molecular orbital codes could be adapted quite readily to DFT, the unintended consequence was the $O(N^3)$ cost scaling noted at the outset.

We fill out needed details of conventional and OFDFT forms of KSDFT in Section 2. Also there we catalog relevant exact properties of $T_s[n]$. For perspective, however, suppose again, for the moment, that one could construct all the terms in U_{ee} (the familiar challenge of XC DFAs). The remaining challenge would be to construct reliable, orbital-free approximations for $T_s[n]$ (KEDFs). That is the subject at hand. The remainder of this section is both a brief guide to the kinds of approximations that have been contrived as well as a guide to the subsequent sections of this review.

Both TF and TvW are what are called one-point functionals. Their origins in the HEG and inhomogeneity, respectively, suggest the generic form

$$T_{s,1}[n] = c_{TF}\int d\mathbf{r} n^{5/3}(\mathbf{r}) F_t(n(\mathbf{r}), \nabla n(\mathbf{r}), \nabla^2 n(\mathbf{r}), ...) \tag{11}$$

TF ($F_t = 1$) is strictly local. Adding spatial derivative dependence is said to make a functional "semi-local". The sense of that phrase is that while the mathematics is strictly local (one-point), the derivative dependence provides some indication of nearby density behavior. (Remark: We caution that some of the older DFT literature uses "non-local" rather than "semi-local" to describe gradient dependence. Mathematically it is strictly local.) KEDFs in which F_t depends only on n and ∇n are called generalized gradient approximations (GGAs or also GEAs if the Kirzhnitz gradient expansion approximation[31] is adopted; see eq 8) in correspondence with terminology already established for XC DFAs with the same dependencies. Those that depend upon $\nabla^2 n$ and higher order derivatives as well as n and ∇n are called "meta-GGAs". As the names imply, development of these KEDFs is influenced strongly by the gradient expansion for the weakly inhomogeneous electron gas.[117,125,136−139]

Nonlocal functionals go back to Hohenberg and Kohn,[3] who proposed a solution to the inability of TF and TFvW to describe quantum oscillations by employing the Lindhard response function[140] for the HEG as an approximation to the electronic dielectric function. This function gives the response of the electrons at an arbitrary point to the introduction of a charge at some other point. Somewhat later, this line of thinking gave rise to investigation of nonlocal KEDFs. Most generally they would have the form

$$T_s^{\mathrm{nl}}[n] = \int d\mathbf{r}_1 d\mathbf{r}_2 d\mathbf{r}_3 ... d\mathbf{r}_m n^{5/3m}(\mathbf{r}_1) n^{5/3m}(\mathbf{r}_2) n^{5/3m}(\mathbf{r}_3) \times ... n^{5/3m}(\mathbf{r}_m)\omega[n](\mathbf{r}_1, \mathbf{r}_2, \mathbf{r}_3, ... \mathbf{r}_m) \tag{12}$$

where $\omega(\mathbf{r}_1...\mathbf{r}_m)$ is an m-body kernel to be determined. This form appears in the original Hohenberg–Kohn paper[3] as a formal expansion of the exact density functional. After a brief discussion of the two-body term, they dismiss the rest: "The higher order terms will not be further discussed here." In that same vein, so far as we are aware, the form has not been used for $m > 3$ and only once for $m = 3$.[44] In that case, the three-point structure was induced by a tour de force perturbation approach that strongly resembles the iterative form of the Dyson equation[141] for the two-particle Green function.

Since the two-particle reduced density matrix (2-rdm) determines all the ground-state properties of a Coulombic fermion system,[142] it similarly is appropriate to focus efforts at direct (nonperturbative) construction of KEDFs upon the two-point case. For reasons of physical clarity and constraint satisfaction (see Section 2), it is convenient to write two-point KEDFs in the generic form

$$T_{s,2}[n] = T_{vW}[n] + T_{TF}[n] + \int d\mathbf{r} d\mathbf{r}' \mathcal{K}[n(\mathbf{r}), n(\mathbf{r}'); \mathbf{r}, \mathbf{r}'] \tag{13}$$

[Remark: For simplicity, here we introduce nonlocal functionals through eq 13. We acknowledge that there are other formulations that preserve the structure of the T_{TF} functional (e.g., the Chacón–Alvarellos–Tarazona (CAT) family of functionals[43,143]) and the structure of the T_{vW} functional (e.g., ref 144). These functionals are well-reviewed in refs 145 and 146. See further discussion in Section 2.] This form incorporates the exactness of T_{TF} in the uniform limit and of T_{vW} in the one-electron or two-electron singlet limit (see Section 2). The explicitly nonlocal contribution then is a sophisticated interpolation between those two extreme cases. Typically it has the structure of a density-weighted kernel

$$\mathcal{K}[n(\mathbf{r}), n(\mathbf{r}'), \mathbf{r}, \mathbf{r}'] = n^{\alpha}(\mathbf{r})\omega[n](\mathbf{r}, \mathbf{r}')n^{\beta}(\mathbf{r}') \tag{14}$$

with α and β constants. Even though eq 13 is formally an approximation, it can be made exact (as can be seen by integration of eq 12 of all coordinates except two) using the general form of the kernel given on the rhs of eq 14. In practice, the kernel is determined, for example, by calibration

https://doi.org/10.1021/acs.chemrev.2c00758
Chem. Rev. 2023, 123, 12039−12104

to linear response of the HEG (Lindhard response)[105] and the resulting KEDF is approximate. We return to this in detail below.

Two-point KEDFs generally are expected to be more accurate than one-point KEDFs simply because the two-pointers probe and encode information about a larger spatial region than is possible with one-point functionals. Figure 3

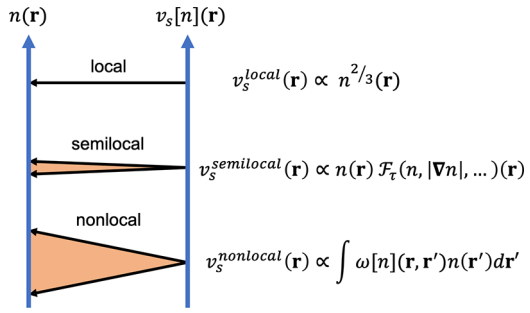

Figure 3. Conceptual depiction of the dependence on the electron density of local, semilocal, and two-point functionals. The corresponding potentials are depicted in the figure. Nonlocal or two-point functionals of $n(\mathbf{r})$ depend on an arbitrary neighborhood of $\mathbf{r}$ whereas semilocal functionals only sample infinitesimally nearby and local functionals sample the single point, $\mathbf{r}$.

provides a simple pictorial comparison. That is, from local one-point, to semilocal one-point (GGA, metaGGA, ...), to two-point functionals, the kinetic energy potential, defined as $v_s(\mathbf{r}) = \frac{\delta T_s[n]}{\delta n(\mathbf{r})}$, is informed by a larger and larger neighborhood of the spatial point $\mathbf{r}$. TF and TFvW are extreme examples of awareness of only the point $\mathbf{r}$. Their forms are inadequate for diverse reasons which will be discussed in Section 2. Note, however, that the curse of computational scaling intrudes because two-point KEDFs depend on the density−density response function of the system; see Sections 2 and 3.

Machine-learnt (ML) KEDFs are the most recent type. They are discussed in Subsection 2.5. Because their explicit form typically is not known, they do not fit easily into the one-point, two-point categorization, though some are built specifically to have a certain maximum order of density gradients. Just as machine learning itself is relatively recent, so also the literature of ML KEDFs is comparatively recent and small.[83,84,147−160]

The imperative for access to the full periodic table with high-quality KEDFs also has motivated efforts such as angular momentum-dependent[161] and projector augmented wave (PAW) implementations[120] of OFDFT. We discuss those briefly at the end of Section 2, along with information-theoretical and other KE approaches. We conclude Section 2 with a brief discussion of some pitfalls of KEDF testing.

Implementation, algorithms, and associated issues are the subject of Section 3. For two-point functionals, implementation is simplified greatly by the employment of regular grids at any reasonable spacing, reciprocal space methods, and Fast Fourier Transforms (FFTs).[53,55] FFT grids also can be used to encode one-point KEDFs, including free-energy versions.[162] Irrespective of KEDF type, however, regular grids are unable to resolve the singular Coulomb potentials originating from point nuclear charges. Thus, several pseudopotentials have been developed.[48,163−165] Those are, of necessity, local in the sense of pseudopotential terminology, that is, orbital-independent. This issue is crucial for expanded applicability of OFDFT, whatever the type of KEDF. We address it in Subsection 3.1.

In Section 4, we discuss a nonexhaustive selection of illustrative applications. Here we simply note that recent applications with one- and two-point KEDFs include warm dense matter[166−168] and molten and zero-temperature metals and semiconductors (bulk,[86,169−172] surfaces and other low-dimensional systems,[173] and clusters[88,126,174]).

We conclude this section with a note on computational scaling of OFDFT versus conventional KSDFT. It is critical to remember that both use the KS decomposition, eq 10, to invoke a specific non-interacting reference system that generates the density. Conventional KSDFT uses the explicit kinetic energy expression for that system, $T_s[\{\varphi_i[n]\}]$, in terms of the N_e orbitals in the KS determinant, $\varphi_i[n](\mathbf{r})$. Obtaining those orthogonal orbitals when using semilocal XC functionals requires a formal $O(N_e^3)$ computational cost (from diagonalizing the KS Hamiltonian matrix) and a $O(N_e^2)$ memory requirement (from storing the wave functions and matrices involved). Therefore, several approaches attempt to evade the cubic scaling of standard implementations of conventional KSDFT by avoiding the diagonalization of the KS Hamiltonian and leveraging sparsity in a variety of different ways.

Other than OFDFT, several propositions have been put forth for achieving sub-cubic scaling (i.e., $O(N_e)$ or $O(N_e^2)$) of

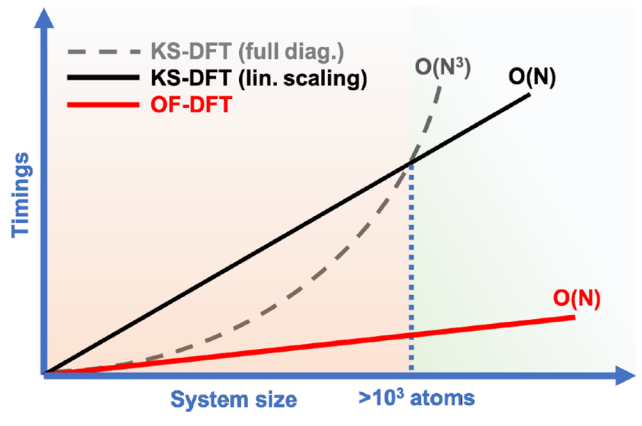

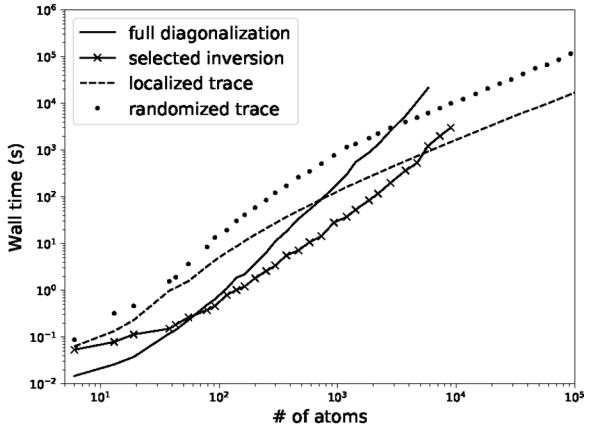

Figure 4. Estimation of the computational scaling of OFDFT (left panel) and conventional KSDFT (right panel) employing both cubic-scaling diagonalization and different sub-cubic-scaling approaches. Conventional KSDFT data from Moussa and Baczewski 2019.[17]

https://doi.org/10.1021/acs.chemrev.2c00758
Chem. Rev. 2023, 123, 12039−12104

conventional KSDFT by combining algorithmic advances with efficient utilization of modern high-performance computer architectures.[10,11,13,17,175−183] Underlying all such schemes, however, is exploitation of nearsightedness in the electronic structure[184−186] to achieve sparse matrices (e.g., by screening certain one- and two-electron integrals or by effective cutoffs applied to the off-diagonal elements of the one-body reduced density matrix, 1-rdm), coupled with efficient solutions to the Poisson equation.

Sub-cubic-scaling approaches to conventional KSDFT are dependent on temperature and on the energy gap of the material. For example, for systems with gap, the 1-rdm decays exponentially, thus sub-cubic-scaling methods are very effective for these systems. Instead, for metals at zero and low temperatures, the 1-rdm decays slowly (algebraically, see eqs 117−119). Thus, sub-cubic-scaling methods are less effective in this regime. However, because at higher temperature the density matrix of metals decays exponentially,[187,188] methods exploiting the sparsity properties of the 1-rdm can be useful and applicable also to metals.

We give an example of the performance of sub-cubic-scaling methods on the right-hand side of Figure 4, where we reproduce data from ref 17. On the left-hand side of the figure, we depict the expected timings for OFDFT compared with linear-scaling KSDFT and its straightforward implementations. The figure shows that both OFDFT and linear-scaling KSDFT are expected to yield linear timings with system size but with very different prefactors.

Given the advantages of OFDFT, the patient reader rightly may ask why it has not supplanted conventional KSDFT. The answer is that, until recently, adequately accurate KEDFs have not been constructed. As we show below, that situation is changing, we believe, rapidly. It is the purpose of this review to report that progress and outlook for achieving the promise of OFDFT in chemical and materials modeling. Additionally, recent years have witnessed the emergence of several schemes that combine conventional KSDFT and OFDFT. Subsystem DFT[180,181,189−191] is one such scheme that is proving to be promising for several classes of systems.

For context, we note several prior OFDFT reviews (in addition to the Thomas−Fermi literature already cited): refs 115, 145, and 192−194 and a book.[195] A convenient listing of one-point KEDFs is in Chapter 16 of that book. Also see the University of Florida online listing.[196] To have some control on the scope of this article, we do not review free-energy (finite temperature) OFDFT except for a bit on successful computational use.[168] For that topic, see refs 194 and 197. Nor do we consider time-dependent OFDFT[198−209] or OFDFT on a lattice.[210]

2. KINETIC ENERGY FUNCTIONALS

This section sets forth DFT in pertinent form, with emphasis on known constraints, limits, and conditions relevant to constructing approximate KEDFs. Then we survey the specific approximations of various kinds (one-point, two-point, machine-learnt) and some of their strong and weak points. There follow some observations on testing, followed by a survey of various "road-less-taken" approaches to recognize angular momentum dependence, apply information theory, and convert to potential functional theory. We conclude the section with a look at OFDFT in the context of embedding schemes (subsystem DFT).

2.1. DFT Basics

For clarity about kinetic energy contributions and notation, we summarize the basic Hohenberg−Kohn (HK) DFT theorems[3] and the KS construction[1] for spin-unpolarized systems. Details are in refs 102, 106, and 211. Nonrelativistic spin-polarization follows easily.[212] For simplicity of presentation and notation therefore, the presentation is spin-unpolarized unless remarked to the contrary. Though DFT is general, chemical and materials interest is in the electronic structure. To that we specialize.

The Hamiltonian for N_e electrons in a fixed external field $v_{ext}(\mathbf{r})$ is

$$\hat{H} := \sum_i^{N_e} \left[-\frac{1}{2}\nabla_i^2 + v_{ext}(\mathbf{r}_i) \right] + \frac{1}{2} \sum_{i \neq j}^{N_e} \frac{1}{|\mathbf{r}_i - \mathbf{r}_j|} \tag{15}$$

in Hartree atomic units. For much of chemistry and materials physics, $v_{ext}(\mathbf{r})$ is the Coulomb potential of a fixed array of nuclei; hence

$$E_{ext}[n] = \int d\mathbf{r} n(\mathbf{r}) v_{ext}(\mathbf{r}) \equiv -\sum_\alpha Z_\alpha \int d\mathbf{r} \frac{n(\mathbf{r})}{|\mathbf{r} - \mathbf{R}_\alpha|} \tag{16}$$

with nuclear charges Z_α and positions $\mathbf{R}_\alpha$. (Remark: Harmonic confinement potentials also have been useful for studying approximate functionals. See for example refs 213−221, among others.)

As already noted at eq 9, the HK theorems prove the existence and key properties of a functional of the electron number density $n(\mathbf{r})$,

$$\mathcal{E}[n] = T[n] + U_{ee}[n] \tag{17}$$

Recall, from Section 1, that $T[n]$ and $U_{ee}[n]$ are the *total* many-electron kinetic energy (KE) and Coulomb interaction energy, respectively. The number density integrates to the total electron number

$$\int d\mathbf{r} n(\mathbf{r}) = N_e \tag{18}$$

Because $\mathcal{E}[n]$ is independent of the external potential $v_{ext}(\mathbf{r})$, the functional is said to be "universal". The Rayleigh−Ritz variational principle gives the ground-state energy E_0 and density n_0 as

$$\min_n \{\mathcal{E}[n] + E_{ext}[n]\} = E_0[n_0] \tag{19}$$

(Remark: A mathematically careful description of the minimization involves differently defined functionals and their extrema. Formally there are three functionals, with different variational properties and different functional derivatives. For most chemistry and physics applications, the subtle mathematical differences among them do not matter enough to be distracted by them here. In this we follow the precedent of Engel and Dreizler,[106] p 36: "As a matter of principle, the subsequent development of the DFT formalism should therefore be based explicitly on the Lieb functional. We will nevertheless ignore the issue...and not distinguish between the various flavors...".)

The HK theorems prove the existence of $\mathcal{E}[n]$ but do not supply an explicit constructive route to it. That fact motivates the connection to non-interacting systems already sketched in Section 1 at eq 10. The connection is made via the insight of Kohn and Sham,[1] namely that the HK theorems apply equally well to non-interacting systems.[106,222] Thus, for most physical

https://doi.org/10.1021/acs.chemrev.2c00758
Chem. Rev. 2023, 123, 12039−12104

systems, it is possible to invoke a special one-electron potential, the Kohn–Sham potential $v_{KS}(\mathbf{r})$, that causes a non-interacting electron system to have exactly the same electron density as the interacting physical system. Those systems for which $v_{KS}(\mathbf{r})$ exists are designated as non-interacting v-representable or simply v_{KS}-representable.[106]

Because the KS system is a non-interacting many-electron system, its variational wave function is a single determinant with orbitals generated by[1]

$$\hat{h}_s[n]\varphi_i(\mathbf{r}) = \varepsilon_i\varphi_i(\mathbf{r}) \tag{20}$$

$$\hat{h}_s[n](\mathbf{r}) := -\frac{1}{2}\nabla^2 + v_{KS}(\mathbf{r}) \rightarrow \hat{H}_s = \sum_i^{N_e} \hat{h}_s(\mathbf{r}_i) \tag{21}$$

$$n(\mathbf{r}) = \sum_i f_i|\varphi_i(\mathbf{r})|^2 \tag{22}$$

where $\hat{H}_s$ is the many-Fermion KS Hamiltonian. At zero temperature the occupation numbers f_i ordinarily are integers (0, 1, or 2). An exception is the case in which the highest occupied level is degenerate.[211,223] For fixed density, $n(\mathbf{r})$, the minimization of the KS energy (i.e., $E_{KS} = \langle\Phi|\hat{H}_s|\Phi\rangle$) is with respect to all single-determinant wave functions, $\Phi(\mathbf{r}_1...\mathbf{r}_{N_e})$, that give $n(\mathbf{r}) = \langle\Phi|\hat{n}(\mathbf{r})|\Phi\rangle$, with $\hat{n}(\mathbf{r}) = \sum_i^{N_e}\delta(\mathbf{r}_i - \mathbf{r})$. The minimizing one that yields the ground-state density $n_0(\mathbf{r})$ is the KS determinant $\Phi_{KS}(\mathbf{r}_1...\mathbf{r}_{N_e})$. Note that the minimization is solely that of the KE expectation value, since the KE is the only many-body operator in the non-interacting Hamiltonian and the density is fixed.

The KS determinant therefore gives an explicit expression for the non-interacting kinetic energy $T_s[\{\varphi_i[n]\}]$:

$$T_s[\{\varphi_i[n]\}] := \frac{1}{2}\sum_i f_i \int d\mathbf{r}|\nabla\varphi_i[n](\mathbf{r})|^2 \equiv \int d\mathbf{r}\tau_s[n(\mathbf{r})] \equiv T_s[n] \tag{23}$$

This object is the center of attention in OFDFT. (Remark: Notice that we use the positive definite form of the KS KE integrand, not the more commonly encountered $T_s[n] = -\frac{1}{2}\sum_i f_i \int d\mathbf{r}\varphi_i^*(\mathbf{r})\nabla^2\varphi_i(\mathbf{r})$. The two differ by a surface term that integrates to zero in virtually all cases.)

The KS determinant also *defines* the DFT exchange energy $E_x[n]$ (for spin unpolarized systems):

$$E_x[n] := -\frac{1}{4}\sum_{i,j} f_i f_j \times \int d\mathbf{r}_1 d\mathbf{r}_2 \frac{\varphi_i^*[n](\mathbf{r}_1)\varphi_j^*[n](\mathbf{r}_2)\varphi_i[n](\mathbf{r}_2)\varphi_j[n](\mathbf{r}_1)}{|\mathbf{r}_1 - \mathbf{r}_2|} \tag{24}$$

It also is a density functional via the fact that the KS orbitals are density functionals.

The remaining step is to connect the physical and KS systems explicitly. In the expression for the total energy of the physical system, it is conventional to identify the classical Coulomb repulsion contribution (the Hartree energy) to the total Coulomb energy

$$E_H[n] := \frac{1}{2}\int d\mathbf{r}_1 d\mathbf{r}_2 \frac{n(\mathbf{r}_1)n(\mathbf{r}_2)}{|\mathbf{r}_1 - \mathbf{r}_2|} \tag{25}$$

The universal density functional eq 17 for the physical system then can be rearranged to expose the non-interacting and classical pieces as

$$\mathcal{E}[n] = T_s[n] + E_H[n] + E_x[n] + \{U_{ee}[n] - E_H[n] - E_x[n] + T[n] - T_s[n]\} \tag{26}$$

$$:= T_s[n] + E_H[n] + E_x[n] + E_c[n] \tag{27}$$

This equation is the KS version of eq 10. The last term in eq 27 *defines* the KSDFT correlation energy as the sum of the final five terms of eq 26. In particular, the difference $T[n] - T_s[n]$ is lumped into E_c along with the Coulomb correlation. Though exchange and correlation are defined separately, they can be obtained (formally and operationally) together via the adiabatic connection.[212,224] It also is common to develop an approximate exchange functional paired with an approximate correlation functional in order to achieve useful cancellation. See, for one much-used example, the PBE approximation.[225] Sometimes exchange and correlation are approximated together in nonseparable form $E_{xc} = E_x + E_c$.[226]

Regardless of whether the functionals are expressed in terms of the KS orbitals or directly in terms of $n(\mathbf{r})$, the variational minimization of $\mathcal{E}[n]$ must be done over electron densities that integrate to N_e. That is equivalent to minimizing the Lagrangian

$$\mathcal{L}[n] = \mathcal{E}[n] + \int d\mathbf{r}n(\mathbf{r})v_{ext}(\mathbf{r}) - \mu\left[\int d\mathbf{r}n(\mathbf{r}) - N_e\right] \tag{28}$$

The Euler–Lagrange equation follows after taking the functional derivative with respect $n(\mathbf{r})$ and requiring that it be null at all $\mathbf{r}$, namely,

$$\frac{\delta T_s[n]}{\delta n(\mathbf{r})} + \frac{\delta E_H[n]}{\delta n(\mathbf{r})} + \frac{\delta E_{xc}[n]}{\delta n(\mathbf{r})} + v_{ext}(\mathbf{r}) \equiv \frac{\delta T_s[n]}{\delta n(\mathbf{r})} + v_{KS}(\mathbf{r}) = \mu \tag{29}$$

Here μ is the electron chemical potential. The last equality comes from the fact that the physical and KS systems have the same chemical potential. That always holds because the potential v_{KS} is determined only up to a constant.

Thus the Kohn–Sham potential in eq 21 is

$$v_{KS}(\mathbf{r}) = v_H(\mathbf{r}) + v_{xc}(\mathbf{r}) + v_{ext}(\mathbf{r})$$
$$v_H(\mathbf{r}) = \int d\mathbf{r}_2 \frac{n(\mathbf{r}_2)}{|\mathbf{r} - \mathbf{r}_2|}, \quad v_{xc}(\mathbf{r}) = \frac{\delta E_{xc}[n]}{\delta n(\mathbf{r})} \tag{30}$$

For a fixed set of nuclei (ions, e.g. at each step in ab initio molecular dynamics, AIMD[227−229]), v_{ext} is as in eq 16 and the electronic force on a given nucleus α is $-\nabla_{\mathbf{R}_\alpha}(\mathcal{E}[n_0] + E_{ext}[n_0] + E_{NN})$. Here $E_{NN}(\{\mathbf{R}\})$ is the internuclear (ion–ion) repulsion energy.

2.2. DFT Context Issues

Before proceeding, some context regarding present-day use of DFT, particularly in chemistry, is relevant. The vast majority of applications use conventional KSDFT, hence $T_s[n]$ in its explicitly orbital-dependent form, eq 23. The only approximate functionals of interest in that case are $E_{xc}[n] = E_x[n] + E_c[n]$. That is why much of the DFT literature uses the phrase

https://doi.org/10.1021/acs.chemrev.2c00758
Chem. Rev. 2023, 123, 12039−12104

"density functional approximations" to mean XC approximations.

In contrast, OFDFT focuses on approximate expressions for $T_s[n]$ that do *not* rely on explicit evaluation of the orbital-dependent expression, $T_s[\{\varphi_i[n]\}]$, in eq 23. A consequence is clear. *If* OFDFT is to grow in utility, there must be sustained, concurrent development of improved orbital-free E_{xc} DFAs. Present-day materials physics practice and priorities illustrate the point. In that arena, the GGA rung of the Perdew–Schmidt[230] ladder of XC DFA complexity dominates, with the PBE[225] functional most widely used. A GGA XC functional has the generic, orbital-free form

$$E_{xc}^{GGA}[n] = \int d\mathbf{r} e_{xc}[n(\mathbf{r}), s] \tag{31}$$

where $e_{xc}[n(\mathbf{r}), s]$ is an XC energy density, the details of which are irrelevant here, except that it depends on both n and the dimensionless reduced density gradient

$$s(\mathbf{r}) := \frac{|\nabla n(\mathbf{r})|}{(3\pi^2)^{1/3} n^{4/3}(\mathbf{r})} \tag{32}$$

(Remark: Beware! In the chemistry literature for XC DFAs it is fairly common to define this variable *without* the constants. Occasionally that form shows up in the OFDFT literature as well.)

The contextual challenge that we do *not* address in this review is the explicit use of KS orbitals in $E_{xc}[n]$ approximations that are on higher rungs of the Perdew–Schmidt complexity ladder than GGAs. In the case of meta-GGA XC functionals, for example, explicit orbital dependence enters via the KS KE density $\tau_s[n(\mathbf{r})]$ as an ingredient. Recent popular examples include the SCAN $E_{xc}[n]$ DFA[231] and its successor, r^{2}SCAN.[232] With certain exceptions, those two are broadly applicable to both molecules and extended systems. Some progress has been made in removing the $\tau_s[n(\mathbf{r})]$ dependence from both SCAN and r^{2}SCAN.[233−235] In stark contrast, the quantum chemistry community has sought accuracy improvements largely by moving to yet higher rungs on the Perdew–Schmidt ladder, specifically with hybrid E_{xc} DFAs, i.e. those that include a single-determinant exchange, eq 24, contribution.

Recall our earlier remark about Pople's coming to DFT via interest in a hybrid XC functional. Inclusion of some single-determinant exchange introduces explicit orbital dependence in $E_{xc}[n]$. That orbital dependency seems to be completely at odds with the OFDFT objective of eliminating such dependence from $T_s[n]$. Conceptually the use of orbital-dependent E_{xc} DFAs poses no issues in conventional KSDFT, as the optimized effective potential (OEP) procedure[236,237] can be used to retrieve the multiplicative KS potential. In practice, however, OEP requires considerable extra computation, so it is little used with orbital-dependent XC DFAs. The generalized KS Euler equation is used instead (i.e., in a short-hand notation, replacing $\frac{\delta E_{xc}}{\delta n}\frac{\delta n}{\delta \phi_i}$ by $\frac{\delta E_{xc}}{\delta \phi_i}$). Observe that the KS and generalized KS equations are not equivalent.[238,239] Anyway, OEP is irrelevant here except to illustrate the potential payoff of OFDFT in an almost sardonic way. Because there is no orbital manifold in OFDFT, there is no generalized KS equation and, hence, no need for the elaborate machinery of OEP.

The irony of emphasis on orbital-dependent XC DFAs not withstanding, from here forward we assume that the $E_{xc}[n]$ DFA is orbital-free. The OFDFT task then is to eliminate the explicit orbital dependence of $T_s[n]$ by constructing approximations to it that depend purely on the electron density, n.

Note also that the kinetic energy approximations discussed here are for $T_s[n]$, not for $T[n]$. Formally the focus upon $T_s[n]$ is to exploit the power of the KS logic of connection to non-interacting systems. Doing so avoids the formidable problem that an attempt to approximate $T[n]$ would amount to an attempt to approximate the entire $\mathcal{E}[n]$ by virtue of the Coulomb virial theorem. (This argument is not original; it was pointed out to SBT by So Hirata in a University of Florida seminar.) Practically, the reason for addressing $T_s[n]$ is that modern $E_{xc}[n]$ DFAs all have been developed in the KS context, i.e., the decomposition in eq 27.

With both $T_s[n]$ and $E_{xc}[n]$ approximations orbital-free, the constrained minimization can be carried out directly via the single variational quantity $n(\mathbf{r})$. See eq 29. This is the justification of the remark at the outset of Section 1 that OFDFT restores the centrality of the density in DFT.

2.3. Constraints

Because there are no mechanical procedures (e.g., order-by-order perturbation expansion) provided by the basic DFT theorems to develop approximate KEDFs, it is important to catalog provable properties of the exact functional $T_s[n]$. Such rigorous results are useful as constraints on KEDF development. An example is the concise list of constraints in ref 240.

The simplest relation is between the full KE $T[n]$ and the non-interacting $T_s[n]$. Because $T_s[n]$ is defined to be the minimum fermion expectation value of the many-fermion KE operator for specified n (recall above), it follows that

$$T_s[n] \le T[n] \tag{33}$$

Constraints often are expressed in terms of $T_{TF}[n]$,[22,23,241] eq 2, and $T_{vW}[n]$,[27] eq 6. Though $T_{TF}[n]$ does not support bound systems (recall Section 1 and ref 39), its simplicity and its exactness for the HEG have made it popular as a plausible initial approximation against which to make corrections. From the perspective of rigorous constraints, that is not, however, the optimal approach. The reason is clear from consideration of $T_{vW}[n]$. It is exact for a fermion system of one orbital (one electron or two electrons in a singlet state). Therefore, $T_{TF}[n]$ is simply wrong for the H atom and for the density associated with the tail region of any isolated molecule or atom.

$T_{vW}[n]$ also is exact for the ground state of any many-boson system, which leads to the observation that fermion anti-symmetrization must raise the non-interacting KE over the corresponding bosonic case; hence

$$T_{vW}[n] \le T_s[n] \tag{34}$$

This lower bound can be proven simply.[242−245] We return to the point in the discussion of information-theoretic KEDFs below.

The T_{vW} lower-bound property motivates the so-called Pauli-term decomposition

$$T_s[n] = T_{vW}[n] + T_\theta[n], \qquad T_\theta[n] \ge 0 \tag{35}$$

as a route to approximate KE functionals. The rigorous non-negativity[246−249] of $T_\theta[n]$ is a powerful constraint on any approximate KEDF, either one- or two-point. Moreover, the functional derivative of $T_\theta[n]$ must be positive semidefinite[249]

https://doi.org/10.1021/acs.chemrev.2c00758
Chem. Rev. 2023, 123, 12039−12104

$$v_\theta(\mathbf{r}) := \frac{\delta T_\theta[n]}{\delta n(\mathbf{r})} \geq 0, \qquad \forall\, \mathbf{r} \tag{36}$$

Because this is a pointwise requirement, it is a particularly stringent constraint on approximate KEDF development.

The Pauli term decomposition enables the rewriting of the DFT Euler−Lagrange equation (eq 29) in a particularly useful way. Substitution of (35) in (29) and recognition that

$$\frac{\delta T_{vW}[n]}{\delta n(\mathbf{r})} = -\frac{1}{2} n^{-1/2}(\mathbf{r}) \nabla^2 n^{1/2}(\mathbf{r}) \tag{37}$$

gives

$$\left\{ -\frac{1}{2}\nabla^2 + v_{KS}(\mathbf{r}) + v_\theta(\mathbf{r}) \right\} n^{1/2}(\mathbf{r}) = \mu n^{1/2}(\mathbf{r}) \tag{38}$$

This one-orbital expression is the OFDFT Kohn−Sham equation. It differs from the conventional KS equation (eq 22) by only a local potential, an advantage unattainable if one were to start from TF and add corrections.

A third, closely related constraint comes into play, namely

$$v_\theta(\mathbf{r}) \geq \frac{\tau_\theta(\mathbf{r})}{n(\mathbf{r})}, \qquad \forall\, \mathbf{r} \tag{39}$$

$$\tau_\theta := \tau_s - \tau_{vW} \tag{40}$$

In this expression, the pointwise positive semi-definiteness of the Pauli term, $\tau_\theta \geq 0$ everywhere makes the constraint on v_θ more stringent than the constraint of its basic semi-definiteness (eq 36).

A related constraint is on the limiting behavior of the Pauli energy density. In terms of the dimensionless reduced density gradient s, eq 32, the constraint is

$$\lim_{s\to\infty} \tau_\theta = 0 \tag{41}$$

This requirement arises from the fact that the density tail of an isolated many-electron atom is dominated by a single orbital that decays exponentially; hence, $s \to \infty$. For a single-orbital system, the von Weizsäcker functional is exact and eq 41 follows.

An upper-bound constraint to T_s that has been conjectured but apparently never proved[250,251] also is useful. It is

$$T_s[n] \leq T_{TF}[n] + T_{vW}[n] \tag{42}$$

This inequality can be rationalized[252] by taking the $N_e \to\infty$ limit of the finite-system inequality due to Gázquez and Robles.[36] Note, however, that their inequality involves a local density approximation and hence is not an exact result. Violations of eq 42 have been discussed recently.[253]

Uniform density scaling[254] is a property that any proper KEDF must have. For the scaled density $n_\lambda(\mathbf{r}) := \lambda^3 n(\lambda\mathbf{r})$ with λ a real, positive constant, the KS KE satisfies

$$T_s[n_\lambda] = \lambda^2 T_s[n] \tag{43}$$

The TF KE satisfies the scaling relation, which motivates the formulation of other KEDFs in terms of dimensionless factors multiplying τ_{TF}. A remarkably early example, prior to the well-known ref 254, is the explicit discussion of uniform density scaling in a KEDF by Alonso and Girifalco.[255] Somewhat after ref 254, there is mention of this scaling in ref 44 in the context of the second kind of kernel they proposed (see their eq 3.39).

A different kind of constraint is associated with the large-Z limit of the neutral atom energy.[256] (Z is the atomic number; recall eq 16). Asymptotically in Z, the KS KE has the expansion

$$T_s = b_0 Z^{7/3} + b_1 Z^2 + b_2 Z^{5/3} + \ldots \tag{44}$$

with $b_0 = 0.768745$, $b_1 = -1/2$, and $b_2 = 0.269900$. Reference 256 gives a procedure by which to extract the asymptotic behavior of a given candidate KEDF from atomic calculations. Comparison with the exact coefficients then provides a route to evaluate or refine the parameters in the candidate KEDF.

An important condition that often is ignored is the N-representability of a KEDF. Regarding N-representability, it is helpful to start with the density itself. The definition of what qualifies as a density[257] is any smooth, differentiable function $f(\mathbf{r}) > 0\ \forall \mathbf{r}$ (subject to boundary conditions) that integrates to N_e on the volume of interest and has finite von Weizäcker KE on that volume. All such candidate densities are themselves N-representable; that is, for each such candidate there is an N_e fermion wave function that yields the specified density.[244,258]

N-representability of functionals is a bit different. The concept is made precise in ref 259, theorem 4. It proves that if a KEDF delivers a KE below the conventional KSDFT value (obtained with the exact orbital-dependent T_s functional) for *any* system, that KEDF is not N-representable because there are no N-representable two-body density matrices (hence, no N_e fermion wave functions) that could yield that energy when traced with the Coulomb Hamiltonian plus v_{ext}.

The risk in use of a non-N-representable KEDF is that it can yield energies below, even grossly so, the correct conventional KSDFT value. Ayers and Liu point out,[259] for example, that T_{vW} is non-N-representable for electron densities integrating to 3 or more electrons because T_{vW} is a lower bound to T_s for those systems (recall above). Further, the TF plus scaled von Weizsäcker functional, TFλvW, eq 8, is non-N-representable for $\lambda < 1$. They illustrate with the ground-state electron density of the xenon atom. For $\lambda = 1/9$ the result is "...far below the true answer: $T_{TF}(1/9) = 7083$, ...$T_{accurate} = 7232$ hartree". Note also that, unhappily for developers of KEDFs, N-representability of a KEDF does not guarantee accuracy. An approximate KEDF could be N-representable simply by being a loose upper bound to T_s.

In contrast to that somewhat gloomy observation, we make two points. While it may not be straightforward to impose N-representability as a constraint in the course of constructing a KEDF, it is straightforward to test N-representability after the fact. Failures on simple systems should, at the least, be viewed as a warning. The other point is that constraints from N-representability have been developed for weighted-density approximation KEDFs based on model 1-rdms. See Chakraborty et al.[260,261] and the discussion below.

Useful constraints on KEDFs also can come from known properties of the densities associated with certain classes of v_{ext}. For v_{ext} from a set of point nuclei, the density is known to satisfy the Kato cusp condition[262] at each nuclear site. For GGA and meta-GGA KEDFs, that has immediate, specific consequences for the form of the KS potential, $v_{KS}(\mathbf{r})$.[249,263−267] Systems in which the physical (i.e., ionic) external potential has been replaced by a pseudopotential have, by construction, no cusp at each nuclear site but typically zero gradient instead. That has different consequences for KEDF construction.[86,265,268] Observe that exploiting these distinctions introduces non-universality, in the sense already mentioned. In principle, the density functional is indifferent to the v_{ext} and, hence, universal. In practice, an effective

https://doi.org/10.1021/acs.chemrev.2c00758
Chem. Rev. 2023, 123, 12039−12104

strategy is to design a KEDF particularized to a specific class of v_{ext}.

A less severe form of non-universality arises in another way. OFDFT calculations require the specification of both an approximation for T_s and an approximation for the XC functional E_{xc}. Another constraint ensues. Those two functionals are connected by the virial relationship[254]

$$T_s = \frac{1}{2}\int d\mathbf{r} n(\mathbf{r})\mathbf{r}\cdot\nabla v_{KS}(\mathbf{r}) \tag{45}$$

Here v_{KS} is the full KS potential, eq 30, which, of course, includes v_{xc}. The implication is that if v_{xc} is from an XC DFA, as virtually always is the case, then the KEDF to be used on the left-hand side should be constructed paired with that specific XC DFA. Otherwise, there is no guarantee that substitution of n_0 would satisfy that equation. One sees that pairing in the Kohn−Sham equation in fact. In it, up to a constant, the functional derivative of T_s evaluated at the equilibrium density n_0 is the negative of $v_{KS}[n_0]$. See also the related discussion in ref 269.

So far as we are aware, this pairing or matching requirement has been imposed strictly on KEDF development only once. The KEDF in ref 255 was developed from their XC approximation. A closely related, converse procedure, deorbitalization of a τ_s-dependent XC functional, was tried first by Perdew and Constantin[270] and pursued more thoroughly by Mejía-Rodríguez and Trickey,[233−235] but neither used the matching as a constraint.

There are several reasons for not using the virial form (but see below about potential functionals). The integrand on the right-hand side of eq 45 is not translationally invariant,[271] so one cannot identify the KE density τ_s with that integrand. For testing a candidate KEDF, the expression can be used directly with atoms (and probably should be). The invariance problem can be evaded via a translationally invariant KE density that integrates to the same value as the original translation-dependent form.[272] But a basic gauge problem remains. Anything that integrates to zero can be added to the integrand on the rhs of eq 45 without changing the functional relationship, so extraction of a KE density is ambiguous.[271,272]

2.4. Orbital-Free T_s Approximations

In Section 1, we distinguished the three main KEDF types of contemporary interest, semilocal or one-point functionals, $T_{s,1}[n]$, two-point functionals, $T_{s,2}[n]$, and machine-learnt, $T_{s,ML}[n]$. As noted just after eq 13, one-point functionals generically are

$$T_{s,1}[n] = \int d\mathbf{r}\tau_s[n(\mathbf{r}), \nabla n(\mathbf{r}), ...] \tag{46}$$

Recall from Section 1 that two-point functionals typically are written as interpolations between T_{TF} and T_{vW} in order to incorporate their exactness properties explicitly. Specifically,

$$T_{s,2}[n] = T_{vW}[n] + T_{TF}[n] + \int d\mathbf{r}d\mathbf{r}'\mathcal{K}[n(\mathbf{r}), n(\mathbf{r}'), \mathbf{r}, \mathbf{r}'] \tag{47}$$

with $\mathcal{K}$ as in eq 14 of Section 1.

Machine-learnt functionals may combine both one-point and two-point contributions in ways that are not expressible in simple analytical form. As such, they may have characteristics that are not easy to analyze in the context of the conventional one-point and two-point formulation.

We consider each type in turn. At the end of the section we consider briefly some other variants.

Before proceeding, a remark on "empirical" functionals is in order. In the development of XC DFAs, it is customary to designate functionals that have multiple parameters fitted to substantial databases (experimental or calculated data or both) as "empirical". In contrast, those DFAs that have parameters constrained by values calculated for small sets of atomic systems ("appropriate norms" per ref 231) are categorized as "nonempirical". We follow that terminology here. Akin with DFA development, however, the construction of a KEDF involves a considerable element of design choice. There simply are not enough known constraints to determine a KEDF completely, so building in desirable physics or conceding some nonuniversality or choosing from a range of allowed parameter values are choices the constructor must address. One might argue whether this genuinely is "nonempirical". We choose not to spend effort on that question and use the conceptual framework and vocabulary consistent with XC DFA development.

2.4.1. One-Point Functionals. Begin with an observation from experience. One-point $T_s[n]$ approximations in principle can depend upon $n(\mathbf{r})$ and all of its spatial derivatives, $\nabla n(\mathbf{r})$, $\nabla^2 n(\mathbf{r})$, ... In practice, the Euler equation that follows even from $\nabla^2 n(\mathbf{r})$ dependence is sufficiently complicated (fourth-order spatial derivatives) that there has been comparatively little consideration of a T_s approximation with higher than $\nabla^2 n$ dependence. Third-order spatial derivatives have been used in machine-learnt KEDFs,[83,150,152,153] as we discuss in Section 2.5. While the sixth-order gradient expansion has a fourth-order spatial derivative contribution,[139] the expansion is divergent.[136,139] Thus it is useless as a KEDF in itself. So far as we are aware, there have been no other candidate KEDFs with fourth-derivative dependence.

Recall from Section 1 that the implicit assumption in the one-point approach is that such functionals can probe nonlocal contributions adequately by selective exploitation of features of the gradient expansion. Because of the just-mentioned divergence, efforts began very early in DFT to formulate useful gradient contributions. Motivated by TFλvW eq 8 and a suggestion by Tomashima and Yonei,[116] Plumer and Stott[273] generalized the λ parameter to a density gradient dependence. A variation on the idea was put forth by Mazin in 1988[274] but in an obscure journal and, hence, was not known in the OFDFT community until posted recently to arXiv. The idea reappeared in ref 69, where the specific form used is attributed to Pearson's 1982 Ph.D. thesis. March and Santamaria[275] presented yet a different type of gradient dependence, based on reasoning from the KS 1-rdm and recognition that exact exchange in KSDFT has the same form as HF.

Neither of those two schemes seems to have been pursued further. Instead, the strategy followed was adapted from density-gradient-dependent XC DFAs.[57,276−278] Analogously with eq 31, generalized gradient approximation (GGA) KEDFs are constructed in the form

$$T_s^{\mathrm{GGA}}[n] = c_{TF}\int d\mathbf{r} n^{5/3}(\mathbf{r})F_\tau(s(\mathbf{r})) \tag{48}$$

$F_\tau(s)$, a function of the dimensionless reduced density gradient s introduced at eq 32, is the "enhancement factor" with respect to TF. It is dimensionless by construction so that the proper KE uniform scaling behavior (mentioned already[254]) provided by the Thomas−Fermi contribution is preserved. From eq 6, it

https://doi.org/10.1021/acs.chemrev.2c00758
Chem. Rev. 2023, 123, 12039−12104

follows that the von Weizsäcker KEDF written as a GGA has the enhancement factor $(5/3)s^2$ and the Pauli term for a GGA KEDF T_θ^{GGA} has

$$F_\theta(s) = F_\tau(s) - \frac{5}{3}s^2 \tag{49}$$

as its enhancement factor. The GGA Pauli KE thus is

$$T_\theta[n] := \int d\mathbf{r}\tau_\theta[n](\mathbf{r}), \qquad \tau_\theta = \tau_s - \frac{1}{8}\frac{|\nabla n|^2}{n} \tag{50}$$

The essence of GGA design strategy is to recover KE gradient expansion behavior for small s but modify it elsewhere so as to avoid the aforementioned[31,136,139] divergent behavior. (Remark: The expressions for the fourth- and sixth-order gradient expansion terms are complicated and not of particular use here. See ref 195.) Thus, the small-s behavior of F_θ should have the form

$$F_\theta = 1 - c_2 s^2 + O(s^4) \tag{51}$$

In the gradient expansion itself, the quadratic coefficient is $c_2 = 40/27 \approx 1.482$.[31]

One way to develop GGA KEDFs is via rational construction, e.g. Padé approximants calibrated against such gradient expansion terms.[61] Another is by extensive fitting[72] to atomic data. Yet another is to exploit the "conjointness conjecture"[58] to rationalize use of the enhancement factor from a GGA exchange functional, E_x^{GGA}, in a GGA KEDF. That allows more than three decades of work on GGA XC DFAs to be exploited. While known not to be correct (see, for example, ref 268 or consider the fact that a GGA exchange DFA cannot satisfy all known constraints on it), the conjecture is instructive and, in fact, it fueled development of the first few GGA KEDFs.[58,67,69,71]

However, none of those conjointness KEDFs would produce binding in test molecules even from post-SCF calculation with the correct conventional KSDFT densities[63] as input. (Here, "correct" is with respect, of course, to the XC DFA used.) The first GGA KEDFs that actually reproduced molecular binding from post-SCF calculation with KSDFT densities were the "modified conjoint" PBEn (n = 2, 3, 4) and exp4 functionals of Karasiev et al.[63,73] The modification with respect to strict conjointness consisted of enforcement of the Pauli term positivity constraint, eq 35. Those modified conjoint KEDFs were not, however, purely nonempirical but were parametrized on very small training sets (a few molecules).

Recently therefore, three strategies have characterized efforts to construct GGA KEDFs: (1) satisfy as many known exact constraints as possible, the approach used to contrive the VT84F,[85] LKT,[86] and RATIONAL[240] KEDFs; (2) devise an enhancement factor that yields as closely as possible the HEG linear response, the method used to obtain the PGint functional;[279] (3) reproduce known semiclassical expansions for neutral atoms, leading to the APBEK and revAPBEK functionals.[59] All three involve, to varying extents, matching of the gradient expansion for small s. In the case of revAPBEK there also is an empirically adjusted parameter.

The APBEK, revAPBEK,[59] APBEKint, and revAPBEKint[60] KEDFs are worth examining a bit more. The PBE XC enhancement factor[225] can be written compactly as

$$F^{pbe}(s) = 1 + \frac{\kappa\mu s^2}{\kappa + \mu s^2} \tag{52}$$

with κ and μ constants in the original XC GGA and in the simpler conjoint or conjoint-like KEDF cases. Thus, in APBEK and revAPBEK, $\mu = \mu^{MGE2} = 0.23899$ from the modified second-order gradient expansion, while $\kappa_{APBEK} = 0.804$ and $\kappa_{revAPBEK} = 1.245$. The modification in MGE2 is to match the asymptotic KE expansion (in Z) for neutral atoms. Though there is evidence of good performance on a small set of molecules, it is demonstrable that both APBEK and revAPBEK violate $v_\theta(\mathbf{r}) > 0$, eq 35, near the nucleus for Kato-cusped densities.[280]

A further refinement was to generalize the coefficient of the s^2 dependence (conventionally denoted μ) into an s dependence, leading to APBEKint and revAPBEKint.[60] The specific approach was to use an interpolation:

$$\mu^{int}(s) = \frac{3\mu^{GE2} + 5s^2\mu^{MGE2}}{3 + 5s^2} \tag{53}$$

with $\mu^{GE2} = 5/27$ from the KE second-order gradient expansion. It appears that both these KEDFs also violate v_θ positivity for Kato-cusped densities however.

Of these various GGAs, so far as we know, VT84F was the first nonempirical GGA KEDF to yield bound systems from solution of the OFDFT Euler equation.[85] Its Pauli enhancement factor reads

$$F_\theta^{VT84F}(s) = 1 - \frac{\mu s^2 e^{-\alpha s^2}}{1 + \mu s^2} + (1 - e^{-\alpha s^{m/2}})(s^{-n/2} - 1) \tag{54}$$

With $m = 8$ and $n = 4$, the functional has two parameters (μ and α) that are related by the gradient expansion at small s. For cusped densities, that relation can be satisfied while maintaining the $v_\theta > 0$ constraint, eq 36, only for a small range of parameter values. An Occam's razor argument was used to choose among them.

The LKT[86] functional, in contrast, is specifically adapted to pseudodensities. It has the very simple Pauli enhancement factor

$$F_\theta^{LKT}(s) = 1/\cosh(as) \tag{55}$$

with the single parameter a set to 1.3 by enforcing $v_\theta > 0$ for low-Z atomic pseudodensities. Subsequently, the PGμ family[87]

$$F_\theta^{PG\mu}(s) = \exp(-\mu s^2) \tag{56}$$

was parametrized to come close to reproducing F_θ^{LKT} by choosing $\mu = 0.75$.[172] (Remark: μ here and in eq 57 is a parameter defining the specific Pauli enhancement factor and is not to be confused with the chemical potential.)

In Figure 5 we compare the Pauli enhancement factors of LKT, PG0.75, and VT84F. Because LKT and VT84F are adapted to specific near-nucleus behavior (zero density gradient or Kato cusp, respectively), they are nonuniversal. The effects of adaptation to nonuniversality are visible in the bump in the VT84F enhancement factor in the vicinity of s = 1. It provides v_θ positivity for Kato-cusped densities. Cuspless densities do not require the bump, as illustrated by LKT.

Numerical results illustrate the difference as well. Values from LKT and VT84F on simple metals and semiconductors are given in Table 2. Three metals, Li, Mg, and Al, each in simple cubic (sc), body-centered cubic (bcc), face-centered cubic (fcc), and hexagonal close-packed (hcp) structures, were treated. Nine zinc-blende structured III−V semiconductors also were treated, AlP, AlAs, AlSb, GaP, GaAs, GaSb, InP,

https://doi.org/10.1021/acs.chemrev.2c00758
Chem. Rev. 2023, 123, 12039−12104

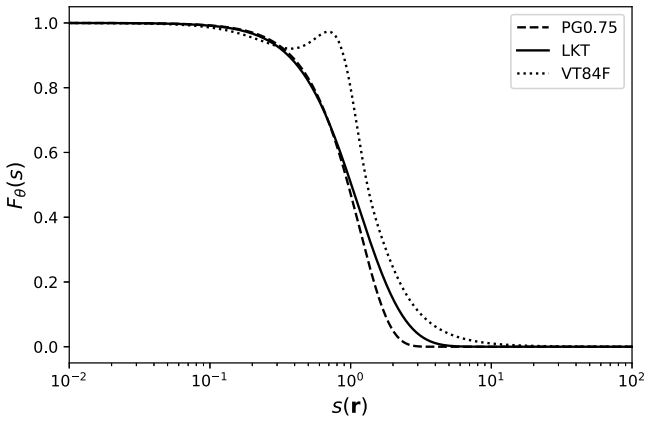

Figure 5. Comparison of the Pauli enhancement factors of LKT, VT84F, and PG0.75. By choice, PG0.75 is close to LKT up to $s \approx 1$.

Table 2. Effect of Nonuniversality Adaptation on KEDF Performance for Solid Metals and Semiconductors: MARE of Equilibrium Volumes, V_0, Energies, E_0, and Bulk Moduli, B_0, as Percentages[a]

	Metals			Semiconductors		
KEDF	V_0	E_0	B_0	V_0	E_0	B_0
LKT	4.0	0.2	7.7	2.1	2.8	4.3
VT84F	6.0	0.1	11.6	10.5	3.6	56.4

[a]See text for notation. Adapted from ref 86.

InAs, and InSb. Mean absolute relative errors (MAREs) referenced to the conventional KS values are reported in that table for equilibrium cell volume V_0, total energy per cell E_0, and bulk modulus B_0. The Perdew−Zunger LDA XC DFA[281] was used. (For other technical details see ref 86 and its Supporting Information.)

All the OFDFT calculations were done with bulk-derived local pseudopotentials (see Subsection 3.1). LKT is adapted to such potentials. VT84F, in contrast, was built with constraint satisfaction for Kato-cusped densities. Table 2 shows substantial improvement when pseudodensities are adopted in all but one case, E_0 for the metals. Even that is an example of a big shift in a small number; the LKT MARE is 0.2%,

The PGint KEDF[279] is interesting because of the unusual way in which it was parametrized. It takes the PGμ form, eq 56, and gives μ an s dependence, the same concept as in the "int" KEDFs just discussed. But instead of eq 53, PGint uses

$$\mu(s) = \mu_1 + (\mu_2 - \mu_1)\frac{\alpha s^2}{1 + \alpha s^2} \tag{57}$$

The parameters are $\mu_1 = 40/27$, $\mu_2 = 20/9$, and $\alpha = 10$. These values were chosen so that PGint recovers the second-order gradient expansion for $s \to 0$ and is close to PGμ with $\mu = 20/9$ for $s > 0.2$. The motivation for these design choices is to retain second-order gradient linear response in PGint. Though it gives some interesting results for atoms and jellium clusters, so far as we are aware, PGint has not been tested against thermochemical properties of molecules or solids nor does it seem to have been used to drive AIMD.

Two basic difficulties with *any* GGA KEDF motivate moving to inclusion of $\nabla^2 n$ dependence. First, for the case of a Kato-cusped density (the density from the physical v_{ext} in the electronic structure problem), $v_\theta(\mathbf{r})$ is singular at the nuclear site,[264] $\lim_{r\to 0} v_\theta(\mathbf{r}) = a_\theta/r$ for any Pauli enhancement factor that for small s goes as $F_\theta^{GGA} = 1 + a_\theta s^2$. Though the singularity is unphysical, the only GGA design choice is to make sure that the constant $a_\theta > 0$. That at least satisfies the $v_\theta > 0$ constraint. Many GGA KEDFs violate that constraint, for example APBEK and revAPBEK (recall above).

This dilemma motivated Karasiev et al.[264] to consider reduced density derivative combinations of s and the dimensionless reduced density Laplacian defined as

$$q := \frac{\nabla^2 n}{4(3\pi^2)^{2/3} n^{5/3}} \tag{58}$$

(Remark: Beware of notational overload. The variable q should not be confused with the canonical position variable of classical phase space mentioned in Section 1 and with the Fourier space variable conjugate with $|\mathbf{r} - \mathbf{r}'|$ discussed later.) Then they rewrote the gradient expansion through fourth-order

$$T_\theta[n] = \int d\mathbf{r}[\tau_\theta^{(0)}[n](\mathbf{r}) + \tau_\theta^{(2)}[n](\mathbf{r}) + \tau_\theta^{(4)}[n](\mathbf{r}) + ...] \tag{59}$$

with

$$\tau_\theta^{(2i)}[n](\mathbf{r}) = \tau_{TF}[n](\mathbf{r}) F_\theta^{(2i)}(s, q, ...) \tag{60}$$

The corresponding enhancement factors are

$$F_\theta^{(0)} + F_\theta^{(2)} = 1 + a_2 s^2$$
$$F_\theta^{(4)} = a_4 s^4 + b_2 q^2 + c_{21} s^2 q \tag{61}$$

Instead of using the gradient expansion coefficients, however, they determined coefficients such that the v_θ for a cusped density would be nonsingular at the origin. That led to, for example, the reduced density derivative combinations which are to be used as arguments of novel enhancement factors, such as $F_\theta(\kappa_4)$.

Reference 264 presented limited consideration of one KEDF constructed with the latter two variables but relied on determination of the parameters by fitting to conventional KSDFT results for two molecules and two atoms. The results were mixed, with some constraint violations but remarkably

$$\kappa_4 := s^4 + \frac{18}{13} q^2 - \frac{30}{13} s^2 q \tag{62}$$

$$\tilde{\kappa}_4 := \sqrt{s^4 + b_2 q^2}, \quad b_2 > 0 \tag{63}$$

$$\kappa_2 := s^2 + b_1 q \tag{64}$$

good performance in post-SCF calculations of T_s for 14 molecules, superior to that of the Perdew−Constantin meta-GGA KEDF[270] that we discuss below. Post-SCF intramolecular forces (evaluated by finite differences) from the two were about equally good (or bad) in that some were rather accurate and some were quite off. Investigation of that ref 264 KEDF was not pursued. In retrospect, it may have been too complicated a form for initial exploration. Moreover, there was no compelling way to pick among possible reduced density derivatives nor to decide the form of the enhancement factor. What the exercise did show was the important role of $\nabla^2 n$ in getting rid of the unphysical v_θ singularities of GGA KEDFs.

A few years later, Xia and Carter[282] pointed out the importance of $\nabla^2 n$ contributions in a different way. In our notation, they observe that the Pauli KE (be it approximate or exact) always can be written as

https://doi.org/10.1021/acs.chemrev.2c00758
Chem. Rev. 2023, 123, 12039−12104

$$T_\theta[n] = c_{TF}\int d\mathbf{r} n^{5/3}(\mathbf{r}) G[n(\mathbf{r})] \tag{65}$$

(Remark: Beware that they use the form of the s variable *without* the constants, as we warned earlier.) For fcc Al, they calculated the KS KE density augmented with a bare Laplacian,

$$\tau(n;\, x) := \tau_s[n] + xq \tag{66}$$

with a constant mixing coefficient $-1 \le x \le 1$. (The calculations used PBE XC and a bulk-derived local pseudopotential, but neither choice affects the outcome.) Then they extracted $G[n;x]$. Plotted as a function of s for various values of x, complicated double-valuedness in G immediately is evident. Not only is $G(n;x) \neq G(s;x)$ but the double-valued behavior depends strongly on the q admixture coefficient x. The Xia−Carter results show that removal (or, at least, substantial suppression) of the double-valuedness would require the mixing to be a function of s, i.e. $x(s)$ at least. Since G is not solely a function of n and s, they concluded that the multivaluedness made the validity of GGA KEDFs questionable.

In a subsequent exchange of comments,[252,283] Trickey, Karasiev, and Chakraborty argued that local imposition of the upper bound, eq 42, essentially cuts off the multivaluedness at least to the extent that a GGA KEDF is able to reproduce the most important features of $G[n]$ on the most important density range. In reply, Xia and Carter pointed out that local upper bound imposition does not remove what may be some critical regions of double-valuedness and that fundamentally such local imposition is not a rigorous constraint because it converts a sufficient condition into a necessary one. They did, however, agree that improved GGA KEDFs merited study.

The reduced density derivative and the $G[n]$ studies just discussed provide solid analytical and numerical motivation for considering Laplacian-dependent KEDFs. The investigation of such KEDFs has a long history because, among other things, of the gradient expansion. Recall from Section 1 that the simplest Laplacian-level functionals were explored in the mid-1980s[124,284] to treat the known failure of GEA functionals to reproduce atomic shell structure in the KE density. A bare Laplacian, as in the Xia and Carter[282] study, has no effect on the kinetic energy potential, $v_s(\mathbf{r})$, delivered by a KEDF but changes the KE density (the gauge issue mentioned above). Empirically it was found that an appropriate admixture of a bare Laplacian term could describe atomic shell structure but at the cost of degrading the description of the near-nucleus kinetic energy density.[124,284] Some recent studies also have included functionals with a bare multiplicative Laplacian term in an enhancement factor,[270,285] as well as more complicated, constraint-based functions of s and q.

All of these can be subsumed in the Laplacian meta-GGA form[268,270,285] already introduced, eq 60,

$$T_s^{mGGA-L}[n] = c_{TF}\int d\mathbf{r} n^{5/3}(\mathbf{r}) F_\tau^L(s^2(\mathbf{r}),\, q(\mathbf{r})) \tag{67}$$

The Perdew−Constantin (PC) meta-GGA has been among the more influential of these.[270] It is designed to recover the fourth-order gradient expansion in the slowly varying case and T_{vW} in the rapidly varying one. Moreover, it is constrained to satisfy eq 34 locally. The form of the PC enhancement factor thus is another example of interpolation between limiting behaviors,

$$F_\tau^{PC} = \frac{5}{3}s^2 + \left(F_\tau^{mGE4} - \frac{5}{3}s^2\right) f_{ab}\left(F_\tau^{mGE4} - \frac{5}{3}s^2\right) \tag{68}$$

Here, F_τ^{mGE4} is a modification of the fourth-order gradient expansion

$$F_\tau^{mGE4} := \frac{F_\tau^{GE4}}{1 + \frac{\Delta_4}{\left(1+\frac{5}{3}s^2\right)^{1/2}}}$$

$$F_\tau^{GE4} = 1 + \frac{5}{27}s^2 + \frac{20}{9}q + \Delta_4$$

$$\Delta_4 := \frac{8}{81}q^2 - \frac{1}{9}s^2 q + \frac{8}{243}s^4 \tag{69}$$

The interpolating function is

$$f_{ab}(z) = 0, \qquad z \le 0$$

$$f_{ab}(z) = \left\{\frac{1 + e^{a/(a-z)}}{e^{a/z} + e^{a/(a-z)}}\right\}^b, \quad 0 < z < a$$

$$f_{ab}(z) = 1, \qquad z \ge a \tag{70}$$

with two parameters $0 < a \le 1$ and $b > 0$. They were fitted to minimize the mean absolute relative error of the KS KE for a suite of neutral atoms, ions, neutral spherical jellium clusters, and liquid-drop model jellium spheres to yield $a = 0.5389$ and $b = 3$. Most of the testing was done on comparatively abstract systems, but the atomization kinetic energy, T_s[separated-atoms] − T_s[molecule], was reported for post-SCF calculations on a set of 12 small molecules. Compared to the TF, GE2, and GE4, oddly the PC meta-GGA MAE was second best. TF was a bit better. However, TF got the sign of the difference wrong in four cases, whereas the PC meta-GGA had only two wrong. This illustrates a difficulty in testing. Seemingly innocent protocols can give misleading results.

A peculiarity in the PC meta-GGA was discovered and analyzed by Cancio and co-workers in the context of meta-GGA X functionals. In those functionals, it is typical to use an indicator function conventionally denoted as $\alpha := (\tau_s - \tau_{vW})/\tau_{TF} \equiv \tau_\theta/\tau_{TF}$. They found mishandling of the behavior for $\nabla^2 n < 0$ and associated difficulties in regions of strong electron localization. Negative $\nabla^2 n$ values are typical of covalent bond formation and for pseudodensities. To deal with these problems, they proposed a smoother enhancement factor[268,286]

$$F_\tau^{CSK} = \frac{5}{3}s^2 + 1 + z_{CSK}\{1 - \exp 1/z_{CSK}[1 - H(z_{CSK})]\}$$

$$z_{CSK} := \frac{20}{9}q - \frac{40}{27}s^2 \tag{71}$$

Here $H(z)$ is the Heaviside unit step function and "CSK" denotes the authors (Cancio, Stewart, and Kuna). Results against the AE6 molecular data set[287] (picked because of its diversity of bonding types) were illuminating. Post-SCF (density from PBE XC DFA in conventional KS) results are shown in Table 3. It compares atomization energy MAEs and KE MAREs. For scale, the MAE against experiment of the conventional KS calculation is 23.0 kcal/mol. Based on the atomization energies, VT84F is best. Thus, the table may seem to present a victory for GGA or a loss for meta-GGA KEDFs, depending on viewpoint. But the reality is more subtle. The

https://doi.org/10.1021/acs.chemrev.2c00758
Chem. Rev. 2023, 123, 12039−12104

Table 3. Post-SCF Atomization Energy MAEs and KE MAREs against the AE6 Data Set Compared for Several mGGA KEDFs[a]

KEDF	Atomization MAE (kcal/mol)	KE MARE
VT84F	182.1	0.2
mGGA-CSK	246.8	0.087
mGGA-PC	595.5	0.139
GE2	560.7	0.112
TF	671.1	0.162

[a]Adapted from ref 286.

actual KE values are very different. For those, VT84F actually was the worst. The design priority for VT84F was to get good ionic forces in AIMD simulations while respecting as many constraints as attainable. The cost was a functional that generates KE values that are too large. Remember, however, that the table compares post-SCF values, not the results of solving eq 29 self-consistently with these KEDFs.

Other single-point functionals based on recovery of the fourth-order gradient expansion are found in refs 83 and 288−291. What is confirmed very convincingly by Golub and Manzhos[83] is that the fourth-order gradient expansion itself is not viable as a KEDF. Its KE density is notably worse than those from the second-order approximation in significant spatial regimes even for Si and Al. With coefficients adjusted for each system separately (hence, a nontransferable KEDF), agreement is much better for metals but not for covalently bonded systems. Those authors turned to machine-learning methods to seek further improvements; see Subsection 2.5.

Reference 291 also attempted to overcome limitations in the Perdew−Constantin KEDF.[270] In our notation, those authors wrote

$$F_\tau^{\mathrm{mod}GE4} := 1 + \frac{5}{27}s^2 + \frac{20}{9}q - \gamma s^2 q + \nu s^4 \tag{72}$$

The constants $\gamma = 0.2608$ and $\nu = 0.1826$ were determined by jellium surface energy and semiclassical neutral atom fitting. Unfortunately, it is difficult to set the recorded performance of this functional in the context of the rest of the literature. Though those authors did calculations on a test set of 21 molecules, they reported results on total KE and atomization KE differences only in terms of a "relative performance indicator" they devised. Ordinary MARE, MAE, etc. information was not provided nor were test results on periodic solids.

More recent investigation of Laplacian dependence has relied on devising an enhancement factor that reproduces as closely as possible the HEG linear response, for example to obtain the PGSL,[87] PGSLr,[172] and GSE2 functionals.[279] PGSL ("Pauli Gaussian supplemented with Laplacian") has the Pauli term enhancement factor

$$F_\theta^{PGSL} := \exp\{-(40/27)s^2\} + \frac{1}{4}q^2 \tag{73}$$

The gradient expansion coefficient of q^2 would be 8/81. The value of 1/4 came from optimization against simple metals. PGSLr retains the good linear response of PGSL by modifying the Pauli term enhancement factor to be

$$F_\theta^{PGSLr} := F_\theta^{PGSL} - \lambda s^2 q + \sigma s^4 \tag{74}$$

The empirical parameters, $\lambda = 0.4$ and $\sigma = 0.2$, were obtained from fitting to equilibrium volume, V_0, total energy, E_0, bulk modulus, B_0, and density errors for a set of 9 metals and 9 semiconductors. The authors noted that optimum values would be $\lambda^2 \approx \sigma$ but that numerical instability attendant with that choice prevented its adoption.

It is already clear that the best recent meta-GGA functionals provide some significant improvements relative to earlier GGA KEDFs but that the improvements are not systematic compared to the best current GGAs. Equally interestingly, however, the best of these GGAs and meta-GGAs are competitive with two-point functionals for calculations on bulk solids,[86,172] on atomic systems,[60] and in subsystem DFT simulations.[60,285,292−296] There is however a problem with Laplacians. High-order spatial derivatives in the Euler equation can cause numerical stability issues. We return to that in Section 3.

Table 4 gives a brief comparison (adapted from ref 172) of GGA and meta-GGA KEDF performance on a slightly larger set of simple metals and semiconductors than was used in the studies just discussed. Four metals, Li, Mg, Al, and Si, each in sc, bcc, fcc, and hcp structures were included. (Elemental Si is metallic in those structures.) Ten semiconductors, cubic diamond Si plus the nine III-Vs in the preceding data set, were used. For stringency, the table compares the performance of one- and two-point KEDFs. Details of the latter class are in the next subsection. Here note only that the two-pointers are the very early Smargiassi−Madden (SM)[46] and more recent Huang−Carter (HC).[77] Observe that HC is parametrized to semiconductors. Again, the OFDFT calculations were done with bulk-derived local pseudopotentials (see Subsection 3.1) but in this case with the PBE GGA XC DFA.[225] Table 4 omits results from the WGC two-point functional[297] because it was parametrized on metals and is known to perform poorly on semiconductors. Results from TFλvW are omitted because it is non-N-representable for the values $\lambda < 1$ ordinarily used.

Table 4. KEDF Performance on Solid Metals and Semiconductors: MARE of Equilibrium Volumes, V_0, Energies, E_0, and Bulk Moduli, B_0, as Percentages[a]

	Metals			Semiconductors		
KEDF	V_0	E_0	B_0	V_0	E_0	B_0
SM (2-pt)	3.82	0.19	4.68	10.6	0.76	42.9
HC (2-pt)	5.84	0.43	11.7	1.98	0.51	11.67
LKT (GGA)	3.61	0.18	23.9	1.33	2.82	13.5
PG0.75 (GGA)	3.72	0.16	25.7	1.16	2.57	9.58
PGSLr (mGGA)	3.68	0.23	12.3	1.11	1.48	7.14

[a]See text for notation about KEDFs. Adapted from Ref 172.

The table shows, somewhat surprisingly perhaps, that the best current GGA KEDFs, LKT and its closely related PG0.75, are rather good at yielding E_0 and V_0 in comparison with the more complicated two-point KEDFs. We do not have an explanation for the seemingly large increase in B_0 MARE for those two from the data set used to generate Table 2 to the data set used in Table 4. The independently calculated B_0 MAREs for LKT reported in refs 86 and 240 are much smaller and agree closely. The data set used in ref 172 differs from that used in the latter two references in having the Si systems. The calculations differ in the XC DFA. But all three studies find nearly the same results for LKT V_0 and E_0 MAREs, so it seems implausible that either of those differences (data set or XC DFA) would cause such a discrepancy in the B_0 MAREs. There

https://doi.org/10.1021/acs.chemrev.2c00758
Chem. Rev. 2023, 123, 12039−12104

may be influences from different fitting procedures (energy vs volume), but we simply do not know.

This situation illustrates, however, a long-standing challenge for KEDFs. Bulk moduli often are a problem. One sees that here in the comparative performance of the PGSLr meta-GGA. Added Laplacian dependence (q dependence) and parametrization to a substantial data set do not make PGSLr any better than LKT for V_0 in either metals or semiconductors nor for metal E_0, but it does improve for semiconductor E_0. The big improvement achieved by PGSLr, at least on this small data set, is for B_0. The step to a meta-GGA makes a major difference, roughly a factor of 2 MARE reduction.

Figure 6 gives a graphical view of the performance of several of the GGA and meta-GGA functionals treated in this section.

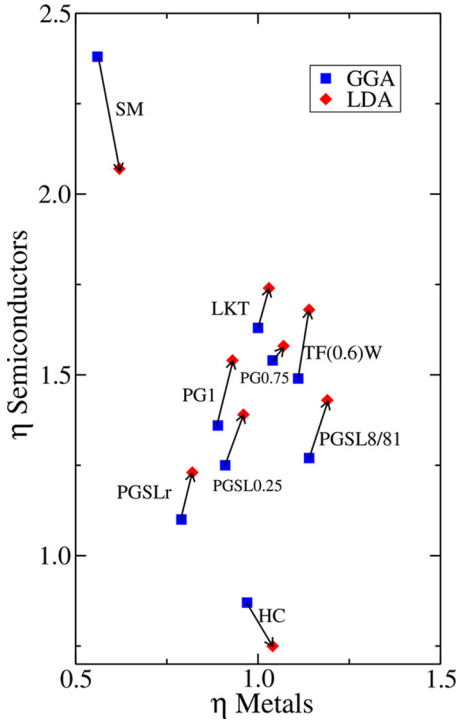

Figure 6. Global performance indicator, η, defined as a weighted average of deviations against benchmark values for metallic systems and semiconductor systems computed with LDA and PBE XC functionals and their associated local pseudopotentials (BLPS; see Section 3.1 for details on the pseudopotentials used in OFDFT simulations). Arrows connect results for LDA and PBE XC functionals for the same KEDF. Reprinted with permission from ref 172. Copyright (2011) American Chemical Society.

The so-called global performance indicator η was defined in ref 172 as a weighted average of MAREs for five properties, V_0; E_0; B_0; density error, $D_0 := \int d\mathbf{r}|n^{KS}(\mathbf{r}) - n^{OFDFT}(\mathbf{r})|$; and the error K_0 in the non-SCF non-interacting KE per cell. The weights were set on the basis of arguments for the relative importance of the five quantities. The indicator η was evaluated for both LDA and GGA (PBE) XC functionals and their associated pseudopotentials. A notable feature is that the one-point functionals do as well on metals as the HC two-point functional. Of course, HC was developed with semiconductors in mind, not metals, another example of the benefits and limitations of nonuniversality. An important observation also is that parametrized functionals, such as PGSLr, improve performance compared to the nonempirical LKT, hinting that improvement of nonempirical one-point KEDFs can, and should be achieved.

We note that at least in the simple meta-GGA KEDFs contrived thus far, Laplacian dependence cannot generate density oscillations from the OFDFT Euler equation, even though such KEDFs give reasonable calculated energies and, often, quite good forces (energy gradients).

As an aside about GGA KEDFs, we remark that, although not shown here, among other somewhat recent ones, the LC94[67] and revAPBEK[60] functionals have been reasonably successful in the context of subsystem DFT simulations.[180,181,190] Recall, however, the comments above about the lack of v_θ positivity in revAPBEK. Another recent development is the WPBEK KEDF,[298] a different example of a modified conjoint GGA. It violates positivity constraints dramatically. That behavior led the authors to an interesting kind of dual representation, with a proper F_θ constructed so as to give the same non-interacting KE as the improper F_θ^{WPBEK}. We return to this idea in Subsection 2.4.3.

2.4.2. Two-Point Functionals. In Section 1 we remarked that interest in the nonlocality provided by two-point functionals originated in the first Hohenberg–Kohn DFT paper.[3] There is a subtlety about that. The HK paper showed that effective approximate treatment of atomic density oscillations involves inclusion in the KE of excitations from occupied to virtual (above Fermi level) orbitals.[40] Because those orbitals are themselves density functionals (albeit implicit), the derived functional is still a density functional.

The HK approach did not catch on until 1985 with the first application of the scheme in materials physics[43] (jellium surfaces and atoms). That paved the way to several subsequent generations of two-point functionals, such as those of Wang–Teter,[44] Smargiassi–Madden[46] (already mentioned), Perrot,[47] Wang–Govind–Carter,[45] Huang–Carter[77] (already mentioned), and, recently, Mi–Genova–Pavanello[81] and its density-dependent kernel version, LMGP,[88] as well as others.[49,80,90]

Two-point KEDFs generally are expected to be more accurate than one-point KEDFs simply because the two-pointers probe and encode information about a larger spatial region than is possible with one-point functionals. Recall the discussion in Section 1 and Figure 3, but keep in mind the recent comparative success of one-pointers just surveyed.

Various of the earlier practical two-point KEDFs used somewhat near-sighted kernels[44] with Coulomb-like corrections for semiconductors.[77,81,88] (Several[45,77,80] also depended on parametrization beyond the level of isolated atoms and, hence, are semiempirical.) In that context it is informative to consider $T_s[n]$ in eq 23 from the perspective of probing an infinitesimal neighborhood of a sample point $\mathbf{r}$. $T_s[n]$ is derived explicitly as a one-electron operator acting on the KS orbitals. By virtue of orthogonality, those orbitals interfere, which gives rise to atomic shell structure. Thus, a proper KEDF must incorporate information about those shell–structure effects. That information is nonlocal because the nodal structure of low-lying orbitals forces the nodal structure of higher ones. This is one rationalization of the oft-stated claim that two-point functionals are essential for incorporation of shell structure.[299] Note, however, that not all nonlocal KEDF formulations will yield good shell structure descriptions.[300] (Remark: Even if one suspects that a a one-point functional with sufficiently high-order spatial derivative contributions could give shell structure, the practical problem of numerical

https://doi.org/10.1021/acs.chemrev.2c00758
Chem. Rev. 2023, 123, 12039–12104

instabilities so far seems formidable.) The Friedel oscillation argument (remarks just above and in Section 1) also is rooted in interference with states lying above the Fermi level.[40,115]

This line of reasoning motivates two-point KEDFs developed from consideration of the perturbed electron gas.[115,145,301] Suppose it to have nonzero average density n_{avg}. Then the weakly varying density is

$$n(\mathbf{r}) = n_{avg} + \Delta(\mathbf{r})$$
$$|\Delta(\mathbf{r})|/n_{avg} \ll 1, \quad \forall \mathbf{r}$$
$$\int d\mathbf{r}\Delta(\mathbf{r}) = 0 \tag{75}$$

and to second order

$$T_s[n_{avg} + \Delta] \approx T_{TF}[n_{avg}] + \frac{1}{2}\int d\mathbf{r}_1 d\mathbf{r}_2 \left.\frac{\delta^2 T_s}{\delta n(\mathbf{r}_1)\delta n(\mathbf{r}_2)}\right|_{n_{avg}} \Delta(\mathbf{r}_1)\Delta(\mathbf{r}_2) \tag{76}$$

The kernel of this integral, $\left.\frac{\delta^2 T_s}{\delta n(\mathbf{r}_1)\delta n(\mathbf{r}_2)}\right|_{n_{avg}}$, has a simple, explicit dependence on the average density, n_{avg}, and on spatial points $\mathbf{r}_1$ and $\mathbf{r}_2$, thereby displaying the two-point structure. Recall the general expression for two-point functionals, eqs 13 and 14. Note, however, a significant difference. In general the kernel $\omega[n](\mathbf{r}, \mathbf{r}')$ has a more complicated and explicit density dependence than the simple n_{avg} in eq 76.

After eq 13 we noted that such nonlocal functionals are exact in principle. Here we provide an alternative route to realize this. It starts from recognition of the strict relationships among the derivatives of a functional and the functional itself. Included is the virial relation of eq 45.[254,302] It is more instructive to consider functional integration relations.[199,303,304] With them, the functional can be recovered from its first functional derivative, and the first functional derivative from the second. For a simple line integral with $n_t(\mathbf{r}) := f(t)n(\mathbf{r})$, T_s is

$$T_s[n] = \int d\mathbf{r}\tau_s[n(\mathbf{r})] = \int d\mathbf{r}\int_C dt \frac{\delta T_s[n_t]}{\delta n_t(\mathbf{r})}\frac{\delta n_t(\mathbf{r})}{\delta t} \tag{77}$$

where C is a smooth curve in $\mathbb{R}$ parametrized by $f(t)$. For the simple case $n_t(\mathbf{r}) = tn(\mathbf{r})$ with $0 \le t \le 1$, we have[81,304]

$$T_s[n] = \int d\mathbf{r}\int_0^1 dt \frac{\delta T_s[n_t]}{\delta n_t(\mathbf{r})} n(\mathbf{r}) \tag{78}$$

(This relationship has been exploited to compute KEDF energy corrections due to a nonlocal contribution to the potential.[48])

The procedure can be iterated to generate $\delta T_s/\delta n_t$ for insertion on the right-hand side of eq 78 to yield

$$T_s[n] = \int d\mathbf{r}\int d\mathbf{r}'\int_0^1 dt'\int_0^1 dt n(\mathbf{r}')\frac{\delta^2 T_s}{\delta n_t(\mathbf{r})\delta n_{t'}(\mathbf{r}')} n(\mathbf{r}) \tag{79}$$

and therefore the kernel in eq 14 can be expressed exactly as

$$\omega[n](\mathbf{r}, \mathbf{r}') = n^{1-\alpha}(\mathbf{r})n^{1-\beta}(\mathbf{r}')\int_0^1 dt' \times \int_0^1 dt \frac{\delta^2(T_s - T_{TF} - T_{vW})}{\delta n_{t'}(\mathbf{r}')\delta n_t(\mathbf{r})} \tag{80}$$

Practical utilization of this result thus involves finding a suitable approximation to the second functional derivative of T_s.

Hohenberg and Kohn[3] established the connection between the KEDF kernel and the linear response function of the HEG. Defined as

$$\delta n(\mathbf{r}) = \int d\mathbf{r}'\chi_s(\mathbf{r}, \mathbf{r}')\delta v_{KS}(\mathbf{r}') \tag{81}$$

the connection of that response function with the KEDF usually is made by considering an additional functional derivative of the KS Euler equation (eq 29). Commonly it is written as[115]

$$\frac{\delta^2 T_s}{\delta n(\mathbf{r})\delta n(\mathbf{r}')} = -\chi_s^{-1}(\mathbf{r}, \mathbf{r}') \tag{82}$$

The relationship was exploited and justified in several studies[44,47,305] and also discussed in ref 115.

But care is needed because the KS Euler equation is not a general density functional. It is a ground-state expression. By virtue of the first Hohenberg–Kohn theorem, eq 29 establishes a one-to-one relationship between an external potential and its ground-state density; hence, $v_{ext}[n_0] \leftrightarrow n_0[v_{ext}]$. Thus, eq 29 should be written

$$\left.\frac{\delta T_s[n]}{\delta n(\mathbf{r})}\right|_{n_0} + v_{KS}([n_0]; \mathbf{r}) = \mu[n_0] \tag{83}$$

Assuming ground-state v-representability and suitable restriction of differentiation to ground-state densities, the second functional derivative of T_s at n_0 is

$$\left.\frac{\delta^2 T_s[n]}{\delta n(\mathbf{r})\delta n(\mathbf{r}')}\right|_{n_0} = \left.\frac{\delta\mu[n]}{\delta n(\mathbf{r}')}\right|_{n_0} - \left.\frac{\delta v_{ks}(\mathbf{r})}{\delta n(\mathbf{r}')}\right|_{n_0} \tag{84}$$

Note the lack of explicit coordinate dependence in the $\mu[n]$. For each n_0, the corresponding $\mu[n_0]$ is a spatial constant. This is crucial. The usual assumption (often unstated) is that μ is a constant from the original Lagrangian; therefore, its functional derivative is zero, and eq 82 follows. In general, however, different ground-state densities (and associated v_{ext}) at the same N_e have different μ. Consider, for example, the first ionization potential for a neutral atom and for the isoelectronic cation, e.g. Li and Be^+. Thus, the usual claim about $\delta\mu/\delta n$ must be proved. So far as we are aware, the following argument is original.

The essential point is that because of Hohenberg–Kohn bijectivity, the first functional derivative of v_{KS} is symmetric in spatial arguments[306]

$$\frac{\delta v_{ks}(\mathbf{r})}{\delta n(\mathbf{r}')} = \frac{\delta v_{ks}(\mathbf{r}')}{\delta n(\mathbf{r})} \tag{85}$$

The same symmetry does not hold for the first functional derivative of $\mu[n_0]$. This follows from proof by contradiction. At fixed N_e, the presence of the proper $\mu[n_0]$ for each n_0 guarantees that

https://doi.org/10.1021/acs.chemrev.2c00758
Chem. Rev. 2023, 123, 12039–12104

$$\int d\mathbf{r}\delta n(\mathbf{r}) = 0 \tag{86}$$

Now multiply eq 84 by $\delta n(\mathbf{r})$ and integrate over the system volume:

$$\int d\mathbf{r}\delta n(\mathbf{r}) \frac{\delta^2 T_s[n]}{\delta n(\mathbf{r})\delta n(\mathbf{r}')}\bigg|_{n_0} = \int d\mathbf{r}\delta n(\mathbf{r}) \frac{\delta \mu[n]}{\delta n(\mathbf{r}')}\bigg|_{n_0} - \int d\mathbf{r}\delta n(\mathbf{r}) \frac{\delta v_{ks}(\mathbf{r})}{\delta n(\mathbf{r}')}\bigg|_{n_0} \tag{87}$$

Invoke the presumed symmetry of $\mathbf{r}$ and $\mathbf{r}'$ in μ and the actual symmetry in v_{ks} to get the second version of eq 87:

$$\int d\mathbf{r}\delta n(\mathbf{r}) \frac{\delta^2 T_s[n]}{\delta n(\mathbf{r})\delta n(\mathbf{r}')}\bigg|_{n_0} = \int d\mathbf{r}\delta n(\mathbf{r}) \frac{\delta \mu[n]}{\delta n(\mathbf{r})}\bigg|_{n_0} - \int d\mathbf{r}\delta n(\mathbf{r}) \frac{\delta v_{ks}(\mathbf{r}')}{\delta n(\mathbf{r})}\bigg|_{n_0} \tag{88}$$

The difference is

$$\begin{aligned} 0 &= \int d\mathbf{r}\delta n(\mathbf{r}) \frac{\delta \mu[n]}{\delta n(\mathbf{r}')}\bigg|_{n_0} - \int d\mathbf{r}\delta n(\mathbf{r}) \frac{\delta \mu[n]}{\delta n(\mathbf{r})}\bigg|_{n_0} \\ &= \frac{\delta \mu[n]}{\delta n(\mathbf{r}')}\bigg|_{n_0} \int d\mathbf{r}\delta n(\mathbf{r}) - \int d\mathbf{r}\delta n(\mathbf{r}) \frac{\delta \mu[n]}{\delta n(\mathbf{r})}\bigg|_{n_0} \\ &= 0 - \int d\mathbf{r}\delta n(\mathbf{r}) \frac{\delta \mu[n]}{\delta n(\mathbf{r})}\bigg|_{n_0} \end{aligned} \tag{89}$$

Since this must hold at n_0 for arbitrary δn that integrates to zero, the conclusion is that $\frac{\delta \mu[n]}{\delta n(\mathbf{r})}\Big|_{n_0} = 0$.

It follows therefore that

$$\frac{\delta^2 T_s[n]}{\delta n(\mathbf{r})\delta n(\mathbf{r}')}\bigg|_{n_0} = -\frac{\delta v_{ks}(\mathbf{r})}{\delta n(\mathbf{r}')}\bigg|_{n_0} \tag{90}$$

and eq 82 follows.

Approximations must be considered for use of eq 82 because knowledge of the KS response function itself would require solution of the KS equations (eq 20), exactly what OFDFT is meant to avoid. Computation of the response function via density functional perturbation theory[307] or directly through the sum-over-states expressions also would be necessary. Since the formulation is a linear response, however, the obvious reference system is the HEG. Then the Fourier transform of the second-functional derivative is the inverse of the Lindhard linear response function.[140] The HEG is an advantageous reference because its response function depends only on $|\mathbf{r} - \mathbf{r}'|$ and, hence, its Fourier transform depends only upon a single reciprocal space variable, q. (Remark: Once again, consistency with the conventional literature notation forces us into symbol overload. But just to be sure, this q is not the reduced density Laplacian of the preceding subsection.) This makes inversion of the response function a simple "one-over" calculation rather than a general operator inverse as shown in eq 82. That may not always be defined.[237]

Common practice therefore is to constrain the two-point kernel ω in eq 13 to recover the HEG linear response in eq 82 evaluated at the equilibrium density. The consensus physical reasoning is that imposing that limit is beneficial, as the electronic structure of solids often resembles that of free electrons. That kind of behavior should be captured by the Lindhard function. A major challenge, however, is capturing the inverse response *beyond* Lindhard. To our knowledge there have been only two attempts at that. One, by Della Sala et al., aimed at encoding band gap behavior in a modified Lindhard function. The approach traces to Rey and Savin.[308] The result was one GGA KEDF[309] and one nonlocal KEDF with a density-independent kernel.[80] The other is by Takahashi.[310−312] It is based on direct employment of the inverted KS response functions computed by a post conventional KS-DFT calculation of the KS response function. Initial results provide accurate but nontransferable functionals. Further work along either or both of these lines would improve the state of the art.

In any event, some implications of constraints immediately are apparent.

- The entire two-point term must vanish for uniform density.
- To obey the conjectured Lieb upper bound, eq 42, requires

$$\omega[n](\mathbf{r}, \mathbf{r}') \leq 0 \tag{91}$$

- To obey Pauli term positivity, eq 35, requires

$$T_{TF}[n] + \int d\mathbf{r}d\mathbf{r}' n^{\alpha}(\mathbf{r})\omega[n](\mathbf{r}, \mathbf{r}')n^{\beta}(\mathbf{r}') \geq 0 \tag{92}$$

  That suggests the kernel $\omega[n](\mathbf{r}, \mathbf{r}')$ should tend to a Dirac delta multiplied by a weight that goes like $n^{5/3-\alpha-\beta}$ for one-electron densities (i.e., when the kinetic energy density is that for von Weizsäcker, $\tau_s(\mathbf{r}) = \tau_{vW}(\mathbf{r})$), such as in the hydrogen atom or in the tail region of isolated atoms.
- Kernels must be dependent explicitly upon $n(\mathbf{r})$ and not solely on its average. Observe the notation, eq 14, repeated here:

$$\mathcal{K}[n(\mathbf{r}), n(\mathbf{r}'), \mathbf{r}, \mathbf{r}'] = n^{\alpha}(\mathbf{r})\omega[n](\mathbf{r}, \mathbf{r}')n^{\beta}(\mathbf{r}') \tag{93}$$

  It is provable that density-independent kernels $\omega(\mathbf{r}, \mathbf{r}')$ yield KEDFs that are variationally unstable[313] whenever they are of the form given by Wang and Teter[44] (which is the most commonly used form). See discussion below.
- Uniform density scaling relations must be satisfied, so $\alpha + \beta = 8/3$ for functionals with density-dependent kernels, ω, which should be functions of dimensionless variables such as reduced density derivatives, $k_F(\mathbf{r})|\mathbf{r} - \mathbf{r}'|$, etc. so that they are homogeneous of degree zero under scaling. The local Fermi wave vector is

$$k_F(\mathbf{r}) := [3\pi^2 n(\mathbf{r})]^{1/3} \tag{94}$$

In principle, another constraint is that the entire two-point integrand should be symmetric with respect to interchange of $\mathbf{r}$ and $\mathbf{r}'$[314] but there are counterexample violations among practical approximations, e.g. ref 77.

Note also that two-point KEDFs with density-independent kernels depend on a reference uniform density, n_0, which is an ill-defined quantity for any unenclosed system, e.g., an atom or molecule.[297,299]

A significant deficiency of the Wang−Teter-like two-point KEDFs with density-independent kernels is the finding by

https://doi.org/10.1021/acs.chemrev.2c00758
Chem. Rev. 2023, 123, 12039−12104

Blanc and Cancès[313] that such KEDFs are variationally unstable except with respect to near-uniform densities. There are many such functionals (Smargiassi–Madden,[46] Perrot,[47] Wang–Govind–Carter 98,[45] Mi–Genova–Pavanello,[81] simplified versions of CAT-like functionals[315,316]) which have been applied successfully to close-to-uniform systems (e.g., simple metals). The problematic variational instability does not seem to occur frequently in practical calculations of bulk systems. However, a recent study by Witt et al.[317] reports instabilities especially from the Perrot functional. The application of WT to warm dense matter also uncovered instabilities.[318]

The issue was identified by Witt et al. as stemming from the violation of condition eq 92 by the Perrot functional as well as (even though infrequently) by the other two-point, density-independent kernel functionals. One can impose strict satisfaction of the positivity condition by applying an exponential stabilization scheme as follows. Rewrite the Pauli term in eq 92 as

$$T_{TF}[n] + \int d\mathbf{r}d\mathbf{r}' n^{\alpha}(\mathbf{r})\omega[n](\mathbf{r}, \mathbf{r}')n^{\beta}(\mathbf{r}') = T_{TF}[n](1 + x) \tag{95}$$

Here $x = \frac{\int d\mathbf{r}d\mathbf{r}' n^{\alpha}(\mathbf{r})\omega[n](\mathbf{r}, \mathbf{r}')n^{\beta}(\mathbf{r}')}{T_{TF}[n]}$. Whenever $x < -1$, Pauli-term positivity is violated. An elegant way to avoid this problem is to replace the $(1 + x)$ term by e^{x}. This substitution ensures the positivity condition always is satisfied and, in fact, no instabilities were observed once it was implemented.[317]

The reader might be concerned that two-point functionals would be computationally expensive because a double spatial integral (six dimensions) must be evaluated. While true that direct evaluation would be unhelpfully costly, use of the HEG inverse response function in the formulation of ω in eq 80 reduces the evaluation cost to quasi-linear, $O(N \ln N)$. This matter is discussed in Subsection 3.4, about related computational aspects. The quasi-linear-scaling also is maintained for density-dependent kernels implemented by aid of spline techniques.[77,88]

The first formulations of a nonlocal KEDF with density-dependent kernels resulted in the so-called average density approximation (ADA) and weighted density approximation (WDA),[43,143,144,255,299,319−323] and later the WGC99 (WGC, hereafter) functional.[297] (Remark: There is a section in ref 44 devoted to extending the Wang–Teter functional to a density-dependent kernel by discretizing the original one, $w_{WT}(\mathbf{r}_1, \mathbf{r}_2)$, over the distance $|\mathbf{r}_1 - \mathbf{r}_2|$ into $\mathcal{N}$ segments, evaluating the local Fermi wavevector on each segment, and then using that in a Gaussian basis expansion (Gaussians centered on each segment) of the original kernel. Structurally the scheme is reminiscent of the Trotter decomposition.[324] To our knowledge, that WT scheme never has been used again.) In all of those kernels, except those of refs 43 and 255, explicit density dependence is introduced through an effective Fermi wavevector, ξ,

$$\omega[n](\mathbf{r}_1, \mathbf{r}_2) = \omega[\xi(\mathbf{r}_1, \mathbf{r}_2)](\mathbf{r}_1, \mathbf{r}_2) \tag{96}$$

with

$$\xi(\mathbf{r}_1, \mathbf{r}_2) = \left(\frac{k_F^{\gamma}(\mathbf{r}_1) + k_F^{\gamma}(\mathbf{r}_2)}{2}\right)^{1/\gamma} \tag{97}$$

where $\gamma > 0$.

Beware that WDA/ADA KEDFs such as the symmetrized CAT functional[299] are written in a somewhat different form than what we have used as canonical, to wit,

$$T_s^{CAT}[n] = T_{vW}[n] + T_{NL}^{CAT}[n]$$
$$T_{NL}^{CAT}[n] := \frac{8}{5}c_{TF}\int d\mathbf{r} n(\mathbf{r})\tilde{n}^{2/3}(\mathbf{r}) - \frac{3}{5}T_{TF}[n]$$
$$\tilde{n}(\mathbf{r}) := \int d\mathbf{r}_2 n(\mathbf{r}_2)[2\xi(\mathbf{r}_1, \mathbf{r}_2)]^3\Omega(2\xi(\mathbf{r}_1, \mathbf{r}_2)|\mathbf{r}_1 - \mathbf{r}_2|) \tag{98}$$

with $\gamma = -1/2$ in eq 97 chosen as a result of numerical experimentation. Ω has the role of a kernel. Note in particular that the "non-local" term in fact has a subtractive local (scaled TF) contribution.

The remarkable advance of the CAT functional was that it gave rather good atomic radial densities from SCF solutions of its Euler equation. From the perspective of 35 years later, CAT posed two difficulties. First, for two of the nine closed-shell atoms treated and one of the group V atoms, CAT gave lower total energies than the reference conventional KS (LDA XC) calculation, a sign of non-N-representability. The other difficulty was the explicit use of double spatial integrals. However, the original formulation of the CAT functional[43] did not feature a symmetrical integrand in the definition of $\tilde{n}(\mathbf{r})$ because it had a one-point effective Fermi wavevector. As we discuss in Subsection 3.4, use of one-point effective Fermi wavevectors enables techniques to avoid the double integration. There are simplified versions of CAT-like functionals[315,316] in which a Fermi wavevector corresponding to an average electron density, k_F^0, is used in place of ξ of eq 97. Simulations of liquid metals were successful with this strategy; see Section 4.3.

The WGC paper[297] unified the formulation of two-point KEDFs in a single structure with the canonical form we have used here. For bulk Al lattice constants and energies per atom as test cases (sc, bcc, fcc, and hcp lattices), they explored the powers α and β from $(\frac{5}{6} \pm 0)$ to $(\frac{5}{6} \pm \sqrt{5}/6)$. The best results with respect to conventional KS calculations with LDA XC were for $(\alpha, \beta) = (\frac{5}{6} + \sqrt{5}/6, \frac{5}{6} - \sqrt{5}/6)$, hence, breaking spatial inversion symmetry $(\mathbf{r}_1 \leftrightarrow \mathbf{r}_2)$. For eq 97 they found γ values from 1.9 to 2.7 were best. From that calibration, they calculated Al vacancy formation energies with success. However, Al surface energies were not as accurate, *unless* the reference average density used was the bulk value. Technically, the WGC formulation provided a clear step forward, namely reduction of the computational scaling by avoiding the double integral through the use of a Taylor expansion of the kernel around the reference constant density. As already mentioned, the reliance of WGC and its predecessors[44,46,47] on such a reference density limits transferability and applicability of such KEDFs.

Several advances in the past decade have resolved the issue. The state of the art two-point functional (at least for bulk systems) is the Huang–Carter (HC) KEDF[77] mentioned already. Instead of the local Fermi-vector average $\xi(\mathbf{r}_1, \mathbf{r}_2)$ used in the WGC functional, the HC KEDF has a fully density-dependent kernel that has no HEG uniform density reference. Written in terms of eq 14, it is

$$\mathcal{K}^{HC}[n(\mathbf{r}_1), n(\mathbf{r}_2), \mathbf{r}_1, \mathbf{r}_2] = n^{8/3-\beta}(\mathbf{r}_1)\omega^{HC}[n](\mathbf{r}_1, \mathbf{r}_2)n^{\beta}(\mathbf{r}_2) \tag{99}$$

https://doi.org/10.1021/acs.chemrev.2c00758
Chem. Rev. 2023, 123, 12039−12104

with

$$\omega^{HC}[n(\mathbf{r}_1)](\mathbf{r}_1, \mathbf{r}_2) = \omega(k_F(\mathbf{r}_1)[1 + \lambda s^2(\mathbf{r}_1)]|\mathbf{r}_1 - \mathbf{r}_2|) \quad (100)$$

Use of a one-point Fermi wavevector is explicit. In the foregoing equation, the s variable is the reduced density gradient defined in eq 32 (but *without* the constants) and β and λ are parameters determined empirically to be $\beta = 0.7143$ and $\lambda = 0.01177$ for III−V semiconductors. They are averages of optimal values over the set for the equilibrium volume, cohesive energy, and bulk modulus relative to conventional KSDFT results from calculations with the same local pseudopotentials (BLPS; see Subsection 3.1 for details on the pseudopotentials used in OFDFT simulations). The simplified two-point dependence in the HC KEDF is important computationally, as we discuss in Subsection 3.4. Above we remarked (in the discussion of constraints) that this kernel also is not symmetric in $\mathbf{r}_1$ and $\mathbf{r}_2$. Despite that, the calculational success of the HC KEDF on systems for which it was developed (discussed below) suggests, at least, that the symmetry violation does not have severe consequences for those systems.

The explicit nonlocality in ω^{HC} via the $\lambda s^2(\mathbf{r}_1)|\mathbf{r}_1 - \mathbf{r}_2|$ dependence is important. Nonzero even when the density is small (e.g., $s \to \infty$ in the tail of an isolated system), the dependence is included to approach the proper limit of the second functional derivative of the KEDF for $|\mathbf{r}_1 - \mathbf{r}_2| \to \infty$ (equivalently, $q \to 0$ in Fourier space; again beware of notational overload). This follows from exact properties of the response function[325,326] given the relationship in eq 82.

In the HEG limit that is the Lindhard function

$$\chi_{\text{Lind}}(\eta) = -\frac{k_F}{\pi^2}\left[\frac{1}{2} + \frac{1-\eta^2}{4\eta}\ln\left(\frac{1+\eta}{1-\eta}\right)\right] \quad (101)$$

where $\eta = \frac{q}{2k_F}$ for spin-compensated systems. (In the HEG, $k_F = (3\pi^2 n_0)^{1/3}$ is a constant of course.) (Remark: For sake of clarity, the variable q in the definition of η is to be considered $q = |\mathbf{G}|$, the absolute value of the reciprocal space variable, $\mathbf{G}$. For reference, the allowed $\mathbf{G}$ vectors satisfy the relation $e^{i2\pi\mathbf{r}\cdot\mathbf{G}} = 1$.) Imposition of eq 82 leads to a first-order differential equation for the ω^{HC} that defines the kernel as a function of η. That ω^{HC} then is used in eq 100 by appropriate change of the kernel variable and consideration of the Fourier transform with respect to the $|\mathbf{r}_1 - \mathbf{r}_2|$ scalar variable.

The HC functional provided a major step forward for OFDFT applied to materials science. For example, for the first time an OFDFT functional could reproduce, at least nearly quantitatively, conventional KSDFT results for bulk semiconductors. See Figure 7.

From the figure, it is clear that OFDFT can approach quantitative treatment of such semiconducting systems. Of course, optimism generated by that good HC KEDF performance is modulated by the reality that the tested semiconductor systems were part of the training set used to parametrize the functional. Subsequent application of the HC KEDF to systems outside the training set showed that HC is nevertheless a quality KEDF.[327]

However, that good performance is restricted to bulk systems. That limitation motivated a modification of HC to extend its applicability to highly inhomogeneous systems.[91] The modification addressed a numerically difficult aspect of the functional, namely the $s^2(\mathbf{r})$ dependence in the kernel eq 100. Simply replacing the $1 + \lambda s^2$ dependence with a PBE-like enhancement factor, $1 + \frac{as^2}{1+bs^2}$ with $a = 0.45$ and $b = 0.1$ (note that the dependence on λ disappears), delivered accurate surface energies and predicted surface morphologies for metals and selected semiconductors. The resulting KEDF is called revised HC (revHC). An important achievement was that revHC reproduced reasonably well the reconstructed Si(111) surface morphology predicted by conventional KSDFT.

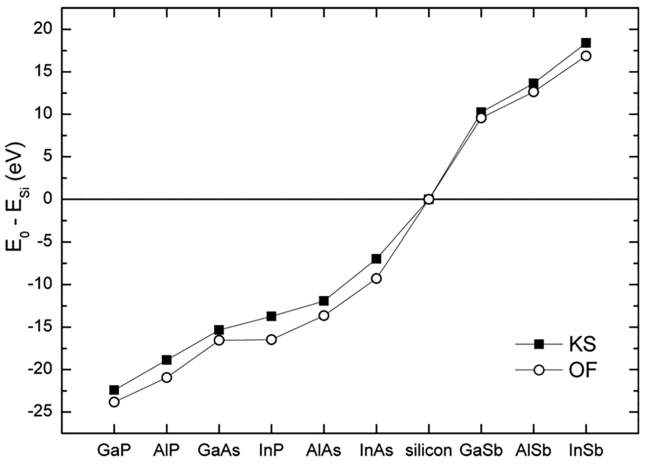

Figure 7. Energy differences (per primitive cell) between the diamond silicon and zinc blende phases of III−V semiconductors. OFDFT was carried out with the HC functional with parameters as in the text. Conventional KSDFT (denoted as "KS") calculations used the same local pseudopotentials for even-handed comparison. Reprinted with permission from ref 77. Copyright (2010) American Physical Society.

What about isolated systems, i.e., gas phase chemistry? The CAT family of functionals[43,299,319−321] gave a clear hint that if nonlocality is taken into account, isolated systems also could be approached by OFDFT in close-to-quantitative accuracy similar to what HC and revHC deliver for bulk systems and surfaces.

To understand recent progress on that issue, it is useful to take a step back historically. Harking back to functional integration, e.g. eq 77, Chai and Weeks[48] went to the potential (in essence v_θ) as the key. They developed a nonlocal functional that reduced properly to the TF and vW forms and had proper low-q or high-q linear response for weakly inhomogeneous systems. (Remark: We remark that q here is used in a way consistent with the literature. A more sensitive variable to use would be $\eta = \frac{q}{2k_F}$ because of its dependence on the local Fermi wavevector.) Both forms have the Pauli potential[328]

$$v_\theta^{CW2} = \frac{5}{3}c_{TF}n^{2/3}(\mathbf{r}) + \frac{10}{9\alpha}c_{TF}n^{\beta}(\mathbf{r}) \int d\mathbf{r}' f(|\mathbf{r} - \mathbf{r}'|; k_F(\mathbf{r}'))n^{\alpha}(\mathbf{r}') \quad (102)$$

with α and β constants related by $\beta = 2/3 - \alpha$. The value for the version that satisfies low-q constraints ("LQ") is $\alpha = \frac{1}{2}$, while large-q constraint satisfaction ("HQ") requires $\alpha = 2/3$. The Fourier transform of $f(|\mathbf{r} - \mathbf{r}'|; k_F(\mathbf{r}'))$ with respect to $|\mathbf{r} - \mathbf{r}'|$ for a fixed $\mathbf{r}'$ is known explicitly, $\hat{f}(\eta(\mathbf{r}')) = F_L(\eta(\mathbf{r}')) - 3\eta(\mathbf{r}')^2 - 1$ with $F_L(\eta)$ the inverse of the Lindhard response, eq 101.

https://doi.org/10.1021/acs.chemrev.2c00758
Chem. Rev. 2023, 123, 12039−12104

Whether to use the LQ or HQ version would seem to be another example of design choice, but the advantage of hindsight, specifically the development of the *N*-representability criteria already discussed,[259] enables a clear conclusion. For all but two of the 13 atoms they treated, self-consistent solution and use of the Herring path[245] with the LQ version gave $E_{tot}^{LQ} < E_{tot}^{KS}$. In contrast $E_{tot}^{HQ} > E_{tot}^{KS}$ for all 13 atoms. At least on that set, the HQ functional imputed from the HQ kinetic potential is *N*-representable. The LQ one is not. Encouragingly, the MARE for the HQ functional on those 13 atomic total energies was only about twice that of the much more complicated CAT functional (discussed above).[43,299,319−321]

The atomic densities at the nucleus $n(0)$ from HQ are much worse than from CAT however. Such differences led Chai and Weeks to discuss nonuniversality of KEDFs and KE potentials with respect to pseudopotentials (recall discussion of LKT above), apparently the first to do so.[48]

For application to solids with near linear-scaling, $O(N \ln N)$ with N the grid count, the HQ weight function was expanded in a Taylor series around a reference density[328] in a way similar to WGC and XWM two-point functionals.[49,297] (We remark that such a Taylor expansion is not strictly needed because of the simple dependence of the Chai−Weeks kernel on the local Fermi wavevector. Thus, spline techniques, such as those discussed next for LMGP and HC, would be applicable to this functional. Those techniques were not in common use at the time the Chai−Weeks functionals were proposed.) For crystalline Al, both the lattice parameters and the energetic sequence of phases (fcc lowest, then bcc, sc, diamond) came out correctly with HQ. For Si, though the lattice parameters were reasonable, the order of crystalline phases was completely wrong, sc, fcc, bcc, dia (most to least bound), vs the proper order of dia, bcc, sc, fcc.

We return to the Chai−Weeks scheme below. Here, we focus on the next use of the functional integration approach, the recent development of the LMGP two-point functional with a density-dependent kernel.[88] Based on the Mi−Genova−Pavanello (MGP) KEDF,[81] LMGP targets isolated systems by proposing a model second functional derivative of T_s. It is used in a manner similar to eq 79 (but limited to a single t integration) to yield a potential. The model second functional derivative is crafted so that it (1) reduces to the inverse Lindhard function for uniform densities; (2) is augmented by a term that imposes correct $1/q^2$ limiting behavior when $q \to 0$; (3) is symmetrized with respect to the interchange $n(\mathbf{r}) \leftrightarrow n(\mathbf{r}')$; and finally, (4) is fully density dependent, like HC and CAT. Full density dependence is computationally achieved in the LMGP family by a numerical scheme that is described in detail in Subsection 3.4.

The LMGP form for the second-functional derivative of the nonlocal part of the KEDF is

$$\frac{\delta^2 T_{NL}}{\delta n(\mathbf{r})\delta n(\mathbf{r}')} = \frac{\pi^2}{(3\pi^2)^{1/3}}(n(\mathbf{r}))^{-1/6} G_{NL}[n(\mathbf{r}), n(\mathbf{r}')] (|\mathbf{r}-\mathbf{r}'|)(n(\mathbf{r}'))^{-1/6} \quad (103)$$

Following eq 82, the Fourier transform of $G_{NL}[n(\mathbf{r}), n(\mathbf{r}')](|\mathbf{r}-\mathbf{r}'|)$ evaluated at the uniform density $n(\mathbf{r}) = n(\mathbf{r}') = n_0$ is related to the inverse Lindhard function:

$$G_{NL}[n_0](\eta) = -\frac{k_F}{\pi^2}\chi_{\mathrm{Lind}}(\eta)^{-1} - 3\eta^2 - 1 \quad (104)$$

with η defined as previously with a constant $k_F = (3\pi^2 n_0)^{1/3}$. Fourier transformation of $G_{NL}[n_0](\eta)$ leads to $G_{NL}[n_0](|\mathbf{r}-\mathbf{r}'|)$. This makes χ_{Lind} effectively a function of n_0. The dependence of $G_{NL}[n_0](|\mathbf{r}-\mathbf{r}'|)$ (shorthand notation G_{NL} below) on $n(\mathbf{r})$ and $n(\mathbf{r}')$ then is included approximately as follows

$$G_{LMGP}[n(\mathbf{r}), n(\mathbf{r}')] = G_{NL}[n_0 = n(\mathbf{r})] \quad (105)$$

The LMGP KEDFs include the correct $q \to 0$ limit by adding a term to eq 103 designed to mimic q^{-2} limiting behavior. Finally, an integration procedure brings the second derivative in eq 103 to the corresponding potential. The outcome is

$$\frac{\delta T_{NL}}{\delta n(\mathbf{r})} = v_{NL}(\mathbf{r}) = \int d\mathbf{r}' n(\mathbf{r}')\left[\int_0^1 dt \frac{\delta^2 T_{NL}}{\delta n(\mathbf{r})\delta n_t(\mathbf{r}')}\right] \quad (106)$$

where $n_t(\mathbf{r}')$ is defined as eq 78. Equivalently, eq 79 gives the energy.

When computing the t-path integral, whether numerically or analytically, we note that because of eq 105, the LMGP kernel imposes $t = t'$ in the integral eq 106. To ameliorate this approximation, kernels of imposed symmetrization were considered. For example, arithmetic symmetrization leads to the LMGPA functional

$$G_{LMGPA}[n_0 t, n_0 t'] \to \frac{1}{2}[G_{NL}[n_0 t] + G_{NL}[n_0 t']] \quad (107)$$

That provides an improved t-path integration compared to LMGP because in obtaining the potential one needs to impose $t' = 1$. A geometric symmetrization also was considered: see the Supporting Information document of ref 81 for more details.

The kernel resulting from the integration then depends on n_0 and is used in a similar way to eq 100 to obtain the potential

$$v_{NL}(\mathbf{r}) = n^{-1/6}(\mathbf{r})\mathcal{F}^{-1}[\Omega[n(\mathbf{r})](\eta(|\mathbf{G}|))\mathcal{F}[n^{5/6}(\mathbf{r}')](\mathbf{G})](\mathbf{r}) \quad (108)$$

Here $\Omega[n(\mathbf{r})](\eta(|\mathbf{G}|)) = \int_0^1 dt \mathcal{F}\left[\frac{\delta^2 T_{NL}}{\delta n(\mathbf{r})\delta n_t(\mathbf{r}')}\Big|_{n(\mathbf{r})=n_0, tn(\mathbf{r}')=tn_0}\right]$, $\mathbf{G}$ is the reciprocal space variable, as before, $\eta = \frac{|\mathbf{G}|}{2(3\pi^2 n_0)^{1/3}}$, and $\mathcal{F}$ is the Fourier transform operator. It is important to remark that while the model second functional derivatives have been symmetrized with respect to the t-path integration variable, the underlying approximation $n(\mathbf{r}), n(\mathbf{r}') \to n_0$ remains. Thus, in eq 108 above, the potential and the density in the kernel are evaluated at point $\mathbf{r}$, effectively imposing $n_0 = n(\mathbf{r})$ in the definition of the kernel. Such an approximate algorithm is dictated by computational scaling, which is kept at $N \ln(N)$. It would be much steeper and computationally prohibitive for the kernel to be formulated as a function of both $n(\mathbf{r})$ and $n(\mathbf{r}')$.

The performance of LMGP is more than satisfactory for metal clusters and III−V semiconductor quantum dots; see the discussion in Section 4. As we discuss later in this section, LMGP also has been employed successfully in subsystem DFT simulations.[89]

The development of HC and LMGP has motivated formulation of at least two further KEDFs, LDAK-X[90] and XWM.[49] "X" in LDAK-X gives the name of a parent functional from which the kernel is borrowed. For example, when X = MGP, the MGP kernel[81] is used. For X = WT, the WT kernel is used. LDAK-X, in essence, exploits the same underlying

https://doi.org/10.1021/acs.chemrev.2c00758
Chem. Rev. 2023, 123, 12039−12104

formalism as LMGP. However, it differs from LMGP in the definition of the energy. It avoids the potential-to-energy integration of eq 79 and instead defines an ad-hoc energy expression from which the corresponding potential is obtained by functional differentiation.[90] LDAK-MGP was shown to improve upon LMGP considerably for an array of clusters and other isolated systems.[90]

The XWM KEDF[49] handles the Fermi wavevector in a way similar to that in symmetrized CAT and WGC (see text after eq 96). Also similarly to WGC, a computationally amenable algorithm arises from Taylor expansion of the kernel around a reference constant density, n_0. As noted with other two-point functionals, that prescription makes XWM primarily suitable for bulk systems unless a recipe for n_0 is invoked (recall what is done with the WGC KEDF). A desirable alternative would be an algorithm or approximation that could evaluate WGC and XWM without explicit double integration or being tied to a reference density. However, as of now, such an algorithm has yet to be proposed.

A different approach has been pursued by the Della Sala group. They proposed two new types of nonlocal KEDFs with density-dependent kernels which are entirely defined in real space and do not rely solely on the Lindhard function: yGGA[329] and uGE4m.[291] These KEDFs extend meta-GGA functionals with the inclusion of nonlocal ingredients. Their energy expressions are based on enhancement factors

$$T_s^{uGE4m} = c_{TF}\int d\mathbf{r} n^{5/3}(\mathbf{r}) F_s(s^2(\mathbf{r}), q(\mathbf{r}), y_\alpha(\mathbf{r})) \quad (109)$$

$$T_s^{yGGA} = c_{TF}\int d\mathbf{r} n^{5/3}(\mathbf{r}) F_s(s^2(\mathbf{r}), q(\mathbf{r}), u(\mathbf{r})) \quad (110)$$

Here q is the reduced density Laplacian introduced at eq 58 and

$$u(\mathbf{r}) \equiv v_H(\mathbf{r}) = \int d\mathbf{r}' \frac{n(\mathbf{r}')}{|\mathbf{r}-\mathbf{r}'|} \quad (111)$$

$$y_\alpha(\mathbf{r}) = \frac{3\pi^2\alpha^2}{4k_F(\mathbf{r})}\int d\mathbf{r}' \frac{n(\mathbf{r}')}{|\mathbf{r}-\mathbf{r}'|} e^{-\alpha k_F(\mathbf{r})|\mathbf{r}-\mathbf{r}'|} \quad (112)$$

The enhancement factors were developed to satisfy a number of conditions. For example, uGE4m recovers the semiclassical expansion of neutral atoms for $Z \to \infty$.[291] Instead, yGGA focuses on reproducing the Lindhard response for uniform densities in the low q region. To achieve this, several enhancement factors were proposed, such as (we use a short-hand notation for the functions involved with all of the following being functions of $\mathbf{r}$: s, q, u, y_α, η_u, ν_u, n, x_1, and x_2),

$$F_s^{uGE4m} = +\frac{8}{81}q^2 - \left[\frac{1}{9} + \left(\nu - \frac{8}{243}f_1\right)\right]s^2 q + f_2 \nu s^4 \quad (113)$$

$$F_s^{yGGA} = \frac{5}{3}s^3 + y_\alpha G(s^2, q) \quad (114)$$

For F_s^{uGE4m} the values are $\nu = 0.1826$, $f_1 = (1 + a\,\nu_u^{1/2})^{-1/2}$, $f_2 = (1 + \nu_u^{1/2} + b\,\nu_u)^{-1}$, and $\nu_u = \frac{1}{1+\eta_u}$, where $\eta_u = \frac{u}{3(3/\pi)^{1/3}n^{1/3}}$. The parameters defining f_1 and f_2 are $a = 450$ and $b = 240$. For F_s^{yGGA}, i.e., the *yuk*4 functional from ref 329, the G function is defined as $G(s^2, q) = T_{3,3}(x_1)T_2(x_2)$, where $x_1 = -\frac{40}{27}s^2$, $x_2 = \frac{40}{27}q$, and $T_{\lambda(x)} = \frac{4}{\lambda}\frac{e^{\lambda x}}{e^{\lambda x}+1} + \frac{\lambda-2}{\lambda}$.

Although the uGE4m KEDF is applicable solely to finite systems (the u function is undetermined for periodic systems due to its divergence, which is canceled by charge neutrality in those systems), in application to a variety of isolated systems (jellium clusters, atoms, and molecules) it delivered good results. The yGGA KEDFs were benchmarked against jellium clusters and their ground-state response to external perturbations as well as atoms (non-self-consistently) and showed promising results. An implementation of yGGA functionals for nonspherical systems is not yet available. The recent introduction of these functionals suggests the need and opportunity for further assessment of them.

Another interesting approach[310−312] develops two strategies to obtain inverse KS response functions to be used to define KEDFs and their functional derivatives. The strategies differ in the way the response functions are represented. In the first case,[310,311] the response functions are mapped on an ad-hoc 1D coordinate. The map applied to the electron density is given by $n^e(\varepsilon) = \int d\mathbf{r} n(\mathbf{r})\delta(\varepsilon - v_{ext}(\mathbf{r}))$, which is valid only for isolated atoms and pure elemental crystalline solids. The KS response function therefore is transformed as $\chi_s(\mathbf{r}, \mathbf{r}') \to \chi_s(\varepsilon, \varepsilon')$, a form which can be handled more efficiently for inversion. In ref 312, the inversion is handled instead by a spectral representation of the response function. Once χ_s^{-1} is obtained, approximations for the non-interacting kinetic energy and its derivative are formulated as an expansion around a reference density, $n_0(\mathbf{r})$. Following eq 76

$$T_s[n] \simeq T_s[n_0] + \int d\mathbf{r} v_{T_s}(\mathbf{r})\delta n(\mathbf{r}) + \frac{1}{2}\int d\mathbf{r} d\mathbf{r}' \delta n(\mathbf{r})\chi_s^{-1}(\mathbf{r}, \mathbf{r}')\delta n(\mathbf{r}') \quad (115)$$

where $\delta n = n - n_0$. Even though the results in refs 310−312 seem encouraging, the approach needs further exploration and the underlying approximations need to be characterized and delineated more clearly before it can be considered viable for broad applicability.

Another interesting and potentially promising real-space route to construct KEDFs is to define a model 1-rdm that depends purely on the electron density. This was attempted by Chakraborty et al.[260,261] Given a 1-rdm, $\gamma(\mathbf{r}, \mathbf{r}')$, the kinetic energy associated with it is

$$T_s[n] = -\frac{1}{2}\int d\mathbf{r} d\mathbf{r}' \delta(\mathbf{r}-\mathbf{r}')(\nabla_{\mathbf{r}}^2 \gamma[n; \mathbf{r}, \mathbf{r}']) \quad (116)$$

Chakraborty et al. proposed model 1-rdms of the form

$$\gamma[n; \mathbf{r}, \mathbf{r}'] = \sqrt{n(\mathbf{r})n(\mathbf{r}')}\, g(k_F|\mathbf{r}-\mathbf{r}'|) \quad (117)$$

This form is motivated by DFA development for the exchange energy, as well as having some resemblance to two-point functional ingredients already encountered. The effective wavevector, k_F, however, is a function to be defined. It can be either local or nonlocal. In principle eq 117 is exact, as it is derived directly from the formal definition of the exchange energy in terms of the exchange hole.[102] Substitution of eq 117 in eq 116 gives

$$T_s[n] = \int d\mathbf{r}\frac{|\nabla n(\mathbf{r})|^2}{8n(\mathbf{r})} - \frac{3g''(0)}{2}\int d\mathbf{r} n(\mathbf{r})k_F^2(\mathbf{r}) \quad (118)$$

https://doi.org/10.1021/acs.chemrev.2c00758
Chem. Rev. 2023, 123, 12039−12104

where the double prime means second derivative.

Even though the function $g(x)$ should satisfy several known conditions (e.g., $g(0) = 1$, $g'(0) = 0$, $g''(0) < 0$, and $-1 < g(x) \leq 1$ for the case of $x \leq 0$), those are not sufficient to determine the function fully. In ref 260, the $g(x)$ for the HEG was chosen to ensure that the constructed KEDFs are exact for uniform densities, i.e.,

$$g_{HEG}(x) = 3\left(\frac{\sin x - x\cos x}{x^3}\right) \tag{119}$$

The remaining important step to generate a KEDF in this approach is to construct the effective Fermi wavevector, k_F, that appears in the argument of g in eq 117. A straightforward option is LDA in eq 94. That choice simply yields TFvW. Another option is the symmetrized two-point form defined in eq 97. In principle there are others. What Chakraborty et al. did was to impose the diagonal idempotency condition

$$\int d\mathbf{r}'\gamma(\mathbf{r}, \mathbf{r}')\gamma(\mathbf{r}', \mathbf{r}) = n(\mathbf{r}) \tag{120}$$

That leads to nonlinear integral equations that correspond either to the weighted density approximation (WDA) in the one-point case (1WDA) or the two-point WDA (2WDA) for k_F.

Benchmarks for the kinetic energies of H-Ar atoms and some small molecules showed that those functionals do not deliver quantitative accuracy. However, both the 1WDA and 2WDA improve considerably on the LDA results (i.e., $k_F(\mathbf{r}) = (3\pi^2 n(\mathbf{r}))^{1/3}$). Table 1 of ref 260 shows that the 2WDA KEDF gives kinetic energies lower than the reference for atoms larger than Si, an indication of non-N-representability. Figure 8

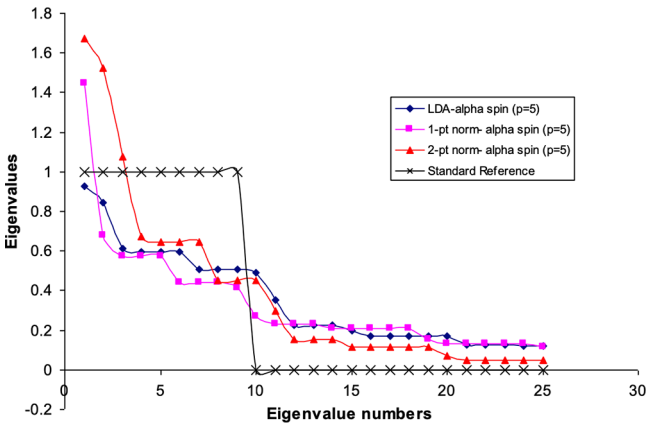

Figure 8. Natural orbital occupation numbers for the model 1-rdms for three choices of the effective Fermi wavevector to be used as the argument of the $g(x)$ function in eq 117: LDA, 1WDA (1 pt norm), and 2WDA (2 pt norm) for the argon atom. Calculations are spin polarized, and p corresponds to the value of the exponent γ (not to be confused with the 1-rdm which bears the same symbol) defined in eq 97), which is a parameter used in the symmetrization procedure of the model 1-rdms. Reprinted with permission from ref 260. Copyright (2017) Springer.

(taken from the paper) shows the eigenvalues of the model 1-rdms to have Pauli principle violations (i.e., eigenvalues larger than 1) for Ar, one of the atoms for which the KEDF gave a value below the exact T_s from conventional KSDFT. Interestingly, the figure also hints that the violations occur mostly for core orbitals. That suggests that non-N-representability might be more problematic for all-electron calculations than for pseudopotential-based OFDFT calculations.

Another interesting observation is the fact that, at least for Ar, the various approximations for the effective k_F function (LDA, 1WDA, 2WDA) lead to at most ensemble-N-representable densities with occupations smeared across several natural orbitals.

To recapitulate, though there is no two-point KEDF yet that works equally well for both isolated and bulk systems, substantial progress has been made. Density-dependent kernels are essential, both formally and practically. The double-integral computational burden can be avoided by a combination of splines and convolutions; see Subsection 3.4. At present, the HC and revHC functionals are perhaps still the best two-point functionals for bulk systems and surfaces. Encouragingly, as shown in Table 4 and Figure 6, there also are one-point KEDFs such as LKT[86] that exhibit comparable (or nearly so) accuracy. This suggests judicious use of both forms together as a possible way forward, as exemplified by the uGE4 and yGGA KEDFs we discussed. For isolated systems, the most advanced two-pointers are LDAK-MGP and LMGP. However, a better and more physical approach to the density dependence of the kernel is given by the CAT, WGC, and XWM functionals. The unresolved challenge to a full implementation of those functionals is to avoid double integrations or Taylor expansions.

2.4.3. Other Explicit KEDFs. Improvement of one- and two-point KEDFs of the types we have described thus far comprises the great majority of effort. We treat machine-learnt functionals separately below. But there are other lines of exploration of analytical forms. This section therefore provides a brief survey of those other lines of which we are aware, with a *crucial* caveat. Given the significance of DFT and of T_s in its utilization, it is essentially inevitable that we will have failed to notice some of those logic roads less-traveled. The reader thus cautioned, we press on.

Sporadically in DFT development since the publication of the HK theorems, the relationship of T_s to information theory concepts has drawn interest.[330] Such investigations date to Sears, Parr, and Dinur[243] in 1980. The part of their discussion that has remained relevant to OFDFT goes as follows.[192] Factor the number density $n(\mathbf{r})$ out of the squared-modulus of some N_e-body wave function of interest to get a conditional $N_e - 1$ electron density:

$$N_e\frac{\Psi^*(\mathbf{r}_1 \ldots \mathbf{r}_{N_e})\Psi(\mathbf{r}_1 \ldots \mathbf{r}_{N_e})}{n(\mathbf{r}_1)} := f(\mathbf{r}_2 \ldots \mathbf{r}_{N_e}||\mathbf{r}_1) \tag{121}$$

The expectation value of the N_e body KE operator then is

$$T[\Psi] = \frac{1}{8}\int d\mathbf{r}_1 \ldots d\mathbf{r}_{N_e}\frac{|\nabla_1 nf|^2}{nf}$$
$$= T_{vW}[n] + \frac{1}{8}\int d\mathbf{r}_1 \int d\mathbf{r}_2 \ldots d\mathbf{r}_{N_e-1}\frac{|\nabla_1 f(\mathbf{r}_1 \ldots \mathbf{r}_{N_e}||\mathbf{r}_1)|^2}{f(\mathbf{r}_1 \ldots \mathbf{r}_{N_e}||\mathbf{r}_1)} \tag{122}$$

The von Weizsäcker term is identified with the Fisher information entropy, a measure of localization. If the state $\Psi(\mathbf{r}_1 \ldots \mathbf{r}_{N_e})$ of interest is the full many-fermion ground state, the nonlocal term beyond T_{vW} has been called the correlation part[65,66,331,332] and is discussed in terms of the Shannon

https://doi.org/10.1021/acs.chemrev.2c00758
Chem. Rev. 2023, 123, 12039−12104

information entropy. (Note that this is *not* the correlation KE as defined in KS DFT; recall above.)

Of more direct relevance for OFDFT, if the state $\Psi(\mathbf{r}_1...\mathbf{r}_{N_e})$ is chosen to be the KS determinant, $\Phi_{KS}(\mathbf{r}_1...\mathbf{r}_{N_e})$, then eq 122 yields

$$T_s[\Phi_{KS}] = T_{vW}[n] + \frac{1}{8}\int d\mathbf{r}_1 \int d\mathbf{r}_2 ... d\mathbf{r}_{N_e-1} \times \frac{|\nabla_1 f_{KS}(\mathbf{r}_1 ... \mathbf{r}_{N_e}||\mathbf{r}_1)|^2}{f_{KS}(\mathbf{r}_1 ... \mathbf{r}_{N_e}||\mathbf{r}_1)} \quad (123)$$

Manifestly, the second term is $T_\theta[n]$, eq 35. Since $f_{KS}(\mathbf{r}_1...\mathbf{r}_{N_e}||\mathbf{r}_1) \geq 0$, this decomposition is a direct demonstration of Pauli term positivity and, hence, also of the lower-bound property of T_{vW}.

The same factorization route in fact was taken by Levy, Perdew, and Sahni[333] to demonstrate the existence, independent of the HK formulation of DFT, of a density eigenvalue equation akin to eq 38,

$$\left\{-\frac{1}{2}\nabla^2 + v_{\text{effective}}(\mathbf{r})\right\} n^{1/2}(\mathbf{r}) = \mu n^{1/2}(\mathbf{r}) \quad (124)$$

but with detailed contributions directly from the N_e-electron wave function and $N_e - 1$ conditional factor. Equivalent routes have been explored[334,335] in specific applications of the exact factorization approach.[336]

A different way to exploit the decomposition is to do a Levy–Lieb constrained search on the conditional factor $f(\mathbf{r}_2...\mathbf{r}_{N_e}||\mathbf{r}_1)$ via Monte Carlo calculations.[65,337] The approach is to use a model form for $f(\mathbf{r}_2...\mathbf{r}_{N_e})$ constructed by considering necessary conditions on the N_e-fermion wave function in conjunction with Monte Carlo sampling on the HEG over a finite range of comparatively high densities $0.55 \leq r_s \leq 1.81$. The result was a proposed KE functional which, in our notation, is

$$T_{GDS08}[n] = T_W[n] + \int d\mathbf{r} n(\mathbf{r})[A_1 + B_1 \ln n(\mathbf{r})] \quad (125)$$

with $A_1 = 0.860 \pm 0.022$ and $B_1 = 0.224 \pm 0.012$. Later another version[66] led to what was denoted as GHDS10,

$$T_{GHDS10}[n] = T_W + T_{TF} + \int d\mathbf{r} n(\mathbf{r})[A_2 + B_2 \ln n(\mathbf{r})] \quad (126)$$

with $A_2 = 1.02$ and $B_2 = 0.163$.

Both functionals have an evident information-theoretic structure and, as well, the same structure as the intrinsic free energy of the classical ideal gas; see ref 338, Secttion 3.1. That illustrates a problem discussed in ref 339. Both functionals violate the positivity constraint eq 35 except for certain density ranges. The analysis led to a proposed modified information-theoretical form that also is positive definite. How to implement that modified form is not obvious, since it relies on the use of a maximal bounding function for the density. The examples given in ref 339 suffice for the purposes of analysis but do not seem practical.

The GDS08 and CHDS10 KEDFs also violate uniform scaling requirements, a difficulty addressed by Delle Site[340] with an exponential ansatz for the conditional factor. That paper also connected the conditional factor to a classical partition function. Additional analysis in the broader context of information theory is in ref 341. More recently, Seshaditya et al.[342] have used the same approach to discuss changes in approximate functionals associated with changes in system dimensionality.

Two other connections deserve mention. There is a version of DFT formulated as a local thermodynamics which Nagy recently has shown to be connected with information theory. See ref 330 and citations therein. A version of the conditional probability factorization as an approach to the XC energy has appeared very recently.[343] In it, a classical approximation for the effect of the selected electron is exploited. So far as we know, the approach has not been applied to the KEDF problem.

An alternative route to constructing an approximate KEDF is one we have mentioned already, namely to approximate $v_s := v_{vW} + v_\theta$ directly. Given that, one could solve eq 38 self-consistently for $n(\mathbf{r})$. Then the total energy could be evaluated by either the virial relation, eq 45, or the line integral, eq 77, already mentioned. The approach via the virial relation (or similar "bi-functional"; see below) is particularly well adapted to single-point approximations. Such schemes are examples of potential functional theory.[344−347] They exemplify the observation that "An energy functional of the density is often useful even though the density is obtained by a separate method."[348]

Regarding OFDFT specifically, the potential functional approach in the one-point context seems to have been taken up first in earnest by Chai and Weeks[48,349] (their two-point scheme, discussed already, came later). In a way it was a confirmation of earlier study by Herring.[245] He had concluded that it seemed formidably difficult to devise a v_s approximation that satisfied the counterpart to the nonlocal spatial symmetry differentiation requirement, eq 85. Chai and Weeks argued, on the other hand, that the nonlocality of τ_s is substantially more complicated than that of v_s because the integral of τ_s over all space is required (recall the two-point argument) whereas v_s is local. In ref 349 therefore, they contrived a one-point scheme for the kinetic potential that, in our notation, has the Pauli part

$$v_\theta^{MTF} = \frac{5}{3}c_{TF}n^{2/3} - \frac{|\nabla n|^2}{8n^2} + \frac{1-\alpha}{4}\frac{\nabla^2 n}{n} \quad (127)$$

("MTF" means modified Thomas–Fermi, Chai and Weeks' term.) The value $\alpha = 1$ gives the correct Kato cusp condition behavior of $n(r)$ at atomic nuclei but poor $n(r = 0)$ values, a result that is unsurprising since the $\nabla^2 n$ contribution is removed from v_θ^{MTF} for that α. For the H atom for example, $v_\theta^{C-W} < 0$ for $r > 1.12$ au. To keep v_θ^{MTF} from going negative asymptotically for an exponential density requires $\alpha \leq \frac{1}{2}$. Chai and Weeks chose $\alpha = \frac{1}{2}$ for further investigation of MTF because that value gave the correct asymptotic behavior for n. That choice sacrifices the nuclear cusp condition, because v_θ^{MTF} has a negative singularity at the origin.

The bare density Laplacian in v_θ^{MTF} does not contribute to the linear response, so the MTF linear response is the same as from TFλvW with $\lambda = \frac{1}{2}$. Atomic total energies obtained from v_θ^{MTF} by the line integral method are below the KS values, so if v_θ^{MTF} corresponds to the functional derivative of some (unknown) T_θ^{MTF}, that putative KEDF is not N-representable.

As MTF is strictly local, Chai and Weeks addressed its deficiencies by constructing the nonlocal kinetic potential[48] that we discussed above; see eq 102 and text therewith.

https://doi.org/10.1021/acs.chemrev.2c00758
Chem. Rev. 2023, 123, 12039−12104

Construction of explicit potential functionals for OFDFT via exploitation of virial-type relations seems to have lain fallow until taken up again by Finzel and co-workers.[350−355] To summarize an extensive series of papers, introduction of explicit atomic shell structure is undertaken by exploitation of expressions akin to the virial relation, eq 45. Critically, however, they take it as a "bi-functional" of both $n(\mathbf{r})$ and some generating potential v_g,

$$T_\theta = -\frac{1}{2}\int d\mathbf{r} n(\mathbf{r})\mathbf{r}\cdot\nabla v_g(\mathbf{r}) \tag{128}$$

See Lemma 2, corollary in the Appendix of ref 35 for justification. If v_g were to be v_θ, the resulting T_θ value would be exact for the exact density. Instead what Finzel and co-workers consider is the construction of physically and chemically sensible approximations to v_g that may in fact not be the functional derivative of anything but nevertheless give T_θ estimates of useful accuracy.

Perhaps the starkest example is to use a stepped potential.[350] Here we give a slight generalization of that in the bifunctional setting to get to the proper result for a central-field atom of N_{shell} shells. Assume that the N_e-electron density is entirely inside a radius R_{shell}. Then

$$N_e = 4\pi\int_0^{R_{shell}} dr r^2 n(r) \tag{129}$$

Choose

$$v_g(r) = -\frac{1}{2\pi}\sum_{i=1}^{N_{shell}} k(r/R_{shell})\ln(r/R_{shell}) \tag{130}$$

and positive constants k_i such that

$$k(r/R_{shell}) := k_i; \quad r_{i-1} \le r < r_i; \quad i = 1, ..., N_{shells} \tag{131}$$

with $k_{i+1} > k_i$ to mimic mean shell energies, $r_0 = 0$, and the other r_i spaced in some chemically sensible way. Observe that the only character this v_g shares self-evidently with a proper atomic v_θ is that it is everywhere positive and decreases radially. For candidate density, eq 128 then gives

$$\begin{aligned} T_\theta[n] &= -2\pi\int_0^{R_{shell}} dr r^2 n(r) r\frac{\partial v_g}{\partial r} \\ &= R_{shell}\sum_{i=1}^{N_{shell}} k_i\int_{r_{i-1}}^{r_i} dr r^2 n(r) \end{aligned} \tag{132}$$

Ergo, one can get a sensible numerical value for the Pauli KE with a step-structured potential v_g that has no obvious relationship (indeed, may have none other than generic character) to the functional derivative $\delta T_\theta/\delta n$.

Much more realistic generating potentials can be constructed from atomic constituents or fragments of molecules or prototype molecules ("pro-molecules") assembled from atomic arrays. See refs 352−354. The challenge of this approach is, of course, that precisely because v_g does not have a known connection with some $\delta T_\theta/\delta n$, development of better v_g models requires very detailed and inventive analysis of the shell structure and bonding regions of highly diverse types of densities. The other issue is the candidate density itself. Again, pro-molecules are promising candidates.

Direct solution for the Pauli potential also has been considered via a differential equation. For that line, see refs 356 and 357. The essential idea is that the OFDFT Euler equation for $n^{1/2}(\mathbf{r})$, eq 38, and the differential equation for $v_\theta(\mathbf{r})$ can be solved self-consistently by cycling between solving for the density for a given $v_\theta(\mathbf{r})$ and then updating $v_\theta(\mathbf{r})$ with the new density. As actually implemented in the proof-of-concept calculation on the Be atom in ref 357, the differential equation for v_θ had contributions from the known solution to the ordinary KS problem. The argument in favor of pursuing the approach without such knowledge is that it may be easier to construct functions of $\mathbf{r}$ that approximate those contributions than it is to construct KEDFs, which are functionals of n.

A different kind of decoupling of the Pauli KE and the Pauli potential appeared very recently. Recall mention, at the end of Section 2.4.1, of the WPBEK GGA KEDF.[298] To cope with its positivity violations, those authors proposed a remedy that does not, in fact, depend on the details of F_θ^{WPBEK} but can be presented usefully for any GGA F_θ^{approx}.

As a first step, ref 298 introduces two reference enhancement factors [their eq 43],

$$F_{\theta,i}(s) = \frac{\exp \alpha s^2}{(1 + b_i s^4)^2} \qquad i = 1, 2 \tag{133}$$

They set $\alpha = \mu_T - (5/3)$ with $\mu_T = 5/27$ (from the gradient expansion) or 0.23889 (from the semiclassical neutral atom). The parameters b_i were determined by calculating

$$I_i = \int d\mathbf{r}\tau_{TF}(\mathbf{r})F_{\theta,i}(\mathbf{r}) \tag{134}$$

with the HF Li atom density for $i = 1$ and the HF Rn density for $i = 2$ and requiring that the results satisfy

$$\begin{aligned} T_{\theta,1} &< T_{\theta,Li} \\ T_{\theta,2} &> T_{\theta,Rn} \end{aligned} \tag{135}$$

The reference values on the RHS come directly from the atomic calculation by simple subtraction of the von Weizsäcker KE. The result is $b_1 = 50$ and $b_2 = 0.5$.

With the parameters set, the next step is to impose the condition

$$\begin{aligned} T_\theta^{approx} &:= \int d\mathbf{r}\tau_{TF}(n(\mathbf{r}))F_\theta^{approx}n(\mathbf{r}) = A_\theta I_1(n(\mathbf{r})) \\ &+ (1 - A_\theta)I_2(n(\mathbf{r})) \Rightarrow A_\theta = \frac{I_2 - T_\theta^{approx}}{I_1 - I_2} \end{aligned} \tag{136}$$

One therefore has a different Pauli enhancement factor that is properly positive but yields the same KE as the original F_θ^{approx}, namely

$$F_\theta^{mix} := A_\theta F_{\theta,1} + (1 - A_\theta)F_{\theta,2} \tag{137}$$

It is this F_θ^{mix} that would form the $v_\theta = \delta T_\theta/\delta n$ in the OFDFT Euler equation. Though ref 298 obtained numerical results solely post-SCF with HF atomic densities, a reasonably obvious next step would be to evaluate A_θ on a pro-molecule (to avoid having to calculate $\delta A_\theta/\delta n$ at each SCF cycle) and use the result as a GGA KEDF for the physical system for which the pro-molecule is the counterpart.

We conclude this section with pointers to three other elements of the literature. First, there is a relatively recent effort to formulate corrections to the TF density without the conventional gradient expansion.[358] The essential idea[359] is to

https://doi.org/10.1021/acs.chemrev.2c00758
Chem. Rev. 2023, 123, 12039−12104

"trotterize" the density written in terms of the time evolution given by the KS Hamiltonian

$$n(\hat{H}_{KS}(\hat{\mathbf{q}}, \hat{\mathbf{p}})) := \int_C \frac{dt}{2\pi i t} e^{-i\hat{H}_{KS}(\hat{\mathbf{q}},\hat{\mathbf{p}})t} \tag{138}$$

The contour is the real axis from $-\infty$ to ∞ with the exclusion of a small circle in the lower half-plane centered on the origin. Expressed in terms of the quantum mechanical position and momentum operators, the KS Hamiltonian is

$$\hat{H}_{KS}(\hat{\mathbf{q}}, \hat{\mathbf{p}}) = \frac{\hat{p}^2}{2} + \mu_{KS}(\hat{\mathbf{q}}|n) \equiv \frac{\hat{p}^2}{2} + \mu - v_{KS}(\hat{\mathbf{q}}|n) \tag{139}$$

With these expressions, one can construct approximate factorizations of the exponential. For example, the first correction past TF given in ref 358 is

$$U_5(t) = e^{-iy_1 t(\hat{p}^2/2)} e^{ix_1 t\mu_{KS}(\hat{\mathbf{q}}|n)} e^{-iy_0 t(\hat{p}^2/2)} e^{ix_2 t\mu_{KS}(\hat{\mathbf{q}}|n)} e^{-iy_2 t(\hat{p}^2/2m)} \tag{140}$$

with parameters x_1, x_2, y_0, y_1, and y_2 determined by analysis of the requirement $\nabla\nabla\mu_{KS} = 0$. Whether the various approximations that result from this procedure can be used to construct or constrain better KEDFs remains to be seen.

Second, semiclassical corrections to the TF model also have been attempted[25,40] and still are an active avenue of research.[360] For the sake of a contained presentation, we do not discuss these schemes further.

Third, though there has been considerable effort on local-scaling approaches to KEDFs, little seems to have occurred recently. Therefore, we refer the reader to refs 192 and 217 and references therein.

2.5. Machine-Learnt KEDFs

In recent years, machine learning (ML) methods have permeated most fields of science, including electronic structure theory.[361−365] The main focus has been to accelerate the computationally intensive parts of an atomistic model, from electronic structure with correlated wave function methods,[366−369] to the fitting of potential energy surfaces,[370,371] to the prediction of quantities specific to KSDFT.[82,83,147−154,372−381]

When fitting energy surfaces (either for small molecular systems or for condensed phases) the total electronic energy or potential energy surface is learned using an appropriate representation of the nuclear positions

$$\{Z_\alpha, R_\alpha\} \xrightarrow{ML} E(\{Z_\alpha, R_\alpha\}) \tag{141}$$

In the present context, this section focuses on ML techniques that can be used to predict electron densities, KEDFs, and other pure functionals of the density. The learning procedure therefore is centered on the founding theorems of DFT. Recall that they establish the bijective maps

$$n(\mathbf{r}) \leftrightarrow \mathcal{E}[n] \tag{142}$$

$$n(\mathbf{r}) \leftrightarrow v_{ext}(\mathbf{r}) \tag{143}$$

The map eq 142 has been exploited to learn XC DFAs in recent years with encouraging results for model systems[376] and molecules.[375,377,380] A general purpose double-hybrid XC DFA also has been optimized with supervised learning techniques.[382] Perhaps the most impressive achievement is the DeepMind21 (DM21) DFA.[381] It derives completely from a ML model trained on molecular data as well as fictitious systems carrying a fractional number of electrons. DM21 is found to treat systems successfully that are problematic for physics-based XC functionals (i.e., over-delocalization of the spin density and the treatment of electronic strong correlation). In a follow-up analysis,[383] DM21 was found to overestimate the hydrogen bond strength in water systematically, thereby pointing to the need for further improvement of the functional in order for predictive chemistry and materials science simulations to be undertaken with confidence.

Moving closer to the subject of this review, several works have focused on either the non-interacting kinetic energy or the general case,[82,83,147−150,152−154,360,373,374,378] eq 17, of the universal functional. As of now, ML KEDFs have not supplanted those developed from physical and mathematical reasoning as discussed in the preceding subsections. However, the general trend is that ML functionals improve as ML techniques also improve.[154]

An interesting and important hurdle that developers of ML-based functionals need to overcome is the inability, so far, of such functionals to provide accurate functional derivatives. Specifically, learning the energy functional does not guarantee the generation of an accurate functional derivative (the associated potential). Without that, the calculation of the density by direct minimization methods would be extremely challenging. Instead, the issue was tackled first by nonlinear denoising techniques.[373] Meyer et al.[155] as well as Ryczko et al.[160] showed that a neural network trained concurrently on the functional and its derivative achieved excellent results for both one-dimensional and complex three-dimensional systems. Ryczko et al.[160] also showed that it is possible to increase the number of training data points by utilizing density-KEDF pairs for non-self-consistent v_{KS} potentials. They could train a neural network with data extracted from only two single-point conventional KSDFT simulations.

In a recent study, Imoto et al. reported[158] encouraging results for selected bulk materials, ranging from metals to semiconductors and rock salt. The electron densities obtained from a ML model (neural network) improve upon the densities resulting from modern GGA KEDFs (such as PGSL[172] and LKT[86]). However, bulk properties derived from the model still are not competitive with physics-based KEDFs.

A fresh approach is simply to learn both the density-to-energy map and the external potential-to-density map as in eq 143.[148] It is worthwhile to sketch how the map in eq 143 was learned in ref 148 by use of kernel ridge regression. The density, $n(\mathbf{r})$, is given as a functional of the external potential, $n[v_{ext}](\mathbf{r})$, using a regression with a Gaussian kernel,

$$n[v_{ext}](\mathbf{r}) = \sum_i^{N_s} \beta_i(\mathbf{r}) k[v_{ext}, v_i] \tag{144}$$

Observe that the kernel function depends on the external potential v_{ext} as well as the external potentials considered in the training set, $\{v_i\}$, whose number of samples is N_s. The chosen Gaussian kernel has the form

$$k[v_{ext}, v_i](\mathbf{r}) = \exp\left[-\frac{\int (v_{ext}(\mathbf{r}) - v_i(\mathbf{r}))^2 d\mathbf{r}}{2\sigma^2}\right] \tag{145}$$

where σ is a hyperparameter of the regression. (Remark: Hyperparameters are adjustable parameters to fine tune the regression.) The electron density and the unknown functions,

https://doi.org/10.1021/acs.chemrev.2c00758
Chem. Rev. 2023, 123, 12039−12104

$\beta_i(\mathbf{r})$, were expanded in a plane wave basis. With that, eq 144 is cast as a linear system which is solved with order $O(N_s^3)$ operations. The scaling of the algorithm is deceptive because the linear system needs to be solved only once. Once the solution is found, the map in eq 143 has been learnt and can be evaluated with order $O(N_s)$ complexity through eq 144.

Once the map of eq 143 is known, it is natural to use the map in eq 142 to learn the electronic energy. This also was done in refs 84 and 148, which showed that the resulting method could be employed in an AIMD simulation of a medium-sized organic molecule recovering known dynamical processes. The regression in eq 144 naturally recovers the potential-to-density map for potentials close to the training set. Reference 84 further dwelled on this issue and showed that it is possible to learn a single map for a small set of chemically similar molecules (resorcinol, phenol, and benzene were tested).

The same research groups showed that the ML procedure can be improved further by relating high-level total energies (e.g., computed by coupled cluster methods) with the electron density from conventional KSDFT calculations with a GGA DFA (termed Δ learning). The outcome was results very close to those of the CCSD(T) reference. Those are much improved compared even to the conventional KSDFT values.[84]

Besides the work in refs 84 and 148, other lines of research for generating ML KEDFs have been to construct density-based descriptors (such as $n(\mathbf{r})$, $|\nabla n(\mathbf{r})|$, $\nabla^2 n(\mathbf{r})$) to be used as a basis to train neural networks (NN). In principle, however, only the electron density should be needed as its derivatives are purely dependent on the density itself. Meyer et al.,[155] for example, employed only $n(\mathbf{r})$ as the main descriptor.

There are studies that seek to learn the kinetic energy density,[83,150,153,154] an approach that implicates the gauge problem discussed previously. Interestingly, the ML focus in that context so far has been on the nonpositive definite KS KE density, i.e., $\tau_s(\mathbf{r}) = -\frac{1}{2}\sum_i^{\mathrm{occ}} \varphi_i(\mathbf{r})\nabla^2\varphi_i(\mathbf{r})$. However, because it differs from the positive-definite form (see eq 23) only in a surface term that depends solely on the density, $\frac{1}{4}\nabla^2 n(\mathbf{r})$, the learning procedure can be carried out on either form of the KS KE density.

An alternative to that approach proposed recently[159] is to learn a quantity that carries information about the Pauli potential, defined in eq 36, rather than the KE density. Reference 159 proposes to use the source of the Pauli potential, defined as $\rho_c(\mathbf{r}) = 4\pi\ \nabla^2 v_\theta(\mathbf{r})$, rather than v_θ itself. Though the results seem encouraging for predicting the electronic structure of atomic systems, the concept is fairly unusual and needs additional exploration and validation.

In the studies mentioned above, once the descriptors and the KS KE density, $\tau_s(\mathbf{r})$, and/or potential, $v_s(\mathbf{r})$, are generated by a conventional KSDFT calculation of the electron density, the NN can be trained against $\tau_s(\mathbf{r})$. There are various options for approximating energy and potentials by regression. However, it appears that convolutional NNs provide superior representation of both potential and energy[155] in comparison to kernel ridge regression because of their ability to capture nonlocal correlations (i.e., the ones that are captured by two-point functionals).

Another important line of research related to ML and DFT has been the quest to predict molecular and periodic system electron densities directly. The challenge addressed is this: given atom-centered descriptors, is it possible to predict the electron density of molecules and periodic systems? For example, in refs 384−387 the electron density is the target of various ML approaches. Virtually all methods surveyed utilize atom-centered basis functions to represent the electron density around each atom. The functions range from Gaussians multiplied by spherical harmonics to numerical functions. These produce electron densities with surprising transferability,[385] even though the deviation of the predicted densities from the parent KSDFT method averages a few percent (or a few tens of meV/atom when energies are considered[384,387]). While such accuracy can be regarded as already quite impressive, it still does not reach chemical accuracy.

It is clear that ML is making important contributions to KEDF development. They are almost certain to increase in number and impact, in parallel with ML development of XC functionals.[381,388] It also is clear that the same exact conditions that constrain the development of physics-based KEDFs should play an increasingly important role in ML-based KEDFs to guide the training toward accurate and transferable KEDFs.[149,372,389] See, for example, refs 381, 390, and 391.

2.6. Testing

From early on, KEDFs were tested for accuracy of their KE values calculated on HF densities. Though reasonably motivated in the sense of historical context, in our opinion there is little value to that procedure now (except perhaps for comparison with earlier literature). More than 15 years ago, ref 63 showed that a more meaningful post-SCF screening of KEDFs is to evaluate whether they give molecular binding when evaluated on the correct KS density (for a prescribed XC DFA of course). The argument is plain. A perfect KEDF would reproduce the binding energy and electron density (both as a function of geometric parameters) from the ordinary KS solution with a prescribed XC DFA. Evaluation of a candidate KEDF on the conventional KS density therefore tests whether that KEDF can deliver the right energy for the right density. If, at that stage, the deviations are larger than the target accuracy for the KEDF, then it is not worthwhile to test the v_θ for that KEDF in the OFDFT Euler equation. This is precisely the identification of functional-driven errors as distinct from density-driven errors as done for XC potentials in the conventional KS context, except that here the reference density is, of course, that from the conventional KS treatment.[392,393]

Reference 63 also made an explicit choice of criteria for testing. The limitations of simple GGA KEDFs led them to a design choice: "... we are compelled to refocus on the original objective: an OF-KE functional parametrization solely for reproducing the KS forces, irrespective of the resulting total energy." Because the forces on the atoms depend solely on the electron density, the requirement to match the forces determined by OFDFT with an approximate KEDF with the conventional KSDFT forces is equivalent to requiring matching of the electron densities of the two methods.

It is not uncommon to study results from a KEDF for which the errors may be below the conventional (orbital) T_s. Such cases are clear violations of N-representability. Therefore, it would seem to be more appropriate to emphasize those energy deviations that are below the conventional (orbital) T_s compared to those that lie above. Doing so would bias construction of KEDFs to minimize the likelihood of non-N-representability.

https://doi.org/10.1021/acs.chemrev.2c00758
Chem. Rev. 2023, 123, 12039−12104

As an example of retrospective testing, note that the non-N-representability of TFλvW with $\lambda < 1$ also means that both the HCD-1 and HCD-2[122] KEDFs also are not N-representable, since $T_{HCDi}[n] \leq T_{TF(1/5)VW}[n]$.

The gauge ambiguity of the KE density discussed above should be taken into consideration when devising measures for assessment of a KEDF. García-Aldea and Alvarellos[146] introduced what they called a quality factor, defined as

$$\sigma_{GAA} := \frac{\int d\mathbf{r}|\tau_s(\mathbf{r}) - \tau_{approx}(\mathbf{r})|}{T_s} \tag{146}$$

This measure tends to favor TF compared to many other one-point functionals. Considering the Teller nonbinding theorem,[39] that is not good. (Note that testing based on the mean absolute relative error, or MARE, also can favor TF, for example, with the Perdew−Constantin KEDF; recall the discussion just after eq 70 above.) However, the García-Aldea−Alvarellos measure does discriminate very clearly between Laplacian-dependent KEDFs and GGAs; see Table 1 in ref 233. This reinforces focus on the objective of the testing. The σ_{GAA} tests the approximate KE density, not the electron density or the possible non-N-representability of the functional.

Above we noted that other quality measures have been introduced and used sparingly, e.g. the "relative performance indicator"[291] and "global performance indicator".[172]

This summary illustrates that the OFDFT community is lacking an agreed-upon and comprehensive set of indicators of the quality of proposed KEDFs. Also missing are data sets of molecules, solids, and model systems on which to benchmark KEDFs. The contrast with quantum chemistry validation of XC DFAs via widely accepted data sets, for example refs 287, 394−398, is striking and needs to be addressed to expedite development and at the same time weed out unpromising avenues of research.

2.7. Going beyond Typical KEDF and Local Pseudopotentials

As already mentioned and as is discussed in detail in Section 3, current OFDFT simulation implementations for materials chemistry and physics applications rely on local pseudopotentials (LPPs). That effectively limits OFDFT simulations at present to that portion of the periodic table for which LPP-based KSDFT calculations reproduce the results of nonlocal pseudopotential conventional KSDFT calculations. We defer detailed discussion of LPPs to Section 3. Here we consider ways to avoid or reduce the challenge.

In addition to the LPP hurdle, as we have seen in the previous discussion, several of the currently best-available KEDFs are not broadly transferable. Recall, for example, the limitations from parametrization of the HC and WGC KEDFs.

Given these obstacles to wider use of OFDFT, it is unsurprising that approaches aimed at going beyond the basic OFDFT scheme have turned up. Some exploit a density decomposition approach in which $n(\mathbf{r})$ is split into regions that are treated individually with a suitably adapted KEDF. Others attempt to recognize orbital angular momentum locally in the KEDF and pseudopotentials. A third scheme is an approximate all-electron treatment via the projector augmented wave (PAW) scheme.[399] We review these approaches in what follows.

2.7.1. Density Decomposition-Based OFDFT. The insight behind the density decomposition approach[78,400] is that it is possible to distinguish regions wherein the local density variations dominate contributions to τ_s from those regions wherein nonlocal (delocalized) variations dominate. (The conceptualization resembles the cellular decomposition into spherical and interstitial regions of the augmented plane wave method.[401,402]) An early one-point version of the idea was put forth by Tal and Bader.[246] They wrote the density as the sum of an atomic-core-like part $n_1(\mathbf{r})$ and a more diffuse remainder $n_2(\mathbf{r})$ and wrote the KE density as $\tau_{vW}[n_1] + \tau_{vW}[n_2] + \tau_{TF}[n_2]$. We do not know of any subsequent exploration of this scheme. The present-day versions of density decomposition take the perspective that a one-point KEDF, $T_s^{(1)}$, should be adequate in the regions of localized densities while a two-point KEDF, $T_s^{(2)}$, would be used in the delocalized ("interstitial") type regions. As we have seen before, nonlocal KEDF kernels must have different limiting behaviors for $q \to 0$ for metallic or insulating systems. A density decomposition approach attempts to exploit this fact via the hope that the decomposed densities correspond closely enough to either metallic or insulating systems to be described by corresponding KEDFs.

A critical ingredient of any density decomposition scheme is a scale (or switching) function $F(\mathbf{r})$ which distinguishes the sought-after density regions, localized n_{loc} and delocalized n_{del}. Typically[78,403] $F(\mathbf{r})$ is chosen as a simple function of $n(\mathbf{r})$. Thus, the delocalized density is

$$n_{\mathrm{del}}(\mathbf{r}) = n(\mathbf{r})F(\mathbf{r}) \tag{147}$$

and the localized density is $n_{\mathrm{loc}} = n - n_{\mathrm{del}}$. The KS KE becomes

$$T_s[n] = (T_s^{(1)}[n] - T_s^{(1)}[n_{\mathrm{del}}]) + T_s^{(2)}[n_{\mathrm{del}}] \tag{148}$$

The accuracy of the approach depends on the choices for $T_s^{(1)}$ and $T_s^{(2)}$ (eq 148) and $F(\mathbf{r})$. A physically reasonable choice is to employ a semilocal functional for $T_s^{(1)}$ and either HC[403] or WGC[78] for $T_s^{(2)}$. When the WGC KEDF is adopted, the functional is named WGCD.

Such a decomposition scheme can be cast in a subsystem DFT framework,[78]

$$T_s[n] = T_s^{(1)}[n_{\mathrm{loc}}] + T_s^{(2)}[n_{\mathrm{del}}] + \underbrace{(T_s^{(1)}[n] - T_s^{(1)}[n_{\mathrm{loc}}] - T_s^{(1)}[n_{\mathrm{del}}])}_{\text{Non-additive } T_s^{\mathrm{nad}}[n_{\mathrm{loc}}, n_{\mathrm{del}}]} \tag{149}$$

However, as distinct from subsystem DFT[190] (see subsection below), the variational parameter is still the total electron density, n, not the decomposed densities. The variations in the localized and delocalized densities are propagated through eq 147, with the resulting contribution to the Euler equation

$$\frac{\delta T_s[n]}{\delta n} = \frac{\delta T^{(1)}[n]}{\delta n} - \left[\frac{\delta T^{(1)}[n_{\mathrm{del}}]}{\delta n} - \frac{\delta T^{(2)}[n_{\mathrm{del}}]}{\delta n}\right] \times \left(F(\mathbf{r}) + n(\mathbf{r})\frac{\delta F}{\delta n}\right) \tag{150}$$

The switching function must be chosen judiciously to avoid overcomplicated structure that makes implementation itself overly complicated.[169] One issue of complication is whether to make $F(\mathbf{r})$ a function independent of the electron density. In ref 78 that was not the case. Instead, the density-dependence of $F[n(\mathbf{r})]$ was determined from an extra self-consistent loop on the density; see Figure 4 of that paper and the attendant

https://doi.org/10.1021/acs.chemrev.2c00758
Chem. Rev. 2023, 123, 12039−12104

discussion. Such a loop amounts to approximating the $\frac{\delta F}{\delta n}$ contribution to eq 150. A simple numerical example[404] shows that the functional derivative has a change in sign with respect to n/n_{del}, behavior not found in the double-loop implementation of ref 78. To our knowledge, the effects of that discrepancy have not been studied.

The Carter group applied the density decomposition scheme to transition metals,[403] amorphous Li−Si alloys,[169] and covalently bonded molecules and materials.[78] The results, however, indicated that while the decomposition scheme can improve on the conventional OFDFT methodology (i.e., use of a single KEDF), it does not lead to a substantive, quantitative improvement. Renewed investigation may be an opportunity.

2.7.2. Angular-Momentum-Dependent OFDFT. Another spatial decomposition scheme to get around the limitations of LPPs for OFDFT applications was proposed by Ke et al.[161,405] Angular-momentum-dependent OFDFT (AMD-OFDFT; almost a misnomer) is a local hybrid approach in which an orbital-angular-momentum-dependent KE for each atom is constructed by way of auxiliary atom-centered 1-rdms. They connect an interstitial density (with no orbital dependence) with ionic cores that are represented by both nonlocal (NLPPs) and local pseudopotentials. The cores are treated solely with the auxiliary 1-rdms. Thus, the KS KE is partitioned into core contributions and an interstitial contribution. The partitioning is achieved by the KE density ansatz

$$\tau_{AMD}(\mathbf{r}) = \sigma(\mathbf{r})\tau_s(\mathbf{r}) + (1 - \sigma(\mathbf{r}))\tau_{KEDF}(\mathbf{r}) \tag{151}$$

where $\sigma(\mathbf{r})$ is a switching function and τ_s and τ_{KEDF} are the KE densities from the auxiliary 1-rdms and the approximate KEDF chosen for the interstitial region, respectively. Clearly there are some similarities with the decomposition methods just discussed, but both the regional treatment and manner of switching are different.

The auxiliary 1-rdms are generated starting from a muffin tin (MT) geometry[401,402] wherein atom-centered spheres are constructed, with the remaining volume being the interstitial region. Then the electron density is expanded in atomic-centered basis functions $\Psi_R(\mathbf{r})$ combined with the on-site density matrix elements, N_R, and the interstitial density, $n_I(\mathbf{r})$. Putting all this together

$$n(\mathbf{r}) = n_I(\mathbf{r}) + \sum_R N_R \Psi_R^*(\mathbf{r})\Psi_R(\mathbf{r}) \tag{152}$$

In doing so, the angular-momentum-dependent parts of the NLPPs can be accounted for though the use of the nondiagonal parts of the auxiliary 1-rdms. Note that the switching encoded by $\sigma(\mathbf{r})$ takes place at a radius greater than or equal to the cutoff radius of the NLPP.

In this way, the energy functional can be expressed in the general form

$$E^{OF}[\{N_R\}, n_I] = T_s^{KEDF}[n] + E_{XC}[n] + E_H[n] + E_{i-e}^{local}[n] + E^{NL}[\{N_R\}, n_I] \tag{153}$$

(The subscript "$i-e$" denotes ion−electron.)

The key part of this scheme is the nonlocal correction term which accounts for errors from the approximation of T_s^{KEDF} in the near-ion core region and includes the NLPP contributions. Ideally, E_{NL} would be precisely the difference between the conventional KSDFT and ordinary OFDFT total energies, namely

$$E^{NL} = E_{i-e}^{NLPS} + T_s - T_s^{KEDF} \tag{154}$$

AMD-OFDFT reproduces the bulk properties of titanium[405] (a transition metal, thus outside of the applicability of OFDFT with LPPs, at least so far). However, since its introduction, to our knowledge there has been no follow-up work to demonstrate applicability to the broader periodic table.

2.7.3. OFDFT with Nonlocal Pseudopotentials. To employ a NLPP in OFDFT, one can use a model 1-rdm. Recalling the subject of the work by Chakraborty et al.,[260,261] several approaches have been proposed for formulating a model 1-rdm. Xu et al.[406] exploited a prescription in which a Gaussian decaying 1-rdm is linked to a local KEDF energy density as follows,

$$\gamma[n](\mathbf{r}, \mathbf{r}') = \rho_q(\mathbf{r}, \mathbf{r}')e^{-s^2(\mathbf{r})/2\beta(\mathbf{r},\mathbf{r}')}\left[1 + A\left(\frac{s^2(\mathbf{r})}{2\beta(\mathbf{r}, \mathbf{r}')}\right)^2\right] \tag{155}$$

Here $\beta(\mathbf{r}, \mathbf{r}') = \frac{\beta(\mathbf{r}) + \beta(\mathbf{r}')}{2}$ with $\beta(\mathbf{r}) = \frac{3}{2}\frac{n(\mathbf{r})}{\tau_s[n](\mathbf{r})}$ and $\rho_q(\mathbf{r}, \mathbf{r}') = \left[\frac{n^q(\mathbf{r}) + n^q(\mathbf{r}')}{2}\right]^{1/q}$.

This model 1-rdm, evaluated with approximate KEDF energy densities was employed to determine the nonlocal part of pseudopotentials by tracing the 1-rdm with the nonlocal pseudopotential operator,

$$E_{NL}[\gamma, v_{NL}] = \int d\mathbf{r}d\mathbf{r}'\gamma(\mathbf{r}, \mathbf{r}')v_{NL}(\mathbf{r}, \mathbf{r}') \tag{156}$$

Results reproducing the structure of molten simple metal alloys were presented. In addition, and most importantly, encouraging results for bulk Be and Cd were presented.[406]

2.7.4. OFDFT with the PAW Method. Another interesting development along somewhat similar lines as the AMD-OFDFT scheme is the work by Lehtomäki et al.[120] It provides an implementation of semilocal OFDFT within the PAW scheme. The PAW method[399] is nowadays among the most widely used computational approaches to conventional KSDFT because of the clear advantage it provides over typical pseudopotentials. Specifically, PAW provides a way to reconstruct (approximately in practice) the total KS orbitals rather than just the pseudo-orbitals. This is an interesting advantage also in OFDFT because functionals can be evaluated on all-electron densities.

However, the PAW implementation of OFDFT is still in a relatively early stage. Thus far, it can support only semilocal KEDFs, thereby limiting its applicability and delivered accuracy. Comparison with two-point KEDFs (which only have implementations in more traditional pseudopotential schemes) also obviously is limited.[120,407]

2.7.5. Subsystem DFT: A Distinct Form of OFDFT Challenge. Quantum embedding is a divide-and-conquer strategy to partition a system (the "full system", hereafter) into interacting fragments with the aim of avoiding the calculation of full-system quantities[408,409] while maintaining an accurate quantum-mechanical description at least in the neighborhood of a subsystem of interest and, perhaps, globally as well. Several methods of this type have been developed, e.g., subsystem DFT,[180,181,189−191,410] density matrix embedding,[411−414] and Greens function embedding.[415−418] The quantum embedding methods differ mainly in two aspects. First is the way in which they define subsystems (using the electron density, the Greens

https://doi.org/10.1021/acs.chemrev.2c00758
Chem. Rev. 2023, 123, 12039−12104

function, or other quantities). Second is the way in which they describe the interactions between subsystems. This review focuses on OFDFT; thus, we concentrate our discussion on subsystem DFT.

Subsystem DFT is an appealing approach for large-scale simulations because it defines subsystems based on a partition of the electron density. Specifically, it uses a sum of subsystem electron densities

$$n(\mathbf{r}) = \sum_I n_I(\mathbf{r}) \tag{157}$$

Those replace the density of the full system, n, as the variational functions. In the same spirit as ordinary OFDFT, subsystem DFT exploits this decomposition via a reformulation of the non-interacting kinetic energy functional. It does so with an ansatz similar to eq 149, to wit

$$T_s[n] = T_s\left[\sum_I n_I\right] = \sum_I T_s[n_I] + \underbrace{\left(T_s[n] - \sum_I T_s[n_I]\right)}_{\text{Non-additive } T_s^{\text{nad}}[\{n_I\}]} \tag{158}$$

This decomposed form provides an important opportunity. The subsystem-additive part of T_s can be evaluated with KS orbitals specific to each subsystem. Those subsystem KS orbitals are not the same as the full system KS orbitals. For one thing, they are not required to be orthogonal with orbitals of other subsystems. The subsystem nonadditive part of T_s can be evaluated in practice with pure density functionals. Therefore, the ansatz in eq 158 provides a route for combining conventional KSDFT with OFDFT in a way that benefits the speedy calculation of molecular condensed phases.

The full energy given as a functional of $n = \sum_I n_I$ is found by substituting eq 158 in eq 27 and including the interaction with the external potential,

$$E\left[\sum_I n_I\right] = \sum_I T_s[n_I] + T_s^{\text{nad}}[\{n_I\}] + E_H\left[\sum_I n_I\right] + E_x\left[\sum_I n_I\right] + E_c\left[\sum_I n_I\right] + \int d\mathbf{r} v_{ext}(\mathbf{r}) \sum_I n_I(\mathbf{r}) \tag{159}$$

Note the explicit replacement of the full system density in the arguments of the functionals by the sum of subsystem densities.

We acknowledge that the first use of eqs 157−159 (as well as the derived functional derivatives and KS-like equations which are presented below in eqs 160−161) is credited to the works of Senatore and Subbaswamy[191] and later, provided a formal footing, by Cortona.[410]

We remark that the energy functional in eq 159 is formally equivalent to $E[n]$. Therefore, it can be used in a variational minimization equivalent to eq 19 achieved by searching over particle-conserving variations of each of the subsystem densities, $\frac{\delta E}{\delta n_I} = 0, \quad \forall I$. Doing so yields the so-called KS equations with constrained electron density,

$$\left[\frac{-\nabla^2}{2} + v_{KS}(\mathbf{r}) + v_{emb}^I(\mathbf{r})\right]\phi_i^I(\mathbf{r}) = \epsilon_i^I(\mathbf{r})\phi_i^I(\mathbf{r}) \tag{160}$$

In this expression, the KS-like potential, v_{KS}, is defined in eq 30 and is evaluated with the external potential $v_{ext}^I(\mathbf{r})$ associated with subsystem I, and $\phi_i^I(\mathbf{r})$ and $v_{emb}^I(\mathbf{r})$ are the KS orbitals and embedding potential of subsystem I, respectively. Equation 160 has the same structure as the KS equations for the isolated subsystem I. The crucial observation is that in eq 160 the effective external potential is not the external potential of the isolated subsystem but rather the sum of that external potential and the embedding potential, $v_{ext}^I(\mathbf{r}) + v_{emb}^I(\mathbf{r})$, which leads to a subsystem electron density, n_I, that generally differs from the electron density of the isolated subsystem. The embedding potential contains the functional derivative of the nonadditive KEDF given in eq 158. Specifically,

$$v_{emb}^I(\mathbf{r}) = \sum_{J\neq I}^{N_s}\left[\int d\mathbf{r}' \frac{n_J(\mathbf{r}')}{|\mathbf{r}-\mathbf{r}'|} + \sum_J v_{ext}^J(\mathbf{r})\right] + \frac{\delta T_s^{\text{nad}}[\{n_I\}]}{\delta n_I(\mathbf{r})} + \frac{\delta E_{xc}^{\text{nad}}[\{n_I\}]}{\delta n_I(\mathbf{r})} \tag{161}$$

with $\{v_{ext}^J\}$ being the external potentials associated with each fragment relating to the total external potential as $v_{ext}(\mathbf{r}) = \sum_I v_{ext}^I(\mathbf{r})$. We also have introduced the nonadditive XC functional, $E_{xc}^{\text{nad}}[\{n_I\}] = E_{xc}[n] - \sum_I E_{xc}[n_I]$. We remark that the decomposition of the external potential into subsystem contributions is not a necessary step.

Clearly, the accuracy of practical implementations of subsystem DFT is determined by the quality of the nonadditive KEDF employed as well as by the accuracy of the XC DFAs used to solve the KSDFT problems for the fragments. To control computational costs, semilocal nonadditive KEDFs typically are employed,[419] at most at the Laplacian level of complexity.[285] However, it is now common knowledge that semilocal nonadditive KEDFs do not provide a proper description of a regime in which the fragment electron densities overlap strongly.[180,181,420] As originally indicated by Wesolowski and Weber,[421] subsystem DFT carried out with approximate nonadditive functionals should target weakly interacting subsystems.

Mi et al.[89] adopted new-generation nonlocal nonadditive KEDFs in subsystem DFT calculations and showed that they improve the computed interaction energies and electron densities considerably compared to commonly employed GGA nonadditive KEDFs. This is especially the case when interfragment electron density overlap is non-negligible. In Section 3 we discuss that application in more depth.

An interesting line of research exploits a "bottom-up" approach rather than a "top-down" approach. That is, what are called the nondecomposable, nonadditive potentials (most commonly for the kinetic energy) rely on an ad-hoc ansatz for the nonadditive potential in an effort to obtain accurate densities and to impose known conditions on the potential[422] comparatively easily. Lastra et al. proposed the first nondecomposable, nonadditive kinetic energy potential,[423] followed by others.[424,425] We refer to ref 422 for additional details and a review of the relevant literature. We also note that error cancellation benefiting the value of KEDF approximants does not necessarily translate to advantageous error cancellation for the derived nonadditive functionals and nonadditive potentials (and thus electron densities).[189,426,427] Therefore, the bottom-up approach emerges as a viable alternative foregoing the definition of a parent KEDF and aiming to exploit beneficial

https://doi.org/10.1021/acs.chemrev.2c00758
Chem. Rev. 2023, 123, 12039−12104

error cancellation tailored specifically for nonadditive potentials.

Though our survey is not a complete overview of subsystem DFT, we point out some theoretical and practical complications about this method of which the reader should be aware. Gritsenko[428] showed that for subsystem DFT to have a properly defined minimum of the energy functional, eq 159, with respect to variations of each of the n_I, it is not enough to impose the requirement that n_I be v_{KS}-representable[106] (see discussion above eq 22). This is because at most one can define an *infimum* of the functional. A simple mathematical counterpart problem is one in which a function of a single variable, $f(x)$, is expressed as a function of two variables, e.g., $f(x) \rightarrow f(y + z)$. While $f(x)$ may have a well-defined minimum at $x = x_{min}$, the same cannot be said about $f(y + z)$ because the equation $y + z = x_{min}$ has infinitely many solutions. Though this nonuniqueness problem is severe in principle, convergence problems related to it (or traced to it) never have been reported to our knowledge for practical calculations that used finite basis set expansions of the subsystem KS orbitals and approximate nonadditive KEDFs.[180,181,429]

The formal framework of subsystem DFT requires that the subsystem densities be non-negative. That is, assuming a system is split into two subsystems with one having density $n_1(\mathbf{r})$ and the other $n_2(\mathbf{r})$, then the formal definition, from eq 157, requires $n_1(\mathbf{r}) = n(\mathbf{r}) - n_2(\mathbf{r})$. Therefore, if n_1 is chosen such that at some spatial points $n(\mathbf{r}) - n_2(\mathbf{r}) < 0$, the subsystem DFT procedure breaks down because of the non-N-representability of $n_1(\mathbf{r})$.[430] Such violation of the non-negativity condition is a critical problem for frozen-density embedding simulations.[431] In those, the environment density, n_2, typically is the one kept frozen. The violation is circumvented by subsystem DFT because the subsystem densities always are maintained as N-representable throughout the variational minimization by construction. We must remark that frozen-density embedding does not suffer from the nonuniqueness problem mentioned above,[428] as the energy density functional admits a unique minimum for a given choice of the frozen-density environment. (We note that the unique solution does not guarantee that the total density, given by the sum of subsystem and frozen densities, yields the true ground-state density; see ref 432.)

Beyond non-negativity, it is useful to consider cases in which a subsystem density vanishes. While that is unexpected in practical calculations, the implications nonetheless must be considered.[433] A clear limitation of the definition of the nonadditive functionals in eq 159 is that the functionals should share the same domain of functional differentiation. However, that can be the case only if all subsystem densities are nonzero everywhere in space. If one subsystem density goes precisely to zero inside a Lebesgue measurable volume element, then such a density is not v_{KS}-representable in a space that includes that volume. Therefore, the existence of the functional derivatives (and therefore the existence of the embedding potential in eq 161) on the entire space is subject to a positive definite condition for all subsystem densities.

Returning to the formal nonuniqueness of the partitioning in eq 158, it motivated the development of a number of embedding methods that provide a unique embedding potential. For example, partition DFT (PDFT)[434] and density functional embedding theory[435,436] partition the electron density in a way that reproduces the total density of a reference KSDFT calculation (even though the conventional KSDFT calculation is avoided[437]). There are approximate formulations of PDFT that exploit nonadditive KEDFs in a fashion akin to subsystem DFT.[437] When applied to PDFT, semilocal nonadditive KEDFs seem to yield comparatively better results than in subsystem DFT.[294] For example, preliminary results show that covalent bonds could be tackled by this method when a parametrized GGA nonadditive KEDF is employed.[293]

3. OFDFT IN PRACTICE

Along with construction of accurate KEDFs, it is critical to have appropriate OFDFT algorithms implemented in reliable, highly efficient codes. Unsurprisingly, for achievement of quasi-linear scaling, $O(N \ln N)$, the devil is in the details, with each of the total energy terms needing attention to obtain a fast codebase. Particular issues include construction of appropriate pseudopotentials for OFDFT (which, as already pointed out, differ from those for conventional KSDFT), approaches for optimization of the electron density, choices of basis sets for representing the density and potentials, and efficient algorithms for system sizes up to and beyond millions of atoms.

3.1. The Need for Local Pseudopotentials

In conventional KS calculations, treatment of the sharp cusps in the KS orbitals induced by nuclear attraction often is avoided by use of pseudopotentials (PPs) or effective core potentials. The reasons are twofold: (1) in periodic systems, PPs generate pseudo-orbitals that are smooth and, thus, can be expanded in a modest number of plane waves, and (2) elimination of explicit core electrons reduces the number of KS states to be computed, be they in a molecule or periodic system.

In OFDFT, PPs are needed for related reasons. First, use of a rather smooth pseudodensity allows evaluation of convolutions [an important class of integrals as will appear later, e.g., in eq 171] with numerical, discrete Fourier transforms. Second, as described in the preceding section, many modern KEDFs are calibrated in some way to the HEG and, thus, can be expected to yield best results for systems with comparatively smooth electron densities. In parallel, therefore, with many implementations of conventional KSDFT,[178,438−441] accurate and transferable electron−ion PPs are crucial ingredients for OFDFT simulations.[121,163−165,442]

In the context of conventional KSDFT, PPs have a local part and a nonlocal part and, hence, are nonlocal PPs, or NLPPs. To reproduce the effect of orthogonality between the valence and core orbitals, they use spherical harmonic projectors centered on the atoms. Those give rise to the so-called angular momentum channels of an NLPP. Observe that the meaning of "nonlocal" in connection with NLPPs is quite distinct from the meaning for nonlocal KEDFs. For NLPPs, the term signifies the explicit orbital dependence of the potential, not the spatial separation dependence of two-point functionals.

The typical approach is motivated by the plain fact that since the KS orbitals do not appear explicitly in OFDFT, any PP employed for OFDFT must not include angular momentum dependence and, hence, must be "local". These are denoted (recall above) as LPPs. However, it is possible, in principle, to use orbital-free prescriptions for the 1-rdm, for example eqs 118−120 as developed in ref 260 as well as prescriptions developed recently by Xu et al.[406] (see Subsection 2.7.3). Given the novelty of those approaches, they have not seen

https://doi.org/10.1021/acs.chemrev.2c00758
Chem. Rev. 2023, 123, 12039−12104

wide usage yet. Therefore, this section focuses on LPP development.

3.1.1. Early OFDFT Pseudopotential Prescriptions. Various LPPs proposed early on for OFDFT can be put into three broad categories.

Empirical or model LPPs[443−450] typically are comparatively simple analytic functions with parameters adjusted so that several physical properties (e.g., electron density, equilibrium volume, bulk modulus) calculated with the LPP fit experimental results or values from other (presumably reliable) electronic structure calculation such as conventional KSDFT. Empirical LPPs played an important role in early KEDF development, though they were derived mostly for metallic systems.[46,305,451−453] Empirical LPPs can be adapted successfully to complex simulations whenever the fitting procedure is successful.[450,454] However, fitting limits their transferability. That, no doubt, is a major reason why such PPs no longer see wide use.

An LPP can be contrived by selecting one of the l angular momentum channels of an extant NLPP. Such a simplified local pseudopotential cannot describe correctly the energetic properties of solid phases, even for simple alkali metal solids (bcc Cs and Rb).[455] Therefore, these no longer are used.

Atomic LPPs (ALPs) are derived by inverting the Kohn−Sham equations to reproduce the pseudodensity from a NLPP KSDFT calculation.[163,456] For group-IV elements, conventional KSDFT simulations with such potentials yield good results for bond lengths and lattice constants, but not for total energies and KS orbital energies.[456] Additionally, ALPs have been found to lack sufficient transferability and accuracy to be applicable to simple semiconductors such as Si.[163]

3.1.2. LPPs Currently Available for OFDFT. To obtain transferable LPPs, approaches have been devised to account for the specific chemical environment of an ion. Among them the bulk-derived LPP [BLP] type is perhaps the most widely used.[163,164,457] (Remark: In this section and beyond we use BLP, and the more frequently used acronym in the literature, BLPS or BLPSs, to indicate bulk-derived LPPs.) Compared with ALPs, BLPSs are obtained by inversion of the KSDFT electron pseudodensity from one or more bulk crystal systems instead of from atom densities. The first BLPSs, proposed by Watson et al.,[457] used OFDFT with a selected KEDF to reproduce, exactly, the reference density from a conventional KSDFT calculation with NLPP. The resulting LPP therefore was *KEDF-dependent*. Those LPPs gave good results for metallic systems, e.g., Li, Na, and Al, but had limited transferability beyond that range. To improve transferability, Carter's group proposed *KEDF-independent* BLPSs based upon inversion of the conventional KSDFT equations rather than the OFDFT equation.[163,164,458] The main algorithmic steps involved are

1. Obtain the target bulk crystal electron pseudodensity from conventional KSDFT calculations with a norm-conserving NLPP.
2. Obtain the effective conventional KSDFT potential, $v_{eff}(\mathbf{r})$, for the entire crystal from that target pseudodensity via the inverse approach[459]
3. Obtain the corresponding LPP for the bulk crystal, $v_{loc}(\mathbf{r})$, from that $v_{eff}(\mathbf{r})$, by removing the Hartree and XC potentials,

$$v_{loc}(\mathbf{r}) = v_{eff}(\mathbf{r}) - v_H(\mathbf{r}) - v_{xc}(\mathbf{r}) \tag{162}$$

4. Obtain the atomic pseudopotential, $v^{atom}(g)$ (where $g = |\mathbf{G}|$ and $\mathbf{G}$ is a reciprocal space vector), by dividing the Fourier transform of $v_{loc}(\mathbf{r})$, $v_{loc}(\mathbf{G}) = \mathcal{F}[v_{loc}(\mathbf{r})]$, by the structure factor $S(\mathbf{G})$ (which is the Fourier transform of the density of nuclear point charges (see Section 3.5.1):

$$v^{atom}(g) = \frac{1}{N_g} \sum_{|\mathbf{G}|=g} \frac{v_{loc}(\mathbf{G})}{S(\mathbf{G})} \tag{163}$$

Here N_g is the number of $\mathbf{G}$ vectors satisfying $|\mathbf{G}| = g$.

To gain transferability of the BLPSs, multiple bulk structures are considered in the process so as to include a large, varied sample of $\mathbf{G}$ points in eq 163. (The number of allowed $\mathbf{G}$ points is dictated by the specific crystal lattice.) Thus, the utility of $v^{atom}(g)$ depends strongly on the sampling of $v^{atom}(\mathbf{G})$ for the low-$\mathbf{G}$ vectors which, unfortunately, are not plentiful. Moreover, the inversion scheme to obtain $v_{loc}(\mathbf{r})$ typically does not yield the correct Coulombic tail decay. Therefore, additional fitting schemes are needed to obtain reliable BLPSs. Here, we do not review those technical details. The main principles are to try to obtain as closely as possible the correct Coulombic tail of the PP, while reproducing the bulk properties as well as possible. See refs 163, 164, and 442, 456.

BLPSs have been applied successfully to various bulk materials,[163,164] including the elemental Li, Mg, Al, Si, Ag, Ga, In, P, As, and Sb crystals and various III−V semiconductors;[77−79] liquid Li,[460] and to the melting temperature of Li.[461] In sum, KEDF-independent BLPSs seem to be the most accurate, transferable LPPs available presently for bulk systems.[462]

There have been attempts to improve BLPSs for liquid phases, leading to a strategy to construct "globally optimized" LPPs (goLPSs).[442] In that approach, BLPSs are modified by adding Gaussians with parameters fitted to minimize the difference between OFDFT and conventional KSDFT for calculated bulk properties and for forces on individual atoms in liquid phases. The goLPSs have been constructed for elements such as, Li, Ge, and Ga but are not available yet for other atom types. We remark that the procedure to obtain goLPSs does not rest on a formally justifiable footing and should, in our view, be considered to be a semiempirical parametrization of the OFDFT procedure.

Another constructive approach is the neutral pseudoatom (NPA) method.[463−465] It constructs LPPs referenced to an atom immersed in an approximate environment. Specifically, the atom is centered in a spherical cavity, subject to a uniform positive background of density equal to the mean valence electron density of the system under consideration. Often that reference is a liquid metal.[316,466,467] The cavity radius is determined by equalizing the positive charge removed from the hole with the total number of atomic valence electrons, hence the NPA name.[468] Anta and Madden[469] used such a reference system to develop KEDF-dependent ab initio LPPs, which were applied to liquid metal studies.[470] See also ref 471. Essentially the same approach has been used for many years in high-temperature systems, both as NPA and in "average atoms". The topic has become a specialty in its own right that no longer is strongly connected to OFDFT, so we leave it to refs 472−475 for leads to that literature.

Returning to explicit LPPs, the fitted normalized linear combination (FNLC) potentials are quite different. Karasiev and Trickey[121] proposed that alternative scheme. It uses information from each of the angular momentum channels,

https://doi.org/10.1021/acs.chemrev.2c00758
Chem. Rev. 2023, 123, 12039−12104

$v_{\mathrm{NL}}^{l}(\mathbf{r})$, of a reference NLPP in the form of a normalized average, to wit,

$$v_{\mathrm{FNLC}}(\mathbf{r}) = \frac{1}{\sum_{l=0}^{l_{\max}} c_l} \sum_{l=0}^{l_{\max}} c_l v_{\mathrm{NL}}^{l}(\mathbf{r}) \tag{164}$$

The weight of the contribution of each angular momentum channel, c_l, is adjusted so that conventional KSDFT calculation with the FNLC yields a good fit to selected equilibrium bulk material properties calculated with the original NLPP. Benchmark studies of Li and Al indicated that this approach can yield very good LPPs for Li and Al. However, those authors recognized the issue in their approach: "A remaining challenge for the OFDFT agenda is to construct a good LPP from an existing non-LPP without appeal to any bulk or aggregate system KS calculations".[121]

Mi et al.[165] took up that challenge with their proposal of optimal effective LPPs (OEPP). Inspired by the importance of the norm-conserving conditions satisfied by NLPPs for conventional KSDFT, they uncovered a fundamental relation between a norm-conserving PP and what could be construed as the ideal norm-conserving LPP, $v_{\mathrm{NCLPP}}(\mathbf{r})$,

$$\int_{\Omega} d\mathbf{r}(v_{\mathrm{NCLPP}}(\mathbf{r}) - v_{\mathrm{NL}}^{l}(\mathbf{r}))n_l(\mathbf{r}) = 0 \quad , \forall l \tag{165}$$

Here $v_{\mathrm{NL}}^{l}(\mathbf{r})$, $n_l(\mathbf{r})$, and Ω are, respectively, the l-th angular momentum channel of a norm-conserving NLPP, the pseudodensity of the l-th atomic orbital, and the region inside the core radius. By combining this relation with the optimized effective potential (OEP) concept already mentioned,[236,237,476−479] they showed that an optimized LPP should be constructed via a Slater-type pseudodensity-weighted average of the orbital-dependent norm-conserving PPs subject to preservation of the norm-conserving condition,

$$v_{\mathrm{OEPP}}(\mathbf{r}) = \frac{1}{n(\mathbf{r})} \sum_{l=0}^{l_{\max}} v_{\mathrm{NL}}^{l}(\mathbf{r}) f_l n_l(\mathbf{r}) \tag{166}$$

In the foregoing expression, f_l is the occupation number and $n(\mathbf{r}) = \sum_{l=0}^{l=\max} f_l\, n_l(\mathbf{r})$.

The corresponding algorithmic steps are simple. For a given electronic configuration and a given set of core radii r_l^c in the selected NLPP,

1. Obtain the LPP by calculating the density-weighted average as in eq 166;
2. For a single atom, compute the norm-conserving conditions and the deviations of the eigenvalues and pseudo-orbitals from a conventional KSDFT calculation with the OEPP versus those from the original NLPP;
3. Repeat the process by adjusting the r_l^c and electron configuration to optimize the OEPP.

We should clarify that there is a certain freedom in choosing r_{ell}^c when constructing NLPPs as long as their transferability and accuracy are maintained. However, OEPP depends on the parent NLPP through eq 166. Thus, r_{ell}^c can be used within that range to fine-tune the accuracy of the OEPP.

Benchmark tests demonstrated that high-quality OEPPs indeed can be constructed from a given norm-conserving PP without empirical fits for several atom types (e.g., most s/p-block elements except for the second row). Unfortunately, for second-row and 3−5d metals, a valid LPP with high transferability cannot be constructed because the NLPP potentials for different l's differ greatly and the norm-conserving condition of eq 165 for the LPP in eq 166 cannot be satisfied. Figure 9 provides a pictorial view of the

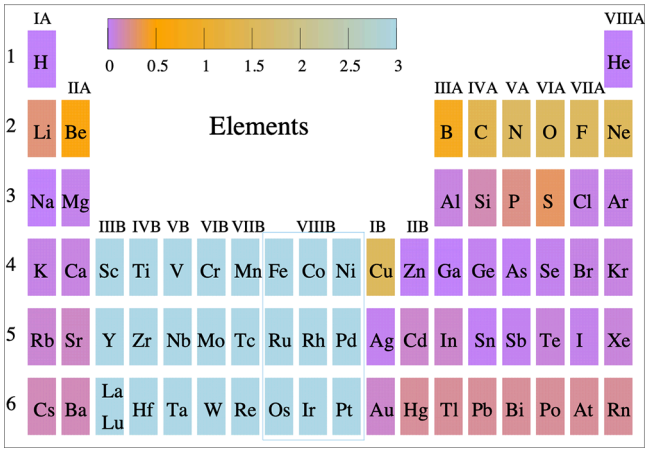

Figure 9. Color map representing the accuracy of OEPP pseudopotentials. The accuracy is assessed by the ability of the OEPP to reproduce the atomic pseudodensity of the parent NLPP as quantified by $\delta_n := \int dr 4\pi r^2 |n_{OEPP}^{ps}(r) - n_{NLPP}^{ps}(r)|$. Here $n_{OEPP}^{ps}(r)$ and $n_{NLPP}^{ps}(r)$ are the corresponding OEPP and NLPP radial pseudodensities, both computed with conventional KSDFT. The LDA XC functional was adopted. Reprinted with permission from ref 165. Copyright (2016) American Institute of Physics.

effectiveness of the OEPP method for each element of the periodic table. The metric used is the preservation of pseudodensity from NLPP to OEPP. Observe that the foregoing remark about the second row and the challenge of the 3d, 4d, and 5d metals is quite apparent.

In summary, there are two important comments to be made regarding pseudopotentials use in OFDFT. First, even though reasonably accurate and transferable LPPs are available for most light metallic elements and some main group elements, for most transition metals and second-row elements, the construction of LPPs with high transferability has proven difficult and may be essentially intractable. Second, our discussion makes clear that developing LPPs for OFDFT is a daunting exercise. Several guiding principles and procedures are available for their construction, but a clear winning strategy has yet to emerge. Thus, the requirement for LPPs is still very much an open problem for OFDFT and perhaps may be its Achilles' heel. New approaches, such as the one based on model 1-rdms summarized in Subsection 2.7, and very recent efforts involving machine-learning pseudopotentials[480] might prove to be breakthroughs for extending the applicability of OFDFT to a wide selection of elements in the periodic table.

3.2. Variational Optimization

Determination of the OFDFT variational minimum obviously is an optimization problem. The function to minimize is the number-conserving total energy Lagrangian, $\mathcal{L}[n]$, eq 28,

$$n_0 = \mathrm{argmin}_n \left\{ \mathcal{L}[n];\ n \geq 0,\ \int |\nabla n^{1/2}|^2 d\mathbf{r} < +\infty \right\} \tag{167}$$

$$E_0[n_0] = \mathcal{E}[n_0]; \tag{168}$$

The second line reproduces eq 19. Recall that the Lagrangian includes the chemical potential μ to enforce electron number

https://doi.org/10.1021/acs.chemrev.2c00758
Chem. Rev. 2023, 123, 12039−12104

conservation. The system volume for the integrations, Ω, can be the simulation cell for the case of periodic boundary conditions or the entirety of $\mathbb{R}^3$ for isolated systems.

As with conventional KSDFT, at least superficially there would seem to be two main approaches for carrying out the optimization. An "indirect" approach converts the minimization into a nonlinear self-consistent field (SCF) problem, while a "direct" approach proceeds as a constrained minimization problem.[481,482] We summarize key aspects of both.

3.2.1. Solution of the Euler Equation: The SCF and OE-SCF Methods. The indirect approach begins with the one-orbital, OFDFT Euler equation, eq 38, for the square root of the density,

$$\left\{-\frac{1}{2}\nabla^2 + v_\theta[n](\mathbf{r}) + v_{KS}[n](\mathbf{r})\right\}\psi(\mathbf{r}) = \mu\psi(\mathbf{r}) \tag{169}$$

where $n(\mathbf{r}) = |\psi(\mathbf{r})|^2$.

Because of the kinship of this equation to the conventional KS equation, one might expect that efficient basis-set methods developed for solution of that equation could be applicable straightforwardly to the OFDFT problem. There are statements to that effect in the literature.[333] The idea is that a conventional KSDFT SCF code could be converted to SCF solution of eq 169 simply by adding v_θ to v_{KS}, changing the normalization (from 1 to $N_e^{1/2}$), and selecting the lowest eigenvalue. What Chan et al.[119] found is that the prescription does not work in practice and, hence, that more robust minimization techniques were needed.[119] Subsequently, Karasiev and Trickey[121] confirmed that finding for both atoms and diatomic molecules and for both a Gaussian-type and numerical orbital basis. Note that both papers reported all-electron calculations. Quoting from ref 121, "... use of standard KS codes to solve the OFDFT Euler equation as a modified KS eigenvalue problem is problematic at best. At least for the all-electron case, it seems implausible as a productive route to routine OFDFT calculations."

Shao et al.[462] explored this issue with the pseudopotential code DFTpy and showed that the main reason for the failure of customary SCF techniques in the OFDFT context is HOMO−LUMO orbital swapping that arises quite commonly in nearly degenerate systems. As system sizes increase, the HOMO−LUMO gap computed from the OFDFT Hamiltonian with eq 169 decreases; see Figure 10.

To resolve that near-degeneracy problem in conventional KSDFT calculations, it suffices to level shift or to open the minimization to the set of *ensemble N*-representable densities computed from several states above the HOMO level and then to smear the occupations[483] (typically with the Fermi−Dirac distribution). Doing so for the OFDFT one-orbital equation would defeat the purpose, since it would involve solving the eigenvalue problem for several levels, hence a regression to a $O(N^3)$ scaling method.

A modified SCF procedure, termed the one-orbital ensemble SCF (OE-SCF), solves that problem.[462,484] To consider ensemble *N*-representable densities in OFDFT, OE-SCF begins by direct minimization of $T_{vW}[n] + E_H[n] + E_{xc}[n]$. The Pauli potential is fixed for that minimization and then updated and a new optimization done. These steps are cycled until self-consistency (hence the name OE-SCF, even though no diagonalization ever occurs). Tests show that OE-SCF converges as well as the commonly adopted direct energy minimization of the full energy functional (see next section)

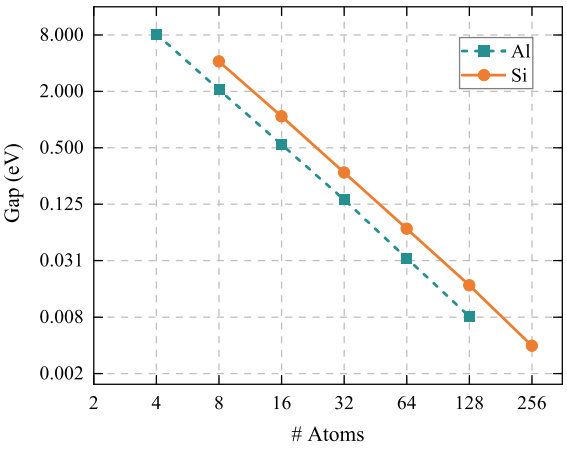

Figure 10. Energy gap between the lowest two energy levels associated with the eigenvalues of the OFDFT Hamiltonian in eq 169 for supercells of Al and Si bulk systems. The plot, in log scale, displays a monotonically decreasing gap with system size. The LMGP KEDF and LDA XC functionals were used. Reprinted with permission from ref 462. Copyright (2021) American Chemical Society.

with one important additional benefit. The Pauli potential needs to be evaluated only a handful of times during the minimization (i.e., once per SCF cycle). For complicated two-point KEDFs, that can yield a large reduction in computational cost, as much as by orders of magnitude.[462] In Section 4, we report how OE-SCF enables large-scale simulations of complex systems to be done with otherwise computationally expensive nonlocal functionals with a density-dependent kernel, such as LMGP.

OE-SCF currently is implemented in the DFTpy[54] and ATLAS[53] codes. As OE-SCF is rather new, most OFDFT codes still exploit direct energy minimization, to which we turn next.

3.2.2. Optimization by Direct Minimization. There is an immense literature on generic direct optimization, so we note only the aspects directly pertinent to OFDFT implementation here.

Algorithms for direct address of eq 167 must explore variations of a single function of three-dimensional space. To do so typically requires parametrization of the argument function, *n*, either by expansion in a basis set or by direct discretization of space (which logically is a basis set of delta functions). Thus, the problem becomes the minimization of a function of many variables (proportional to the number of discrete points or basis functions). That can be a simple task for atomic systems rendered in an atom-centered basis. But even in modeling of clusters, the number of variational parameters becomes large enough to require the development of ad-hoc optimizers.[119,485] When bulk materials are considered, discretization of space with regular grids is the usual choice. That allows use of discrete Fourier transforms to represent the electron density and the potentials and for solving the Poisson equation associated with the classical Coulomb energy (see next section).

Energy minimization algorithms typically include the following steps to obtain the quasi-orbital, ψ, see eq 169:

1. Obtain the optimization direction vector in the space of the variational parameters, $\mathbf{p}_k$.
2. Find a reasonable step size λ_k along the vector $\mathbf{p}_k$.

https://doi.org/10.1021/acs.chemrev.2c00758
Chem. Rev. 2023, 123, 12039−12104

3. Generate an improved quasi-orbital, $\psi_{k+1}(\mathbf{r})$, updating the one from the previous optimization step, $\psi_k(\mathbf{r})$, with $\mathbf{p}_k$ and λ_k.
4. Iterate until convergence criteria are satisfied.

Many algorithms from the optimization literature can be employed for step (1). Some of those provided in the available OFDFT software[53,54,486] include steepest-descent (SD), nonlinear conjugate gradient (CG),[487−493] limited memory Broyden−Fletcher−Goldfarb−Shanno (L-BFGS),[494] and truncated Newton (TN) methods.[495] Because of efficiency limitations on SD and storage limitations for L-BFGS, CG is the most widely used of these. It is possible to improve its computational efficiency by adopting a precondition procedure, an option that has been explored for OFDFT by Hung et al.[496]

We note that L-BFGS stands out for its stability, with several available options for updating the search direction, p_k. Because, however, it requires the storage of prior $\psi_k(\mathbf{r})$ and gradients, its memory cost is larger than that of any of the other methods mentioned.

For step (2), the step size, λ_k could be determined by direct approximation[485] (as in the SD method) or by line search.[53,54,486] Determination by direct approximation, however, causes the stability of the optimization to be quite system dependent. In contrast, line search is numerically stable, so it is used rather generally in OFDFT codes. Line search stability arises from imposition of the so-called Wolfe conditions; see ref 497.

The most direct way to accomplish the third step, update of ψ_{k+1}, would be $\psi_{k+1} = \psi_k + \lambda_k p_k$, followed by normalization of the total density to N_e. That procedure is not always stable. The problem has an elegant solution in the form of a scheme that makes the p_k contribution orthogonal to ψ_k. Thus, the update becomes[485]

$$\psi_{k+1} = \psi_k \cos(\lambda_k) + p_k \sin(\lambda_k) \tag{170}$$

which maintains the normalization of electron density at every step.

The Trust-Region Image Method (TRIM)[498] is another elegant solution to the problem of energy minimization subject to the constraint $\int d\mathbf{r}\, n(\mathbf{r}) = N_e$. In short, TRIM exploits a grand canonical formulation of OFDFT, finding that the minimum problem with respect to $n(\mathbf{r})$ is actually a saddle point minimax optimization with respect to n and the chemical potential, μ. The energy functional is found to be convex with respect to n and concave with respect to μ. Ryley et al.[498] derive expressions for the gradient and the Hessian with respect to variation of the chemical potential and the electron density (which they parametrize in terms of Gaussian-type orbitals). That provides a density optimization method that is robust and requires fewer iteration to convergence than the method of Chan et al.[119] Unfortunately, no comparisons to the method of Jiang and Yang[485] have been reported. Therefore, it is difficult to assess the relative robustness of TRIM compared to the density optimization methods exploiting eq 170 as commonly implemented in pseudopotential codes such as PROFESS and DFTpy.[54,486]

3.3. Basis Sets

As just surveyed, whether the energy minimization is direct or indirect, it is always necessary to express functions in terms of a basis. Though any complete set would do in principle, in practice the choice of basis is critical to determining the range of applicability of the software. Basis sets employed currently include plane waves (PWs),[481,482,499] atomic orbitals (AOs) (e.g., Gaussian-type-orbitals (GTOs)[500]), finite differences (FDs),[501,502] finite elements (FEs),[501] and wavelets.[503−505] The majority of OFDFT software to date is targeted at materials problems (hence, periodic boundary conditions); thus, a discretization of space well-adapted to that periodicity is used. Therefore, in this section we discuss the PW, FE, and FD approaches and refer the reader to the references above regarding the other ones.

3.3.1. Plane Wave Basis. Plane waves (PWs) are the most widely used basis functions in electronic structure calculations for materials science.[481,482,499,506] Generally, PWs confer the following advantages:[481,482,499]

1. Independence from nuclear (ionic) positions avoids Pulay forces[507] and provides a uniform resolution description in all space;
2. Calculation of derivatives of $n(\mathbf{r})$ requires only algebraic operations in reciprocal space. [Remark: The derivative of any real-space function, $f(\mathbf{r})$, is straightforward in reciprocal space, $\nabla f(\mathbf{r}) = \frac{1}{(2\pi)^3}\int d\mathbf{G}\, i\mathbf{G}\tilde{f}(\mathbf{G})e^{i\mathbf{G}\cdot\mathbf{r}}$, where $\tilde{f}(\mathbf{G})$ is the Fourier transform of $f(\mathbf{r})$.] Depending on the pseudopotential used, derivatives of the total energy with respect to geometrical parameters (e.g., force and stress) are simple;
3. Imposition of periodic boundary conditions is straightforward;
4. Systematic improvement of the basis set is provided simply by setting the wave vector cutoff;
5. Quantities expressed in real space can be transformed efficiently to reciprocal space by use of Fast Fourier Transforms (FFTs), with a computational effort that is almost linear scaling, $O(N \ln N)$.

Even though recent progress on one-point KEDFs[86,87] has resulted in functionals capable of describing condensed phase systems (recall Section 2), two-point functionals continue to dominate in materials science applications.[145] For them, the basis set employed must permit efficient KEDF evaluation to retain the quasi-linear scalability of OFDFT. PWs are well suited for that because the double-integration formula in eq 13 can be simplified greatly when a homogeneous system is considered. In that case, the kernel $\omega(\mathbf{r}, \mathbf{r}') \equiv \omega(|\mathbf{r} - \mathbf{r}'|)$ and the convolution theorem can be exploited to turn eq 13 into

$$T_s^{\mathrm{nl}}[n] = T_{TF}[n] + T_{vW}[n] + \int d\mathbf{G}\tilde{n}^{\alpha}(\mathbf{G})\tilde{\omega}[n](|\mathbf{G}|)\tilde{n}^{\beta}(-\mathbf{G}) \tag{171}$$

Because $n(\mathbf{r})$ is a real function, the integral can be simplified further by exploiting $\tilde{n}(-\mathbf{G}) = \tilde{n}(\mathbf{G})$. Overall, the $O(N \ln N)$ scaling is retained.

The quasi-linear scaling is maintained roughly even when more complicated nonlocal functionals are considered, such as those with density-dependent kernels, $\omega(n(\mathbf{r}), |\mathbf{r} - \mathbf{r}'|)$ as in HC,[77] LMGP[88] and LDAK;[90] or $\omega(\xi(\mathbf{r}, \mathbf{r}')|\mathbf{r} - \mathbf{r}'|)$, as in WGC[297] and XWM.[49] Recall the discussion in Subsection 2.4.2. At first glance, the computational cost for such functionals would seem to scale quadratically with the number of grid points. In Subsection 3.4, we discuss the details of the evaluation in a PW basis set for functionals of this type such that linear scaling with system size is maintained with a moderate prefactor.

PW basis sets are not without drawbacks. Probably the most significant is the one we have discussed already, the necessity

https://doi.org/10.1021/acs.chemrev.2c00758
Chem. Rev. 2023, 123, 12039−12104

of pseudopotentials.[481,482,499,506,508] Recall Subsection 3.1. That removes all-electron calculations from the picture. (There is KSDFT software for the all-electron linearized augmented plane wave basis (LAPW).[402,509−512] However, that basis is atom-centered and muffin-tin-based and, hence, quite ill-suited to AIMD.) An excellent compromise for the PW basis is provided by the PAW method.[120,399] In conventional KSDFT calculations, PAWs seem largely to have supplanted NLPPs. As we noted in Subsection 2.7.4, the PAW ansatz needs substantial further exploration in connection with OFDFT.

Another drawback of the PW basis is the inherently three-dimensional periodicity in the computation of the classical electrostatic potential. This is introduced by use of the periodic Coulomb kernel, $f_h(G) = \frac{4\pi}{G^2}$ for reciprocal space vector $\mathbf{G}$, yielding a Hartree potential in reciprocal space

$$v_H(\mathbf{G}) = \frac{4\pi}{G^2} n(\mathbf{G}) \tag{172}$$

Unfortunately, for intrinsic system periodicity lower than three dimensions, the common algorithm is not ideal.[513] Corrections, however, exist, both at the level of the energy functional[514] and for the electrostatic potential.[515−517] Those typically only add a small prefactor to the simulations. Alternatively, real-space Poisson solvers can be employed.[501,502,517] Note that this problem occurs in both OFDFT and conventional KSDFT.

A potential drawback for massively parallel implementations is the need for "all-to-all" communication among the processors needed by the FFT.[502,518] Though this problem cannot be circumvented entirely, currently available parallelization schemes are robust and have been shown to maintain linear scalability of the algorithm.[519,520] We discuss this aspect further in Subsection 3.5.2. Again, we point out that parallel limitations for FFTs are not specific to OFDFT. Conventional PW-basis KSDFT codes have the same problem.

3.3.2. Real-Space Representations. Among real-space basis sets, perhaps the most direct and easy approach is FD.[521] In it, the values of both $n(\mathbf{r})$ and the potentials are given on a discrete grid of real-space points.[522] Accordingly, the Hamiltonian also must be discretized. Thus, the key aspects of the FD method are the discretization of the Laplacian operator for the evaluation of the von Weizsäcker kinetic potential and solution of the Poisson equation for the electrostatic potential. Denoting the grid point positions as (x_i, y_i, z_i), the expansion of the Laplacian operator acting on ψ for coordinate x is

$$\frac{\partial^2 \psi(\mathbf{r})}{\partial x^2} = \sum_{n=-N_f}^{N_f} C_n \psi(x_i + nh, y_j, z_k) + O(h^{2N+2}) \tag{173}$$

where h and N_f are the grid spacing and order of the FD expansion, respectively, and C_n are Taylor expansion coefficients. Algorithmic details and results are found in refs 501 and 502.

The truncation error $O(h^{2N+2})$ introduced by the Taylor expansion can be controlled by tuning the expansion order and grid spacing. For low-order FD expansions, sparse linear algebra leads to further computational efficiency. Note that when $\psi(\mathbf{r})$ is used to evaluate physical quantities such as the Hartree energy, the error originating from the series truncation can be of either sign and cannot be controlled systematically. Thus, the FD approximation may lead to nonpositive definite Hamiltonian approximations that could result in variational breakdown.[501]

For a non-Cartesian grid, an additional important detail is that a direct discretization of the Laplacian operator contains $O(N_f^2)$ terms in the summation because of the need to include off-diagonal neighboring points in a square of size $(2N_f + 1)^2$ around any given point. That would impose a high computational scaling prefactor. To solve the problem, Tiago et al.[523] presented a generalized high-order FD method that bypasses the evaluation of mixed-derivative terms by employing a weighted combination of derivatives along the three original directions and three additional nearest-neighboring directions. That reduces computational cost significantly. The approach has been adopted in the ATLAS code.[53] To improve FD computational efficiency further, it is possible to define grids of different resolution depending on the spatial region.[502,524] Though double-grid and multigrid methods[501,525] have been deployed in ordinary KSDFT solvers, their usefulness in OFDFT implementations has yet to be assessed.

FD provides some advantages over PW for the evaluation of semilocal functionals. From Figure 11 it is clear that for large systems FD outperforms PW for the von Weizsäcker functional. FD, however, is not well-suited to evaluate nonlocal functionals. Thus, typically PW and FFTs are favored for them. However, real-space approaches to evaluate nonlocal functionals exist (*vide infra*).

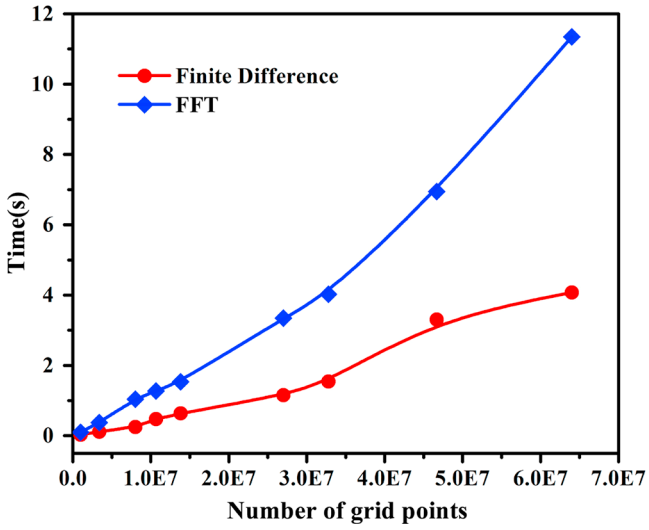

Figure 11. Timings for the computation of the von Weizsäcker potential in different numbers of grid points. The FD basis set implemented with efficient computation of the Laplacian outperforms the PW basis set formulation implemented with FFTs. Reprinted with permission from ref 53. Copyright (2016) Elsevier.

Lastly, because FD methods represent the electron density in real space, they are well-suited to aid AIMD accelerators. This was described in detail in ref 526, where a simple FD method was employed to track the electron density and its associated potential with free-space (open) boundary conditions in adaptively restrained particle simulations (ARPSs). An ARPS decomposes the system into slow- and fast-moving particles. An ARPS[527] accelerates AIMD by freezing some of the slow-moving particles along a molecular dynamics

https://doi.org/10.1021/acs.chemrev.2c00758
Chem. Rev. 2023, 123, 12039−12104

trajectory. Coupling ARPSs with an FD solver for OF-DFT provides the possibility to compute good initial guesses for the electron densities and their associated Hartree potential during the AIMD easily. That is, because of the real-space representation of the density, the frozen ions remain fixed also during the OF-DFT density optimization, thereby achieving a computational saving. Even though such schemes could be implemented in a PW basis (as PW basis methods have access to a real-space representation of the electron densities on the FFT grid), to our knowledge such PW counterparts have not appeared so far in the literature.

Moving on to the finite element method (FE), generically it uses sets of strictly local piecewise polynomials as basis functions. Those functions only overlap with immediate neighbors.[528−530] Various choices for those basis functions involve their dimensionality, polynomial order, and continuities (preservation of value and derivatives across interelement boundaries).[528,529,531] The two main steps needed to construct a FE basis set are

1. Partitioning of the domain Ω into subdomains (elements).
2. Definition of the local basis function within each element and piecing them together to obtain the final piecewise polynomial basis $\{\phi_j\}$. Generally, any function ψ defined in the domain Ω can be expanded with

$$\psi(\mathbf{r}) = \sum_j u_j \phi_j(\mathbf{r}) \tag{174}$$

In step 1, the elements are chosen to optimize computational efficiency. For example, triangles and quadrilaterals commonly are used as two-dimensional elements, while tetrahedra, parallelopipeds, and wedges are common in three-dimensional systems.[528,529,531]

In step 2, interpolation nodes are set in each element for the selected piecewise polynomial functions. The basis functions typically are chosen such that ϕ_j is 1 on the j-th FE interpolation node while it is 0 on all the other nodes. Typically only function continuity is imposed. First- and higher-order derivative continuity typically is not. Thus, differential equations for solution of the electronic structure problem need to be reformulated into integral equations. Once this is accomplished, such problems as the real-space Laplacian, Poisson equation, Poisson−Boltzmann equation, and eigenvalue equation can be transformed to a corresponding sparse matrix problem, which can be solved in various efficient and scalable approaches. Details of these techniques can be found in refs 530 and 532.

A general drawback of FE methods is that typically they require more memory than FD-based approaches and are more difficult to implement as well. Until now, they have proven advantageous primarily for very large system sizes.

A specific issue arises in the context of density-independent two-point KEDFs. Equation 171 shows how the PW basis and the convolution theorem combine to form an elegant reduction of the 6-dimensional integrals. In real-space basis set schemes an alternative is needed. It has two requirements, handling of the long-range Coulomb interaction and of nonlocal functionals (two-point KEDF and, sometimes, XC). Choley and Kaxiras[50] proposed a method with scaling close to $O(N)$. They noted that the kernel of a density-independent two-point KEDF can be fitted with reasonable accuracy by rational functions. Further, its Fourier transform can be approximated as a sum of subkernels

$$\omega(g) = \sum_{j=1}^{m} \frac{P_j g^2}{g^2 + Q_j} \tag{175}$$

where P_j and Q_j are complex numbers determined by fit to the original Fourier transformed kernel. With this expression, the convolution of a function $f(\mathbf{r})$ with a kernel $\omega(|\mathbf{r} - \mathbf{r}'|)$

$$v(\mathbf{r}) = \int d\mathbf{r}' f(\mathbf{r}') \omega(|\mathbf{r} - \mathbf{r}'|) \tag{176}$$

becomes

$$v(\mathbf{G}) = \sum_{j=1}^{m} v_j(\mathbf{G}) \tag{177}$$

where

$$v_j(\mathbf{G}) = \frac{P_j g^2}{g^2 + Q_j} f(\mathbf{G}) \tag{178}$$

Then, the $v_i(\mathbf{r})$ can be obtained efficiently by solving the corresponding Helmholtz equation.

$$\left[-\frac{1}{(2k_F)^2} \nabla^2 + Q_j \right] v_j(\mathbf{r}) = -\frac{P_j}{(2k_F)^2} \nabla^2 f(\mathbf{r}) \tag{179}$$

Benchmarks for the WGC[297] functional (which, by Taylor expansion of the kernel around a reference constant density, requires the evaluation of integrals involving only density-independent kernels; see below) indicated that the error introduced by the approximation is negligible. The scheme also was adopted to simulate tens of thousands of atoms with full atomic resolution and millions of atoms using coarse-graining techniques.[533]

3.4. Computationally Efficient Evaluation of Nonlocal Functionals

For nonlocal KEDFs with density-dependent kernels, the convolution integral no longer is directly applicable because such functionals involve integrals (in both the energy and the potential) of the type

$$P(\mathbf{r}) = \int d\mathbf{r}' f(\mathbf{r}') \mathcal{K}(k_F(\mathbf{r}), \mathbf{r} - \mathbf{r}') \tag{180}$$

$$Q(\mathbf{r}) = \int d\mathbf{r}' f(\mathbf{r}') \mathcal{K}(k_F(\mathbf{r}'), \mathbf{r} - \mathbf{r}') \tag{181}$$

As just noted, the WGC and XWM functionals[49,297] bypass that complication by use of a Taylor expansion of the kernel (i.e., the $\mathcal{K}$ function in eqs 180 and 181) around a constant density, n_0 (or equivalently around a constant Fermi wavevector, $k_F^0 = (3\pi^2 n_0)^{1/3}$). The remaining integrals are evaluable by simple convolutions. While the technique reduces computational complexity, it jeopardizes transferability. Specifically, the WGC and XWM KEDFs are applicable only to bulk systems for which a reference density is well-defined and in which $n(\mathbf{r})$ does not exhibit large variations. Without a system-dependent prescription for the reference density, WGC and XWM are inapplicable to finite systems. In some instances they also are affected by convergence problems.[49,79]

The LMGP KEDF provides a way around this difficulty by defining the potential with an integral equivalent to eq 180. It can be evaluated by a spline technique based upon use of a

https://doi.org/10.1021/acs.chemrev.2c00758
Chem. Rev. 2023, 123, 12039−12104

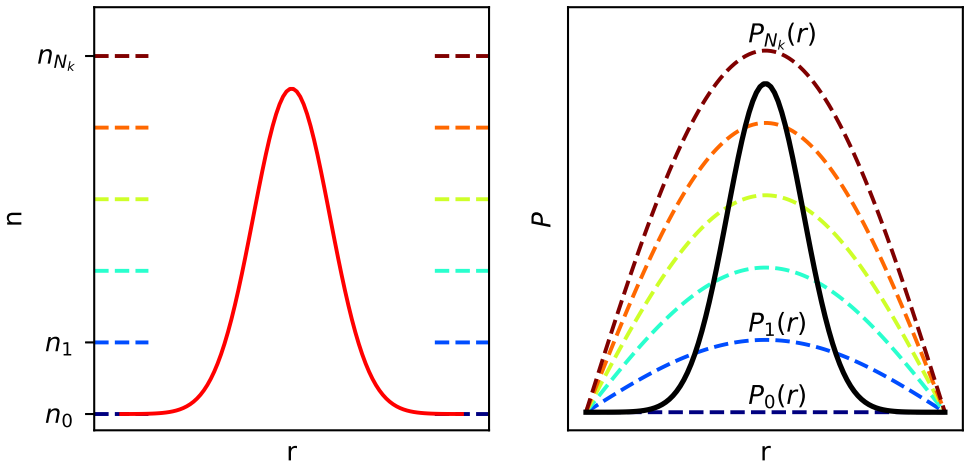

Figure 12. Depiction of the procedure to compute the integral, $P(\mathbf{r})$, in eq 180. On the left, the electron density is sampled by N_k values, $\{n_k\}$. On the right, the function $P(\mathbf{r})$ is approximated at every point by splining the values for each of the $P_k(\mathbf{r})$ functions.

discrete set of reference densities. For N_k selected density values $\{n_k\}$, there is a corresponding set of Fermi wavevectors, $\{k_F^k\}$. It follows[534] that

1. For each k_F^k value, the integral eq 180 can be evaluated by convolutions to generate N_k functions, $P_k(\mathbf{r}) = P(k_F^k, \mathbf{r}) = \int d\mathbf{r}' f(\mathbf{r}')\mathcal{K}(k_F^k, \mathbf{r} - \mathbf{r}')$.

2. The final objective function, $P(\mathbf{r})$ then can be recovered by spline representation of the $P_k(\mathbf{r})$ functions for each $\mathbf{r}$ point. That is, for each $\mathbf{r}$, the spline identifies k_F^k points near $k_F(\mathbf{r})$, {..., $P_{k-1}(\mathbf{r})$, $P_k(\mathbf{r})$, $P_{k+1}(\mathbf{r})$, ...} and splines them to find the best estimate for $P(\mathbf{r}) = P(k_F(\mathbf{r}), \mathbf{r})$.

This spline procedure is depicted in Figure 12. For it, a linear quadrature was chosen for $\{n_k\}$ (i.e., $n_k = k \times \Delta$, with Δ a positive real number). In practice, it often is advantageous to employ a logarithmic quadrature (i.e., $n_k = \alpha n_{k-1}$ with α a positive real number). The motive is to improve accuracy and aid convergence for nonperiodic systems (e.g., clusters and surfaces). In them, the electron density has large variations, from a maximum to arbitrarily close to zero, in contrast to bulk systems. For nonperiodic systems, large N_k values are reported[462] to be necessary, so judicious choice of grid becomes critical to computational performance.

The HC and LDA-K KEDFs define an energy functional of the kind shown in eq 47. The functional derivative (potential) involves integrals of both types, eq 180 and eq 181. For HC and LDA-K, evaluation of the integral eq 181therefore requires additional steps that typically are done in reciprocal space. For a periodic system with cell volume V_{cell}, the Fourier transform of $Q(\mathbf{r})$ is[535]

$$\tilde{Q}(\mathbf{G}) = \frac{1}{V_{cell}} \int d\mathbf{r}' f(\mathbf{r}') e^{-i\mathbf{G}\cdot\mathbf{r}'} \tilde{\mathcal{K}}(k_F(\mathbf{r}'), \mathbf{G}) \tag{182}$$

thus

$$\tilde{\mathcal{K}}(k_F(\mathbf{r}'), \mathbf{G}) = \int d\mathbf{r} \mathcal{K}(k_F(\mathbf{r}'), \mathbf{r} - \mathbf{r}') e^{-i\mathbf{G}\cdot(\mathbf{r}-\mathbf{r}')} \tag{183}$$

The resulting set of functions, $\{\tilde{\mathcal{K}}(k_F^k, \mathbf{G})\}$, then is used to approximate the integral in eq 182 by Riemann summation. Inverse Fourier transform to real space then recovers $Q(\mathbf{r})$ of eq 181.

It worth mentioning that it is more computationally demanding to evaluate eq 181 than eq 180 because all N_k points need to be considered for all $\mathbf{r}$ values in eq 181 compared to the spline for eq 180. That typically requires only the k_F^k points in the neighborhood of the $k_F(\mathbf{r})$ of interest. In conclusion, the computational evaluation of both integrals scales quasi-linearly because the FFTs involved scale like $O(N \log(N))$ and at most the algorithm requires N_k such FFT evaluations, independent of system size.

3.5. Algorithms for Million-Atom Simulations

Application of the increasingly accurate one- and two-point KEDFs we have described to simulation of extremely large systems (10^6 atoms or more) exposes some further algorithmic challenges. That also is true for exploitation of modern high-performance computing architectures. Issues of interest relate to the cost of evaluating the ion−ion and electron−ion interaction contributions and, hence, the structure factor. Related to that is solution of the Poisson problem (needed for the electrostatic potential). In what follows we summarize advances regarding both as embodied in contemporary OFDFT software. We also describe common strategies for distributing data and work in the most computationally intensive steps of the OFDFT simulation.

3.5.1. Structure Factors. Use of FFTs (and splining) gives $O(N \ln N)$ computational cost scaling for evaluating two-point KEDFs. But the electrostatic interaction terms (Hartree, ion−ion, and electron−ion) involve a computational cost that at first sight is quadratic scaling. Though the separate electrostatic sums are divergent in periodic systems,[536−540] the divergences cancel for neutral cells.[541] The Hartree term can be evaluated by using FFT to achieve $O(N \ln N)$ scaling; see eq 172. But if the ion−ion interaction is evaluated by standard Ewald summation,[541] the quadratic computational cost with the number of atoms in the simulation cell M, $O(M^2)$, becomes the bottleneck at system sizes of a few thousand atoms. The problematic term is the ionic structure factor. To simplify, here we consider only the ion−electron interaction E_{ext}, but a similar treatment applies to the ion−ion interaction. Also for simplicity we give the argument for the bare Coulomb interaction. Use of pseudopotentials changes only the details, not the essence.

Equation 16 can be re-expressed as

$$E_{ext}[n] = -\int d\mathbf{r} d\mathbf{r}' n(\mathbf{r}) \frac{n_a(\mathbf{r}')}{|\mathbf{r} - \mathbf{r}'|} \tag{184}$$

https://doi.org/10.1021/acs.chemrev.2c00758
Chem. Rev. 2023, 123, 12039−12104

where

$$n_a(\mathbf{r}) = \sum_{\alpha}^{N_a} Z_\alpha \sum_{k}^{n_\alpha} \delta(\mathbf{r} - \mathbf{R}_k) := \sum_{\alpha}^{N_a} Z_\alpha S^\alpha(\mathbf{r}) \quad (185)$$

Here N_a is the number of atomic species (or atom types), $\mathbf{R}_k$ is the position of the k-th atom of type α, n_α is the number of atoms of type α, and Z_α is their ionic charge. $S^\alpha(\mathbf{r})$ is the structure factor. Fourier transformation and application of the convolution theorem then gives

$$E_{ext}[n] = \sum_{\alpha}^{N_a} Z_\alpha \int d\mathbf{G} \tilde{n}(\mathbf{G}) \tilde{S}^\alpha(\mathbf{G}) \frac{4\pi}{|\mathbf{G}|^2} \quad (186)$$

$$\tilde{S}^\alpha(\mathbf{G}) = \sum_{k}^{n_\alpha} \exp(i\mathbf{G}\cdot\mathbf{R}_k) \quad (187)$$

$\tilde{S}^\alpha(\mathbf{G})$ is simply the Fourier transform of $S^\alpha(\mathbf{r})$ in eq 185.

As there are N_g grid points for $\mathbf{G}$, the direct evaluation of eq 187 scales as $O(n_\alpha \cdot N_g)$.[53,486,542] This is effectively quadratic scaling with system size. For system size $n_\alpha \approx 1,000$, the structure factor calculation begins to dominate the computational time relative to other terms in the OFDFT energy functional. That degrades the total computational cost to quadratic scaling.[53,486,542,543] This crossover seldom is encountered in conventional KSDFT simulations, as their inherent $O(N^3)$ scaling dominates, with the result that system sizes greater than a few thousand atoms rarely are treated by conventional KSDFT.

To address the problem, Darden et al. proposed the particle-mesh Ewald (PME) method.[544] In it, Lagrangian interpolation is used to evaluate the reciprocal space Ewald sums and the resulting convolution is evaluated via FFT. The approach reduces the cost to $O(N \ln N)$. The Lagrangian interpolation is effectively an approximation of the real-space structure factor in which the Dirac delta functions in eq 185 are approximated by spline basis functions with compact support (i.e., they decay exactly to zero within a finite number of grid points). Cardinal B-splines typically are chosen for this.[545] The compact support is important, as it assures the locality of the functions around the ions that is the cause of the linear scalability of the method. Typically only a handful of grid points in each direction from the ion is needed. (Note that the ion position may not coincide with a grid point.)

Choley et al. apparently were the first to use the B-spline plus FFT convolution PME scheme for evaluating the structure factor in electronic structure calculations. The first implementation in OFDFT software was by Hung et al.[542]

It also is possible to avoid the computation of the structure factor altogether by representing the atomic local pseudopotential (LPP) through its source pseudocharge density. The pseudocharge is localized and can be represented fully on a small subset of grid points (a crucial property also shared by the cardinal B-spline function). After summing all the pseudocharges, followed by multiplication by the Coulomb kernel $(\frac{4\pi}{q^2})$, a single FFT operation recovers the full LPP. The scheme has been implemented in the ATLAS software package and benchmarked on large-scale simulations.[543]

3.5.2. Parallelizing FFT for Large Systems: Small Box FFT and 2D-FFT. It should be abundantly clear by now that an important component of the computational cost in OFDFT with two-point KEDFs is the ubiquitous use of FFTs. Though they provide favorable $O(N \ln N)$ scaling (N total number of grid points), exploitation of that fact is hampered by the need for all-to-all communications among the CPUs involved. Jiang et al.[546] proposed an efficient "small-box" FFT (SBFFT) algorithm to address this problem for the Hartree term and, in fact, for any convolution integral with a radially decaying kernel. The kernel is presumed to be decomposable into long- and short-ranged parts. As depicted in Figure 13 (in cubic symmetry for simplicity), SBFFT is a divide-and-conquer strategy. The simulation cell volume is subdivided into small boxes. Each small box has an internal structure consisting of a cube decorated by a buffer region. In the small box, the Poisson equation for the short-range kernel is solved on a dense FFT grid. Then a long-range (but smooth) kernel is used in a Poisson equation solver over the entire simulation cell on a coarse FFT grid. The Hartree potential thus is the sum of localized potentials over the small boxes and a long-range potential represented on a coarse grid which provides efficient evaluation. SBFFT yielded a speed-up of 8.6 for a 10-fold increase in the number of CPUs, which is quite good for a parallel algorithm for massive systems. In addition, the relative error was estimated to be 4×10^{-5} (or 0.1 meV maximum error in the potential) for a massive simulation using 24,000 processors with a large FFT grid of $2,400^3$ points.[546]

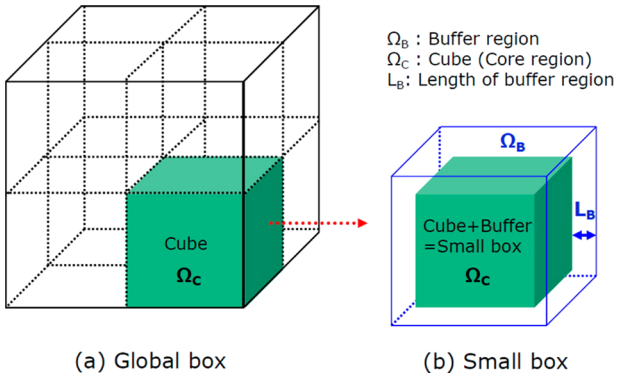

Figure 13. Small-box FFT algorithm distributes work and data for the computation of Coulomb and KEDF terms in the OFDFT energy functional. The large simulation cell is divided into small boxes. Each is composed of a physical small box and a buffer region which is introduced for evaluating the derivative of the density function needed for the evaluation of KEDFs. Reprinted with permission from ref 519. Copyright (2016) American Chemical Society.

Following the same strategy, SBFFT can be used to evaluate two-point KEDFs by introducing a real-space truncation of the nonlocal KEDF kernel. Chen et al.[519] performed an optimization of 1,024,000 Li atoms by distributing the work on 65,536 processes. That is a striking improvement over a "vanilla" FFT parallelization.

Two additional methods for implementing parallel FFTs, slab and pencil decompositions,[547,548] have been introduced recently to OFDFT by Shao et al.[520] in the ATLAS package.

In the slab decomposition, slices of the simulation cell along one axis are distributed evenly among all processes, while in the pencil decomposition the spatial partitions are done along two axes. As a result, the theoretical limit on the number of processors is larger in the pencil decomposition. The limits can be estimated from the mesh grid. With an $N = N_x \times N_y \times N_z$ point grid, the maximum number of processes is $\max(N_x, N_y,$

https://doi.org/10.1021/acs.chemrev.2c00758
Chem. Rev. 2023, 123, 12039−12104

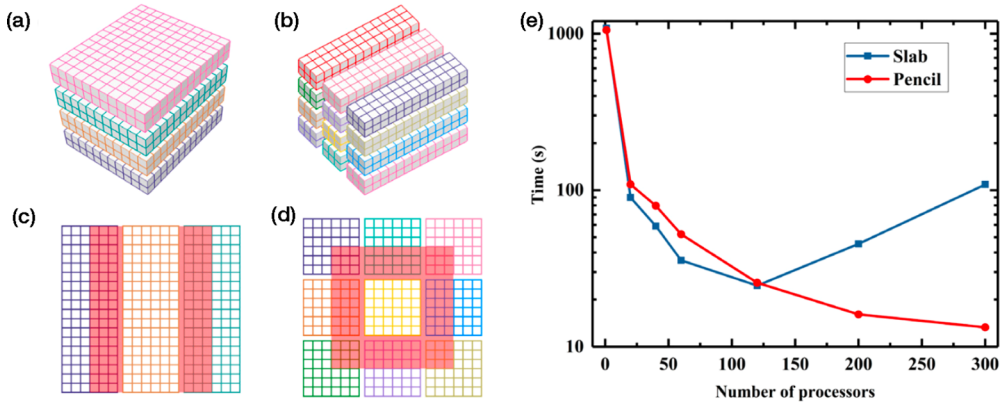

Figure 14. 2D-FFT algorithm. (a) Slab domain decomposition using four processors. (b) Pencil domain decomposition using a 4 × 3 processor grid. The buffer region (in red) is used to store information for the points near a domain boundary for the center processor in slab (c) and pencil (d) decompositions. (e) Comparison of wall time for a density optimization of 32,000 atoms of bulk Al with slab and pencil domain decompositions. Reprinted with permission from ref 520. Copyright (2018) Elsevier.

N_z) and $N/\min(N_x, N_y, N_z)$ for the slab and pencil decompositions, respectively. As illustrated in Figure 14(c) and (d), an additional buffer region is needed to store information for the points near a domain boundary. That region is used to perform finite difference schemes for each processor and can reduce the massive communication frequency.

In the form implemented in the ATLAS code, these approaches were benchmarked by comparison of total (wall clock) time for density optimization of Al with a 32,000 atom supercell. Both slab and pencil domain decompositions were used. Those results also are shown in Figure 14(e). Below 200 processors, the performance of the two approaches is comparable. Above that, the pencil outperforms the slab decomposition significantly. Shao et al.[520] showed that the parallel efficiency of the pencil decomposition reached 0.92 for a 2,048,000 atom simulation distributed on up to 4,096 processors.[520] Another impressive achievement by those authors is the recent successful optimization of the electron density of cubic aluminum using the WT KEDF and LDA XC functional for a sample of 100,271,632 atoms.[549]

3.5.3. Real-Space Algorithms for OFDFT Simulations of Million-Atom Systems. The FE and FD real-space representations introduced in Subsection 3.3.2 are generally efficient and scalable. However, when multimillion-atom systems are considered, real-space methods have the opportunity to use a lower spatial resolution for the space far away from notable features (e.g., vacancies in bulk systems and clusters in vacuum) and reduce computational complexity thereby.[518,530,550] A realization of this idea has been implemented by Gavini et al., who proposed the quasi-continuum OFDFT scheme.[533,550] In it, three feature-centered grids of different resolutions are adopted. We refer the interested reader to refs 518, 530, and 550 for additional information about the quasi-continuum approach as well as other FE methods. We also refer the reader to additional references describing other scalable real-space methods that have found success in DFT codes, namely refs 11 and 551−557.

3.6. Software for OFDFT Simulations of Materials

As discussed in Section 1, the TF and TFD approximations applied to atoms yield one-dimensional differential equations that have analytical solutions. They attracted interest in no small measure because of the extremely limited computational capacity of that era. To our knowledge, the first computational solution to the TFD equations was reported in 1950 by Reitz.[28] Other numerical solutions followed.[37,38,116,558−561] Given limitations of both the KEDFs and the available computational resources back then, those efforts targeted small systems, e.g. single atoms or small molecules.

Beginning in the 1980s, OFDFT software became more general and capable of treating wider system classes, including condensed phases,[43,44,451] surfaces,[562] and metal clusters[563] It seems fair to say, however, that those calculations were largely proof-of-principle efforts with limited impact outside the OFDFT method development community.

With the development of more accurate KEDFs and, concurrently, the betterment of pseudopotentials, since 2007 several groups have developed general-purpose codes, aimed at large-scale (up to hundreds of millions of atoms[549]) OFDFT simulations.[53−55,162,486,520,533,564] A summary of available and recently reported OFDFT software follows.

1. PROFESS:

   The PRinceton Orbital-Free Electronic Structure Software (PROFESS)[55,486,564] package is an open source code released under a CPC license.[565] It appears to be the most comprehensive OFDFT code currently available, as it can perform a wide range of simulations under diverse conditions. It employs a PW basis set; hence, Coulomb interactions, gradient, and Laplacian operations are evaluated in reciprocal space by FFT. The electron density is found by direct minimization of the total energy functional. Several minimization algorithms are available (SD, CG, TN, BFGS, and more). Besides electron density optimization, with use of forces and stresses, PROFESS can run molecular dynamics and structure relaxations with most GGA and two-point KEDFs. In terms of pseudopotentials, PROFESS not only supports LPP but also supports recent experimental schemes that go beyond LPP[161,169] (see Subsection 2.7). Recently, libKEDF, a library for the efficient and accelerated evaluation of local, semilocal, and nonlocal functionals, was released.[566] The library will be integrated in PROFESS. PROFESS also has been coupled to Quantum Espresso and augmented with finite-temperature KEDFs and XC DFAs to provide a

https://doi.org/10.1021/acs.chemrev.2c00758
Chem. Rev. 2023, 123, 12039−12104

general platform for even-handed comparison of OFDFT-based and conventional KSDFT-based AIMD calculations.[162]

2. ATLAS:
   Ab-initio orbiTaL-free density functionAl theory Software (ATLAS) is a FD implementation (both the Laplacian operator and the Poisson equation) of OFDFT. PW basis sets and associated FFTs also are provided for the evaluation of two-point KEDFs and use as Poisson solvers. The primary electron density optimization algorithm is direct energy minimization. It can be used for both periodic and nonperiodic systems. For two-point functionals with density-dependent kernels, ATLAS uses OE-SCF instead.[53,90,462,520] The source code can be obtained from the ATLAS Web site (atlas-ch.cn[549]).
3. GPAW:
   GPAW[51] is released under the GNU Public License version 3 or any later version.[567] In GPAW, there is an OFDFT implementation[120] consisting of a modified KSDFT solver adapted for tackling indirect solution of the OFDFT Euler equation via an SCF algorithm (recall Subsection 3.2.1). The OFDFT implementation in GPAW features local and semilocal KEDFs. Two-point KEDFs are yet to be implemented.
4. DFTpy:
   DFTpy[54] is open source, released under an MIT license.[568] It relies on Fourier space for the treatment of Coulomb interactions, for the computation of gradient and Laplacian operations, and for evaluation of two-point KEDF kernels. Various density optimization algorithms are provided, including OE-SCF.[462] DFTpy is a flexible, object-oriented OFDFT implementation with friendly APIs for Jupyter Notebooks. It thus is adapted to prototyping of new features. It can be used as a module for computing energy, forces, and stress. It also provides an API to the Atomic Simulation Environment[569,570] for AIMD and other functionalities. In addition, it provides a hydrodynamic time-dependent OFDFT implementation.[54]
5. CONUNDrum:
   CONUNDrum[52] is released under the GNU GPL v3 license.[567] Both a high-order central FD method and FFT are used for calculation of various energy and potential terms. Density optimization is via direct energy minimization with SD and nonlinear CG algorithms. In addition to one- and two-point KEDFs, machine-learnt KEDFs also are available.

Besides the packages just listed, other software implementing real-space OFDFT algorithms has surfaced but apparently is not publicly available.[484,533,571,572] There have been various materials simulations with these.[573−576]

We conclude by remarking that OFDFT software currently is under development in several research groups around the world. The overall trend seems to favor material science applications and pseudopotential implementations. As multiscale software continues to improve and new multiscale schemes evolve (such as embedding[577−579]), the role of OFDFT software will grow in importance. The future likely will see OFDFT solvers and conventional KSDFT solvers being used together in comparatively unconventional multiscale computational protocols. To achieve this goal, OFDFT software seems to be following the trend of other materials science software, namely, transition from stand-alone codes to modules and libraries that can be used independently (nearly "black box") by other software in flexible ways.

4. APPLICATIONS

In most cases, the prediction of structure−function relationships requires ab initio molecular dynamics (AIMD) simulations to represent configurational sampling and evaluate thermodynamic functions. Thus, the complexity of the requisite simulations can become intractable even for comparatively computationally efficient methods, such as semilocal conventional KSDFT. Doing AIMD with OFDFT is, in contrast, expected to be cost-effective for geometry optimizations and molecular dynamics of clusters, surfaces, and bulks. Aside from MD, OFDFT simply allows tackling of much larger systems than possible with conventional KSDFT, thereby helping to bridge the divide between few-atom system results and reality.

Note also that it is possible to accelerate OFDFT-based AIMD by applying techniques akin to what is done in conventional KSDFT.[580] Even though acceleration methods such as the extended-Lagrangian Born−Oppenheimer molecular dynamics techniques have been proposed and benchmarked for model systems,[581] they have not yet been employed in OFDFT simulations. However, we expect they will be.

Here we give examples of what already has been achieved. In the subsections that follow, we review several applications of OFDFT that enabled modeling of systems that clearly would be outside the applicability range of conventional KSDFT. These include models of the mechanical properties of bulk metallic systems (including alloys), metallic clusters, and nanostructures. Even though OFDFT currently is limited by the systems it can approach (because of limitations of present-day approximate KEDFs and local pseudopotentials), the set of systems benefiting from OFDFT-based modeling is large and growing as approximate KEDFs become more refined, transferable, and accurate.

We review bulk solid studies first and then move on to nanostructures and clusters, liquids and matter under extreme conditions. Then we survey applications of those subsystem DFT methods that rely on KEDFs in their formulation.

4.1. Solids

Since the bronze age (3000 BC) human beings have understood that alloying metals modifies their bulk properties: mechanical, thermal, and optical. Even today, metallurgy is an active field of research and engineering. OFDFT has played a key role in this context, providing accurate models for alloys and defective metals.

Thematically in this review, we have noted that the $O(N^3)$ computational scaling of conventional KSDFT poses a severe incremental cost barrier regarding treatable system sizes. Yet system size matters. For example, to control finite-size effects, predictive models of alloys and defective metals require large system sizes (hundreds or even millions of atoms in the simulation cell). Radhakrishnan and Gavini[576] found "remarkable cell-size effects that are present in computational domains consisting of up to 10^3−10^4 atoms, even in simple defects such as vacancies" either in bulk Al[576] or in alloys.[572] Strong finite-size effects required Das et al.[572] to use a 879-atom cell to converge the OFDFT electronic structure of a monovacancy in

https://doi.org/10.1021/acs.chemrev.2c00758
Chem. Rev. 2023, 123, 12039−12104

bulk Al. Additionally, Qiu et al.[582] reported that vacancy migration and formation energies display strong finite-size effects (fcc-Al needed supercells with up to 10,976 atoms). They employed the WT and WGC KEDFs and LDA and PBE XC functionals. Validation was carried out against conventional KSDFT for feasible system sizes (up to 256 atoms). While they found little difference between predictions with LDA and PBE XC functionals, the WT KEDF overestimated the vacancy formation energy by about 0.7 eV (out of an experimental value of 0.61 eV). WGC gave much improved vacancy formation energies (0.80−0.72 eV depending on the XC functional employed). Their study shows that practical implementations of OFDFT are predictive for studying vacancy formation, such as the collision cascade process in irradiated materials[582] or materials under loading shock conditions.[583]

Zhuang et al.[171] employed the WT KEDF and PBE XC functional implemented in PROFESS to investigate the elastic and thermodynamic properties of complex Mg−Al intermetallic compounds. First they benchmarked the performance of OFDFT as compared with both conventional KSDFT and experimental results and found good agreement. For example, the lattice constant of $Mg_{13}Al_{14}$ is 10.314, 10.437, and 10.183 Å from experiment, OFDFT, and conventional KSDFT, respectively. They also found similarly good agreement for phonon spectra of hcp Mg and fcc Al. In a second step, they evaluated the dynamical stability of alloys by computing phonon spectra on 3 × 3 × 3 supercells for all the compounds considered, including $Mg_{23}Al_{30}$. This resulted in a 1431-atom system. Their computations enabled the determination of thermodynamic properties, such as the temperature-dependent formation energy, heat capacity, and thermal expansion coefficient. The simulation yielded linear thermal expansion coefficients of 22.8 and 22.6 × 10^{-6} K^{-1} at T = 298 K for Mg and Al, respectively. Those results compare well with the experimental values, 24.8 and 23.1 × 10^{-6} K^{-1}, an indication that OFDFT is quantitatively reliable for computing properties of Mg−Al intermetallic compounds.

A detailed account regarding various kinds of defects in metals and metal alloys (such as vacancies and vacancy clusters, interstitials, dislocations, and grain boundaries) can be found in the recent review by Witt et al., ref 145. It is worth highlighting a few specific examples to showcase the usefulness of OFDFT to materials science. For one, Xia et al. employed the WGC-decomposition approach (see Section 2.7.1) and HC KEDFs, the PBE XC functional, and BLPS pseudopotentials implemented in PROFESS to study several Li−Si alloys (LiSi, $Li_{12}Si_7$, Li_7Si_3, $Li_{13}Si_4$, $Li_{15}Si_4$, and $Li_{22}Si_5$). They found that over 80% of the OFDFT results had errors in the equilibrium lattice constants within 1% of the conventional KSDFT reference values, with the largest deviation less than 2%. The bulk moduli errors lie within 5 GPa (or approximately 10%) of the conventional KSDFT values.

Atomic-scale characterization and understanding of dislocations in bulk systems is another topic of importance for materials science. Because dislocation formation is difficult to monitor in situ, theory and modeling potentially are of very high value. Shin and Carter[584] tackled the problem by employing the WT and WGC KEDFs, the LDA XC functional, and BLPS pseudopotentials with the PROFESS code. They benchmarked against conventional KSDFT with the same pseudopotentials and XC functional. The differences are quite small, within 25.8 (5.8) meV/atom for the total energy from the WT (respectively WGC) KEDF, and 5.5 (5.2) GPa for elastic constants, and 16.3 (28.9) mJ m^{-2} for stacking fault energies. The same authors also presented a thorough analysis of screw and edge dislocations in magnesium. They analyzed dislocation width and dynamics for the first time with an ab initio method which is much more accurate than the embedded-atom force fields[585] typically employed in the engineering community. In another study, Hung and Carter[586] analyzed the ductile properties of aluminum and showed that Al metal is much more resistant to plastic deformation than is predicted by commonplace engineering methods such as continuum models.

4.2. Metal Clusters, Quantum Dots, and Nanostructures

As mentioned, OFDFT-based AIMD (OFDFT-AIMD) can be quite useful for modeling metallic systems, including metal clusters. Multiple OFDFT-AIMD studies of metal clusters have been done dating to the early 1990s. We summarize a representative selection in what follows.

Despite its fundamental flaws (recall Section 2), historically the $T_{TF} + \lambda T_{vW}$ (TFλvW) KEDF has been used in ways that encouraged further exploration of OFDFT treatment (with LDA XC) of clusters. Kanhere et al. treated simple Na and Mg dimers and trimers[587] with the λ = 1/9 version. It also was used to study the most probable low-energy configurations of diverse clusters including the ground-state geometries and energetics of small Li clusters and the Li_nAl_m cluster,[588−591] as well as melting of Al_{13}.[592,593] Despite its deficiencies, the TFλvW functional yielded bond lengths within 5% of the conventional KSDFT values,[589] an encouraging indication of the promising nature of OFDFT-AIMD for study of nonperiodic metallic systems. Thus, for example, Blaise et al.[594] used OFDFT-AIMD with TFλvW, λ = 1/9 to study the structural and dynamical properties of neutral and charged Na clusters up to sizes of several hundred atoms. Their ab initio calculations confirmed the validity of the so-called "liquid drop" model (often used in the nuclear physics community) as a function of the total cluster charge.[595] Moreover, the Guo group[562] adopted OFDFT to study the equilibrium structure and bonding of small silicon clusters.[563] They also used TFλvW KEDF, but with λ = 1/5. Although the values of cohesive energy they obtained were only semiquantitative, the bond lengths and angles compared very well to values from conventional KSDFT.[563] The OFDFT-AIMD approach was exploited by Aguado and coauthors as well in a number of studies of alkali clusters and alkali metal alloy clusters.[126,127,453,596−599]

The first application of two-point KEDFs to clusters is credited to the Carter group.[174] They used the WGC[297] two-point KEDF and LDA XC functional to study two-dimensional arrays of Al quantum dots. The issue investigated was the induction of a metal−insulator transition by increase of interdot separation. The only input to their model was a measure of the electron density decay as a function of intercluster separation. Their study was important because it showed that two-point functionals, even if developed for applications to bulk systems, could be applied to systems with remarkable inhomogeneity. (Note that the authors of ref 174 were careful to clarify that very low density values are probably unreliable because the Taylor expansion in WGC, mentioned in Subsection 2.4.2, may not be able to recover an appropriate kernel in low-density regions.)

https://doi.org/10.1021/acs.chemrev.2c00758
Chem. Rev. 2023, 123, 12039−12104

Applications of OFDFT ventured to investigating tensile yielding of metal nanowires, behavior that is important for predicting how the metal behaves under extreme stress. In ref 173, Hung and Carter adopted the WGC KEDF, LDA XC functional, and BLPS pseudopotentials in the PROFESS code to model large-sized Al (111) nanowires (up to 20 nm in length). Interestingly, they found that such nanowires develop specific slip planes or amorphization of the crystal structure depending on wire size (see Figure 15). Employing the same

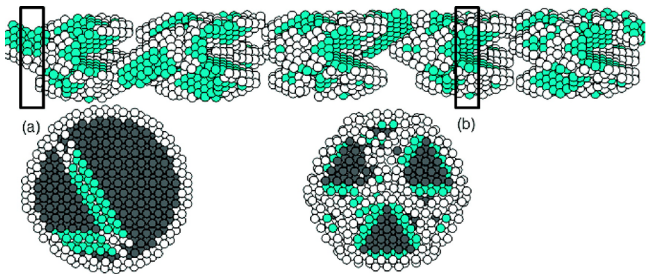

Figure 15. Aluminum wires under tensile stress. The wires break in specific ways (slip planes are made visible by the color coding) predicted by OFDFT with the two-point KEDF WGC. Green atoms correspond to hcp structure, gray to fcc structure, and white to an unknown structure. Reprinted with permission from ref 173. Copyright (2011) American Chemical Society.

approach, the Carter group went further and studied plastic properties of body-centered-cubic (bcc) Mg–Li alloys as potential lightweight metals. In the model, they used simulation cells containing up to 8640 atoms.[454]

Aguado et al. adopted a two-point functional developed in the group of Stott by simplifying the CAT KEDF[316] (similar in spirit to the WT functional[44]) in conjunction with the LDA XC functional to study melting of various-sized sodium clusters.[600−604] Quite interestingly, calorimetry experiment results[605] were reproduced quantitatively by the simulations,[601] as shown in Figure 16. Detailed information is in the review by Aguado et al.[606,607]

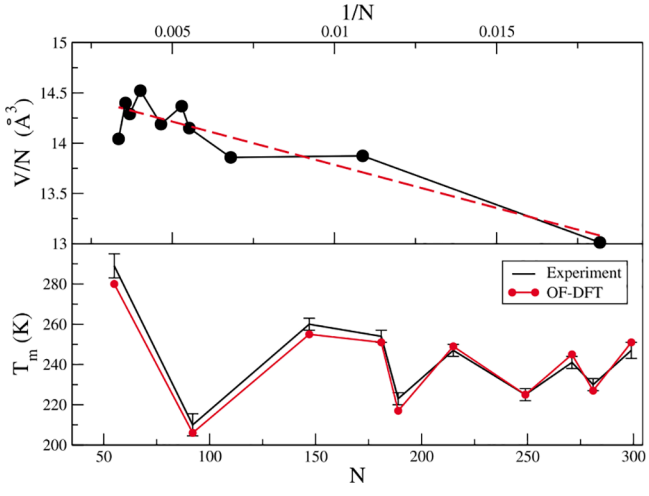

Figure 16. Size variation of the volume per atom (top) and melting temperature (bottom) in Na clusters from OFDFT simulations and experiment. The dashed line in the upper panel is the best linear fit to the data. Reprinted with permission from ref 601. Copyright (2005) American Physical Society.

Recall from Subsection 2.4.2 that the LMGP KEDF[88] recently developed is applicable to quite inhomogeneous systems, including clusters.

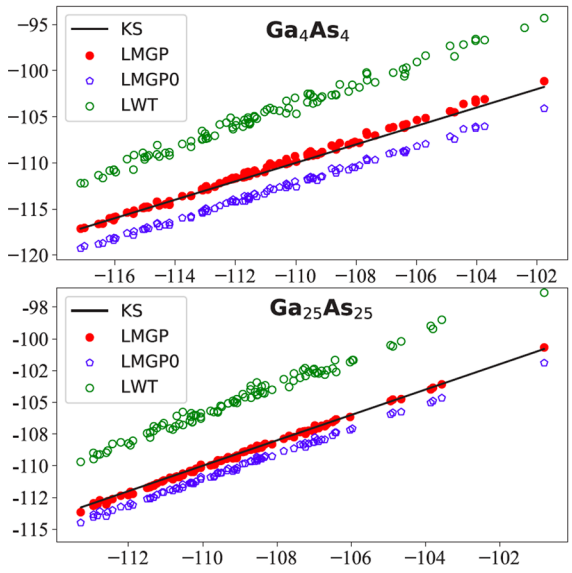

Figure 17. Energies (eV/atom) of 100 random structures of Ga_4As_4 and $Ga_{25}As_{25}$ compared to conventional KSDFT results (on the x axis) as well those from other KEDFs. LMGP0 is LMGP with the corrective $1/q^2$ as the $q \to 0$ term removed. LWT is the result of using the integrand in eq 106 simply evaluated at $t = 1$; hence, it is LMGP0 with the kernel terms arising from the functional integration removed. Adapted with permission from ref 88. Copyright (2019) American Physical Society.

Figure 17 and Table 5 show the results of benchmark studies for several hundred random-structured metal and semiconducting clusters. The LDA XC functional was adopted in all these OFDFT calculations, which were done with the ATLAS code. The outcomes indicate that two-point functionals with fully density-dependent kernels (such as LMGP) improve the performance of OFDFT considerably in modeling finite metal clusters and quantum dots compared with values from the semilocal functionals mentioned above. This is true for both total energy and electron density. The results also indicate that OFDFT can treat systems with highly inhomogeneous electron density, such as clusters and quantum dots, as accurately as conventional KSDFT at a fraction of the computational cost.

Because of the computational cost, until recently there have been no applications of two-point functionals with density-dependent kernels to nanoscale systems[79] such as materials interfaces and nanoparticles. That state of affairs changed with the introduction of the OE-SCF method (Section 3.2.1). It requires only ≈15 nonlocal KEDF evaluations for each geometry (depending weakly on system size and type). As an example, Figure 18 shows results for a nanoscale metal–semiconductor interface and a semiconductor nanoparticle, each containing hundreds of thousands of atoms. Both were studied with the LMGP KEDF.

We have mentioned already the avoidance of finite-size effects via OFDFT. For obvious computational cost reasons, it is rather common for conventional KSDFT calculations to be done on system sizes that are small compared to the scale of

https://doi.org/10.1021/acs.chemrev.2c00758
Chem. Rev. 2023, 123, 12039−12104

Table 5. Mean Unsigned Error (MUE) for the Total Energy in eV/atom and, in Parentheses, Percentage Mean Unsigned Relative Error (MURE) for the Electron Density[a]

Systems	LMGP	LMGP0	LWT	TF+15vW	WT
Mg_8	0.18(3.79)	0.63(4.12)	1.19(4.05)	1.09(11.36)	8.79(16.0)
Si_8	0.22(4.84)	2.17(4.90)	4.86(4.74)	1.46(8.28)	41.7(17.5)
Ga_4As_4	0.34(5.40)	2.21(5.43)	6.15(4.89)	1.55(8.94)	51.8(19.3)
Mg_{50}	0.05(3.31)	0.35(3.42)	0.84(2.38)	0.95(9.56)	3.23(10.3)
Si_{50}	0.11(4.59)	0.95(4.65)	3.73(3.60)	1.53(7.24)	16.4(14.2)
$Ga_{25}As_{25}$	0.13(5.21)	1.06(5.26)	4.29(3.19)	1.67(7.79)	22.7(16.8)
Mg_8^S	0.28(5.20)	1.16(5.34)	2.66(5.29)	0.27(7.63)	19.4(18.6)
Mg_8^{VS}	0.09(3.94)	1.67(4.10)	3.88(4.87)	0.10(5.60)	24.0(17.5)

[a]MUE is defined as $\frac{100\%}{2N}\int|n_{\mathrm{OFDFT}}(\mathbf{r}) - n_{\mathrm{KSDFT}}(\mathbf{r})|d\mathbf{r}$ relative to conventional KSDFT values. Superscripts *S* and *V S* stand for "strained" and "very strained", where the minimal interatomic distances between atom pairs are 1.2 and 0.8 Å, respectively. Both are much shorter than the equilibrium bond distance, 2.4 Å. Reproduced from Mi *et al.*[88].

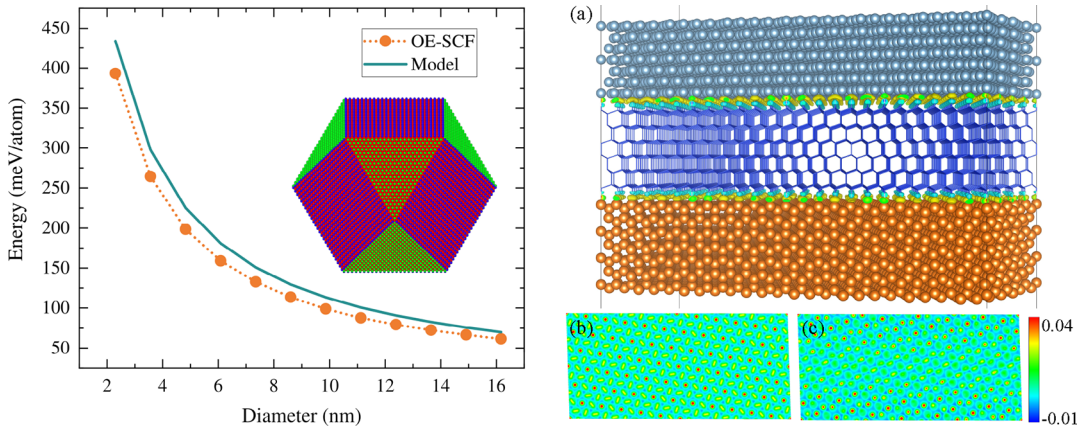

Figure 18. Left: Energy per atom of large icosahedral Si nanoparticles containing up to 102,501 atoms (dashed orange curve with dots is for the LMGP functional with OE-SCF solver; solid green curve is the empirical formula taken from ref 608). Right: Inset (a): depiction of a 3-layer interface, Al(111) (top), Si(111) (middle), and Mg(100) (bottom). Slabs of large dimensions were required in order to match the lattices of the materials at the interfaces. The charge flow across the Si−Al and Mg−Si interfaces (computed as the difference between the electron density of the 3-layer interface and the electron densities of the isolated slabs) is displayed with an isosurface volume plot visible in inset (a). Insets (b) and (c): Two-dimensional cut of the charge flow across the interface for the Si−Al and Mg−Si interfaces, respectively, which is seen to range between −0.01 and +0.04 electrons. Adapted with permission from ref 462. Copyright (2021) American Chemical Society.

experimental samples. That is particularly the case for modeling of nanoparticles and materials interfaces. For the latter systems, models often are unable to reproduce the correct crystal lattices at the interface because resolution of the differing lattice constants would require excessively large simulation cell sizes to reach a commensurate length. Reference 462 showed that with accurate KEDFs it is possible to overcome this difficulty and use appropriate system sizes. Shao et al.[462] in particular found that LMGP reproduced, quantitatively, the energy as a trend of nanoparticle radius (culminating in the largest nanoparticle depicted in the figure). For the metal−semiconductor interface in Figure 18 (right panels), the authors showed that the charge rearrangement across the interface reproduces known trends for passivated and unpassivated Si surfaces. (The charge rearrangement was computed by subtracting from the electron density of the interface the electron densities of the isolated slabs.)

4.3. Liquid Metals and Alloys

We turn next to the applications of OFDFT to liquid metals (including alloys) and their surfaces. We refer the reader to the reviews by Aguado et al. in ref 607 and by Witt et al. in ref 145 for additional and complementary details.

OFDFT-AIMD was used with success for studying the structure of simple liquid metals (such as Li, Na, Mg, Al, and Cs) beginning in the 1990s.[452,469,609,610] Typically that was with the LDA XC functional. That progress exploited the relevance of the HEG to such metals as embodied in use of the linear response formulation of two-point functionals beginning with WT[44] and continuing with SM,[46] WGC,[297] and other KEDFs.[43,299,320] Recall details in Section 2.4.2. In those simulations, first-principles LPPs (such as NPA and BLPS; see Section 3.1.2 for details), as well as empirical or model LPPs (such as the Topp-Hopfield LPP[447] for Na and the Fiolhair model potential[444] for Cs), were used. Note that empirical LPPs still are useful, as there exist parametrizations for those ions that are not approachable, so far, by first-principles LPPs, such as transition metals.[611] We also note that the KEDFs mentioned are broadly useful for simulating complex liquids, including their surfaces.[612]

An early success from Madden et al. was calculation of the dynamic structure factor of liquid Na[609] using the LDA XC, their SM KEDF,[46] and the Topp-Hopfield LPPs.[447] They obtained excellent agreement with experimental results for static and dynamic structure factors.[609] In subsequent work that used first-principles LPPs,[457] the liquid phases of Na, Mg, and Al[610] were studied at temperatures close to their melting points. It was found that the calculated average coordination numbers and radial distribution functions (RDFs) agreed well

https://doi.org/10.1021/acs.chemrev.2c00758
Chem. Rev. 2023, 123, 12039−12104

with both conventional KSDFT and experimental outcomes. Recently, the same KEDF and XC functional were used with the PROFESS code to study the dynamic properties of liquid Sn. The simulations reproduced the experimental results for the collective fluid dynamic behavior quite well.[613]

Significant improvements over the SM functional were introduced with the simplified CAT functional[316] (recall Section 2.4.2). It was developed to study the structure and dynamics of diverse liquids. In the simulations listed next, the LDA XC DFA was used and the temperatures were chosen to be close to experimental values. The studies were as follows:

1. Simple and alkaline earth liquid metals: Cs,[452] Li,[469] Na,[614] Mg,[615] and Al[316] plus liquid alkaline earth metals (Be, Ga, and Ba);[471]
2. Liquid alloys: liquid Na−Cs and Na−Cs alloys,[616] Li−Na alloy,[617] Ga, In, and binary alloy Ga−In;[618]
3. Liquid surfaces and interfaces: surface of liquid Li and Na,[619] liquid−vapor interface in liquid binary alloys,[620] and liquid surface of Sn,[621] interface of the liquid metals Al,[622] liquid−vapor interfaces of Ga and In,[618] liquid−vapor interfaces of liquid binary alloys (NaK, NaCs, and LiNa),[623] and the liquid In surface.[612]
4. Nonmetals and transition metals: liquid Si at near melting point[624] and high-pressure conditions,[625] bulk liquid Ga,[626] liquid noble metals,[627] transition metals,[611] and liquid Zn, Cd, and Hg divalent metals.[628]

Most of the studies in the foregoing list employed the simplified CAT KEDF. The earlier works presented comparisons among results obtained with the simplified CAT and the one-point functional TFλvW with λ = 1. Perhaps unsurprisingly, the simplified CAT KEDF was found to be more accurate and to provide a better description of the structure of the liquid metals considered on the basis of comparison with experimentally determined structure factors.[452] An additional take-home message from the list of studies above is that the simplified CAT KEDFs in conjunction with pseudopotentials provide a nearly quantitative description of the structure and dynamics of bulk as well as liquid metal surfaces without incurring limitations from the finite-size effects[619] which had plagued conventional KSDFT simulations of similar types of systems.[629]

In a related application, the Carter group adopted the two-point WGC KEDF in conjunction with the PBE XC functional and BLPS LPPs to study the melting point of Li using the PROFESS code.[461] Figure 19 shows their OFDFT-AIMD results for both the RDF and static structure factors at ion temperatures 470 and 725 K as compared with X-ray diffraction and neutron diffraction data, respectively. The agreement is evident. These results on liquid metals are encouraging indicators of the value of OFDFT-AIMD simulations. Moreover, the OFDFT-AIMD predictions of structure factors predicted from ab initio dynamics for liquid Li are in better agreement with experimental data than the predictions from classical force fields.[460]

4.4. Matter under Extreme Conditions

Most materials physics is done in the same pressure−temperature (P, T) domain as the chemistry of the molecular constituents of those materials, roughly $T \lesssim 2000$ K, $P \lesssim 1$ Kbar. Electronic structure calculations at T = 0 K generally suffice therefore, so zero-temperature AIMD is used successfully to calculate the equation of state (EOS) and various properties of the condensed systems. Immediately, the

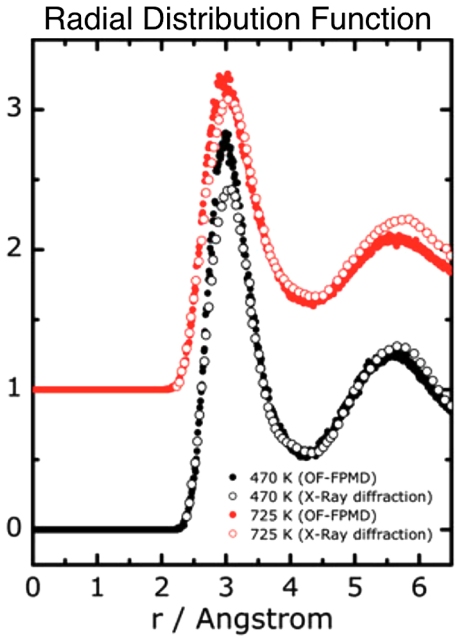

Figure 19. Radial distribution functions (RDFs) of liquid Li at 470 and 725 K. The simulations used 128 independent atoms in the simulation cell in the canonical ensemble. The results at 725 K are shifted upward by one unit for ease of viewing. The legend "OF-FPMD" denotes what we term OFDFT-AIMD. Adapted with permission from ref 461. Copyright (2013) Taylor & Francis.

computational cost-scaling advantage of zero-temperature OFDFT and the KEDFs we have discussed is relevant for such studies.

However, there are systems in which both the chemistry and the condensed phase physics occur at much higher T and P. Especially spectacular examples are found in the interiors of giant planets and exoplanets.[630] Other examples of this so-called warm dense matter (WDM) regime occur in inertial confinement fusion.[631] For WDM, one can have $T \lesssim 10-15$ eV (with 1 eV = 11,604.5 K) and $P \lesssim 1$ Mbar or even higher.

Systems in the WDM $P-T$ domain have electron populations that are highly excited. But they are not so thoroughly excited as to make the system into a two-component plasma (electrons, ions) with small quantum corrections. Because quantum mechanics still is dominant, it has proven efficacious to use finite-T AIMD. (Remark: Chemists may be surprised (or bemused) to learn that it is conventional in the physics literature to refer to nonzero T as "finite T" even though zero is, of course, finite.) Immediately that implicates free-energy DFT.[632] For present purposes, it suffices to say that free-energy DFT differs from ground-state DFT in three ways. First, the non-interacting kinetic energy T_s, eq 23, becomes the non-interacting free energy $\mathcal{T}_s = T_s[n] - TS_s[n]$ (where $S_s[n]$ is the non-interacting entropy). Second, the exchange-correlation energy, eq 27, becomes the exchange-correlation free energy $\mathcal{F}_{xc}[n; T]$. And third, the occupation numbers, eq 22, take on Fermi−Dirac T-dependence. Observe that the KS equation is unchanged in form.

The relevance of OFDFT is plain. The simple presence of another physical parameter, T, means that there are more simulations to do than at T = 0 K. Moreover, at least in principle all the KS levels are occupied. In practice, many more occupation numbers can be numerically significant than at T =

https://doi.org/10.1021/acs.chemrev.2c00758
Chem. Rev. 2023, 123, 12039−12104

0 K, so the benefit of OFDFT $O(N \ln N)$ scaling relative to conventional KSDFT cubic scaling is amplified compared to the ground state (T = 0 K).

We do not review free-energy OFDFT here in detail, but only sketch the key ingredients and give a few examples as a guide to the recent literature and a connection to the ground-state OFDFT methods and KEDFs that are our focus. In parallel with the ground-state case, the critical ingredient is $\mathcal{T}_s$. For brevity, we refer to approximations for it as KEDFs, even though they have an entropic contribution. The most widely used have been finite-T Thomas–Fermi[29] or TFvW. The finite-T von Weizsäcker term was given by Perrot[633] more than 40 years ago, while TF-based finite-T AIMD studies first appeared almost 30 years ago.[634,635] Despite the fact that TF and TFvW obviously are far from satisfactory on fundamental grounds, they continue to be used.[636−639] (Remark: It is a misleading peculiarity of the literature that many of the finite-T TF or TFvW-based papers state, incorrectly, that OFDFT is *defined* by the use of those functionals.)

Connection with modern ground-state OFDFT was made in 2012 when Karasiev et al.[640] presented a method for generalizing a ground-state gradient-dependent (GGA) KEDF into a gradient-dependent $\mathcal{F}_s$. They demonstrated the workings and effectiveness of that scheme by use on their semiempirical PBE2 GGA KEDF (recall discussion in Subsection 2.4.1 about "modified conjoint" KEDFs). A bit over a year later, the first nonempirical finite-T GGA KEDF was presented, namely VT84F.[85] Constraint-based, it was constructed with both proper T = 0 K limiting behavior and large-T behavior.

As we discussed in Subsection 2.4.1, the constraint satisfaction in VT84F (as a T = 0 KEDF) is predicated on physical densities with nuclear-site cusps that satisfy the Kato condition. That property carries over to $T > 0$ K. Recall, from that same discussion, that the LKT KEDF[86] was constructed to satisfy positivity constraints for typical pseudodensities. By means of the procedure in ref 640. LKT recently also was extended to being a free-energy KEDF,[641] LKTF.

So far as we are aware, those are the only two nonempirical one-point free-energy KEDFs to date. Two-point $\mathcal{F}_s$ approximations are equally rare. To our knowledge, there are only two, both the work of Sjostrom and Daligault.[166,318,642] They have the structure of eqs 13 with kernel (eq 14), but of course with T-dependent densities and kernels. The first of the Sjostrom–Daligault functionals is straightforwardly the Wang–Teter kernel[44] extended by calibration to the finite-T Lindhard response. It has a deficiency, namely that for large wavevectors (small distances), the kernel $\omega(\mathbf{k}, T)$ goes strongly negative (see Figure 1 in ref 44). That behavior can yield "... unphysical densities with infinite negative energy".[318] Reference 318 cured that problem by changing the T_{vW} term to scaled two-point form (temperature-dependence suppressed for clarity),

$$\mathcal{F}_{\beta vW} := \frac{1}{2}\int d\mathbf{r}d\mathbf{r}'[\nabla n^{1/2}(\mathbf{r})\cdot\nabla n^{1/2}(\mathbf{r}')][\delta(\mathbf{r}-\mathbf{r}') + \beta(|\mathbf{r}-\mathbf{r}'|)] \quad (188)$$

The nonlocal scaling function $\beta(|\mathbf{r}-\mathbf{r}'|)$ and kernel ω then are determined by enforcing the Lindhard response in the HEG limit while requiring that the kernel vanish for large k. In ref 641, this $\mathcal{T}_s$ approximation was denoted "sdβ-vW14F".

Regarding the XC free energy, ground-state E_{xc} forms evaluated with finite-T densities often have been used. This "ground-state approximation" is reasonable up to about T = 1 eV in many but not all cases and certainly is not valid generally.[643−645] Until 2014[646] there was no strict $\mathcal{F}_{xc}$ counterpart of the Perdew–Zunger LDA E_{xc}.[281] A partial counterpart to the PBE GGA E_{xc}[225] was presented in 2014,[647] but a strict counterpart did not appear until 2018.[648] While there is a hybrid $\mathcal{F}_{xc}$,[649] that is not relevant to OFDFT, the history of prior development of $\mathcal{F}_{xc}$ approximations is irrelevant here.

With this brief introduction, we turn to a few illustrative examples of calculations. First are two examples of Thomas–Fermi-based calculations. The simpler of the two was by Lambert et al.[636] It used simple Thomas-Fermi for $\mathcal{F}_s$ and had no exchange-correlation free-energy contribution in the OFDFT-AIMD. Nevertheless, the prediction for the principal Hugoniot (the locus in P, T of all final states of a material at density ρ reachable by passage of a single shock wave) for iron is rather good for $T \gtrsim 100$ eV when compared to the SESAME table EOS 2140.[650] See Figure 20. Below that temperature the

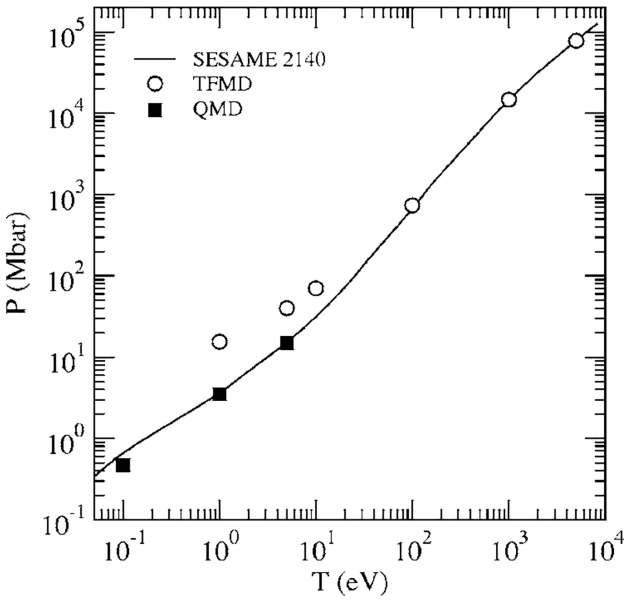

Figure 20. Principal Hugoniot for Fe from free-energy OFDFT with only finite-T TF and no $\mathcal{F}_{xc}$ compared to the SESAME library EOS 2140 and, for lower temperatures, conventional free energy KSDFT AIMD (denoted here as "KSMD", widely called "QMD") done with LDA XC. Reprinted with permission from ref 636. Copyright (2006) American Physical Society.

deviations with respect to conventional free-energy KSDFT-AIMD are a clear sign of both the deficiencies of TF and the lack of a $\mathcal{F}_{xc}$ term. This diagnosis is confirmed by a more recent study that includes $\mathcal{F}_{xc}$ contributions (at the level of the ground-state approximation); see ref 651.

The second example is the calculation of the EOS and dynamic structure factor of aluminum by White et al.[167] for 0.1 $\leq T \leq$ 10 eV. The finite-T OFDFT simulations used 864 atoms in the simulation cell, compared to 108 for the conventional KSDFT finite-T validation calculations, an illustration of the computational cost scaling advantage of OFDFT. Figure 21 shows the resulting EOSs. Once again, one

https://doi.org/10.1021/acs.chemrev.2c00758
Chem. Rev. 2023, 123, 12039−12104

sees the low-temperature deficiency of the TF approximation. Also obvious is the importance of the inclusion of the XC free energy.

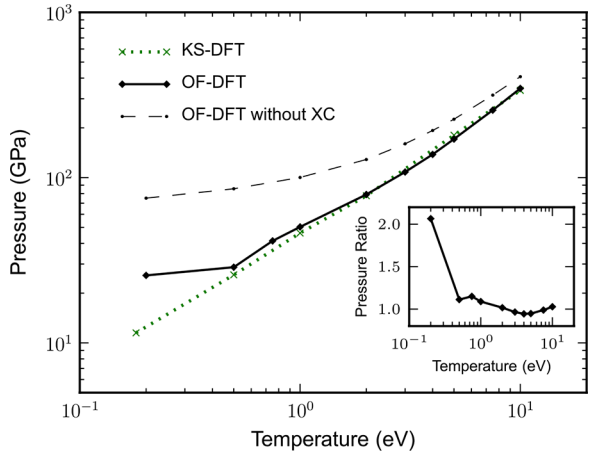

Figure 21. Al EOS at ρ = 2.7 g/cm^3 from free-energy OFDFT with finite-T TF and with (and without) LDA $\mathcal{F}_{xc}$ (ground-state approximation) compared with conventional free-energy KSDFT results. The inset shows the pressure ratio between OFDFT and conventional KS values. Reprinted with permission from ref 167. Copyright (2013) American Physical Society.

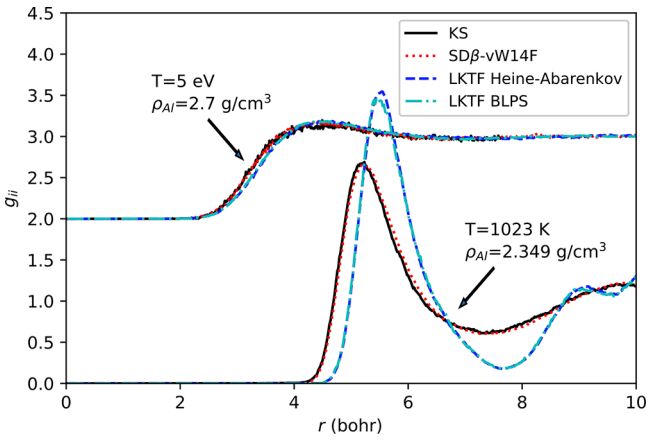

Figure 22. Comparison of calculated RDFs for Al at two state conditions. Conventional free-energy KSDFT results are the black solid curves. Free-energy OFDFT results from the one-point LKTF $\mathcal{T}_s$ are the blue dashed curves; those from the two-point sdβ-vW14F functional are the red dotted curves. The RDFs for the case T = 5 eV, ρ = 2.7 g/cm^3 are shifted upward by two units for clarity (the caption in the original is incorrect). Reprinted with permission from ref 641. Copyright (2020) American Physical Society.

Figure 22 shows a comparison between the best current one- and two-point approximations for $\mathcal{T}_s$, namely LKTF and sdβ-vW14F. The physical quantity is the RDF. What is apparent is that the one-point functional is quite competitive at larger T and ρ but that the two-point functional clearly represents the low-T, low-ρ regime better. The calculations were done for two different pseudopotentials, BLPS[163,164,458] and Heine–Abarenkov.[445,652] Reassuringly, the two yield very similar results. The isothermal EOS also is interesting. Figure 23 shows that

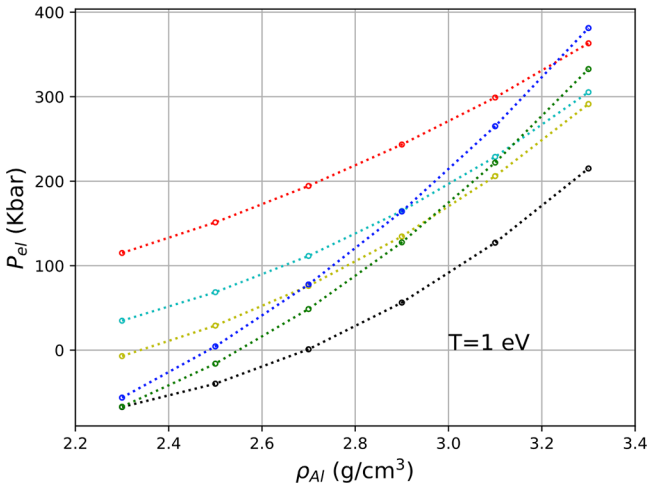

Figure 23. Al EOS at T = 1 eV from various $\mathcal{T}_s$ KEDFs. Top to bottom curves at lowest ρ are TF (red), Perrot (teal), TF$\frac{1}{5}$vW (olive), VT84F (blue), and LKTF (green). Conventional free energy KSDFT curve is black. Reprinted with permission from ref 641. Copyright (2020) American Physical Society.

LKTF actually is closest to conventional KSDFT in the region of low bulk density, unlike the comparison for the RDF. Finally, Figure 24 shows the scaling of the wall time per AIMD

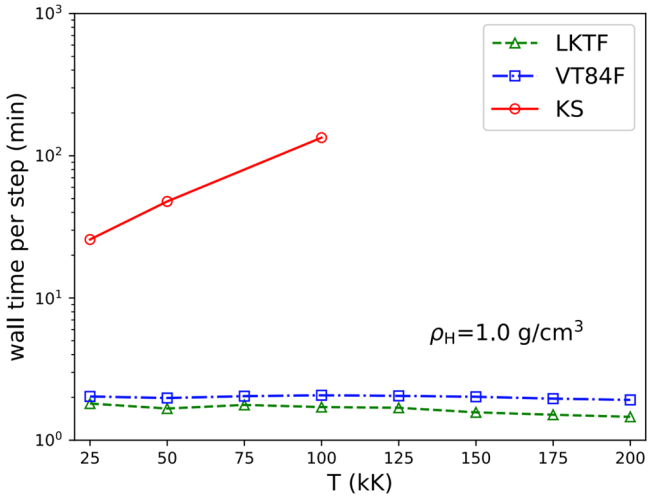

Figure 24. Wall-clock time per MD step for 108 H atoms for conventional free-energy KSDFT vs OFDFT with the LKTF and VT84F KEDFs. Reprinted with permission from ref 641. Copyright (2020) American Physical Society.

step as a function of T from about 25 kK to 200 kK for LKTF and VT84F compared to conventional free-energy KSDFT. The system is 108 H atoms. The promised OFDFT cost scaling, independent of thermal occupation, is obvious. Note that the conventional free-energy KSDFT calculations end at the temperature shown because they were unaffordable above that T. A similar plot is given in ref 315 for the sdβ-vW14F $\mathcal{T}_s$ KEDF as a function of T over 2 orders of magnitude for the case of 128 H atoms placed randomly.

4.5. Applications with Orbital-Free Embedding Schemes

In Subsection 2.7.5 we discussed the central importance of the so-called nonadditive KEDF eq 158 in subsystem DFT (sDFT). A high-fidelity nonadditive KEDF approximation is

https://doi.org/10.1021/acs.chemrev.2c00758
Chem. Rev. 2023, 123, 12039−12104

essential; hence, we provide a brief review of LDA, GGA, and two-point nonadditive KEDFs with respect to the type of simulations they can support. This is not a comprehensive survey; rather our intent is to sketch what sDFT can do nowadays as it is enabled by progress in KEDF development. Additional details can be obtained from embedded method reviews.[180,181,190,408,409,430,653] We also remark that, unless specified differently, all the examples given in this section regard subsystem DFT simulations wherein all subsystem densities are driven to self-consistency.

Obviously, the Thomas−Fermi KEDF is the most rudimentary functional that can be used as a nonadditive KEDF. As originally determined by Wesolowski and Weber,[421] because the nonadditive KEDF magnitude is small for most weakly interacting subsystems, TF may be a utilitarian choice in some situations[421] even though it generally gives overly repulsive nonadditive KEDF values and incorrect energy curves.[296,654,655]

GGA nonadditive KEDF functionals generally are superior to TF for reproducing ground-state densities and energies.[181,296,656,657] For those systems in which the interaction between the constitutive subsystems is weak, GGA nonadditive KEDFs have been studied thoroughly. Overall, it was found that GGA nonadditive KEDFs reach sub-5-kcal/mol accuracy in the prediction of most weak intermolecular interaction energies as defined by standard test sets such as S22 or S66.[658,659] Systems studied include van der Waals complexes,[660,661] hydrogen-bonded complexes,[654,656,662,663] and their combinations.[60,425,426,655] In particular, recent work on partition DFT (related to sDFT but formulated in such a way that the density partitioning is unique while allowing self-consistent solutions for all subsystem densities[434]) shows that GGA nonadditive KEDFs even can provide a quantitative description of the energetics and electron density for selected diatomics connected by a single covalent bond compared to conventional KSDFT of the full system.[293,664]

Semilocal nonadditive KEDFs employed in sDFT have enabled AIMD simulations of liquids such as water,[296,665] and supercritical CO_2,[295] as well as solvated systems.[666] In them, GGA nonadditive KEDFs produced accurate results while providing dramatic computational cost reduction via improved scaling (from cubic to linear). Interestingly, an intrinsic error cancellation between the repulsive nonadditive KEDF and the attractive nonadditive XC led to semilocal sDFT giving improved results compared to those from semilocal conventional KSDFT.[296]

OFDFT can play an even greater role in sDFT simulations. For example, the combination, in a single subsystem DFT simulation, of conventional KSDFT solvers for molecular subsystems and OFDFT solvers for metallic surfaces recently was reported by Shao et al.[667] In that work, the binding energies of molecules at Al(111) surfaces were reported to be within a few meV of the conventional KSDFT values. Additionally, thanks to the advantageous computational scaling of OFDFT, the hybrid OFDFT/KSDFT subsystem DFT method yielded the electronic structure of large water/Al(111) interfaces in record wall times.

Perhaps the most spectacular application to date of sDFT with semilocal nonadditive KEDFs is credited to the VandeVondele group.[668] They tackled a tobacco virus completely ab initio by combining sDFT with linear-scaling conventional KSDFT techniques for the subsystems. The virus is effectively a protein with quaternary structure. It was geometry optimized in a simulation cell that was filled by water molecules. In Figure 25 we show the electronic structure of the tobacco virus computed by them colored by features of the electrostatic potential. While there is no particular reason for carrying out the geometry optimization of a virus, the simulation of ref 668 is a source of excitement and makes one realize that the all-electron, ab initio description of biological systems is an achievable goal and not science fiction.

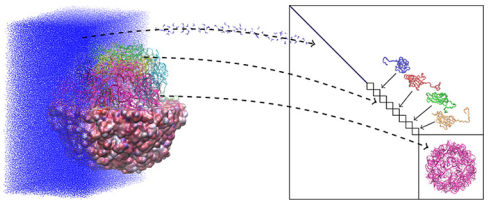

Figure 25. Electronic structure of a tobacco virus computed with sDFT combined with linear-scaling conventional KSDFT for the monomers making up the protein and the solvent. The figure maps portions of the virus onto its density matrix as defined by sDFT, with each diagonal block corresponding to one subsystem. The off-diagonal blocks are zero because orbitals of different subsystems belong to different KS systems which have independent Hilbert spaces and therefore need not be orthogonal. The nonadditive KEDF used is Lee−Lee−Parr.[58] Reprinted with permission from ref 668. Copyright (2016) American Chemical Society.

Beside these applications, a vast array of chemical problems, for instance, solvation free energies,[666] solvent effects on different types of spectroscopies,[669,670] magnetic properties,[671−675] charge-transfer states,[676−680] open-shell systems,[681] and excited states,[657,682−687] have been explored by semilocal sDFT and its time-dependent extension.[653,657,684,688] The fact that research continues to yield improved KEDFs suggests strongly that nonadditive KEDFs also will improve and, with that, the applicability of sDFT also will expand.

In addition, ways to expand the applicability of nonadditive KEDFs arise by coupling them with innovative embedding schemes. For example, the 3FDE method[689,690] handles strong interactions, for which nonadditive KEDFs would fail, by using a constraining potential derived from capping groups. That constraining potential also maintains a correct electron density in the regions of strong inter-subsystem density overlap. The recent adoption of sDFT to improve many-body expansions also is an interesting way to expand the applicability of sDFT.[691,692]

Along these lines of thought, Laricchia et al. tested various Laplacian-level meta-GGA nonadditive KEDFs for sDFT calculations.[285] They found improved sDFT results compared to GGA nonadditive KEDFs when testing interaction energies of small diatomics.

A step forward in accuracy and applicability has been achieved recently by employing two-point KEDFs. The reasons for the comparatively late employment of two-point KEDFs as nonadditive KEDFs are twofold. First, most such KEDFs are primarily suitable for weakly inhomogeneous systems (such as bulk metals). This limitation is at odds with sDFT. In it, the subsystem densities decay at the boundaries. Second, while there exist two-point KEDFs suitable for non-homogeneous systems, most either suffer from numerical instability, can only handle weak non-homogeneity,[297] or are too expensive to be employed in large-scale sDFT simulations.[77] However, the LMGP functionals discussed in Subsection 2.4.2 can be used as

https://doi.org/10.1021/acs.chemrev.2c00758
Chem. Rev. 2023, 123, 12039−12104

nonadditive KEDFs because they are particularly well suited to describe finite systems.[89] LMGP provides considerable performance improvement relative to the best GGA functionals in terms of both interaction energies and predicted electron densities.[89] Evaluation of the full significance of two-point nonadditive KEDFs for sDFT awaits comparable large-scale sDFT calculations. Note, however, that recently Shao et al.[425] constructed a GGA functional that mimics the behavior of two-point functionals (i.e., on one hand to cut off the von Weizsäcker functional in high-density regions and on the other hand to cut off the TF functional in low-density, asymptotic regions). Their functional improved upon existing GGA nonadditive KEDF performance by matching the accuracy of two-point nonadditive KEDFs for interaction energies and electron densities for the S22-5 and S66[658,659] test sets.

Thus far, we have discussed the accuracy of sDFT simulations by citing their ability to reproduce interaction energies (and energy curves) between molecules, and the structure and dynamics of molecular condensed phases (hence, we inferred also the quality of the computed atomic forces). There are, however, other properties that can be adjudged, such as dipole moments, NMR properties, optical spectra, etc. Clearly, the quality of the predicted molecular properties depends on the quality of the electron density, which in turn depends on the quality of the potential employed. In sDFT this translates to the quality of the embedding potential and, as in all KS-DFT calculations, the quality of the XC functional. While we have not dwelled on some of these important details, we refer the interested reader to excellent and comprehensive reviews on the subject (see, e.g., pp 335−337 and 345−346 of ref 181 and sections 5.2−5.6 of ref 190).

For more details on high-efficiency implementations, parallelization schemes, and other details of sDFT implementations, we refer the interested reader to refs 577−579, 665, 667, 668, and 693−695.

5. CONCLUSION

With this review, we have attempted to provide the reader with systematic access to the emerging value and quality of orbital-free density functional theory (OFDFT), both in advances of understanding the theory itself and in improved kinetic energy density functionals (KEDFs). Our claim is that because of steady and strong advances in the development of approximate KEDFS, OFDFT has already played a significant role in understanding materials and cluster chemistry and physics. We expect that role to grow and expand. That expectation is rooted in the growing number of investigators of OFDFT and codes implementing OFDFT. Given promising recent developments surveyed here, applications to catalysis, for example, as well as other parts of chemistry and materials science are expected to surface soon, either with pure OFDFT simulations or with other, related methods such as embedding and decomposition schemes.

In the modeling of chemical processes, atom dynamics and finite-size effects constitute the biggest bottlenecks in current simulation protocols. As we showed in Section 4, OFDFT already resolves those issues for a large class of systems. The challenge now is to widen its applicability to embrace an even larger set of system types. One of the persistent roadblocks to universal applicability of OFDFT has been the limited accuracy of available KEDFs. Another is the lack of local pseudopotentials for second-row elements and transition metals. While such roadblocks affect pure OFDFT, we have described several hybrid schemes that are less affected by these shortcomings.

The historical account of the development of OFDFT given in Section 1 and the theoretical background presentation in Section 2 show clearly that only by following a rigorous, constraint-satisfaction strategy can one formulate generally applicable (transferable) KEDFs. Thus, we hope this review will help guide OFDFT developers as well as spark interest in employing OFDFT among those research groups that customarily have employed only conventional KSDFT in their research. This is particularly relevant, as OFDFT is now accessible through several software suites (see Section 3).

Obviously, we are indebted to the OFDFT research community that came before us and until recently was rather small. Spanning chemistry, physics, and materials science, that hardy band has inspired us and our research groups over the years, with healthy and constructive debate aimed at the goal of serving the broader scientific community with useful, predictive, swift, ab initio electronic structure methods.

AUTHOR INFORMATION

Corresponding Authors

Wenhui Mi − *Key Laboratory of Material Simulation Methods & Software of Ministry of Education, College of Physics, State Key Laboratory of Superhard Materials, and International Center of Future Science, Jilin University, Changchun 130012, PR China*; orcid.org/0000-0002-1612-5292; Email: mwh@jlu.edu.cn

Kai Luo − *Department of Applied Physics, Nanjing University of Science and Technology, Nanjing 210094, PR China*; Email: kluo@njust.edu.cn

S. B. Trickey − *Quantum Theory Project, Department of Physics and Department of Chemistry, University of Florida, Gainesville, Florida 32611, United States*; orcid.org/0000-0001-9224-6304; Email: trickey@qtp.ufl.edu

Michele Pavanello − *Department of Physics and Department of Chemistry, Rutgers University, Newark, New Jersey 07102, United States*; orcid.org/0000-0001-8294-7481; Email: m.pavanello@rutgers.edu

Complete contact information is available at: https://pubs.acs.org/10.1021/acs.chemrev.2c00758

Author Contributions

†All authors contributed equally to this work. CRediT: **Wenhui Mi** funding acquisition, writing-original draft, writing-review & editing; **Kai Luo** funding acquisition, writing-original draft, writing-review & editing; **Samuel B. Trickey** conceptualization, funding acquisition, project administration, writing-original draft, writing-review & editing; **Michele Pavanello** conceptualization, funding acquisition, project administration, writing-original draft, writing-review & editing.

Notes

The authors declare no competing financial interest.

Biographies

Wenhui Mi is a professor of computational physics at Jilin university. He received his Ph.D. degree in condensed matter physics from Jilin University in 2016 under the supervision of Prof. Yanming Ma. Then he moved to Duke University (2016−2017), working with Prof. Volker Blum, and Rutgers University (2017−2021), working with

https://doi.org/10.1021/acs.chemrev.2c00758
Chem. Rev. 2023, 123, 12039−12104

Prof. Michele Pavanello as a postdoctoral researcher. He began to work as a tenure-track professor at Jilin University in 2021 and was promoted to full professor in 2022. He was awarded the national high-level overseas talents introduction youth project of China in 2022. His research interests mainly focus on the development of electronic structure methods for large-scale, mesoscopic systems, focusing on such methods as orbital-free DFT and density embedding for materials science applications.

Kai Luo is an associate professor in Applied Physics at Nanjing University of Science and Technology. He received his Ph.D. from City University of New York in 2015 under the supervision by Neepa T. Maitra. Then he continued his postdoctoral research with Robert A. DiStasio at Cornell University (2015-2016), S. B. Trickey and James W. Dufty at University of Florida (2017-2019), and Ronald E. Cohen at Carnegie Institution for Science (2019-2021). His research interests are in density and density matrix based electronic structure methods and their applications to matter under extreme conditions.

S. B. Trickey is Prof. (emeritus) of Physics and Chemistry, Univiversity of Florida. He received his Ph.D. from Texas A&M in 1968 and joined the faculty at Florida that same year. His research interests are in density functional theory of many-Fermion systems, especially constraint-based, orbital-free functionals for ab initio molecular dynamics, and the formal underpinnings of free-energy DFT and its connections to and constraints from rigorous many-body theory. The motivation is predictive simulations of matter under extreme conditions, for example, warm dense matter. He is a Fellow of the American Physical Society, an APS Outstanding Referee, and Miembro Correspondiente de la Academia Mexicana de Ciencias.

Michele Pavanello is a professor of Chemistry and Physics in the Newark campus of Rutgers University. Michele graduated in 2010 with a Ph.D. in Chemistry from the University of Arizona working with Prof. Ludwik Adamowicz on describing few-particle Coulomb systems such as the H_3^+ molecular ion as accurately as possible. A Marie Curie fellowship took him to The Netherlands to work on density embedding and its formulations for describing charge-transfer reactions with Prof. Johannes Neugebauer (now at the University of Münster, Germany). Since 2012, Michele has been leading the Pavanello Research Group (PRG), focusing on electronic structure method development for material science problems, funded by NSF, DOE, and ACS-PRF grants. Michele received the ACS-COMP OpenEye junior faculty award in 2016, and in the same year he received the NSF CAREER award. In 2018 and 2020 Michele was awarded the Rutgers Board of Trustees Award for Excellence in Research for recently promoted as well as for tenured faculty. In 2022, the Physical Chemistry division of ACS awarded him the ACS-PHYS Early Career Award in Theoretical Chemistry.

ACKNOWLEDGMENTS

Over the years, we have benefited from discussions and presentations by many of the colleagues referenced here. MP and SBT are particularly grateful to current and former members of their respective groups. We also thank Andrew Baczewski for his comments on the computational scaling (both theoretical and in practice) of conventional KSDFT methods. WM acknowledges funding support from the National Natural Science Foundation of China under Grant No. 12274171. KL was supported by the National Natural Science Foundation of China Grant No.12104230. MP acknowledges support by the U.S. National Science Foundation under Grants No. CHE-1553993, CHE-2154760, and OAC-1931473 and the U.S. Department of Energy, Office of Basic Energy Sciences, under Award Number DE-SC0018343. SBT was supported by U.S. Department of Energy Grant No. DE-SC0002139.

REFERENCES

(1) Kohn, W.; Sham, L. J. Self-consistent Equations Including Exchange and Correlation Effects. *Phys. Rev.* **1965**, *140*, A1133−A1138.
(2) Burke, K. Perspective on Density Functional Theory. *J. Chem. Phys.* **2012**, *136*, 150901.
(3) Hohenberg, P.; Kohn, W. Inhomogeneous Electron Gas. *Phys. Rev.* **1964**, *136*, B864.
(4) Gould, T. Welcome to Lab 2.0 Where Computers Replace Experimental Science. https://theconversation.com/welcome-to-lab-2-0-where-computers-replace-experimental-science-57271, Accessed on 10/03/2022.
(5) Jain, A.; Ong, S. P.; Hautier, G.; Chen, W.; Richards, W. D.; Dacek, S.; Cholia, S.; Gunter, D.; Skinner, D.; Ceder, G.; Persson, K. A. The Materials Project: A Materials Genome Approach to Accelerating Materials Innovation. *APL Mater.* **2013**, *1*, 011002.
(6) Pizzi, G.; Cepellotti, A.; Sabatini, R.; Marzari, N.; Kozinsky, B. AiiDA: Automated Interactive Infrastructure and Database for Computational Science. *Comput. Mater. Sci.* **2016**, *111*, 218−230.
(7) Hylleraas, E. A. Neue Berechnung Der Energie Des Heliums Im Grundzustande, Sowie Des Tiefsten Terms Von Ortho-helium. *Z. Phys.* **1929**, *54*, 347−366.
(8) Facit Model, S. Odhner Pinwheel Calculator. 1935; http://www.johnwolff.id.au/calculators/Facit/Facit.htm, Accessed on 10/03/2022.
(9) Corporation, E.-M. C. Electronic Numerical Integrator and Computer. Patent Specification 709,407, 1948.
(10) Aidas, K.; et al. The Dalton Quantum Chemistry Program System. *Wiley Interdiscip. Rev. Comput. Mol. Sci.* **2014**, *4*, 269−284.
(11) Bowler, D.; Miyazaki, T. O(N) Methods in Electronic Structure Calculations. *Rep. Prog. Phys.* **2012**, *75*, 036503.
(12) Hartree, D. R. Results of Calculations of Atomic Wave Functions. I. Survey, and Self-consistent Fields for Cl and Cu. *Proc. Math. Phys. Eng. Sci.* **1933**, *141*, 282−301.
(13) VandeVondele, J.; Borštnik, U.; Hutter, J. Linear Scaling Self-consistent Field Calculations with Millions of Atoms in the Condensed Phase. *J. Chem. Theory Comput.* **2012**, *8*, 3565−3573.
(14) Khaliullin, R. Z.; VandeVondele, J.; Hutter, J. Efficient Linear-scaling Density Functional Theory for Molecular Systems. *J. Chem. Theory Comput.* **2013**, *9*, 4421−4427.
(15) Shimojo, F.; Kalia, R. K.; Nakano, A.; Vashishta, P. Linear-scaling Density-functional-theory Calculations of Electronic Structure Based on Real-space Grids: Design, Analysis, and Scalability Test of Parallel Algorithms. *Comput. Phys. Commun.* **2001**, *140*, 303−314.
(16) Clark, S. J.; Segall, M. D.; Pickard, C. J.; Hasnip, P. J.; Probert, M. I.; Refson, K.; Payne, M. C. First Principles Methods Using Castep. *Z. Kristallogr. Cryst. Mater.* **2005**, *220*, 567−570.
(17) Moussa, J. E.; Baczewski, A. D. Assessment of Localized and Randomized Algorithms for Electronic Structure. *Electron. Struct.* **2019**, *1*, 033001.
(18) Bartlett, R. J. Coupled-cluster Theory and Its Equation-of-motion Extensions. *Wiley Interdiscip. Rev. Comput. Mol. Sci.* **2012**, *2*, 126−138.
(19) Chan, G. K.-L.; Dorando, J. J.; Ghosh, D.; Hachmann, J.; Neuscamman, E.; Wang, H.; Yanai, T. An Introduction to the Density Matrix Renormalization Group Ansatz in Quantum Chemistry. *Frontiers in Quantum Systems in Chemistry and Physics*; Springer Netherlands, 2008; pp 49−65.
(20) Zhang, I. Y.; Grüneis, A. Coupled Cluster Theory in Materials Science. *Front. Mater.* **2019**, *6*, 123.
(21) Baiardi, A.; Reiher, M. The Density Matrix Renormalization Group in Chemistry and Molecular Physics: Recent Developments and New Challenges. *J. Chem. Phys.* **2020**, *152*, 040903.

https://doi.org/10.1021/acs.chemrev.2c00758
Chem. Rev. 2023, 123, 12039−12104

(22) Fermi, E. Un Metodo Statistico Per La Determinazione Di Alcune Proprietà Dell'Atomo. *Rend. Accad. Naz. Lincei* **1927**, *6*, 32.
(23) Thomas, L. H. The calculation of atomic fields. *Math. Proc. Camb. Philos. Soc.* **1927**, *23*, 542−548.
(24) Baker, E. B. The Application of the Fermi-Thomas Statistical Model to the Calculation of Potential Distribution in Positive Ions. *Phys. Rev.* **1930**, *36*, 630−647.
(25) Dirac, P. A. M. Note on Exchange Phenomena in the Thomas Atom. *Proc. Camb. Philos. Soc.* **1930**, *26*, 376−385.
(26) Slater, J. C.; Krutter, H. M. The Thomas-Fermi Method for Metals. *Phys. Rev.* **1935**, *47*, 559−568.
(27) von Weizsäcker, C. F. Zur Theorie Der Kernmassen. *Z. Phys.* **1935**, *96*, 431−458.
(28) Reitz, J. R. The Effect of Screening on Beta-ray Spectra and Internal Conversion. *Phys. Rev.* **1950**, *77*, 10−18.
(29) Feynman, R. P.; Metropolis, N.; Teller, E. Equations of State of Elements Based on the Generalized Fermi-Thomas Theory. *Phys. Rev.* **1949**, *75*, 1561−1573.
(30) March, N. H. The Thomas-Fermi Approximation in Quantum Mechanics. *Adv. Phys.* **1957**, *6*, 1−101.
(31) Kirzhnitz, D. A. Quantum Corrections to the Thomas-Fermi Equation. *Soviet Phys. JETP* **1957**, *5*, 64.
(32) Acharya, P. K.; Bartolotti, L. J.; Sears, S. B.; Parr, R. G. An Atomic Kinetic Energy Functional with Full Weizsäcker Correction. *Proc. Nat. Acad. Sci. (USA)* **1980**, *77*, 6978−6982.
(33) Baltin, R. The Energy-density Functional of an Electron Gas in Locally Linear Approximation of the One-body Potential. *Z. Naturforsch. A* **1972**, *27*, 1176−1186.
(34) Golden, S. Statistical Theory of Many-electron Systems. General Considerations Pertaining to the Thomas-Fermi Theory. *Phys. Rev.* **1957**, *105*, 604−615.
(35) Ghosh, S. K.; Parr, R. G. Density-determined Orthonormal Orbital Approach to Atomic Energy Functionals. *J. Chem. Phys.* **1985**, *82*, 3307−3315.
(36) Gázquez, J.; Robles, J. On the Atomic Kinetic Energy Functionals with Full Weizsäcker Correction. *J. Chem. Phys.* **1982**, *76*, 1467−1472.
(37) Lieb, E. H. Thomas-Fermi and Related Theories of Atoms and Molecules. *Rev. Mod. Phys.* **1981**, *53*, 603−641.
(38) Yonei, K.; Tomishima, Y. On the Weizsäcker Correction to the Thomas-Fermi Theory of the Atom. *J. Phys. Soc. Jpn.* **1965**, *20*, 1051−1057.
(39) Teller, E. On the Stability of Molecules in the Thomas-Fermi Theory. *Rev. Mod. Phys.* **1962**, *34*, 627.
(40) Kohn, W.; Sham, L. J. Quantum Density Oscillations in an Inhomogeneous Electron Gas. *Phys. Rev.* **1965**, *137*, A1697.
(41) Benguria, R.; Brezis, H.; Lieb, E. H. The Thomas-Fermi-von Weizsäcker Theory of Atoms and Molecules. *Commun. Math. Phys.* **1981**, *79*, 167−180.
(42) Berk, A. Lower-bound Energy Functionals and Their Application to Diatomic Systems. *Phys. Rev. A* **1983**, *28*, 1908−1923.
(43) Chacón, E.; Alvarellos, J. E.; Tarazona, P. Nonlocal Kinetic Energy Functional for Nonhomogeneous Electron Systems. *Phys. Rev. B* **1985**, *32*, 7868−7877.
(44) Wang, L.-W.; Teter, M. P. Kinetic-energy Functional of the Electron Density. *Phys. Rev. B* **1992**, *45*, 13196−13220.
(45) Wang, Y. A.; Govind, N.; Carter, E. A. Orbital-free Kinetic-energy Functionals for the Nearly Free Electron Gas. *Phys. Rev. B* **1998**, *58*, 13465−13471.
(46) Smargiassi, E.; Madden, P. A. Orbital-free Kinetic-energy Functionals for First-principles Molecular Dynamics. *Phys. Rev. B* **1994**, *49*, 5220.
(47) Perrot, F. Hydrogen-hydrogen Interaction in an Electron Gas. *J. Phys.: Condens. Matter* **1994**, *6*, 431.
(48) Chai, J.-D.; Weeks, J. D. Orbital-free Density Functional Theory: Kinetic Potentials and *ab Initio* Local Pseudopotentials. *Phys. Rev. B* **2007**, *75*, 205122.
(49) Xu, Q.; Wang, Y.; Ma, Y. Nonlocal kinetic energy density functional via line integrals and its application to orbital-free density functional theory. *Phys. Rev. B* **2019**, *100*, 205132.
(50) Choly, N.; Kaxiras, E. Kinetic Energy Density Functionals for Non-periodic Systems. *Solid State Commun.* **2002**, *121*, 281−286.
(51) Mortensen, J. J.; Hansen, L. B.; Jacobsen, K. W. Real-space Grid Implementation of the Projector Augmented Wave Method. *Phys. Rev. B* **2005**, *71*, 035109.
(52) Golub, P.; Manzhos, S. CONUNDrum: A Program for Orbital-free Density Functional Theory Calculations. *Comput. Phys. Commun.* **2020**, *256*, 107365.
(53) Mi, W.; Shao, X.; Su, C.; Zhou, Y.; Zhang, S.; Li, Q.; Wang, H.; Zhang, L.; Miao, M.; Wang, Y.; Ma, Y. ATLAS: A Real-space Finite-difference Implementation of Orbital-free Density Functional Theory. *Comput. Phys. Commun.* **2016**, *200*, 87−95.
(54) Shao, X.; Jiang, K.; Mi, W.; Genova, A.; Pavanello, M. DFTpy: An Efficient and Object-oriented Platform for Orbital-free DFT Simulations. *Wiley Interdiscip. Rev. Comput. Mol. Sci.* **2021**, *11*, e1482.
(55) Chen, M.; Xia, J.; Huang, C.; Dieterich, J. M.; Hung, L.; Shin, I.; Carter, E. A. Introducing PROFESS 3.0: An Advanced Program for Orbital-free Density Functional Theory Molecular Dynamics Simulations. *Comput. Phys. Commun.* **2015**, *190*, 228−230.
(56) Perdew, J. P.; Yue, W. Accurate and Simple Density Functional for the Electronic Exchange Energy: Generalized Gradient Approximation. *Phys. Rev. B* **1986**, *33*, 8800−8802.
(57) Perdew, J. P. Density-functional Approximation for the Correlation Energy of the Inhomogeneous Electron Gas. *Phys. Rev. B* **1986**, *33*, 8822−8824.
(58) Lee, H.; Lee, C.; Parr, R. G. Conjoint Gradient Correction to the Hartree-Fock Kinetic- and Exchange-energy Density Functionals. *Phys. Rev. A* **1991**, *44*, 768−771.
(59) Constantin, L. A.; Fabiano, E.; Laricchia, S.; Della Sala, F. Semiclassical Neutral Atom As a Reference System in Density Functional Theory. *Phys. Rev. Lett.* **2011**, *106*, 186406.
(60) Laricchia, S.; Fabiano, E.; Constantin, L. A.; Della Sala, F. Generalized Gradient Approximations of the Noninteracting Kinetic Energy from the Semiclassical Atom Theory: Rationalization of the Accuracy of the Frozen Density Embedding Theory for Nonbonded Interactions. *J. Chem. Theory Comput.* **2011**, *7*, 2439−2451.
(61) DePristo, A. E.; Kress, J. D. Kinetic-energy Functionals via Padé Approximations. *Phys. Rev. A* **1987**, *35*, 438−441.
(62) Ernzerhof, M. The Role of the Kinetic Energy Density in Approximations to the Exchange Energy. *J. Mol. Struct.: THEOCHEM* **2000**, *501*−*502*, 59−64.
(63) Karasiev, V. V.; Trickey, S. B.; Harris, F. E. Born−Oppenheimer Interatomic Forces from Simple, Local Kinetic Energy Density Functionals. *J. Comput. Aided Mol. Des.* **2006**, *13*, 111−129.
(64) Fuentealba, P.; Reyes, O. Further Evidence of the Conjoint Correction to the Local Kinetic and Exchange Energy Density Functionals. *Chem. Phys. Lett.* **1995**, *232*, 31−34.
(65) Ghiringhelli, L. M.; Delle Site, L. Design of Kinetic Functionals for Many-body Electron Systems: Combining Analytical Theory with Monte Carlo Sampling of Electronic Configurations. *Phys. Rev. B* **2008**, *77*, 073104.
(66) Ghiringhelli, L. M.; Hamilton, I. P.; Delle Site, L. Interacting Electrons, Spin Statistics, and Information Theory. *J. Chem. Phys.* **2010**, *132*, 014106.
(67) Lembarki, A.; Chermette, H. Obtaining a Gradient-corrected Kinetic-energy Functional from the Perdew-wang Exchange Functional. *Phys. Rev. A* **1994**, *50*, 5328−5331.
(68) Ou-Yang, H.; Levy, M. Approximate Noninteracting Kinetic Energy Functionals from a Nonuniform Scaling Requirement. *Int. J. Quantum Chem.* **1991**, *40*, 379−388.
(69) Lacks, D. J.; Gordon, R. G. Tests of Nonlocal Kinetic Energy Functionals. *J. Chem. Phys.* **1994**, *100*, 4446−4452.
(70) Pearson, E. W.; Gordon, R. G. Local Asymptotic Gradient Corrections to the Energy Functional of an Electron Gas. *J. Chem. Phys.* **1985**, *82*, 881−889.

https://doi.org/10.1021/acs.chemrev.2c00758
Chem. Rev. 2023, 123, 12039−12104

(71) Perdew, J. P. Generalized Gradient Approximation for the Fermion Kinetic Energy As a Functional of the Density. *Phys. Lett. A* **1992**, *165*, 79−82.
(72) Thakkar, A. J. Comparison of Kinetic-energy Density Functionals. *Phys. Rev. A* **1992**, *46*, 6920−6924.
(73) Karasiev, V. V.; Jones, R. S.; Trickey, S. B.; Harris, F. E. Recent Advances in Developing Orbital-free Kinetic Energy Functionals. In *New Developments in Quantum Chemistry*; Paz, J. L.; Hernández, A. J., Eds.; Research Signpost, Kerala, 2009; pp 25−54.
(74) Tran, F.; Wesołowski, T. A. Link between the Kinetic-and Exchange-energy Functionals in the Generalized Gradient Approximation. *Int. J. Quantum Chem.* **2002**, *89*, 441−446.
(75) Vitos, L.; Johansson, B.; Kollár, J.; Skriver, H. L. Local Kinetic-energy Density of the Airy Gas. *Phys. Rev. A* **2000**, *61*, 052511.
(76) Vitos, L.; Skriver, H. L.; Kollár, J. Kinetic-energy Functionals Studied by Surface Calculations. *Phys. Rev. B* **1998**, *57*, 12611−12615.
(77) Huang, C.; Carter, E. A. Nonlocal Orbital-free Kinetic Energy Density Functional for Semiconductors. *Phys. Rev. B* **2010**, *81*, 045206.
(78) Xia, J.; Carter, E. A. Density-decomposed Orbital-free Density Functional Theory for Covalently Bonded Molecules and Materials. *Phys. Rev. B* **2012**, *86*, 235109.
(79) Shin, I.; Carter, E. A. Enhanced Von Weizsäcker Wang-Govind-Carter Kinetic Energy Density Functional for Semiconductors. *J. Chem. Phys.* **2014**, *140*, 18A531.
(80) Constantin, L. A.; Fabiano, E.; Della Sala, F. Nonlocal Kinetic Energy Functional from the Jellium-with-gap Model: Applications to Orbital-free Density Functional Theory. *Phys. Rev. B* **2018**, *97*, 205137.
(81) Mi, W.; Genova, A.; Pavanello, M. Nonlocal Kinetic Energy Functionals by Functional Integration. *J. Chem. Phys.* **2018**, *148*, 184107.
(82) Snyder, J. C.; Rupp, M.; Hansen, K.; Müller, K.-R.; Burke, K. Finding Density Functionals with Machine Learning. *Phys. Rev. Lett.* **2012**, *108*, 253002.
(83) Golub, P.; Manzhos, S. Kinetic Energy Densities Based on the Fourth Order Gradient Expansion: Performance in Different Classes of Materials and Improvement via Machine Learning. *Phys. Chem. Chem. Phys.* **2019**, *21*, 378−395.
(84) Bogojeski, M.; Vogt-Maranto, L.; Tuckerman, M. E.; Müller, K.-R.; Burke, K. Quantum Chemical Accuracy from Density Functional Approximations via Machine Learning. *Nat. Commun.* **2020**, *11*, 5223.
(85) Karasiev, V. V.; Chakraborty, D.; Shukruto, O. A.; Trickey, S. B. Nonempirical Generalized Gradient Approximation Free-energy Functional for Orbital-free Simulations. *Phys. Rev. B* **2013**, *88*, 161108.
(86) Luo, K.; Karasiev, V. V.; Trickey, S. B. A Simple Generalized Gradient Approximation for the Noninteracting Kinetic Energy Density Functional. *Phys. Rev. B* **2018**, *98*, 041111.
(87) Constantin, L. A.; Fabiano, E.; Della Sala, F. Semilocal Pauli−gaussian Kinetic Functionals for Orbital-free Density Functional Theory Calculations of Solids. *J. Phys. Chem. Lett.* **2018**, *9*, 4385−4390.
(88) Mi, W.; Pavanello, M. Orbital-free Density Functional Theory Correctly Models Quantum Dots When Asymptotics, Nonlocality, and Nonhomogeneity Are Accounted for. *Phys. Rev. B* **2019**, *100*, 041105.
(89) Mi, W.; Pavanello, M. Nonlocal Subsystem Density Functional Theory. *J. Phys. Chem. Lett.* **2020**, *11*, 272−279.
(90) Xu, Q.; Lv, J.; Wang, Y.; Ma, Y. Nonlocal Kinetic Energy Density Functionals for Isolated Systems Obtained via Local Density Approximation Kernels. *Phys. Rev. B* **2020**, *101*, 045110.
(91) Shao, X.; Mi, W.; Pavanello, M. Revised Huang-Carter nonlocal kinetic energy functional for semiconductors and their surfaces. *Phys. Rev. B* **2021**, *104*, 045118.
(92) Dirac, P. A. M. Quantum Mechanics of Many-electron Systems. *Proc. Roy. Soc. A* **1929**, *123*, 714−733.
(93) Brillouin, L. Le Modèle D'atome De Fock-Dirac Et L'existence Des Potentiels D'ionisation. *J. Phys. Radium* **1934**, *5*, 185−192.
(94) Hartree, D. R. The Wave Mechanics of an Atom with a Non-coulomb Central Field. Part I. Theory and Methods. *Math. Proc. Camb. Philos. Soc.* **1928**, *24*, 89−110.
(95) Hartree, D. R. The Wave Mechanics of an Atom with a Non-coulomb Central Field. Part II. Results and Discussion. *Math. Proc. Camb. Philos. Soc.* **1928**, *24*, 111−132.
(96) Hartree, D. R.; Hartree, W. Self-consistent Field, with Exchange, for Beryllium. *Proc. Math. Phys. Eng. Sci.* **1935**, *150*, 9−33.
(97) Lieb, E. H.; Simon, B. Thomas-Fermi Theory of Atoms. *Molecules and Solids. Adv. Math.* **1977**, *23*, 22−116.
(98) Spruch, L. Pedagogic Notes on Thomas-Fermi Theory (and on Some Improvements): Atoms, Stars, and the Stability of Bulk Matter. *Rev. Mod. Phys.* **1991**, *63*, 151−209.
(99) March, N. H. Origins—The Thomas-Fermi Theory. In *Theory of the Inhomogeneous Electron Gas*; Lundqvist, S., March, N. H., Eds.; Springer US: Boston, MA, 1983; pp 1−77.
(100) Solovej, J. P. A New Look at Thomas-Fermi Theory. *Mol. Phys.* **2016**, *114*, 1036.
(101) Englert, B.-G. *Semiclassical Theory of Atoms*; Springer: Berlin, 1988.
(102) Parr, R. G.; Yang, W. *Density-functional Theory of Atoms and Molecules*; Oxford University Press, 1989.
(103) Slater, J. C. *Quantum Theory of Atomic Structure*; McGraw-Hill: New York, 1960; Vol. *1*.
(104) Slater, J. *Insulators, Semiconductors and Metals: Quantum Theory of Molecules and Solids*; McGraw-Hill: New York, 1967; Vol. *3*.
(105) Guliani, G. F.; Vignale, G. *Quantum Theory of the Electron Liquid*; Cambridge University Press: Cambridge, 2005.
(106) Engel, E.; Dreizler, R. M. *Density Functional Theory*; Springer, 2013.
(107) Hartree, D. R. Some Methods of Estimating the Successive Ionisation Potentials of Any Element. *Math. Proc. Camb. Philos. Soc.* **1924**, *22*, 464−474.
(108) Hillery, M.; O'Connell, R. F.; Scully, M. O.; Wigner, E. P. Distribution Functions in Physics: Fundamentals. *Phys. Rep.* **1984**, *106*, 121−167.
(109) Mukamel, S. *Principles of Nonlinear Optical Spectroscopy*; Oxford Series in Optical and Imaging Sciences 6; Oxford University Press: New York, 2009.
(110) Weyl, H. Quantenmechanik Und Gruppentheorie. *Z. Phys.* **1927**, *46*, 1−46.
(111) Wigner, E. On the Quantum Correction For Thermodynamic Equilibrium. *Phys. Rev.* **1932**, *40*, 749−759.
(112) Fermi, L. *Atoms in the family: my life with Enrico Fermi (1954)*; University of Chicago Press, 2014.
(113) Berg, R.; Wilets, L. On the Validity of the Weizsäcker Inhomogeneity Correction Term. *Proc. Phys. Soc. A* **1955**, *68*, 229−239.
(114) Gázquez, J. L.; Ludeña, E. V. The Weizsäcker Term in Density Functional Theory. *Chem. Phys. Lett.* **1981**, *83*, 145−148.
(115) Wang, Y. A.; Carter, E. A. Orbital-free Kinetic-energy Density Functional Theory. In *Theoretical Methods in Condensed Phase Chemistry*; Schwartz, S., Ed.; Kluwer: New York, 2000; pp 117−184. Republished in 2002 by Springer.
(116) Tomishima, Y.; Yonei, K. Solution of the Thomas-Fermi−Dirac Equation with a Modified Weizsäcker Correction. *J. Phys. Soc. Jpn.* **1966**, *21*, 142−153.
(117) Murphy, D. R.; Parr, R. G. Gradient Expansion of the Kinetic Energy Density Functional: Local Behavior of the Kinetic Energy Density. *Chem. Phys. Lett.* **1979**, *60*, 377−79.
(118) Goodisman, J. Modified Weizsäcker Corrections in Thomas-Fermi Theories. *Phys. Rev. A* **1970**, *1*, 1574−1576.
(119) Chan, G. K.-L.; Cohen, A. J.; Handy, N. C. Thomas−Fermi−Dirac−von Weizsäcker Models in Finite Systems. *J. Chem. Phys.* **2001**, *114*, 631−638.
(120) Lehtomäki, J.; Makkonen, I.; Caro, M. A.; Harju, A.; Lopez-Acevedo, O. Orbital-free Density Functional Theory Implementation

https://doi.org/10.1021/acs.chemrev.2c00758
Chem. Rev. 2023, 123, 12039−12104

with the Projector Augmented-wave Method. *J. Chem. Phys.* **2014**, *141*, 234102.
(121) Karasiev, V. V.; Trickey, S. B. Issues and Challenges in Orbital-free Density Functional Calculations. *Comput. Phys. Commun.* **2012**, *183*, 2519−2527.
(122) García-Aldea, D.; Martín-Blas, T.; Alvarellos, J. E. Local Behavior of the First-order Gradient Correction to the Thomas−Fermi Kinetic Energy Functional. *J. Chem. Phys.* **2009**, *131*, 164117.
(123) Friedel, J. XIV. The Distribution of Electrons Round Impurities in Monovalent Metals. *London Edinb. Dublin Philos. Mag.* **1952**, *43*, 153−189.
(124) Yang, W.; Parr, R. G.; Lee, C. Various Functionals for the Kinetic Energy Density of an Atom or Molecule. *Phys. Rev. A* **1986**, *34*, 4586−4590.
(125) Alonso, J. A.; Girifalco, L. A. Gradient Corrections in the Energy Density Functional. *Chem. Phys. Lett.* **1978**, *53*, 190−191.
(126) Aguado, A. Orbital-free Molecular Dynamics Study of Melting in K_{20}, K_{55}, K_{92}, K_{142}, Rb_{55},and Cs_{55}Clusters. *Phys. Rev. B* **2001**, *63*, 115404.
(127) Aguado, A.; López, J. M. Molecular Dynamics Simulations of the Meltinglike Transition in $Li_{13}Na_{42}$and $Na_{13}Cs_{42}$Clusters. *Phys. Rev. B* **2005**, *71*, 075415.
(128) Aguado, A.; González, L. E.; López, J. M. Thermal Properties of Impurity-doped Clusters: Orbital-free Molecular Dynamics Simulations of the Meltinglike Transition in $Li_1Na_{54}$and Cs_1Na_{54}. *J. Phys. Chem. B* **2004**, *108*, 11722−11731.
(129) Slater, J. C. A Simplification of the Hartree-Fock Method. *Phys. Rev.* **1951**, *81*, 385−390.
(130) Slater, J. C. A Generalized Self-consistent Field Method. *Phys. Rev.* **1953**, *91*, 528−530.
(131) Medvedev, M. G.; Bushmarinov, I. S.; Sun, J.; Perdew, J. P.; Lyssenko, K. A. Density Functional Theory Is Straying from the Path Toward the Exact Functional. *Science* **2017**, *355*, 49−52.
(132) Kohn, W. Nobel Lecture: Electronic Structure of Matter - Wave Functions and Density Functionals. *Rev. Mod. Phys.* **1999**, *71*, 1253−1266.
(133) Pople, J. Nobel Lecture: Quantum Chemical Models. *Rev. Mod. Phys.* **1999**, *71*, 1267−1274.
(134) Gill, P.; Johnson, B.; Pople, J.; Frisch, M. An Investigation of the Performance of a Hybrid of Hartree-Fock and Density Functional Theory. *Int. J. Quantum Chem.* **1992**, *44* (S26), 319−331.
(135) Jones, R. O. Density Functional Theory: Its Origins, Rise to Prominence, and Future. *Rev. Mod. Phys.* **2015**, *87*, 897−923.
(136) Hodges, C. H. Quantum Corrections to the Thomas−Fermi Approximation—the Kirzhnits Method. *Can. J. Phys.* **1973**, *51*, 1428−1437.
(137) Wang, W. P.; Parr, R. G.; Murphy, D. R.; Henderson, G. A. Gradient Expansion of the Atomic Kinetic Energy Functional. *Chem. Phys. Lett.* **1976**, *43*, 409−412.
(138) Oliver, G. L.; Perdew, J. P. Spin-Density Gradient Expansion of the Kinetic Energy. *Phys. Rev. A* **1979**, *20*, 397−403.
(139) Murphy, D. R. Sixth-order Term of the Gradient Expansion of the Kinetic-energy Density Functional. *Phys. Rev. A* **1981**, *24*, 1682−1688.
(140) Lindhard, J. On the Properties of a Gas of Charged Particles. *Kgl. Danske Videnskab. Selskab Mater.-fys. Medd.* **1954**, *28*, 8.
(141) Fetter, A. L.; Walecka, J. D. *Quantum Theory of Many-particle Systems*; McGraw-Hill, 1971.
(142) Löwdin, P. O. Quantum Theory of Many-particle Systems. I. Physical Interpretation by Means of Density Matrices, Natural Spin-orbitals and Convergence Problems in the Method of Configuration Interaction. *Phys. Rev.* **1955**, *97*, 1474−1489.
(143) García-Aldea, D.; Alvarellos, J. Kinetic Energy Density Study of Some Representative Semilocal Kinetic Energy Functionals. *J. Chem. Phys.* **2007**, *127*, 144109.
(144) García-Aldea, D.; Alvarellos, J. E. Generalized Nonlocal Kinetic Energy Density Functionals Based on the Von Weizsäcker Functional. *Phys. Chem. Chem. Phys.* **2012**, *14*, 1756−1767.
(145) Witt, W. C.; del Rio, B. G.; Dieterich, J. M.; Carter, E. A. Orbital-free Density Functional Theory for Materials Research. *J. Mater. Res.* **2018**, *33*, 777−795.
(146) García-Aldea, D.; Alvarellos, J.; Roy, A. The Construction of Kinetic Energy Functionals and the Linear Response function. In *Theoretical and Computational Developments in Modern Density Functional Theory*; Roy, A., Ed.; Physics Research and Technology; Nova Science Publishers, 2012; pp 255−280.
(147) Yao, K.; Parkhill, J. Kinetic Energy of Hydrocarbons As a Function of Electron Density and Convolutional Neural Networks. *J. Chem. Theory Comput.* **2016**, *12*, 1139−1147.
(148) Brockherde, F.; Vogt, L.; Li, L.; Tuckerman, M. E.; Burke, K.; Müller, K.-R. Bypassing the Kohn-Sham Equations with Machine Learning. *Nat. Commun.* **2017**, *8*, 872.
(149) Hollingsworth, J.; Li, L.; Baker, T. E.; Burke, K. Can Exact Conditions Improve Machine-learned Density Functionals? *J. Chem. Phys.* **2018**, *148*, 241743.
(150) Seino, J.; Kageyama, R.; Fujinami, M.; Ikabata, Y.; Nakai, H. Semi-local Machine-learned Kinetic Energy Density Functional with Third-order Gradients of Electron Density. *J. Chem. Phys.* **2018**, *148*, 241705.
(151) Dick, S.; Fernandez-Serra, M. Learning from the Density to Correct Total Energy and Forces in First Principle Simulations. *J. Chem. Phys.* **2019**, *151*, 144102.
(152) Seino, J.; Kageyama, R.; Fujinami, M.; Ikabata, Y.; Nakai, H. Semi-local Machine-learned Kinetic Energy Density Functional Demonstrating Smooth Potential Energy Curves. *Chem. Phys. Lett.* **2019**, *734*, 136732.
(153) Fujinami, M.; Kageyama, R.; Seino, J.; Ikabata, Y.; Nakai, H. Orbital-free Density Functional Theory Calculation Applying Semi-local Machine-learned Kinetic Energy Density Functional and Kinetic Potential. *Chem. Phys. Lett.* **2020**, *748*, 137358.
(154) Manzhos, S.; Golub, P. Data-driven Kinetic Energy Density Fitting for Orbital-free DFT: Linear vs Gaussian Process Regression. *J. Chem. Phys.* **2020**, *153*, 074104.
(155) Meyer, R.; Weichselbaum, M.; Hauser, A. W. Machine Learning Approaches Toward Orbital-free Density Functional Theory: Simultaneous Training on the Kinetic Energy Density Functional and Its Functional Derivative. *J. Chem. Theory Comput.* **2020**, *16*, 5685−5694.
(156) von Lilienfeld, O. A.; Burke, K. Retrospective on a Decade of Machine Learning for Chemical Discovery. *Nat. Commun.* **2020**, *11*, 4895.
(157) Alghadeer, M.; Al-Aswad, A.; Alharbi, F. H. Highly accurate machine learning model for kinetic energy density functional. *Phys. Lett. A* **2021**, *414*, 127621.
(158) Imoto, F.; Imada, M.; Oshiyama, A. Order-N Orbital-free Density-functional Calculations with Machine Learning of Functional Derivatives for Semiconductors and Metals. *Phys. Rev. Res.* **2021**, *3*, 033198.
(159) Ghasemi, S. A.; Kühne, T. D. Artificial Neural Networks for the Kinetic Energy Functional of Non-interacting Fermions. *J. Chem. Phys.* **2021**, *154*, 074107.
(160) Ryczko, K.; Wetzel, S. J.; Melko, R. G.; Tamblyn, I. Toward Orbital-Free Density Functional Theory with Small Data Sets and Deep Learning. *J. Chem. Theory Comput.* **2022**, *18*, 1122.
(161) Ke, Y.; Libisch, F.; Xia, J.; Wang, L.-W.; Carter, E. A. Angular-Momentum-Dependent Orbital-free Density Functional Theory. *Phys. Rev. Lett.* **2013**, *111*, 066402.
(162) Karasiev, V. V.; Sjostrom, T.; Trickey, S. B. Finite-temperature Orbital-free DFT Molecular Dynamics: Coupling PROFESS and Quantum Espresso. *Comput. Phys. Commun.* **2014**, *185*, 3240−3249.
(163) Zhou, B.; Wang, Y. A.; Carter, E. A. Transferable Local Pseudopotentials Derived via Inversion of the Kohn-Sham Equations in a Bulk Environment. *Phys. Rev. B* **2004**, *69*, 125109.
(164) Huang, C.; Carter, E. A. Transferable Local Pseudopotentials for Magnesium, Aluminum and Silicon. *Phys. Chem. Chem. Phys.* **2008**, *10*, 7109.

https://doi.org/10.1021/acs.chemrev.2c00758
Chem. Rev. 2023, 123, 12039−12104

(165) Mi, W.; Zhang, S.; Wang, Y.; Ma, Y.; Miao, M. First-principle Optimal Local Pseudopotentials Construction via Optimized Effective Potential Method. *J. Chem. Phys.* **2016**, *144*, 134108.
(166) Sjostrom, T.; Daligault, J. Nonlocal Orbital-free Non-interacting Free-energy Functional for Warm Dense Matter. *Phys. Rev. B* **2013**, *88*, 195103.
(167) White, T. G.; Richardson, S.; Crowley, B. J. B.; Pattison, L. K.; Harris, J. W. O.; Gregori, G. Orbital-Free Density-functional Theory Simulations of the Dynamic Structure Factor of Warm Dense Aluminum. *Phys. Rev. Lett.* **2013**, *111*, 175002.
(168) Kang, D.; Luo, K.; Runge, K.; Trickey, S. B. Two-temperature Warm Dense Hydrogen As a Test of Quantum Protons Driven by Orbital-free Density Functional Theory Electronic Forces. *Matter Radiat. at Extremes* **2020**, *5*, 064403.
(169) Xia, J.; Carter, E. A. Orbital-free Density Functional Theory Study of Amorphous Li−Si Alloys and Introduction of a Simple Density Decomposition Formalism. *Model. Simul. Mater. Sci. Eng.* **2016**, *24*, 035014.
(170) Xia, J.; Carter, E. A. Orbital-free Density Functional Theory Study of Crystalline Li−Si Alloys. *J. Power Sources* **2014**, *254*, 62−72.
(171) Zhuang, H.; Chen, M.; Carter, E. A. Elastic and Thermodynamic Properties of Complex Mg-Al Intermetallic Compounds via Orbital-free Density Functional Theory. *Phys. Rev. Applied* **2016**, *5*, 064021.
(172) Constantin, L. A.; Fabiano, E.; Della Sala, F. Performance of Semilocal Kinetic Energy Functionals for Orbital-free Density Functional Theory. *J. Chem. Theory Comput.* **2019**, *15*, 3044−3055.
(173) Hung, L.; Carter, E. A. Orbital-Free DFT Simulations of Elastic Response and Tensile Yielding of Ultrathin [111] Al Nanowires. *J. Phys. Chem. C* **2011**, *115*, 6269−6276.
(174) Watson, S. C.; Carter, E. A. Linear-scaling Parallel Algorithms for the First Principles Treatment of Metals. *Comput. Phys. Commun.* **2000**, *128*, 67−92.
(175) Hohenstein, E. G.; Luehr, N.; Ufimtsev, I. S.; Martínez, T. J. An Atomic Orbital-based Formulation of the Complete Active Space self-consistent Field Method on Graphical Processing Units. *J. Chem. Phys.* **2015**, *142*, 224103.
(176) Mohr, S.; Ratcliff, L. E.; Genovese, L.; Caliste, D.; Boulanger, P.; Goedecker, S.; Deutsch, T. Accurate and Efficient Linear Scaling DFT Calculations with Universal Applicability. *Phys. Chem. Chem. Phys.* **2015**, *17*, 31360−31370.
(177) Sena, A. M. P.; Miyazaki, T.; Bowler, D. R. Linear Scaling Constrained Density Functional Theory in CONQUEST. *J. Chem. Theory Comput.* **2011**, *7*, 884−889.
(178) Schlipf, M.; Gygi, F. Optimization Algorithm for the Generation of ONCV Pseudopotentials. *Comput. Phys. Commun.* **2015**, *196*, 36−44.
(179) Skylaris, C.-K.; Haynes, P. D.; Mostofi, A. A.; Payne, M. C. Introducing ONETEP: Linear-scaling Density Functional Simulations on Parallel Computers. *J. Chem. Phys.* **2005**, *122*, 084119.
(180) Krishtal, A.; Sinha, D.; Genova, A.; Pavanello, M. Subsystem Density-functional Theory As an Effective Tool for Modeling Ground and Excited States, Their Dynamics and Many-body Interactions. *J. Phys.: Condens. Matter* **2015**, *27*, 183202.
(181) Jacob, C. R.; Neugebauer, J. Subsystem Density-functional Theory. *Wiley Interdiscip. Rev. Comput. Mol. Sci.* **2014**, *4*, 325−362.
(182) Chen, M.; Baer, R.; Neuhauser, D.; Rabani, E. Overlapped Embedded Fragment Stochastic Density Functional Theory for Covalently-bonded Materials. *J. Chem. Phys.* **2019**, *150*, 034106.
(183) Goedecker, S. Linear Scaling Electronic Structure Methods. *Rev. Mod. Phys.* **1999**, *71*, 1085.
(184) Kohn, W. Density Functional and Density Matrix Method Scaling Linearly with the Number of Atoms. *Phys. Rev. Lett.* **1996**, *76*, 3168−3171.
(185) Prodan, E.; Kohn, W. Nearsightedness of Electronic Matter. *Proc. Nat. Acad. Sci. (USA)* **2005**, *102*, 11635−11638.
(186) Prodan, E. Nearsightedness of Electronic Matter in One Dimension. *Phys. Rev. B* **2006**, *73*, 085108.
(187) Goedecker, S. Decay properties of the finite-temperature density matrix in metals. *Phys. Rev. B* **1998**, *58*, 3501−3502.
(188) Ismail-Beigi, S.; Arias, T. A. Locality of the density matrix in metals, semiconductors, and insulators. *Phys. Rev. Lett.* **1999**, *82*, 2127.
(189) Wesolowski, T. A.; Warshel, A. Frozen Density Functional Approach for Ab Initio Calculations of Solvated Molecules. *J. Phys. Chem.* **1993**, *97*, 8050−8053.
(190) Wesolowski, T. A.; Shedge, S.; Zhou, X. Frozen-Density Embedding Strategy for Multilevel Simulations of Electronic Structure. *Chem. Rev.* **2015**, *115*, 5891−5928.
(191) Senatore, G.; Subbaswamy, K. Density dependence of the dielectric constant of rare-gas crystals. *Phys. Rev. B* **1986**, *34*, 5754.
(192) Ludeña, E. V.; Karasiev, V. V. Kinetic Energy Functionals: History, Challenges, and Prospects. *Reviews of Modern Quantum Chemistry: a Celebration of the Contributions of Robert Parr*; World Scientific, 2002; Vol. *1*, pp 612−665.
(193) Chen, H.; Zhou, A. Orbital-Free Density Functional Theory for Molecular Structure Calculations. *Numer. Math.* **2008**, *1*, 1−28.
(194) Karasiev, V. V.; Chakraborty, D.; Trickey, S. B. Progress on New Approaches to Old Ideas: Orbital-free Density Functionals. *Many-Electron Approaches in Physics, Chemistry and Mathematics*; Delle Site, L.; Bach, V., Eds.; Springer, 2014; pp 113−134.
(195) Tran, F.; Wesolowski, T. Semilocal Approximations for the Kinetic Energy. In *Recent Progress in Orbital-free Density Functional Theory*; Wesolowski, T. A., Wang, Y. A., Eds.; World Scientific, 2013; pp 429−442.
(196) Luo, K.; Rodríguez, D. M.; Trickey, S. B. University Florida Odft. 2009−2020; http://www.qtp.ufl.edu/ofdft/research/KE_refdata_27ii18/Explanatory_Post_HF_OFKE_23xi20.pdf. Accessed on 10/03/2022.
(197) Smith, J. C.; Sagredo, F.; Burke, K. Warming Up Density Functional Theory. In *Frontiers of Quantum Chemistry*; Wójcik, M., Nakatsuji, H., Kirtman, B., Ozaki, Y., Eds.; Springer: Singapore, 2018; pp 249−271, https://link.springer.com/chapter/10.1007/978-981-10-5651-2_11.
(198) Domps, A.; Reinhard, P.-G.; Suraud, E. Time-dependent Thomas-Fermi Approach for Electron Dynamics in Metal Clusters. *Phys. Rev. Lett.* **1998**, *80*, 5520.
(199) Hessler, P.; Park, J.; Burke, K. Several Theorems in Time-dependent Density Functional Theory. *Phys. Rev. Lett.* **1999**, *82*, 378−381.
(200) Ding, Y.; White, A. J.; Hu, S.; Certik, O.; Collins, L. A. Ab Initio Studies on the Stopping Power of Warm Dense Matter with Time-dependent Orbital-free Density Functional Theory. *Phys. Rev. Lett.* **2018**, *121*, 145001.
(201) White, A. J.; Certik, O.; Ding, Y.; Hu, S.; Collins, L. A. Time-dependent Orbital-free Density Functional Theory for Electronic Stopping Power: Comparison to the Mermin-Kohn-Sham Theory at High Temperatures. *Phys. Rev. B* **2018**, *98*, 144302.
(202) Neuhauser, D.; Pistinner, S.; Coomar, A.; Zhang, X.; Lu, G. Dynamic Kinetic Energy Potential for Orbital-free Density Functional Theory. *J. Chem. Phys.* **2011**, *134*, 144101.
(203) Jiang, K.; Shao, X.; Pavanello, M. Nonlocal and nonadiabatic Pauli potential for time-dependent orbital-free density functional theory. *Phys. Rev. B* **2021**, *104*, 235110.
(204) Jiang, K.; Pavanello, M. Time-dependent orbital-free density functional theory: Background and Pauli kernel approximations. *Phys. Rev. B* **2021**, *103*, 245102.
(205) Della Sala, F. Orbital-free methods for plasmonics: Linear response. *J. Chem. Phys.* **2022**, *157*, 104101.
(206) Baghramyan, H. M.; Della Sala, F.; Ciracì, C. Laplacian-level quantum hydrodynamic theory for plasmonics. *Phys. Rev. X* **2021**, *11*, 011049.
(207) Ciracì, C.; Della Sala, F. Quantum hydrodynamic theory for plasmonics: Impact of the electron density tail. *Phys. Rev. B* **2016**, *93*, 205405.
(208) Bhan, L.; Covington, C. L.; Varga, K. Laser-Driven Petahertz Electron Ratchet Nanobubbles. *Nano Lett.* **2022**, *22*, 4240.

(209) Covington, C.; Malave, J.; Varga, K. Coupled Maxwell and time-dependent orbital-free density functional calculations. *Phys. Rev. B* **2021**, *103*, 075119.
(210) Theophilou, I.; Buchholz, F.; Eich, F. G.; Ruggenthaler, M.; Rubio, A. Kinetic-Energy Density-functional Theory on a Lattice. *J. Chem. Theory Comput.* **2018**, *14*, 4072−4087.
(211) Dreizler, R. M.; Gross, E. K. U. *Density Functional Theory: An Approach to the Quantum Many-body Problem*; Springer, 1990.
(212) Gunnarsson, O.; Lundqvist, B. I. Exchange and Correlation in Atoms, Molecules, and Solids by the Spin-density-functional Formalism. *Phys. Rev. B* **1976**, *13*, 4274−4298.
(213) Filippi, C.; Umrigar, C. J.; Taut, M. Comparison of Exact and Approximate Density Functionals for an Exactly Soluble Model. *J. Chem. Phys.* **1994**, *100*, 1290−1296.
(214) Qian, Z.; Sahni, V. Physics of Transformation from Schrödinger Theory to Kohn-Sham Density-functional Theory: Application to an Exactly Solvable Model. *Phys. Rev. A* **1998**, *57*, 2527−2538.
(215) Burke, K.; Cruz, F. G.; Lam, K. Unambiguous Exchange-correlation Energy Density for Hooke's Atom. *Int. J. Quantum Chem.* **1998**, *70*, 583−589.
(216) Howard, I. A.; March, N. H.; Nieto, L. M. Complete Functional Theory for the Fermion Density of Independent Particles Subject to Harmonic Confinement. *Phys. Rev. A* **2002**, *66*, 054501.
(217) Ludeña, E. V.; Gómez, D.; Karasiev, V. V.; Nieto, P. Exact Analytic Total Energy Functional for Hooke's Atom Generated by Local-scaling Transformations. *Int. J. Quantum Chem.* **2004**, *99*, 297−307.
(218) Capuzzi, P.; March, N. H.; Tosi, M. P. Differential Equation for the Ground-state Density of Artificial Two-electron Atoms with Harmonic Confinement. *J. Phys. A: Mathematics, General* **2005**, *38*, L439−L442.
(219) Zhu, W.; Trickey, S. B. Exact Density Functionals for Two-electron Systems in an External Magnetic Field. *J. Chem. Phys.* **2006**, *125*, 094317.
(220) Katriel, J.; Roy, S.; Springborg, M. Nonuniversality of Commonly Used Correlation-energy Density Functionals. *J. Chem. Phys.* **2006**, *124*, 234111.
(221) Gál, T.; March, N. H. Density Functional for the Ground-state Energy of Artificial Two-electron Atoms with Harmonic Confinement. *J. Phys. B: Atomic Molecular, Optical Phys.* **2009**, *42*, 025001.
(222) Levy, M. Universal Variational Functionals of Electron Densities, First-order Density Matrices, and Natural Spin-orbitals and Solution of the V-representability Problem. *Proc. Nat. Acad. Sci. (USA)* **1979**, *76*, 6062−6065.
(223) Schipper, P. R. T.; Gritsenko, O. V.; Baerends, E. J. One - Determinantal Pure State Versus Ensemble Kohn-Sham Solutions in the Case of Strong Electron Correlation: CH_2 and C_2. *Theor. Chem. Acc.* **1998**, *99*, 329−343.
(224) Langreth, D.; Perdew, J. Exchange-correlation energy of a metallic surface: Wave-vector analysis. *Phys. Rev. B* **1977**, *15*, 2884−2901.
(225) Perdew, J. P.; Burke, K.; Ernzerhof, M. Generalized Gradient Approximation Made Simple. *Phys. Rev. Lett.* **1996**, *77*, 3865−3868. Erratum: *Phys. Rev. Lett.* **1997**, *78*, 1396.
(226) Albavera-Mata, A.; Botello-Mancilla, K.; Trickey, S. B.; Gázquez, J. L.; Vela, A. Generalized Gradient Approximations with Local Parameters. *Phys. Rev. B* **2020**, *102*, 035129.
(227) Barnett, R. N.; Landman, U. Born-Oppenheimer Molecular-Dynamics Simulations of Finite Systems: Structure and Dynamics of $(H_2O)_2$. *Phys. Rev. B* **1993**, *48*, 2081−2097.
(228) Tse, J. S. Ab Initio Molecular Dynamics with Density Functional Theory. *Annu. Rev. Phys. Chem.* **2002**, *53*, 249−290.
(229) Marx, D.; Hutter, J. *Ab Initio Molecular Dynamics: Basic Theory and Advanced Methods*; Cambridge University Press, 2009.
(230) Perdew, J. P.; Schmidt, K. Jacob's Ladder of Density Functional Approximations for the Exchange-correlation Energy. In *AIP Conference Proceedings*; Vol. 577, 2001; pp 1−20.
(231) Sun, J.; Ruzsinszky, A.; Perdew, J. P. Strongly Constrained and Appropriately Normed Semilocal Density Functional. *Phys. Rev. Lett.* **2015**, *115*, 036402.
(232) Furness, J. W.; Kaplan, A. D.; Ning, J.; Perdew, J. P.; Sun, J. Accurate and Numerically Efficient r^2SCAN Meta-generalized Gradient Approximation. *J. Phys. Chem. Lett.* **2020**, *11*, 8208−8215.
(233) Mejía-Rodríguez, D.; Trickey, S. B. Deorbitalization Strategies for Meta-generalized-gradient-approximation Exchange-correlation Functionals. *Phys. Rev. A* **2017**, *96*, 052512.
(234) Mejía-Rodríguez, D.; Trickey, S. B. Deorbitalized Meta-GGA Exchange-correlation Functionals in Solids. *Phys. Rev. B* **2018**, *98*, 115161.
(235) Mejía-Rodríguez, D.; Trickey, S. B. Meta-GGA Performance in Solids at Almost GGA Cost. *Phys. Rev. B* **2020**, *102*, 121109.
(236) Yang, W.; Wu, Q. Direct Method for Optimized Effective Potentials in Density-functional Theory. *Phys. Rev. Lett.* **2002**, *89*, 143002.
(237) Görling, A. Orbital- and State-dependent Functionals in Density-functional Theory. *J. Chem. Phys.* **2005**, *123*, 062203.
(238) Yang, Z.-h.; Peng, H.; Sun, J.; Perdew, J. P. More Realistic Band Gaps from Meta-generalized Gradient Approximations: Only in a Generalized Kohn-Sham Scheme. *Phys. Rev. B* **2016**, *93*, 205205.
(239) Perdew, J. P.; Yang, W.; Burke, K.; Yang, Z.; Gross, E. K. U.; Scheffler, M.; Scuseria, G. E.; Henderson, T. M.; Zhang, I. Y.; Ruzsinszky, A.; Peng, H.; Sun, J.; Trushin, E.; Görling, A. Understanding Band Gaps of Solids in Generalized Kohn−Sham Theory. *Proc. Nat. Acad. Sci. (USA)* **2017**, *114*, 2801.
(240) Lehtomäki, J.; Lopez-Acevedo, O. Semilocal Kinetic Energy Functionals with Parameters from Neutral Atoms. *Phys. Rev. B* **2019**, *100*, 165111.
(241) Fermi, E. Eine Statistische Methode Zur Bestimmung Einiger Eigenschaften Des Atoms Und Ihre Anwendung Auf Die Theorie Des Periodischen Systems Der Elemente. *Z. Phys.* **1928**, *48*, 73−79.
(242) Hoffmann-Ostenhof, M.; Hoffmann-Ostenhof, T. "Schrödinger Inequalities" and Asymptotic Behavior of the Electron Density of Atoms and Molecules. *Phys. Rev. A* **1977**, *16*, 1782.
(243) Sears, S. B.; Parr, R. G.; Dinur, U. On the Quantum-mechanical Kinetic Energy As a Measure of the Information in a Distribution. *Israel J. Chem.* **1980**, *19*, 165−173.
(244) Harriman, J. E. A Kinetic Energy Density Functional. *J. Chem. Phys.* **1985**, *83*, 6283−6287.
(245) Herring, C. Explicit Estimation of Ground-state Kinetic Energies from Electron Densities. *Phys. Rev. A* **1986**, *34*, 2614.
(246) Tal, Y.; Bader, R. Studies of the Energy Density Functional Approach. I. Kinetic Energy. *Int. J. Quantum Chem.* **1978**, *14*, 153−168.
(247) Bartolotti, L.; Acharya, P. On the Functional Derivative of the Kinetic Energy Density Functional. *J. Chem. Phys.* **1982**, *77*, 4576−4585.
(248) Harriman, J. E. The interface between reduced density matrices and density functional theory. *Density Matrices and Density Functionals*; Erdahl, R.; Smith Jr., V. H., Eds.; Springer, 1987; pp 359−373.
(249) Levy, M.; Hui Ou-Yang. Exact Properties of the Pauli Potential for the Square Root of the Electron Density and the Kinetic Energy Functional. *Phys. Rev. A* **1988**, *38*, 625.
(250) Lieb, E. H. Some Open Problems About Coulomb Systems. In *Mathematical Problems in Theoretical Physics*; Osterwalder, K., Ed.; Springer, 1980; pp 91−102.
(251) Lewin, M.; Lieb, E. H.; Seiringer, R. Universal Functionals in Density Functional Theory. *arXiv* **2020**, 1912.10424.
(252) Trickey, S. B.; Karasiev, V. V.; Chakraborty, D. Comment on "Single-point Kinetic Energy Density Functionals: a Pointwise Kinetic Energy Density Analysis and Numerical Convergence Investigation. *Phys. Rev. B* **2015**, *92*, 117101.
(253) Witt, W. C.; Jiang, K.; Carter, E. A. Upper Bound to the Gradient-based Kinetic Energy Density of Noninteracting Electrons in an External Potential. *J. Chem. Phys.* **2019**, *151*, 064113.

(254) Levy, M.; Perdew, J. P. Hellmann-Feynman, Virial, and Scaling Requisites for the Exact Universal Density Functionals. Shape of the Correlation Potential and Diamagnetic Susceptibility for Atoms. *Phys. Rev. A* **1985**, *32*, 2010.
(255) Alonso, J.; Girifalco, L. Nonlocal Approximation to the Exchange Potential and Kinetic Energy of an Inhomogeneous Electron Gas. *Phys. Rev. B* **1978**, *17*, 3735.
(256) Lee, D.; Constantin, L. A.; Perdew, J. P.; Burke, K. Condition on the Kohn-Sham Kinetic Energy and Modern Parametrization of the Thomas-Fermi Density. *J. Chem. Phys.* **2009**, *130*, 034107.
(257) Lieb, E. Density Functionals for Coulomb Systems. *Int. J. Quantum Chem.* **1983**, *24*, 243−277.
(258) Harriman, J. E. Orthonormal Orbitals for the Representation of an Arbitrary Density. *Phys. Rev. A* **1981**, *24*, 680−682.
(259) Ayers, P. W.; Liu, S. Necessary and Sufficient Conditions for the N-representability of Density Functionals. *Phys. Rev. A* **2007**, *75*, 022514.
(260) Chakraborty, D.; Cuevas-Saavedra, R.; Ayers, P. W. Two-point Weighted Density Approximations for the Kinetic Energy Density Functional. *Theor. Chem. Acc.* **2017**, *136*, 113.
(261) Chakraborty, D.; Cuevas-Saavedra, R.; Ayers, P. W. Kinetic Energy Density Functionals from Models for the One-electron Reduced Density Matrix. In *Many-body Approaches at Different Scales*; Angilella, G. G. N., Amovilli, C., Eds.; Springer, 2018; pp 199−208.
(262) Kato, T. On the Eigenfunctions of Many-particle Systems in Quantum Mechanics. *Commun. Pure. Appl. Math.* **1957**, *10*, 151−177.
(263) Janosfalvi, Z.; Sen, K. D.; Nagy, A. Cusp Conditions for Non-interacting Kinetic Energy Density of the Density Functional Theory. *Phys. Lett. A* **2005**, *344*, 1−6.
(264) Karasiev, V. V.; Jones, R. S.; Trickey, S. B.; Harris, F. E. Properties of Constraint-based Single-point Approximate Kinetic Energy Functionals. *Phys. Rev. B* **2009**, *80*, 245120.
(265) Karasiev, V. V.; Trickey, S. B. Frank Discussion of the Status of Ground-state Orbital-free DFT. *Adv. Quantum Chem.* **2015**, *71*, 221−245.
(266) Constantin, L. A.; Fabiano, E.; Della Sala, F. Kinetic and Exchange Energy Densities Near the Nucleus. *Computation* **2016**, *4*, 19.
(267) Smiga, S.; Constantin, L. A.; Della Sala, F.; Fabiano, E. The Role of the Reduced Laplacian Renormalization in the Kinetic Energy Functional Development. *Computation* **2019**, *7*, 65.
(268) Cancio, A. C.; Stewart, D.; Kuna, A. Visualization and Analysis of the Kohn-Sham Kinetic Energy Density and Its Orbital-free Description in Molecules. *J. Chem. Phys.* **2016**, *144*, 084107.
(269) Finzel, K.; Bultnick, P. The Influence of the Exchange-correlation Functional on the Non- Interacting Kinetic Energy and Its Implications for Orbital-free Density Functional Approximations. *Acta Phys. - Chim. Sin.* **2018**, *34*, 650−655.
(270) Perdew, J. P.; Constantin, L. A. Laplacian-level Density Functionals for the Kinetic Energy Density and Exchange-correlation Energy. *Phys. Rev. B* **2007**, *75*, 155109.
(271) Anderson, J. S. M.; Ayers, P. W.; Hernandez, J. I. R. How Ambiguous Is the Local Kinetic Energy? *J. Phys. Chem. A* **2010**, *114*, 8884−8895.
(272) Sim, E.; Larkin, J.; Burke, K.; Bock, C. W. Testing the Kinetic Energy Functional: Kinetic Energy Density As a Density Functional. *J. Chem. Phys.* **2003**, *118*, 8140−8147.
(273) Plumer, M. I.; Stott, M. J. Approximate Kinetic Energy Functionals for Atoms in Extended Systems. *J. Phys. C: Solid State Phys.* **1985**, *18*, 4143−4163.
(274) Mazin, I. I. One Method for Building Nonlocal Density Functionals for Energy. *Kratk. Soobshch. Fiz.* **1988**, *1*, 15−17. reposted as arXiv 2209.02807.
(275) March, N. H.; Santamaria, R. Non-local Relation between Kinetic and Exchange Energy Densities in Hartree-Fock Theory. *Int. J. Quantum Chem.* **1991**, *39*, 585−592.
(276) Perdew, J.; Erratum, P. Density-functional Approximation for the Correlation Energy of the Inhomogeneous Electron Gas. *Phys. Rev. B* **1986**, *34*, 7406−7406.
(277) Lee, C.; Yang, W.; Parr, R. G. Development of the Colle-Salvetti Correlation-energy Formula Into a Functional of the Electron Density. *Phys. Rev. B* **1988**, *37*, 785−789.
(278) Carmona-Espíndola, J.; Gázquez, J. L.; Vela, A.; Trickey, S. B. Generalized Gradient Approximation Exchange Functional with Near-best-semilocal Performance. *J. Chem. Theory Comput.* **2019**, *15*, 303−310.
(279) Constantin, L. A. Semilocal Properties of the Pauli Kinetic Potential. *Phys. Rev. B* **2019**, *99*, 155137.
(280) Steiner, E. Charge Densities in Atoms. *J. Chem. Phys.* **1963**, *39*, 2365−2366.
(281) Perdew, J. P.; Zunger, A. Self-interaction Correction to Density-functional Approximations for Many-electron Systems. *Phys. Rev. B* **1981**, *23*, 5048−5079.
(282) Xia, J.; Carter, E. A. Single-point Kinetic Energy Density Functionals: A Pointwise Kinetic Energy Density Analysis and Numerical Convergence Investigation. *Phys. Rev. B* **2015**, *91*, 045124.
(283) Xia, J.; Carter, E. A. Reply to "Comment on 'Single-point Kinetic Energy Density Functionals: a Pointwise Kinetic Energy Density Analysis and Numerical Convergence Investigation'. *Phys. Rev. B* **2015**, *92*, 117102.
(284) Yang, W. Gradient Correction in Thomas-Fermi Theory. *Phys. Rev. A* **1986**, *34*, 4575−4585.
(285) Laricchia, S.; Constantin, L. A.; Fabiano, E.; Della Sala, F. Laplacian-level Kinetic Energy Approximations Based on the Fourth-order Gradient Expansion: Global Assessment and Application to the Subsystem Formulation of Density Functional Theory. *J. Chem. Theory Comput.* **2014**, *10*, 164−179.
(286) Cancio, A. C.; Redd, J. J. Visualization and Orbital-free Parametrization of the Large-z Scaling of the Kinetic Energy Density of Atoms. *Mol. Phys.* **2017**, *115*, 618−635.
(287) Lynch, B. J.; Truhlar, D. G. Small Representative Benchmarks for Thermochemical Calculations. *J. Phys. Chem. A* **2003**, *107*, 8996−8999.
(288) Plindov, G. I.; Pogrebnya, S. K. A Simple Approximation to the Kinetic Energy Functional. *Chem. Phys. Lett.* **1988**, *143*, 535−537.
(289) Engel, E.; Dreizler, R. Extension of the Thomas-Fermi−Dirac-weizsäcker Model: Fourth-order Gradient Corrections to the Kinetic Energy. *J. Phys. B: Atomic, Molecular and Optical Phys.* **1989**, *22*, 1901.
(290) Glossman, M. D. Variational Study of a New Approximation for the Kinetic Energy Functional. *Chem. Phys. Lett.* **1992**, *188*, 310−314.
(291) Constantin, L. A.; Fabiano, E.; Della Sala, F. Modified Fourth-order Kinetic Energy Gradient Expansion with Hartree Potential-dependent Coefficients. *J. Chem. Theory Comput.* **2017**, *13*, 4228−4239.
(292) Śmiga, S.; Fabiano, E.; Constantin, L. A.; Della Sala, F. Laplacian-dependent Models of the Kinetic Energy Density: Applications in Subsystem Density Functional Theory with Meta-generalized Gradient Approximation Functionals. *J. Chem. Phys.* **2017**, *146*, 064105.
(293) Jiang, K.; Nafziger, J.; Wasserman, A. Constructing a Non-additive Non-interacting Kinetic Energy Functional Approximation for Covalent Bonds from Exact Conditions. *J. Chem. Phys.* **2018**, *149*, 164112.
(294) Jiang, K.; Nafziger, J.; Wasserman, A. Non-additive Non-interacting Kinetic Energy of Rare Gas Dimers. *J. Chem. Phys.* **2018**, *148*, 104113.
(295) Mi, W.; Ramos, P.; Maranhao, J.; Pavanello, M. Ab Initio Structure and Dynamics of CO_2 at Supercritical Conditions. *J. Phys. Chem. Lett.* **2019**, *10*, 7554−7559.
(296) Genova, A.; Ceresoli, D.; Pavanello, M. Avoiding Fractional Electrons in Subsystem DFT Based Ab-initio Molecular Dynamics Yields Accurate Models For Liquid Water and Solvated Oh Radical. *J. Chem. Phys.* **2016**, *144*, 234105.
(297) Wang, Y. A.; Govind, N.; Carter, E. A. Orbital-free Kinetic-energy Density Functionals with a Density-dependent Kernel. *Phys. Rev. B* **1999**, *60*, 16350−16358.

https://doi.org/10.1021/acs.chemrev.2c00758
Chem. Rev. 2023, 123, 12039−12104

(298) Francisco, H. I.; Carmona-Espíndola, J.; Gázquez, J. L. Analysis of the Kinetic Energy Functional in the Generalized Gradient Approximation. *J. Chem. Phys.* **2021**, *154*, 084107.
(299) García-González, P.; Alvarellos, J. E.; Chacón, E. Kinetic-energy Density Functional: Atoms and Shell Structure. *Phys. Rev. A* **1996**, *54*, 1897−1905.
(300) Glossman, M. D.; Rubio, A.; Balbas, L. C.; Alonso, J. A. Nonlocal Exchange and Kinetic-energy Density Functionals for Electronic Systems. *Int. J. Quantum Chem.* **1992**, *44*, 347−358.
(301) Stoddart, J. C.; March, N. H. Exact Thomas-Fermi Method in Perturbation Theory. *Proc. Math. Phys. Eng. Sci.* **1967**, *299*, 279−286.
(302) Jiang, K.; Mosquera, M. A.; Oueis, Y.; Wasserman, A. Virial Relations in Density Embedding. *Int. J. Quantum Chem.* **2020**, *120*, e26204.
(303) Gaiduk, A. P.; Chulkov, S. K.; Staroverov, V. N. Reconstruction of Density Functionals from Kohn-Sham Potentials by Integration along Density Scaling Paths. *J. Chem. Theory Comput.* **2009**, *5*, 699−707.
(304) van Leeuwen, R.; Baerends, E. J. Energy Expressions in Density-functional Theory Using Line Integrals. *Phys. Rev. A* **1995**, *51*, 170−178.
(305) Foley, M.; Madden, P. A. Further Orbital-free Kinetic-energy Functionals for Ab Initio Molecular Dynamics. *Phys. Rev. B* **1996**, *53*, 10589.
(306) Gaiduk, A. P.; Staroverov, V. N. Communication: Explicit Construction of Functional Derivatives in Potential-driven Density-functional Theory. *J. Chem. Phys.* **2010**, *133*, 101104.
(307) Baroni, S.; Giannozzi, P.; Testa, A. Green's-function Approach to Linear Response in Solids. *Phys. Rev. Lett.* **1987**, *58*, 1861−1864.
(308) Rey, J.; Savin, A. Virtual Space Level Shifting and Correlation Energies. *Int. J. Quantum Chem.* **1998**, *69*, 581−590.
(309) Constantin, L. A.; Fabiano, E.; Śmiga, S.; Della Sala, F. Jellium-with-gap Model Applied to Semilocal Kinetic Functionals. *Phys. Rev. B* **2017**, *95*, 115153.
(310) Takahashi, H. Density-functional theory based on the electron distribution on the energy coordinate. *J. Phys. B Atom., Molec., Opt. Phys.* **2018**, *51*, 055102.
(311) Takahashi, H. Development of kinetic energy density functional using response function defined on the energy coordinate. *Int. J. Quantum Chem.* **2022**, *122*, e26969.
(312) Takahashi, H. Development of Nonlocal Kinetic-Energy Density Functional for the Hybrid QM/MM Interaction. *J. Chem. Phys.* **2023**, *158*, 014102.
(313) Blanc, X.; Cancès, E. Nonlinear Instability of Density-independent Orbital-free Kinetic-energy Functionals. *J. Chem. Phys.* **2005**, *122*, 214106.
(314) Plumer, M. L.; Geldart, D. J. W. Non-local Approximations to the Kinetic Energy Functional. *J. Phys. C: Solid State Phys.* **1983**, *16*, 677−689.
(315) González, D. J.; González, L. E.; López, J. M.; Stott, M. J. Orbital Free Ab Initio Molecular Dynamics Study of Liquid Al Near Melting. *J. Chem. Phys.* **2001**, *115*, 2373−2376.
(316) González, D. J.; González, L. E.; López, J. M.; Stott, M. J. Dynamical Properties of Liquid Al Near Melting: An Orbital-free Molecular Dynamics Study. *Phys. Rev. B* **2002**, *65*, 184201.
(317) Witt, W. C.; Shires, B. W. B.; Tan, C. W.; Jankowski, W. J.; Pickard, C. J. Random Structure Searching with Orbital-free Density Functional Theory. *J. Phys. Chem. A* **2021**, *125*, 1650−1660.
(318) Sjostrom, T.; Daligault, J. Fast and Accurate Quantum Molecular Dynamics of Dense Plasmas Across Temperature Regimes. *Phys. Rev. Lett.* **2014**, *113*, 155006.
(319) García-González, P.; Alvarellos, J.; Chacón, E. Nonlocal Kinetic-energy-density Functionals. *Phys. Rev. B* **1996**, *53*, 9509.
(320) García-González, P.; Alvarellos, J.; Chacón, E. Nonlocal Symmetrized Kinetic-energy Density Functional: Application to Simple Surfaces. *Phys. Rev. B* **1998**, *57*, 4857.
(321) García-González, P.; Alvarellos, J.; Chacón, E. Kinetic-energy Density Functionals Based on the Homogeneous Response Function Applied to One-dimensional Fermion Systems. *Phys. Rev. A* **1998**, *57*, 4192.
(322) García-Aldea, D.; Alvarellos, J. Fully Nonlocal Kinetic Energy Density Functionals: A Proposal and a General Assessment for Atomic Systems. *J. Chem. Phys.* **2008**, *129*, 074103.
(323) García-Aldea, D.; Alvarellos, J. Approach to Kinetic Energy Density Functionals: Nonlocal Terms with the Structure of the Von Weizsäcker Functional. *Phys. Rev. A* **2008**, *77*, 022502.
(324) Suzuki, M. Fractal Decomposition of Exponential Operators with Applications to Many-body Theories and Monte Carlo Simulations. *Phys. Lett. A* **1990**, *146*, 319.
(325) Adler, S. L. Quantum Theory of the Dielectric Constant in Real Solids. *Phys. Rev.* **1962**, *126*, 413−420.
(326) Pick, R. M.; Cohen, M. H.; Martin, R. M. Microscopic Theory of Force Constants in the Adiabatic Approximation. *Phys. Rev. B* **1970**, *1*, 910−920.
(327) Xia, J.; Huang, C.; Shin, I.; Carter, E. A. Can Orbital-free Density Functional Theory Simulate Molecules? *J. Chem. Phys.* **2012**, *136*, 084102.
(328) Chai, J.-D.; Lignères, V. L.; Ho, G.; Carter, E. A.; Weeks, J. D. Orbital-free Density Functional Theory: Linear Scaling Methods for Kinetic Potentials, and Applications to Solid Al and Si. *Chem. Phys. Lett.* **2009**, *473*, 263−267.
(329) Sarcinella, F.; Fabiano, E.; Constantin, L.; Della Sala, F. Nonlocal Kinetic Energy Functionals in Real Space Using a Yukawa-potential Kernel: Properties, Linear Response, and Model Functionals. *Phys. Rev. B* **2021**, *103*, 155127.
(330) Nagy, A. Fisher and Shannon Information in Orbital-free Density Functional Theory. *Int. J. Quantum Chem.* **2015**, *115*, 1392−1395.
(331) Hamilton, I. P.; Mosna, R. A.; Delle Site, L. Quantum Fluctuations, Dequantization, Information Theory and Kinetic-energy Functionals. In *Recent Progress in Orbital-free Density Functional Theory*; Wesolowski, T. A., Wang, Y. A., Eds.; World Scientific, 2013; pp 401−425.
(332) Delle Site, L. On the Scaling Properties of the Correlation Term of the Electron Kinetic Functional and Its Relation to the Shannon Measure. *EPL* **2009**, *86*, 40004.
(333) Levy, M.; Perdew, J. P.; Sahni, V. Exact Differential Equation for the Density and Ionization Energy of a Many-particle System. *Phys. Rev. A* **1984**, *30*, 2745−2748.
(334) Kocák, J.; Kraisler, E.; Schild, A. On the relationship between the Kohn-Sham potential, the Pauli potential, and the Exact Electron Factorization. *arXiv* **2021**, 2010.14885.
(335) Schild, A.; Gross, E. Exact Single-Electron Approach to the Dynamics of Molecules in Strong Laser Fields. *Phys. Rev. Lett.* **2017**, *118*, 163202.
(336) Abedi, A.; Maitra, N. T.; Gross, E. K. U. Exact Factorization of the Time-Dependent Electron-Nuclear Wave Function. *Phys. Rev. Lett.* **2010**, *105*, 123002.
(337) Delle Site, L.; Ghiringhelli, L. M.; Ceperley, D. M. Electronic Energy Functionals: Levy−Lieb Principle Within the Ground State Path Integral Quantum Monte Carlo. *Int. J. Quantum Chem.* **2013**, *113*, 155−160.
(338) Hansen, J.-P.; McDonald, I. R. *Theory of Simple Liquids with Applications to Soft Matter*, 4th ed.; Academic, 2013.
(339) Trickey, S. B.; Karasiev, V. V.; Vela, A. Positivity Constraints and Information-theoretical Kinetic Energy Functionals. *Phys. Rev. B* **2011**, *84*, 075146.
(340) Delle Site, L. Kinetic Functional of Interacting Electrons: A Numerical Procedure and Its Statistical Interpretation. *J. Stat. Phys.* **2011**, *144*, 663−678.
(341) Delle Site, L. Shannon Entropy and Many-electron Correlations: Theoretical Concepts, Numerical Results, and Collins Conjecture. *Int. J. Quantum Chem.* **2015**, *115*, 1396−1404.
(342) Seshaditya, A.; Ghiringhelli, L.; Delle Site, L. Levy-Lieb-Based Monte Carlo Study of the Dimensionality Behaviour of the Electronic Kinetic Functional. *Computation* **2017**, *5*, 30.

https://doi.org/10.1021/acs.chemrev.2c00758
Chem. Rev. 2023, 123, 12039−12104

(343) McCarty, R. J.; Perchak, D.; Pederson, R.; Evans, R.; Qiu, Y.; White, S. R.; Burke, K. Bypassing the Energy Functional in Density Functional Theory: Direct Calculation of Electronic Energies from Conditional Probability Densities. *Phys. Rev. Lett.* **2020**, *125*, 266401.
(344) Yang, W.; Ayers, P. W.; Wu, Q. Potential Functionals: Dual to Density Functionals and Solution to the V-representability Problem. *Phys. Rev. Lett.* **2004**, *92*, 146404.
(345) Cangi, A.; Lee, D.; Elliott, P.; Burke, K.; Gross, E. K. U. Electronic Structure via Potential Functional Approximations. *Phys. Rev. Lett.* **2011**, *106*, 23644.
(346) Gaiduk, A. P.; Staroverov, V. N. Construction of Integrable Model Kohn-Sham Potentials by Analysis of the Structure of Functional Derivatives. *Phys. Rev. A* **2011**, *83*, 012509.
(347) Cangi, A.; Gross, E. K. U.; Burke, K. Potential Functionals Versus Density Functionals. *Phys. Rev. A* **2013**, *88*, 062505.
(348) Pratt, L. R.; Hoffman, G. G.; Harris, R. A. Statistical Theory of Electron Densities. *J. Chem. Phys.* **1988**, *88*, 1818−1823.
(349) Chai, J.-D.; Weeks, J. D. Modified Statistical Treatment of Kinetic Energy in the Thomas-Fermi Model. *J. Phys. Chem. B* **2004**, *108*, 6870−6876.
(350) Finzel, K. A Simple Approximation for the Pauli Potential Yielding Self-consistent Electron Densities Exhibiting Proper Atomic Shell Structure. *Int. J. Quantum Chem.* **2015**, *115*, 1629−1634.
(351) Finzel, K. Shell-structure-based Functionals for the Kinetic Energy. *Theor. Chem. Acc.* **2015**, *134*, 106.
(352) Finzel, K.; Kohout, M. A Fragment-based Approximation of the Pauli Kinetic Energy. *Theor. Chem. Acc.* **2018**, *137*, 182.
(353) Finzel, K. Chemical Bonding without Orbitals. *Comput. Theor. Chem.* **2018**, *1144*, 50−55.
(354) Finzel, K. The First Order Atomic Fragment Approach: An Orbital-free Implementation of Density Functional Theory. *J. Chem. Phys.* **2019**, *151*, 024109.
(355) Finzel, K. Analytical Shell Models for Light Atoms. *Int. J. Quantum Chem.* **2021**, *121*, e26212.
(356) Nagy, Á. The Pauli Potential From the Differential Virial Theorem. *Int. J. Quantum Chem.* **2010**, *110*, 2117−2120.
(357) Levämäki, H.; Nagy, Á.; Kokko, K.; Vitos, L. Alternative to the Kohn-Sham Equations: The Pauli Potential Differential Equation. *Phys. Rev. A* **2015**, *92*, 062502.
(358) Chau, T. T.; Hue, J. H.; Trappe, M.-I.; Englert, B.-G. Systematic corrections to the Thomas-Fermi approximation without a gradient expansion. *New J. Phys.* **2018**, *20*, 073003.
(359) Dufty, J. W.; Wrighton, J. Comments on Corrections to Thomas-Fermi Approximation. 2022, Unpublished technical note, University of Florida.
(360) Ribeiro, R. F.; Lee, D.; Cangi, A.; Elliott, P.; Burke, K. Corrections to Thomas-Fermi Densities at Turning Points and Beyond. *Phys. Rev. Lett.* **2015**, *114*, 050401.
(361) Behler, J.; Parrinello, M. Generalized Neural-network Representation of High-dimensional Potential-energy Surfaces. *Phys. Rev. Lett.* **2007**, *98*, 146401.
(362) Huang, B.; von Lilienfeld, O. A. Quantum Machine Learning Using Atom-in-molecule-based Fragments Selected on the Fly. *Nat. Chem.* **2020**, *12*, 945−951.
(363) Zhang, L.; Lin, D.-Y.; Wang, H.; Car, R.; E, W. Active Learning of Uniformly Accurate Interatomic Potentials for Materials Simulation. *Phys. Rev. Mater.* **2019**, *3*, 023804.
(364) Qiao, Z.; Welborn, M.; Anandkumar, A.; Manby, F. R.; Miller, T. F. OrbNet: Deep Learning for Quantum Chemistry Using Symmetry-adapted Atomic-orbital Features. *J. Chem. Phys.* **2020**, *153*, 124111.
(365) Fiedler, L.; Shah, K.; Bussmann, M.; Cangi, A. Deep dive into machine learning density functional theory for materials science and chemistry. *Phys. Rev. Mater.* **2022**, *6*, 040301.
(366) Cheng, L.; Kovachki, N. B.; Welborn, M.; Miller, T. F. Regression Clustering for Improved Accuracy and Training Costs with Molecular-orbital-based Machine Learning. *J. Chem. Theory Comput.* **2019**, *15*, 6668−6677.
(367) Nudejima, T.; Ikabata, Y.; Seino, J.; Yoshikawa, T.; Nakai, H. Machine-learned Electron Correlation Model Based on Correlation Energy Density at Complete Basis Set Limit. *J. Chem. Phys.* **2019**, *151*, 024104.
(368) Ma, J.; Zhang, P.; Tan, Y.; Ghosh, A. W.; Chern, G.-W. Machine Learning Electron Correlation in a Disordered Medium. *Phys. Rev. B* **2019**, *99*, 085118.
(369) Smith, J. S.; Nebgen, B. T.; Zubatyuk, R.; Lubbers, N.; Devereux, C.; Barros, K.; Tretiak, S.; Isayev, O.; Roitberg, A. E. Approaching Coupled Cluster Accuracy with a General-purpose Neural Network Potential Through Transfer Learning. *Nat. Commun.* **2019**, *10*, 2903.
(370) Tuckerman, M. E. Machine Learning Transforms How Microstates Are Sampled. *Science* **2019**, *365*, 982−983.
(371) Zhang, L.; Han, J.; Wang, H.; Car, R.; E, W. Deep Potential Molecular Dynamics: A Scalable Model with the Accuracy of Quantum Mechanics. *Phys. Rev. Lett.* **2018**, *120*, 143001.
(372) Kalita, B.; Li, L.; McCarty, R. J.; Burke, K. Learning to Approximate Density Functionals. *Acc. Chem. Res.* **2021**, *54*, 818−826.
(373) Snyder, J. C.; Rupp, M.; Müller, K.-R.; Burke, K. Nonlinear Gradient Denoising: Finding Accurate Extrema from Inaccurate Functional Derivatives. *Int. J. Quantum Chem.* **2015**, *115*, 1102−1114.
(374) Li, L.; Baker, T. E.; White, S. R.; Burke, K. Pure Density Functional for Strong Correlation and the Thermodynamic Limit from Machine Learning. *Phys. Rev. B* **2016**, *94*, 245129.
(375) Zhou, Y.; Wu, J.; Chen, S.; Chen, G. Toward the Exact Exchange-correlation Potential: A Three-dimensional Convolutional Neural Network Construct. *J. Phys. Chem. Lett.* **2019**, *10*, 7264−7269.
(376) Schmidt, J.; Benavides-Riveros, C. L.; Marques, M. A. L. Machine Learning the Physical Nonlocal Exchange-correlation Functional of Density-functional Theory. *J. Phys. Chem. Lett.* **2019**, *10*, 6425−6431.
(377) Lei, X.; Medford, A. J. Design and Analysis of Machine Learning Exchange-correlation Functionals via Rotationally Invariant Convolutional Descriptors. *Phys. Rev. Mater.* **2019**, *3*, 063801.
(378) Sinitskiy, A. V.; Pande, V. S. Deep neural network computes electron densities and energies of a large set of organic molecules faster than density functional theory (DFT). *arXiv* **2018**, 1809.02723.
(379) Ryczko, K.; Strubbe, D. A.; Tamblyn, I. Deep Learning and Density-functional Theory. *Phys. Rev. A* **2019**, *100*, 022512.
(380) Ji, H.; Jung, Y. A Local Environment Descriptor for Machine-learned Density Functional Theory at the Generalized Gradient Approximation Level. *J. Chem. Phys.* **2018**, *148*, 241742.
(381) Kirkpatrick, J.; et al. Pushing the frontiers of density functionals by solving the fractional electron problem. *Science* **2021**, *374*, 1385−1389.
(382) Mardirossian, N.; Head-Gordon, M. Survival of the Most Transferable at the Top of Jacob's Ladder: Defining and Testing the ωb97m(2) Double Hybrid Density Functional. *J. Chem. Phys.* **2018**, *148*, 241736.
(383) Palos, E.; Lambros, E.; Dasgupta, S.; Paesani, F. Density functional theory of water with the machine-learned DM21 functional. *J. Chem. Phys.* **2022**, *156*, 161103.
(384) Lewis, A. M.; Grisafi, A.; Ceriotti, M.; Rossi, M. Learning electron densities in the condensed phase. *J. Chem. Theory Comput.* **2021**, *17*, 7203−7214.
(385) Grisafi, A.; Fabrizio, A.; Meyer, B.; Wilkins, D. M.; Corminboeuf, C.; Ceriotti, M. Transferable machine-learning model of the electron density. *ACS Cent. Sci.* **2019**, *5*, 57−64.
(386) Cuevas-Zuviría, B.; Pacios, L. F. Machine learning of analytical electron density in large molecules through message-passing. *J. Chem. Inf. Model.* **2021**, *61*, 2658−2666.
(387) Schmidt, E.; Fowler, A. T.; Elliott, J. A.; Bristowe, P. D. Learning models for electron densities with Bayesian regression. *Comput. Mater. Sci.* **2018**, *149*, 250−258.
(388) Perdew, J. P. Artificial intelligence "sees" split electrons. *Science* **2021**, *374*, 1322−1323.
(389) Li, L.; Hoyer, S.; Pederson, R.; Sun, R.; Cubuk, E.; Riley, P.; Burke, K. Kohn-Sham Equations As Regularizer: Building Prior

Knowledge Into Machine-learned Physics. *Phys. Rev. Lett.* **2021**, *126*, 036401.
(390) Pokharel, K.; Furness, J. W.; Yao, Y.; Blum, V.; Irons, T. J.; Teale, A. M.; Sun, J. Exact constraints and appropriate norms in machine learned exchange-correlation functionals. *J. Chem. Phys.* **2022**, *157*, 174106.
(391) Nagai, R.; Akashi, R.; Sugino, O. Machine-learning-based exchange correlation functional with physical asymptotic constraints. *Phys. Rev. Res.* **2022**, *4*, 013106.
(392) Kim, M.-C.; Sim, E.; Burke, K. Understanding and Reducing Errors in Density Functional Calculations. *Phys. Rev. Lett.* **2013**, *111*, 073003.
(393) Wasserman, A.; Nafziger, J.; Jiang, K.; Kim, M.-C.; Sim, E.; Burke, K. The importance of being inconsistent. *Annu. Rev. Phys. Chem.* **2017**, *68*, 555−581.
(394) Curtiss, L. A.; Raghavachari, K.; Redfern, P. C.; Pople, J. Assessment of Gaussian-2 and Density Functional Theories for the Computation of Enthalpies of Formation. *J. Chem. Phys.* **1997**, *106*, 1063−1079.
(395) Curtiss, L. A.; Raghavachari, K.; Redfern, P. C.; Pople, J. Assessment of Gaussian-3 and Density Functional Theories for a Larger Experimental test Set. *J. Chem. Phys.* **2000**, *112*, 7374−7383.
(396) Curtiss, L. A.; Redfern, P. C.; Raghavachari, K.; Pople, J. A. Gaussian-3X (g3x) Theory: Use of Improved Geometries, Zero-point Energies, and Hartree-Fock Basis Sets. *J. Chem. Phys.* **2001**, *114*, 108−117.
(397) Staroverov, V. N.; Scuseria, G.; Tao, J.; Perdew, J. P. Comparative Assessment of a New Nonempirical Density Functional: Molecules and Hydrogen-bonded Complexes. *J. Chem. Phys.* **2003**, *119*, 12129−12137. Erratum: *J. Chem. Phys.* **2004**, *121*, 11507.
(398) Peverati, R.; Truhlar, D. G. Quest for a Universal Density Functional: the Accuracy of Density Functionals Across a Broad Spectrum of Databases in Chemistry and Physics. *Philos. Trans. Royal Soc. A* **2014**, *372*, 20120476.
(399) Blöchl, P. Projector Augmented-wave Method. *Phys. Rev. B* **1994**, *50*, 17953−17979.
(400) García-Cervera, C. J.; Lu, J.; E, W. A Sub-linear Scaling Algorithim for Computing the Electronic Structure of Materials. *Commun. Math. Sci.* **2007**, *5*, 999−1026.
(401) Slater, J. C. Wave Functions in a Periodic Potential. *Phys. Rev.* **1937**, *51*, 846−851.
(402) Blaha, P.; Schwarz, K.; Sorantin, P.; Trickey, S. B. Full-potential, Linearized Augmented Plane Wave Programs for Crystalline Systems. *Comput. Phys. Commun.* **1990**, *59*, 399−415.
(403) Huang, C.; Carter, E. A. Toward an Orbital-free Density Functional Theory of Transition Metals Based on an Electron Density Decomposition. *Phys. Rev. B* **2012**, *85*, 045126.
(404) Trickey, S. B. Omitted Scale Factor Functional Derivative in "Density-decomposed orbital-free density functional theory for covalently bonded molecules and materials", (Phys. Rev. B **86**, 235109 (2012). *University of Florida Technical Note*; 2013, unpublished.
(405) Ke, Y.; Libisch, F.; Xia, J.; Carter, E. A. Angular Momentum Dependent Orbital-free Density Functional Theory: Formulation and Implementation. *Phys. Rev. B* **2014**, *89*, 155112.
(406) Xu, Q.; Ma, C.; Mi, W.; Wang, Y.; Ma, Y. Nonlocal pseudopotential energy density functional for orbital-free density functional theory. *Nat. Commun.* **2022**, *13*, 1385.
(407) Espinosa Leal, L. E.; Karpenko, A.; Caro, M.; Lopez-Acevedo, O. Optimizing a Parametrized Thomas−Fermi−Dirac−Weizsäcker Density Functional for Atoms. *Phys. Chem. Chem. Phys.* **2015**, *17*, 31463−31471.
(408) Sun, Q.; Chan, G. K.-L. Quantum Embedding Theories. *Acc. Chem. Res.* **2016**, *49*, 2705−2712.
(409) Wasserman, A.; Pavanello, M. Quantum Embedding Electronic Structure Methods. *Int. J. Quantum Chem.* **2020**, *120*, e26495.
(410) Cortona, P. Self-consistently Determined Properties of Solids without Band-structure Calculations. *Phys. Rev. B* **1991**, *44*, 8454.
(411) Knizia, G.; Chan, G. K.-L. Density Matrix Embedding: A Simple Alternative to Dynamical Mean-field Theory. *Phys. Rev. Lett.* **2012**, *109*, 186404.
(412) Knizia, G.; Chan, G. K.-L. Density Matrix Embedding: A Strong-coupling Quantum Embedding Theory. *J. Chem. Theory Comput.* **2013**, *9*, 1428−1432.
(413) Bulik, I. W.; Scuseria, G. E.; Dukelsky, J. Density Matrix Embedding from Broken Symmetry Lattice Mean Fields. *Phys. Rev. B* **2014**, *89*, 035140.
(414) Wouters, S.; Jiménez-Hoyos, C. A.; Sun, Q.; Chan, G. K.-L. A Practical Guide to Density Matrix Embedding Theory in Quantum Chemistry. *J. Chem. Theory Comput.* **2016**, *12*, 2706−2719.
(415) Inglesfield, J. A Method of Embedding. *J. Phys. C: Solid State Phys.* **1981**, *14*, 3795.
(416) Inglesfield, J. E. *The Embedding Method for Electronic Structure*; IOP Publishing: Bristol, UK, 2015.
(417) Kotliar, G.; Savrasov, S. Y.; Haule, K.; Oudovenko, V. S.; Parcollet, O.; Marianetti, C. Electronic Structure Calculations with Dynamical Mean-field Theory. *Rev. Mod. Phys.* **2006**, *78*, 865.
(418) Chibani, W.; Ren, X.; Scheffler, M.; Rinke, P. Self-consistent Green's Function Embedding for Advanced Electronic Structure Methods Based on a Dynamical Mean-field Concept. *Phys. Rev. B* **2016**, *93*, 165106.
(419) Gotz, A. W.; Beyhan, S. M.; Visscher, L. Performance of Kinetic Energy Functionals for Interaction Energies in a Subsystem Formulation of Density Functional Theory. *J. Chem. Theory Comput.* **2009**, *5*, 3161−3174.
(420) Fux, S.; Jacob, C. R.; Neugebauer, J.; Visscher, L.; Reiher, M. Accurate Frozen-density Embedding Potentials As a First Step Towards a Subsystem Description of Covalent Bonds. *J. Chem. Phys.* **2010**, *132*, 164101.
(421) Wesolowski, T. A.; Weber, J. Kohn-Sham equations with constrained electron density: an iterative evaluation of the ground-state electron density of interacting molecules. *Chem. Phys. Lett.* **1996**, *248*, 71−76.
(422) Polak, E.; González-Espinoza, C. E.; Gander, M. J.; Wesolowski, T. A. A non-decomposable approximation on the complete density function space for the non-additive kinetic potential. *J. Chem. Phys.* **2022**, *156*, 044103.
(423) Lastra, J. M. G.; Kaminski, J. W.; Wesolowski, T. A. Orbital-free Effective Embedding Potential at Nuclear Cusps. *J. Chem. Phys.* **2008**, *129*, 074107.
(424) Jiang, K.; Nafziger, J.; Wasserman, A. Constructing a non-additive non-interacting kinetic energy functional approximation for covalent bonds from exact conditions. *J. Chem. Phys.* **2018**, *149*, 164112.
(425) Shao, X.; Mi, W.; Pavanello, M. GGA-Level Subsystem DFT Achieves Sub-kcal/mol Accuracy Intermolecular Interactions by Mimicking Nonlocal Functionals. *J. Chem. Theory Comput.* **2021**, *17*, 3455−3461.
(426) Wesolowski, T. A.; Chermette, H.; Weber, J. Accuracy of Approximate Kinetic Energy Functionals in the Model of Kohn-Sham Equations with Constrained Electron Density: The FH··· NCH Complex as a Test Case. *J. Chem. Phys.* **1996**, *105*, 9182−9190.
(427) Bernard, Y. A.; Dułak, M.; Kamiński, J. W.; Wesołowski, T. A. The energy-differences based exact criterion for testing approximations to the functional for the kinetic energy of non-interacting electrons. *J. Phys. A: Mathematical and Theoretical* **2008**, *41*, 055302.
(428) Gritsenko, O. V. On the Principal Difference Between the Exact and Approximate Frozen-density Embedding Theory. In *Recent Advances in Orbital-Free Density Functional Theory*; Wesolowski, T. A., Wang, Y. A., Eds.; World Scientific: Singapore, 2013; Chapter 12, pp 355−365.
(429) Humbert-Droz, M.; Zhou, X.; Shedge, S. V.; Wesolowski, T. A. How to choose the frozen density in Frozen-Density Embedding Theory-based numerical simulations of local excitations? *Theor. Chem. Acc.* **2014**, *133*, 1405.
(430) Wesolowski, T. A. One-Electron Equations for Embedded Electron Density: Challenge for Theory and Practical Payoffs in

Multi-level Modeling of Complex Polyatomic Systems. In *Computational Chemistry: Reviews of Current Trends*; Leszczynski, J., Ed.; World Scientific: Singapore, 2006; Vol. *10*, pp 1−82.
(431) Ricardi, N.; González-Espinoza, C. E.; Wesołowski, T. A. N-representability of the target density in Frozen-Density Embedding Theory based methods: Numerical significance and its relation to electronic polarization. *J. Chem. Phys.* **2022**, *157*, 064108.
(432) Wesołowski, T. A. Embedding a multideterminantal wave function in an orbital-free environment. *Phys. Rev. A* **2008**, *77*, 012504.
(433) Wesolowski, T. A. Is the non-additive kinetic potential always equal to the difference of effective potentials from inverting the Kohn-Sham equation? *J. Chem. Phys.* **2022**, *157*, 081102.
(434) Elliott, P.; Burke, K.; Cohen, M. H.; Wasserman, A. Partition Density-functional Theory. *Phys. Rev. A* **2010**, *82*, 024501.
(435) Yu, K.; Carter, E. A. Extending Density Functional Embedding Theory for Covalently Bonded Systems. *Proc. Nat. Acad. Sci.(USA)* **2017**, *114*, E10861−E10870.
(436) Huang, C.; Pavone, M.; Carter, E. A. Quantum Mechanical Embedding Theory Based on a Unique Embedding Potential. *J. Chem. Phys.* **2011**, *134*, 154110.
(437) Nafziger, J.; Wasserman, A. Density-Based Partitioning Methods for Ground-State Molecular Calculations. *J. Phys. Chem. A* **2014**, *118*, 7623−7639.
(438) Pickett, W. E. Pseudopotential Methods in Condensed Matter Applications. *Comput. Phys. Rep.* **1989**, *9*, 115−197.
(439) Troullier, N.; Martins, J. L. Efficient Pseudopotentials for Plane-wave Calculations. *Phys. Rev. B* **1991**, *43*, 1993−2006.
(440) Dal Corso, A. Pseudopotentials Periodic Table: From H to Pu. *Comput. Mater. Sci.* **2014**, *95*, 337−350.
(441) Vanderbilt, D. Soft self-consistent Pseudopotentials in a Generalized Eigenvalue Formalism. *Phys. Rev. B* **1990**, *41*, 7892.
(442) Del Rio, B. G.; Dieterich, J. M.; Carter, E. A. Globally-optimized Local Pseudopotentials for (orbital-free) Density Functional Theory Simulations of Liquids and Solids. *J. Chem. Theory Comput.* **2017**, *13*, 3684−3695.
(443) Ashcroft, N. Electron-ion Pseudopotentials in Metals. *Phys. Lett.* **1966**, *23*, 48−50.
(444) Fiolhais, C.; Perdew, J. P.; Armster, S. Q.; MacLaren, J. M.; Brajczewska, M. Dominant Density Parameters and Local Pseudopotentials for Simple Metals. *Phys. Rev. B* **1995**, *51*, 14001.
(445) Heine, V.; Abarenkov, I. A New Method for the Electronic Structure of Metals. *Philos. Mag.* **1964**, *9*, 451−465.
(446) Shaw, R. W. Optimum Form of a Modified Heine-Abarenkov Model Potential for the Theory of Simple Metals. *Phys. Rev.* **1968**, *174*, 769−781.
(447) Topp, W. C.; Hopfield, J. J. Chemically Motivated Pseudopotential for Sodium. *Phys. Rev. B* **1973**, *7*, 1295−1303.
(448) Starkloff, T.; Joannopoulos, J. Local Pseudopotential Theory for Transition Metals. *Phys. Rev. B* **1977**, *16*, 5212.
(449) Goodwin, L.; Needs, R.; Heine, V. A Pseudopotential Total Energy Study of Impurity-promoted Intergranular Embrittlement. *J. Phys.: Condens. Matter* **1990**, *2*, 351.
(450) Legrain, F.; Manzhos, S. Highly Accurate Local Pseudopotentials of Li, Na, and Mg for Orbital Free Density Functional Theory. *Chem. Phys. Lett.* **2015**, *622*, 99−103.
(451) Pearson, M.; Smargiassi, E.; Madden, P. Ab Initio Molecular Dynamics with an Orbital-free Density Functional. *J. Phys.: Condens. Matter* **1993**, *5*, 3221.
(452) Gómez, S.; González, L.; González, D.; Stott, M.; Dalgiç, S.; Silbert, M. Orbital Free Ab Initio Molecular Dynamics Study of Expanded Liquid Cs. *J. Non Cryst. Solids* **1999**, *250*, 163−167.
(453) Aguado, A.; López, J. M.; Alonso, J. A.; Stott, M. J. Orbital-free Molecular Dynamics Simulations of Melting in Na_8 and Na_20: Melting in Steps. *J. Chem. Phys.* **1999**, *111*, 6026−6035.
(454) Shin, I.; Carter, E. A. First-principles Simulations of Plasticity in Body-centered-cubic Magnesium−lithium Alloys. *Acta Mater.* **2014**, *64*, 198−207.
(455) Cabral, B. J. C.; Martins, J. L. First-principles Molecular Dynamics of Liquid Cesium and Rubidium. *Phys. Rev. B* **1995**, *51*, 872.
(456) Wang, B.; Stott, M. First-principles Local Pseudopotentials for Group-IV Elements. *Phys. Rev. B* **2003**, *68*, 195102.
(457) Watson, S.; Jesson, B.; Carter, E.; Madden, P. Ab Initio Pseudopotentials for Orbital-free Density Functionals. *EPL* **1998**, *41*, 37.
(458) Zhou, B.; Carter, E. A. First Principles Local Pseudopotential for Silver: Towards Orbital-free Density-functional Theory for Transition Metals. *J. Chem. Phys.* **2005**, *122*, 184108.
(459) Wu, Q.; Yang, W. A Direct Optimization Method for Calculating Density Functionals and Exchange−correlation Potentials from Electron Densities. *J. Chem. Phys.* **2003**, *118*, 2498−2509.
(460) Chen, M.; Vella, J. R.; Panagiotopoulos, A. Z.; Debenedetti, P. G.; Stillinger, F. H.; Carter, E. A. Liquid Li Structure and Dynamics: A Comparison between OFDFT and Second Nearest-neighbor Embedded-atom Method. *AIChE J.* **2015**, *61*, 2841−2853.
(461) Chen, M.; Hung, L.; Huang, C.; Xia, J.; Carter, E. A. The Melting Point of Lithium: an Orbital-free First-principles Molecular Dynamics Study. *Mol. Phys.* **2013**, *111*, 3448−3456.
(462) Shao, X.; Mi, W.; Pavanello, M. Efficient DFT Solver for Nanoscale Simulations and Beyond. *J. Phys. Chem. Lett.* **2021**, *12*, 4134−4139.
(463) Ziman, J. M. The Method of Neutral Pseudo-atoms in the Theory of Metals. *Adv. Phys.* **1964**, *13*, 89−138.
(464) Ziman, J. M. Some Non-structural Aspects of the Theory of Metals. *Proc. Phys. Soc.* **1967**, *91*, 701−723.
(465) Dagens, L. A Selfconsistent Calculation of the Rigid Neutral Atom Density According to the Auxiliary Neutral Atom Model. *J. Phys. C: Solid State Phys.* **1972**, *5*, 2333.
(466) Bhuiyan, G. M.; Bretonnet, J. L.; Silbert, M. Liquid Structure of the 3d Transition Metals. *J. Non Cryst. Solids* **1993**, *156*, 145−148.
(467) Chihara, J. Structure Factor and Pseudopotential of Liquid Metallic Lithium Determined from the Nucleus-electron Model. *Phys. Rev. A* **1989**, *40*, 4507−4516.
(468) González, L. E.; González, D. J.; Silbert, M.; Alonso, J. A. A Theoretical Study of the Static Structure and Thermodynamics of Liquid Lithium. *J. Phys.: Condens. Matter* **1993**, *5*, 4283−4298.
(469) Anta, J.; Madden, P. Structure and Dynamics of Liquid Lithium: Comparison of Ab Initio Molecular Dynamics Predictions with Scattering Experiments. *J. Phys.: Condens. Matter* **1999**, *11*, 6099.
(470) González, L.; González, D.; López, J. Pseudopotentials for the Calculation of Dynamic Properties of Liquids. *J. Phys.: Condens. Matter* **2001**, *13*, 7801.
(471) del Rio, B. G.; González, L. E. Orbital Free Ab Initio Simulations of Liquid Alkaline Earth Metals: from Pseudopotential Construction to Structural and Dynamic Properties. *J. Phys.: Condens. Matter* **2014**, *26*, 465102.
(472) Starrett, C. E.; Gill, N. M.; Sjostrom, T.; Greeff, C. W. Wide Ranging Equation of State with Tartarus: a Hybrid Green's Function/orbital-based Average Atom Code. *Comput. Phys. Commun.* **2019**, *235*, 50−62.
(473) Faussurier, G.; Blancard, C. Pressure in Warm and Hot Dense Matter Using the Average-atom Model. *Phys. Rev. E* **2019**, *99*, 053201.
(474) Johnson, W. R.; Nilsen, J. Average-atom Calculations of Bound-free and Free-free Cross Sections in Dense Plasmas. *Phys. Rev. E* **2020**, *102*, 043209.
(475) Dharma-wardana, M. W. C.; Klug, D. D.; Remsing, R. C. Liquid-Liquid Phase Transitions in Silicon. *Phys. Rev. Lett.* **2020**, *125*, 075702.
(476) Sahni, V.; Gruenebaum, J.; Perdew, J. Study of the Density-gradient Expansion for the Exchange Energy. *Phys. Rev. B* **1982**, *26*, 4371.
(477) Grabo, T.; Kreibich, T.; Kurth, S.; Gross, E. Orbital Functionals in Density Functional Theory: The Optimized Effective Potential Method. In *Strong Coulomb Correlations in Electronic Structure: Beyond the Local Density Approximation*; Anisimov, V. I., Ed.; Gordon and Breach: Amsterdam; 2000.

https://doi.org/10.1021/acs.chemrev.2c00758
Chem. Rev. 2023, 123, 12039−12104

(478) Krieger, J.; Li, Y.; Iafrate, G. Systematic Approximations to the Optimized Effective Potential: Application to Orbital-density-functional Theory. *Phys. Rev. A* **1992**, *46*, 5453.
(479) Krieger, J.; Li, Y.; Iafrate, G. Construction and Application of an Accurate Local Spin-polarized Kohn-Sham Potential with Integer Discontinuity: Exchange-only Theory. *Phys. Rev. A* **1992**, *45*, 101.
(480) Advance Article Woo, J.; Kim, H.; Kim, W. Y. Neural network-based pseudopotential: development of a transferable local pseudopotential. *Phys. Chem. Chem. Phys.* **2022**, *24*, 20094−20103.
(481) Payne, M. C.; Teter, M. P.; Allan, D. C.; Arias, T. A.; Joannopoulos, J. D. Iterative Minimization Techniques for Ab Initio Total-energy Calculations: Molecular Dynamics and Conjugate Gradients. *Rev. Mod. Phys.* **1992**, *64*, 1045.
(482) Kresse, G.; Furthmüller, J. Efficient Iterative Schemes for Ab Initio Total-energy Calculations Using a Plane-wave Basis Set. *Phys. Rev. B* **1996**, *54*, 11169−11186.
(483) Slater, J. C.; Mann, J. B.; Wilson, T. M.; Wood, J. H. Nonintegral Occupation Numbers in Transition Atoms in Crystals. *Phys. Rev.* **1969**, *184*, 672−694.
(484) Ghosh, S.; Suryanarayana, P. Higher-order Finite-difference Formulation of Periodic Orbital-free Density Functional Theory. *J. Comput. Phys.* **2016**, *307*, 634−652.
(485) Jiang, H.; Yang, W. Conjugate-gradient Optimization Method for Orbital-free Density Functional Calculations. *J. Chem. Phys.* **2004**, *121*, 2030−2036.
(486) Ho, G. S.; Lignères, V. L.; Carter, E. A. Introducing PROFESS: A New Program for Orbital-free Density Functional Theory Calculations. *Comput. Phys. Commun.* **2008**, *179*, 839−854.
(487) Hestenes, M. R.; Stiefel, E. Methods of Conjugate Gradients for Solving Linear Systems. *J. Res. Natl. Bur. Stnds.* **1952**, *49*, 2379.
(488) Fletcher, R.; Reeves, C. M. Function Minimization by Conjugate Gradients. *Computer J.* **1964**, *7*, 149−154.
(489) Polak, E.; Ribiere, G. Note Sur La Convergence De Méthodes De Directions Conjuguées. *ESAIM Math. Model. Numer. Anal.* **1969**, *3*, 35−43.
(490) Polyak, B. T. The Conjugate Gradient Method in Extremal Problems. *Comput. Math. Math. Phys.* **1969**, *9*, 94−112.
(491) Fletcher, R. *Practical Methods Of Optimization: Vol. 1 Unconstrained Optimization*; John Wiley & Sons, 1980.
(492) Liu, Y.; Storey, C. Efficient Generalized Conjugate Gradient Algorithms, Part 1: Theory. *J. Optim. Theory Appl.* **1991**, *69*, 129−137.
(493) Dai, Y.-H.; Yuan, Y. A Nonlinear Conjugate Gradient Method with a Strong Global Convergence Property. *SIAM J. Optim.* **1999**, *10*, 177−182.
(494) Liu, D. C.; Nocedal, J. On the Limited Memory BFGS Method for Large Scale Optimization. *Math. Programming* **1989**, *45*, 503−528.
(495) Nocedal, J.; Wright, S. *Numerical Optimization*; Springer Science & Business Media, 2006.
(496) Hung, L.; Huang, C.; Carter, E. A. Preconditioners and Electron Density Optimization in Orbital-free Density Functional Theory. *Commun. Comput. Phys.* **2012**, *12*, 135.
(497) Wright, S. J.; Nocedal, J. *Numerical Optimization*; Springer: New York, 1999; Vol. 2.
(498) Ryley, M. S.; Withnall, M.; Irons, T. J.; Helgaker, T.; Teale, A. M. Robust All-Electron Optimization in Orbital-Free Density-Functional Theory Using the Trust-Region Image Method. *J. Phys. Chem. A* **2021**, *125*, 459−475.
(499) Kohanoff, J. *Electronic Structure Calculations for Solids and Molecules: Theory and Computational Methods*; Cambridge University Press, 2006.
(500) Jensen, F. *Introduction to Computational Chemistry*, 3rd ed.; John Wiley & Sons, 2017.
(501) Beck, T. L. Real-space Mesh Techniques in Density-functional Theory. *Rev. Mod. Phys.* **2000**, *72*, 1041.
(502) Kikuji, H.; Tomoya, O.; Yoshitaka, F.; Shigeru, T. *First-principles Calculations in Real-space Formalism: Electronic Configurations and Transport Properties of Nanostructures*; World Scientific, 2005.
(503) Arias, T. A. Multiresolution Analysis of Electronic Structure: Semicardinal and Wavelet Bases. *Rev. Mod. Phys.* **1999**, *71*, 267.
(504) Han, S.; Cho, K.; Ihm, J. Wavelets in All-electron Density-functional Calculations. *Phys. Rev. B* **1999**, *60*, 1437.
(505) Genovese, L.; Neelov, A.; Goedecker, S.; Deutsch, T.; Ghasemi, S. A.; Willand, A.; Caliste, D.; Zilberberg, O.; Rayson, M.; Bergman, A.; Schneider, R. Daubechies Wavelets As a Basis Set for Density Functional Pseudopotential Calculations. *J. Chem. Phys.* **2008**, *129*, 014109.
(506) Martin, R. M. *Electronic Structure: Basic Theory and Practical Methods: Second ed.*; Cambridge University Press, 2020.
(507) Pulay, P. Ab Initio Calculation of Force Constants and Equilibrium Geometries in Polyatomic Molecules: I. Theory. *Mol. Phys.* **1969**, *17*, 197−204.
(508) Schlosser, H.; Marcus, P. M. Composite Wave Variational Method for Solution of the Energy-band Problem in Solids. *Phys. Rev.* **1963**, *131*, 2529−2546.
(509) Blaha, P.; Schwarz, K.; Tran, F.; Laskowski, R.; Madsen, G. K. H.; Marks, L. D. WIEN2k: An APW+lo Program for Calculating the Properties of Solids. *J. Chem. Phys.* **2020**, *152*, 074101.
(510) Singh, D. J.; Nordstrom, L. *Planewaves, Pseudopotentials, and the LAPW Method*, 2nd ed.; Springer Science & Business Media, 2006.
(511) Blaha, P.; Schwarz, K.; Trickey, S. B. Electronic Structure of Solids with Wien2k. *Mol. Phys.* **2010**, *108*, 3147−3166.
(512) Zhang, L.; Kozhevnikov, A.; Schulthess, T.; Trickey, S. B.; Cheng, H.-P. All Electron Full Potential APW+lo Calculation Using Exciting-plus and Sirus Library. *Computation* **2022**, *10*, 43.
(513) Makov, G.; Payne, M. C. Periodic Boundary Conditions In Ab Initio Calculations. *Phys. Rev. B* **1995**, *51*, 4014−4022.
(514) Otani, M.; Sugino, O. First-principles Calculations of Charged Surfaces and Interfaces: A Plane-wave Nonrepeated Slab Approach. *Phys. Rev. B* **2006**, *73*, 115407.
(515) Martyna, G. J.; Tuckerman, M. E. A Reciprocal Space Based Method for Treating Long Range Interactions in Ab Initio and Force-field-based Calculations in Clusters. *J. Chem. Phys.* **1999**, *110*, 2810−2821.
(516) Andreussi, O.; Marzari, N. Electrostatics of Solvated Systems in Periodic Boundary Conditions. *Phys. Rev. B* **2014**, *90*, 245101.
(517) Fisicaro, G.; Genovese, L.; Andreussi, O.; Marzari, N.; Goedecker, S. A Generalized Poisson and Poisson-Boltzmann Solver for Electrostatic Environments. *J. Chem. Phys.* **2016**, *144*, 014103.
(518) Chen, H.; Zhou, A. Finite Element Approximations in Orbital-free Density Functional Theory. In *Recent Progress in Orbital-free Density Functional Theory*; Wesolowski, T. A., Wang, Y. A., Eds.; World Scientific, 2013; pp 251−271.
(519) Chen, M.; Jiang, X.-W.; Zhuang, H.; Wang, L.-W.; Carter, E. A. Petascale Orbital-free Density Functional Theory Enabled by Small-box Algorithms. *J. Chem. Theory Comput.* **2016**, *12*, 2950−2963.
(520) Shao, X.; Xu, Q.; Wang, S.; Lv, J.; Wang, Y.; Ma, Y. Large-scale Ab Initio Simulations for Periodic System. *Comput. Phys. Commun.* **2018**, *233*, 78−83.
(521) Smith, G. D. *Numerical Solution of Partial Differential Equations: Finite Difference Methods*; Oxford University Press, 1985.
(522) Chelikowsky, J. R.; Troullier, N.; Saad, Y. Finite-difference-pseudopotential Method: Electronic Structure Calculations without a Basis. *Phys. Rev. Lett.* **1994**, *72*, 1240.
(523) Natan, A.; Benjamini, A.; Naveh, D.; Kronik, L.; Tiago, M. L.; Beckman, S. P.; Chelikowsky, J. R. Real-space Pseudopotential Method for First Principles Calculations of General Periodic and Partially Periodic Systems. *Phys. Rev. B* **2008**, *78*, 075109.
(524) Ono, T.; Hirose, K. Timesaving Double-grid Method for Real-space Electronic-structure Calculations. *Phys. Rev. Lett.* **1999**, *82*, 5016.
(525) Brandt, A. Multi-level Adaptive Solutions to Boundary-value Problems. *Math. Comput.* **1977**, *31*, 333−390.
(526) Rousse, F.; Redon, S. Incremental solver for orbital-free density functional theory. *J. Comput. Chem.* **2019**, *40*, 2013.

https://doi.org/10.1021/acs.chemrev.2c00758
Chem. Rev. 2023, 123, 12039−12104

(527) Artemova, S.; Redon, S. Adaptively Restrained Particle Simulations. *Phys. Rev. Lett.* **2012**, *109*, 190201.
(528) Zienkiewicz, O. C.; Taylor, R. L.; Nithiarasu, P.; Zhu, J. *The Finite Element Method*; McGraw-Hill: London, 1977; Vol. 3.
(529) Strouboulis, T.; Copps, K.; Babuška, I. The Generalized Finite Element Method. *Comput. Methods Appl. Mech. Eng.* **2001**, *190*, 4081−4193.
(530) Pask, J.; Sterne, P. Finite Element Methods in Ab Initio Electronic Structure Calculations. *Model. Simul. Mater. Sci. Eng.* **2005**, *13*, R71.
(531) Kardestuncer, H.; Norrie, D. H. *Finite Element Handbook*; McGraw-Hill New York NY, Inc.: 1987.
(532) Pask, J. E.; Klein, B. M.; Sterne, P. A.; Fong, C. Y. Finite-element Methods in Electronic-structure Theory. *Comput. Phys. Commun.* **2001**, *135*, 1−34.
(533) Gavini, V.; Bhattacharya, K.; Ortiz, M. Quasi-continuum Orbital-free Density-functional Theory: A Route to Multi-million Atom Non-periodic DFT Calculation. *J. Mech. Phys. Solids* **2007**, *55*, 697−718.
(534) Román-Pérez, G.; Soler, J. M. Efficient Implementation of a van der Waals Density Functional: Application to Double-wall Carbon Nanotubes. *Phys. Rev. Lett.* **2009**, *103*, 096102.
(535) Giannozzi, P. Large-scale Electronic Structure Calculations in Solids. *Computational Approaches to Novel Condensed Matter Systems*; Neilson, D.; Das, M. P., Eds.; Springer, 1995; pp 67−86.
(536) Wigner, E.; Seitz, F. On the Constitution of Metallic Sodium. *Phys. Rev.* **1933**, *43*, 804−810.
(537) Wigner, E.; Seitz, F. On the Constitution of Metallic Sodium. *II. Phys. Rev.* **1934**, *46*, 509−524.
(538) Fuchs, K. A Quantum Mechanical Investigation of the Cohesive Forces of Metallic Copper. *Proc. Roy. Soc. A* **1935**, *151*, 585−602.
(539) Ihm, J.; Zunger, A.; Cohen, M. L. Momentum-space Formalism for the Total Energy of Solids. *J. Phys. C: Solid State Phys.* **1979**, *12*, 4409.
(540) Pask, J.; Sterne, P. Real-space Formulation of the Electrostatic Potential and Total Energy of Solids. *Phys. Rev. B* **2005**, *71*, 113101.
(541) Ewald, P. P. Die Berechnung Optischer Und Elektrostatischer Gitterpotentiale. *Ann. Phys.* **1921**, *369*, 253−287.
(542) Hung, L.; Carter, E. A. Accurate Simulations of Metals at the Mesoscale: Explicit Treatment of 1 Million Atoms with Quantum Mechanics. *Chem. Phys. Lett.* **2009**, *475*, 163−170.
(543) Shao, X.; Mi, W.; Xu, Q.; Wang, Y.; Ma, Y. O (N log N) Scaling Method to Evaluate the Ion−electron Potential of Crystalline Solids. *J. Chem. Phys.* **2016**, *145*, 184110.
(544) Darden, T.; York, D.; Pedersen, L. Particle Mesh Ewald: An Nlog (N) Method for Ewald Sums in Large Systems. *J. Chem. Phys.* **1993**, *98*, 10089−10092.
(545) Essmann, U.; Perera, L.; Berkowitz, M. L.; Darden, T.; Lee, H.; Pedersen, L. G. A Smooth Particle Mesh Ewald Method. *J. Chem. Phys.* **1995**, *103*, 8577−8593.
(546) Jiang, X.-W.; Li, S.-S.; Wang, L.-W. A Small Box Fast Fourier Transformation Method for Fast Poisson Solutions in Large Systems. *Comput. Phys. Commun.* **2013**, *184*, 2693−2702.
(547) Frigo, M.; Johnson, S. G. FFTW: an Adaptive Software Architecture for the FFT. Acoustics, Speech and Signal Processing, 1998. In *Proceedings of the 1998 IEEE International Conference on Acoustics, Speech and Signal Processing, ICASSP '98 (Cat. No.98CH36181)*; 1998; pp 1381−1384.
(548) Li, N.; Laizet, S. 2DECOMP & Fft-a Highly Scalable 2d Decomposition Library and FFT Interface. In *Cray user group 2010 conference*; 2010; pp 1−13.
(549) *ATLAS Website*, available at: http://atlas-ch.cn/. 2019.
(550) Radhakrishnan, B. G.; Gavini, V. Electronic Structure Calculations at Macroscopic Scales Using Orbital-free DFT. In *Recent Progress in Orbital-Free Density Functional Theory*; Wesolowski, T. A., Wang, Y. A., Eds.; World Scientific, 2013; pp 147−163.
(551) Bowler, D. R.; Baker, J. S.; Poulton, J. T. L.; Mujahed, S. Y.; Lin, J.; Yadav, S.; Raza, Z.; Miyazaki, T. Highly Accurate Local Basis Sets for Large-scale DFT Calculations in Conquest. *Jpn. J. Appl. Phys.* **2019**, *58*, 100503.
(552) Soler, J. M.; Artacho, E.; Gale, J. D.; García, A.; Junquera, J.; Ordejón, P.; Sánchez-Portal, D. The SIESTA Method for Ab Initio order-N Materials Simulation. *J. Phys.: Condens. Matter* **2002**, *14*, 2745−2779.
(553) Hernández, E.; Gillan, M. J.; Goringe, C. M. Basis Functions for Linear-scaling First-principles Calculations. *Phys. Rev. B* **1997**, *55*, 13485−13493.
(554) Haynes, P. D.; Skylaris, C.-K.; Mostofi, A. A.; Payne, M. C. Elimination of Basis Set Superposition Error in Linear-scaling Density-functional Calculations with Local Orbitals Optimised in Situ. *Chem. Phys. Lett.* **2006**, *422*, 345−349.
(555) Frediani, L.; Sundholm, D. Real-space Numerical Grid Methods in Quantum Chemistry. *Phys. Chem. Chem. Phys.* **2015**, *17*, 31357−31359.
(556) Saad, Y.; Chelikowsky, J. R.; Shontz, S. M. Numerical Methods for Electronic Structure Calculations of Materials. *SIAM Rev. Soc. Ind. Appl. Math.* **2010**, *52*, 3−54.
(557) Kronik, L.; Makmal, A.; Tiago, M. L.; Alemany, M. M. G.; Jain, M.; Huang, X.; Saad, Y.; Chelikowsky, J. R. PARSEC − the Pseudopotential Algorithm for Real-space Electronic Structure Calculations: Recent Advances and Novel Applications to Nano-structures. *Phys. Status Solidi B* **2006**, *243*, 1063−1079.
(558) Latter, R. Atomic Energy Levels for the Thomas-Fermi and Thomas-Fermi−Dirac Potential. *Phys. Rev.* **1955**, *99*, 510.
(559) Schey, H. M.; Schwartz, J. L. Quantum Corrections in the Thomas-Fermi Model. *Phys. Rev.* **1965**, *137*, A709.
(560) Enstrom, J. E. Solution of the Thomas-Fermi Model with Quantum Corrections. *Phys. Rev. A* **1971**, *4*, 460.
(561) Deb, B.; Ghosh, S. New Method for the Direct Calculation of Electron Density in Many-electron Systems. I. Application to Closed-shell Atoms. *Int. J. Quantum Chem.* **1983**, *23*, 1−26.
(562) Govind, N.; Wang, J.; Guo, H. Total-energy Calculations Using a Gradient-expanded Kinetic-energy Functional. *Phys. Rev. B* **1994**, *50*, 11175.
(563) Govind, N.; Mozos, J.-L.; Guo, H. Equilibrium Structure and Bonding of Small Silicon Clusters Studied Using an Orbital-free Kinetic-energy Functional. *Phys. Rev. B* **1995**, *51*, 7101.
(564) Hung, L.; Huang, C.; Shin, I.; Ho, G. S.; Lignères, V. L.; Carter, E. A. Introducing PROFESS 2.0: A Parallelized, Fully Linear Scaling Program for Orbital-free Density Functional Theory Calculations. *Comput. Phys. Commun.* **2010**, *181*, 2208−2209.
(565) CPC License. https://www.elsevier.com/about/policies/open-access-licenses/elsevier-user-license/cpc-license.
(566) Dieterich, J. M.; Witt, W. C.; Carter, E. A. libKEDF: An Accelerated Library of Kinetic Energy Density Functionals. *J. Comput. Chem.* **2017**, *38*, 1552−1559.
(567) GNU License. http://www.gnu.org/licenses/gpl-3.0.html.
(568) MIT License. https://opensource.org/licenses/mit-license.html.
(569) Larsen, A. H.; et al. The Atomic Simulation Environment − a Python Library for Working with Atoms. *J. Phys.: Condens. Matter* **2017**, *29*, 273002.
(570) Bahn, S. R.; Jacobsen, K. W. An Object-oriented Scripting Interface to a Legacy Electronic Structure Code. *Comput. Sci. Eng.* **2002**, *4*, 56−66.
(571) Suryanarayana, P.; Phanish, D. Augmented Lagrangian Formulation of Orbital-free Density Functional Theory. *J. Comput. Phys.* **2014**, *275*, 524−538.
(572) Das, S.; Iyer, M.; Gavini, V. Real-space Formulation of Orbital-free Density Functional Theory Using Finite-element Discretization: The Case for Al, Mg, and Al-mg Intermetallics. *Phys. Rev. B* **2015**, *92*, 014104.
(573) Gavini, V.; Bhattacharya, K.; Ortiz, M. Vacancy Clustering and Prismatic Dislocation Loop Formation in Aluminum. *Phys. Rev. B* **2007**, *76*, 180101.

https://doi.org/10.1021/acs.chemrev.2c00758
Chem. Rev. 2023, 123, 12039−12104

(574) Gavini, V.; Knap, J.; Bhattacharya, K.; Ortiz, M. Non-periodic Finite-element Formulation of Orbital-free Density Functional Theory. *J. Mech. Phys. Solids* **2007**, *55*, 669−696.
(575) Gavini, V. Role of Macroscopic Deformations in Energetics of Vacancies in Aluminum. *Phys. Rev. Lett.* **2008**, *101*, 205503.
(576) Radhakrishnan, B.; Gavini, V. Effect of Cell Size on the Energetics of Vacancies in Aluminum Studied via Orbital-free Density Functional Theory. *Phys. Rev. B* **2010**, *82*, 094117.
(577) Jacob, C. R.; Neugebauer, J.; Visscher, L. A Flexible Implementation of Frozen-density Embedding for Use in Multilevel Simulations. *J. Comput. Chem.* **2008**, *29*, 1011−1018.
(578) Genova, A.; Ceresoli, D.; Krishtal, A.; Andreussi, O.; DiStasio, R. A.; Pavanello, M. eQE: An Open-source Density Functional Embedding Theory Code for the Condensed Phase. *Int. J. Quantum Chem.* **2017**, *117*, e25401.
(579) Mi, W.; Shao, X.; Genova, A.; Ceresoli, D.; Pavanello, M. eQE 2. 0: Subsystem DFT beyond GGA functionals. *Comput. Phys. Commun.* **2021**, *269*, 108122.
(580) Niklasson, A. M. Extended Born-Oppenheimer molecular dynamics. *Phys. Rev. Lett.* **2008**, *100*, 123004.
(581) Niklasson, A. M. Extended Lagrangian Born−Oppenheimer molecular dynamics for orbital-free density-functional theory and polarizable charge equilibration models. *J. Chem. Phys.* **2021**, *154*, 054101.
(582) Qiu, R.; Lu, H.; Ao, B.; Huang, L.; Tang, T.; Chen, P. Energetics of Intrinsic Point Defects in Aluminium via Orbital-free Density Functional Theory. *Phylos. Mag.* **2017**, *97*, 2164−2181.
(583) Ho, G.; Ong, M. T.; Caspersen, K. J.; Carter, E. A. Energetics and Kinetics of Vacancy Diffusion and Aggregation in Shocked Aluminium via Orbital-free Density Functional Theory. *Phys. Chem. Chem. Phys.* **2007**, *9*, 4951−4966.
(584) Shin, I.; Carter, E. A. Orbital-free Density Functional Theory Simulations of Dislocations in Magnesium. *Model. Simul. Mater. Sci. Eng.* **2012**, *20*, 015006.
(585) Sun, D.; Mendelev, M.; Becker, C.; Kudin, K.; Haxhimali, T.; Asta, M.; Hoyt, J.; Karma, A.; Srolovitz, D. J. Crystal-melt Interfacial Free Energies in hcp Metals: A Molecular Dynamics Study of Mg. *Phys. Rev. B* **2006**, *73*, 024116.
(586) Hung, L.; Carter, E. A. Ductile Processes at Aluminium Crack Tips: Comparison of Orbital-free Density Functional Theory with Classical Potential Predictions. *Model. Simul. Mater. Sci. Eng.* **2011**, *19*, 045002.
(587) Shah, V.; Nehete, D.; Kanhere, D. Ab Initio Molecular Dynamics via Density Based Energy Functionals. *J. Phys.: Condens. Matter* **1994**, *6*, 10773−10781.
(588) Shah, V.; Kanhere, D. Ground-state Geometries and the Stability of Some \prmLi$_7$\prmAl$_n$ (n = 1, 7) Clusters Investigated Using Density-based Ab Initio Molecular Dynamics. *J. Phys.: Condens. Matter* **1996**, *8*, L253−L260.
(589) Nehete, D.; Shah, V.; Kanhere, D. Ab Initio Molecular Dynamics Using Density-based Energy Functionals: Application to Ground-state Geometries of Some Small Clusters. *Phys. Rev. B* **1996**, *53*, 2126−2131.
(590) Shah, V.; Kanhere, D.; Majumder, C.; Das, G. An Ab Initio Molecular Dynamics Investigation of Li$_n$ Al$_n$ Clusters. *J. Phys.: Condens. Matter* **1997**, *9*, 2165.
(591) Majumder, C.; Das, G.; Kulshrestha, S.; Shah, V.; Kanhere, D. Ground State Geometries and Energetics of Al$_n$ Li (n= 1, 13) Clusters Using Ab Initio Density-based Molecular Dynamics. *Chem. Phys. Lett.* **1996**, *261*, 515−520.
(592) Vichare, A.; Kanhere, D. Density-based Molecular Dynamics Study of Melting in a Finite-sized Cluster Al$_{13}$. *J. Phys.: Condens. Matter* **1998**, *10*, 3309−3320.
(593) Ghosh, S. K.; Balbás, L. C. Study of the Kinetic Energy Density Functional in the Locally Linear Potential Approximation. *J. Chem. Phys.* **1985**, *83*, 5778−5783.
(594) Blaise, P.; Blundell, S.; Guet, C. Extended Thomas-Fermi Molecular Dynamics of Sodium Clusters. *Phys. Rev. B* **1997**, *55*, 15856−15867.
(595) Seidl, M.; Brack, M. Liquid Drop Model for Charged Spherical Metal Clusters. *Annals Phys.* **1996**, *245*, 275−310.
(596) Aguado, A.; López, J. M.; Alonso, J. A.; Stott, M. J. Melting in Large Sodium Clusters: An Orbital-free Molecular Dynamics Study. *J. Phys. Chem. B* **2001**, *105*, 2386−2392.
(597) Aguado, A.; López, J. M. Structural and Thermal Behavior of Compact Core-shell Nanoparticles: Core Instabilities and Dynamic Contributions to Surface Thermal Stability. *Phys. Rev. B* **2005**, *72*, 205420.
(598) Aguado, A.; López, J. M. Melting-like Transition in a Ternary Alkali Nanoalloy: Li_{13} Na_{30} Cs_{12}. *J. Chem. Theory Comput.* **2005**, *1*, 299−306.
(599) Aguado, A.; López, J. M.; Núñez, S. Molecular Dynamics Simulation of the Melting-like Transition in K_1 Na_{54}. *Comput. Mater. Sci.* **2006**, *35*, 174−178.
(600) Aguado, A. Competing Thermal Activation Mechanisms in the Meltinglike Transition of Na$_n$ (n= 135- 147) Clusters. *J. Phys. Chem. B* **2005**, *109*, 13043−13048.
(601) Aguado, A.; López, J. M. Anomalous Size Dependence in the Melting Temperatures of Free Sodium Clusters: An Explanation for the Calorimetry Experiments. *Phys. Rev. Lett.* **2005**, *94*, 233401.
(602) Aguado, A.; López, J. M. Small Sodium Clusters That Melt Gradually: Melting Mechanisms in Na_{30}. *Phys. Rev. B* **2006**, *74*, 115403.
(603) Núñez, S.; López, J. M.; Aguado, A. Atomic Layering and Related Postmelting Effects in Small Liquid Metal Clusters. *Phys. Rev. B* **2009**, *79*, 165429.
(604) Hock, C.; Bartels, C.; Straßburg, S.; Schmidt, M.; Haberland, H.; von Issendorff, B.; Aguado, A. Premelting and Postmelting in Clusters. *Phys. Rev. Lett.* **2009**, *102*, 043401.
(605) Schmidt, M.; Kusche, R.; von Issendorff, B.; Haberland, H. Irregular Variations in the Melting Point of Size-selected Atomic Clusters. *Nature* **1998**, *393*, 238−240.
(606) Kanhere, D. G.; Shah, V. Ab initio Orbital-free Molecular Dynamics - Technique and Applications. In *Electronic Structure of Alloys, Surfaces and Clusters*; Mookerjee, A.; Sarma, D. D., Eds.; CRC Press, 2002; pp 308−347.
(607) Aguado, A.; González, D. J.; González, L. E.; López, J. M.; Núñez, S.; Stott, M. J. An Orbital Free *ab initio* Method: Applications to Liquid Metals and Clusters. In *Recent Progress in Orbital-Free Density Functional Theory*; Wesolowski, T. A., Wang, Y. A., Eds.; World Scientific, 2013; pp 55−145.
(608) Zhao, Y.; Kim, Y.-H.; Du, M.-H.; Zhang, S. First-principles Prediction of Icosahedral Quantum Dots for Tetravalent Semiconductors. *Phys. Rev. Lett.* **2004**, *93*, 015502.
(609) Foley, M.; Smargiassi, E.; Madden, P. The Dynamic Structure of Liquid Sodium from Ab Initio Simulation. *J. Phys.: Condens. Matter* **1994**, *6*, 5231.
(610) Anta, J.; Jesson, B.; Madden, P. Ion-electron Correlations in Liquid Metals from Orbital-free Ab Initio Molecular Dynamics. *Phys. Rev. B* **1998**, *58*, 6124.
(611) Bhuiyan, G.; Molla, M. R.; Ahmed, A. Z.; González, L.; González, D. Orbital Free Ab Initio Study of Static and Dynamic Properties of Some Liquid Transition Metals. In *EPJ Web of Conferences*; 2017; p 03001.
(612) del Rio, B. G.; Gonzalez, L. E. Depth-dependent Dynamics of Liquid Metal Surfaces with First Principles Simulations. *Acta Mater.* **2020**, *198*, 281−289.
(613) Del Rio, B. G.; Chen, M.; González, L. E.; Carter, E. A. Orbital-free Density Functional Theory Simulation of Collective Dynamics Coupling in Liquid Sn. *J. Chem. Phys.* **2018**, *149*, 094504.
(614) Marqués, M.; González, D.; González, L. Structure and Dynamics of High-pressure Na Close to the Melting Line: An Ab Initio Molecular Dynamics Study. *Phys. Rev. B* **2016**, *94*, 024204.
(615) Şengül, S.; González, D.; González, L. Structural and Dynamical Properties of Liquid Mg. An Orbital-free Molecular Dynamics Study. *J. Phys.: Condens. Matter* **2009**, *21*, 115106.

https://doi.org/10.1021/acs.chemrev.2c00758
Chem. Rev. 2023, 123, 12039−12104

(616) Blanco, J.; González, D. J.; González, L. E.; López, J. M.; Stott, M. J. Collective Ionic Dynamics in the Liquid Na−Cs Alloy: An Ab Initio Molecular Dynamics Study. *Phys. Rev. E* **2003**, *67*, 041204.
(617) González, D. J.; González, L. E.; López, J. M.; Stott, M. J. Microscopic Dynamics in the Liquid Li-Na Alloy: An Ab Initio Molecular Dynamics Study. *Phys. Rev. E* **2004**, *69*, 031205.
(618) González, D.; González, L. Structure of the Liquid−vapor Interfaces of Ga, In and the Eutectic Ga−In Alloy: an Ab Initio Study. *J. Phys.: Condens. Matter* **2008**, *20*, 114118.
(619) González, D.; González, L.; Stott, M. Surface Structure of Liquid Li and Na: an Ab Initio Molecular Dynamics Study. *Phys. Rev. Lett.* **2004**, *92*, 085501.
(620) González, D.; González, L.; Stott, M. Liquid-vapor Interface in Liquid Binary Alloys: An Ab Initio Molecular Dynamics Study. *Phys. Rev. Lett.* **2005**, *94*, 077801.
(621) del Rio, B. G.; González, L. E. Orbital-free Ab Initio Molecular Dynamics Study of the Static Structure and Dynamic Properties of the Free Liquid Surface of Sn. *EPJ. Web Conf.* **2017**, *151*, 03003.
(622) González, L. E.; González, D. J. Orbital-free Ab-initio Study of the Structure of Liquid Al on a Model fcc Metallic Wall: The Influence of Surface Orientation. *J. Phys.: Conf. Ser.* **2008**, *98*, 062024.
(623) González, D. J.; González, L. E. Structure and Motion at the Liquid-vapor Interface of Some Interalkali Binary Alloys: An Orbital-free Ab Initio Study. *J. Chem. Phys.* **2009**, *130*, 114703.
(624) Delisle, A.; González, D.; Stott, M. Structural and Dynamical Properties of Liquid Si: An Orbital-free Molecular Dynamics Study. *Phys. Rev. B* **2006**, *73*, 064202.
(625) Delisle, A.; González, D.; Stott, M. Pressure-induced Structural and Dynamical Changes in Liquid Si: An Ab Initio Study. *J. Phys.: Condens. Matter* **2006**, *18*, 3591.
(626) González, L. E.; González, D. J. Structure and Dynamics of Bulk Liquid Ga and the Liquid-vapor Interface: An Ab Initio Study. *Phys. Rev. B* **2008**, *77*, 064202.
(627) Bhuiyan, G.; González, L.; González, D. Orbital Free Ab Initio Molecular Dynamics Simulation Study of Some Static and Dynamic Properties of Liquid Noble Metals. *Condens. Matter. Phys.* **2012**, *15*, 33604−33623.
(628) Molla, M. R.; Ahmed, A. Z.; Sarker, H.; Bhuiyan, G.; Amin, M.; González, L.; González, D. Static and Dynamic Properties of Liquid Zn, Cd and Hg Divalent Metals: An Orbital Free Ab Initio Molecular Dynamics Study. *J. Non Cryst. Solids* **2014**, *406*, 45−53.
(629) Fabricius, G.; Artacho, E.; Sánchez-Portal, D.; Ordejón, P.; Drabold, D.; Soler, J. M. Atomic Layering at the Liquid Silicon Surface: A First-principles Simulation. *Phys. Rev. B* **1999**, *60*, R16283.
(630) Becker, A.; Bethkenhagen, M.; Kellermann, C.; Wicht, J.; Redmer, R. Material Properties for the Interiors of Massive Giant Planets and Brown Dwarfs. *Astron. J.* **2018**, *156*, 149.
(631) Graziani, F.; Desjarlais, M. P.; Redmer, R.; Trickey, S. B. *Frontiers and Challenges in Warm Dense Matter*; Springer Science & Business: Heidelberg, 2014; Vol. *96*.
(632) Mermin, N. D. Thermal Properties of the Inhomogeneous Electron Gas. *Phys. Rev.* **1965**, *137*, A1441−A1443.
(633) Perrot, F. Gradient Correction to the Statistical Electronic Free Energy at Nonzero Temperatures: Application to Equation-of-state Calculations. *Phys. Rev. A* **1979**, *20*, 586−594.
(634) Zérah, G.; Clérouin, J.; Pollock, E. L. Thomas-Fermi Molecular-dynamics, Linear Screening, and Mean-field Theories of Plasmas. *Phys. Rev. Lett.* **1992**, *69*, 446−449.
(635) Clérouin, J.; Pollock, E. L.; Zérah, G. Thomas-Fermi Molecular Dynamics. *Phys. Rev. A* **1992**, *46*, 5130−5137.
(636) Lambert, F.; Clérouin, J.; Zérah, G. Very-high-temperature Molecular Dynamics. *Phys. Rev. E* **2006**, *73*, 016403.
(637) Mazevet, S.; Lambert, F.; Bottin, F.; Zérah, G.; Clérouin, J. Ab Initio Molecular Dynamics Simulations of Dense Boron Plasmas up to the Semiclassical Thomas-Fermi Regime. *Phys. Rev. E* **2007**, *75*, 056404.
(638) Danel, J.-F.; Kazandjian, L. Equation of State of a Dense Plasma by Orbital-free and Quantum Molecular Dynamics: Examination of Two Isothermal-isobaric Mixing Rules. *Phys. Rev. E* **2015**, *91*, 013103.
(639) Shemyakin, O. P.; Levashov, P. R.; Krasnova, P. A. TFmix:A High-precision Implementation of the Finite-temperature Thomas-Fermi Model for a Mixture of Atoms. *Comput. Phys. Commun.* **2019**, *235*, 378−387.
(640) Karasiev, V. V.; Sjostrom, T.; Trickey, S. B. Generalized-gradient-approximation Noninteracting Free-energy Functionals for Orbital-free Density Functional Calculations. *Phys. Rev. B* **2012**, *86*, 115101.
(641) Luo, K.; Karasiev, V. V.; Trickey, S. B. Towards Accurate Orbital-free Simulations: A Generalized Gradient Approximation for the Noninteracting Free Energy Density Functional. *Phys. Rev. B* **2020**, *101*, 075116.
(642) Sjostrom, T.; Daligault, J. Ionic and Electronic Transport Properties in Dense Plasmas by Orbital-free Density Functional Theory. *Phys. Rev. E* **2015**, *92*, 063304.
(643) Schulz, H.; Görling, A. *Toward a Comprehensive Treatment of Temperature in Electronic Structure Calculations: Non-zero Temperature Hartree-Fock and Exact-exchange Kohn-Sham Methods*. pp 87−121 in ref 631.
(644) Karasiev, V. V.; Calderín, L.; Trickey, S. B. Importance of Finite-temperature Exchange-correlation for Warm Dense Matter Calculations. *Phys. Rev. E* **2016**, *93*, 063207.
(645) Karasiev, V. V.; Trickey, S. B.; Dufty, J. W. Status of Free-energy Representations for the Homogeneous Electron Gas. *Phys. Rev. B* **2019**, *99*, 195134.
(646) Karasiev, V. V.; Sjostrom, T.; Dufty, J.; Trickey, S. B. Accurate Homogeneous Electron Gas Exchange-correlation Free Energy for Local Spin-density Calculations. *Phys. Rev. Lett.* **2014**, *112*, 076403.
(647) Sjostrom, T.; Daligault, J. Gradient Corrections to the Exchange-correlation Free Energy. *Phys. Rev. B* **2014**, *90*, 155109.
(648) Karasiev, V. V.; Dufty, J. W.; Trickey, S. B. Nonempirical Semilocal Free-energy Density Functional for Matter Under Extreme Conditions. *Phys. Rev. Lett.* **2018**, *120*, 076401.
(649) Mihaylov, D. I.; Karasiev, V. V.; Hu, S. X. Thermal Hybrid Exchange-correlation Density Functional for Improving the Description of Warm Dense Matter. *Phys. Rev. B* **2020**, *101*, 245141.
(650) Lyon, S. P.; Johnson, J. D. *SESAME: The Los Alamos National Laboratory Equation of State Database*, la-ur-92-3407 ed.; Los Alamos National Laboratory, 1992.
(651) Sun, H.; Kang, D.; Hou, Y.; Dai, J. Transport Properties of Warm and Hot Dense Iron from Orbital Free and Corrected Yukawa Potential Molecular Dynamics. *Matter Radiat. at Extremes* **2017**, *2*, 287−295.
(652) Abarenkov, I.; Heine, V. The Model Potential for Positive Ions. *Philos. Mag.* **1965**, *12*, 529−537.
(653) Severo Pereira Gomes, A.; Jacob, C. R. Quantum-chemical Embedding Methods for Treating Local Electronic Excitations in Complex Chemical Systems. *Annu. Rep. Prog. Chem., Sect. C: Phys. Chem.* **2012**, *108*, 222−277.
(654) Wesolowski, T. A. Density Functional Theory with Approximate Kinetic Energy Functionals Applied to Hydrogen Bonds. *J. Chem. Phys.* **1997**, *106*, 8516−8526.
(655) Schluns, D.; Klahr, K.; Muck-Lichtenfeld, C.; Visscher, L.; Neugebauer, J. Subsystem-DFT Potential-energy Curves for Weakly Interacting Systems. *Phys. Chem. Chem. Phys.* **2015**, *17*, 14323−14341.
(656) Kiewisch, K.; Eickerling, G.; Reiher, M.; Neugebauer, J. Topological Analysis of Electron Densities from Kohn-Sham and Subsystem Density Functional Theory. *J. Chem. Phys.* **2008**, *128*, 044114.
(657) Pavanello, M. On the Subsystem Formulation of Linear-response Time-dependent DFT. *J. Chem. Phys.* **2013**, *138*, 204118.
(658) Řezáč, J.; Hobza, P. Benchmark Calculations of Interaction Energies in Noncovalent Complexes and Their Applications. *Chem. Rev.* **2016**, *116*, 5038−5071.

https://doi.org/10.1021/acs.chemrev.2c00758
Chem. Rev. 2023, 123, 12039−12104

(659) Řezáč, J.; Riley, K. E.; Hobza, P. S66: A Well-balanced Database of Benchmark Interaction Energies Relevant to Biomolecular Structures. *J. Chem. Theory Comput.* **2011**, *7*, 2427−2438.
(660) Wesołowski, T.; Ellinger, Y.; Weber, J. Density Functional Theory with an Approximate Kinetic Energy Functional Applied to Study Structure and Stability of Weak van der Waals Complexes. *J. Chem. Phys.* **1998**, *108*, 6078−6083.
(661) Jacob, C. R.; Wesolowski, T. A.; Visscher, L. Orbital-free Embedding Applied to the Calculation of Induced Dipole Moments in CO_2··· X (X= He, Ne, Ar, Kr, Xe, Hg) van der Waals Complexes. *J. Chem. Phys.* **2005**, *123*, 174104.
(662) Wesolowski, T. A. Hydrogen-bonding-induced Shifts of the Excitation Energies in Nucleic Acid Bases: an Interplay between Electrostatic and Electron Density Overlap Effects. *J. Am. Chem. Soc.* **2004**, *126*, 11444−11445.
(663) Kevorkyants, R.; Dulak, M.; Wesolowski, T. A. Interaction Energies in Hydrogen-bonded Systems: A Testing Ground for Subsystem Formulation of Density-functional Theory. *J. Chem. Phys.* **2006**, *124*, 024104.
(664) Nafziger, J.; Jiang, K.; Wasserman, A. Accurate Reference Data for the Nonadditive, Noninteracting Kinetic Energy in Covalent Bonds. *J. Chem. Theory Comput.* **2017**, *13*, 577−586.
(665) Iannuzzi, M.; Kirchner, B.; Hutter, J. Density functional embedding for molecular systems. *Chem. Phys. Lett.* **2006**, *421*, 16−20.
(666) Bensberg, M.; Türtscher, P. L.; Unsleber, J. P.; Reiher, M.; Neugebauer, J. Solvation Free Energies in Subsystem Density Functional Theory. *J. Chem. Theory Comput.* **2022**, *18*, 723−740.
(667) Shao, X.; Mi, W.; Pavanello, M. Density Embedding Method for Nanoscale Molecule−Metal Interfaces. *J. Phys. Chem. Lett.* **2022**, *13*, 7147−7154.
(668) Andermatt, S.; Cha, J.; Schiffmann, F.; VandeVondele, J. Combining Linear-scaling DFT with Subsystem DFT in Born−Oppenheimer and Ehrenfest Molecular Dynamics Simulations: From Molecules to a Virus in Solution. *J. Chem. Theory Comput.* **2016**, *12*, 3214−3227.
(669) Umerbekova, A.; Pavanello, M. Many-body Response of Benzene at Monolayer MoS_2: van der Waals Interactions and Spectral Broadening. *Int. J. Quantum Chem.* **2020**, *120*, e26243.
(670) Neugebauer, J. Orbital-free Embedding Calculations of Electronic Spectra. In *Recent Progress in Orbital-free Density Functional Theory*; Wesolowski, T. A., Wang, Y. A., Eds.; World Scientific, 2013; pp 323−354.
(671) Jacob, C. R.; Visscher, L. Calculation of Nuclear Magnetic Resonance Shieldings Using Frozen-density Embedding. *J. Chem. Phys.* **2006**, *125*, 194104.
(672) Bulo, R. E.; Jacob, C. R.; Visscher, L. NMR Solvent Shifts of Acetonitrile from Frozen Density Embedding Calculations. *J. Phys. Chem. A* **2008**, *112*, 2640−2647.
(673) Neugebauer, J.; Louwerse, M. J.; Belanzoni, P.; Wesolowski, T. A.; Baerends, E. J. Modeling Solvent Effects on Electron-spin-resonance Hyperfine Couplings by Frozen-density Embedding. *J. Chem. Phys.* **2005**, *123*, 114101.
(674) Kevorkyants, R.; Wang, X.; Close, D. M.; Pavanello, M. Calculating Hyperfine Couplings in Large Ionic Crystals Containing Hundreds of QM Atoms: Subsystem DFT Is the Key. *J. Phys. Chem. B* **2013**, *117*, 13967−13974.
(675) Wesołowski, T. A. Application of the DFT-based Embedding Scheme Using an Explicit Functional of the Kinetic Energy to Determine the Spin Density of Mg+ Embedded in Ne and Ar Matrices. *Chem. Phys. Lett.* **1999**, *311*, 87−92.
(676) Schulz, A.; Jacob, C. R. Description of intermolecular charge transfer with subsystem density-functional theory. *J. Chem. Phys.* **2019**, *151*, 131103.
(677) Pavanello, M.; Van Voorhis, T.; Visscher, L.; Neugebauer, J. An Accurate and Linear-scaling Method for Calculating Charge-transfer Excitation Energies and Diabatic Couplings. *J. Chem. Phys.* **2013**, *138*, 054101.
(678) Solovyeva, A.; Pavanello, M.; Neugebauer, J. Describing Long-range Charge-separation Processes with Subsystem Density-functional Theory. *J. Chem. Phys.* **2014**, *140*, 164103.
(679) Ramos, P.; Papadakis, M.; Pavanello, M. Performance of Frozen Density Embedding for Modeling Hole Transfer Reactions. *J. Phys. Chem. B* **2015**, *119*, 7541−7557.
(680) Hernández-Fernández, F.; Pavanello, M.; Visscher, L. Effect of Metallation, Substituents and Inter/intra-molecular Polarization on Electronic Couplings for Hole Transport in Stacked Porphyrin Dyads. *Phys. Chem. Chem. Phys.* **2016**, *18*, 21122−21132.
(681) Eschenbach, P.; Neugebauer, J. Subsystem density-functional theory: A reliable tool for spin-density based properties. *J. Chem. Phys.* **2022**, *157*, 130902.
(682) Neugebauer, J.; Louwerse, M. J.; Baerends, E. J.; Wesolowski, T. A. The Merits of the Frozen-density Embedding Scheme to Model Solvatochromic Shifts. *J. Chem. Phys.* **2005**, *122*, 094115.
(683) Neugebauer, J.; Curutchet, C.; Muñoz-Losa, A.; Mennucci, B. A Subsystem TDDFT Approach for Solvent Screening Effects on Excitation Energy Transfer Couplings. *J. Chem. Theory Comput.* **2010**, *6*, 1843−1851.
(684) Casida, M. E.; Wesołowski, T. A. Generalization of the Kohn-Sham Equations with Constrained Electron Density Formalism and Its Time-dependent Response Theory Formulation. *Int. J. Quantum Chem.* **2004**, *96*, 577−588.
(685) García-Lastra, J.; Wesolowski, T.; Barriuso, M.; Aramburu, J.; Moreno, M. Optical and Vibrational Properties of Mnf64- Complexes in Cubic Fluoroperovskites: Insight Through Embedding Calculations Using Kohn-Sham Equations with Constrained Electron Density. *J. Phys.: Condens. Matter* **2006**, *18*, 1519.
(686) Ramos, P.; Pavanello, M. Constrained Subsystem Density Functional Theory. *Phys. Chem. Chem. Phys.* **2016**, *18*, 21172−21178.
(687) Umerbekova, A.; Zhang, S.-F.; Pavanello, M. Dissecting Energy Level Renormalization and Polarizability Enhancement of Molecules at Surfaces with Subsystem TDDFT. *Euro. Phys. J. B* **2018**, *91*, 214.
(688) Neugebauer, J. Chromophore-Specific Theoretical Spectroscopy: From Subsystem Density Functional Theory to Mode-specific Vibrational Spectroscopy. *Phys. Rep.* **2010**, *489*, 1−87.
(689) Goez, A.; Neugebauer, J. Benchmarking Electron Densities and Electrostatic Potentials of Proteins from the Three-partition Frozen Density Embedding Method. *J. Chem. Theory Comput.* **2016**, *12*, 4843−4855.
(690) Jacob, C. R.; Visscher, L. A Subsystem Density-functional Theory Approach for the Quantum Chemical Treatment of Proteins. *J. Chem. Phys.* **2008**, *128*, 155102.
(691) Schmitt-Monreal, D.; Jacob, C. R. Frozen-density Embedding-based Many-body Expansions. *Int. J. Quantum Chem.* **2020**, *120*, e26228.
(692) Schmitt-Monreal, D.; Jacob, C. R. Density-Based Many-Body Expansion as an Efficient and Accurate Quantum-Chemical Fragmentation Method: Application to Water Clusters. *J. Chem. Theory Comput.* **2021**, *17*, 4144−4156.
(693) Niemeyer, N.; Eschenbach, P.; Bensberg, M.; Tölle, J.; Hellmann, L.; Lampe, L.; Massolle, A.; Rikus, A.; Schnieders, D.; Unsleber, J. P.; et al. The subsystem quantum chemistry program Serenity. *Wiley Interdisciplinary Reviews: Computational Molecular Science* **2023**, *13*, e1647.
(694) Sharma, M.; Sierka, M. Efficient implementation of density functional theory based embedding for molecular and periodic systems using gaussian basis functions. *J. Chem. Theory Comput.* **2022**, *18*, 6892−6904.
(695) Unsleber, J.; Dresselhaus, T.; Klahr, K.; Schnieders, D.; Böckers, M.; Barton, D.; Neugebauer, J. Serenity: A subsystem quantum chemistry program. *J. Comput. Chem.* **2018**, *39*, 788−798.

https://doi.org/10.1021/acs.chemrev.2c00758
Chem. Rev. 2023, 123, 12039−12104